Doctoral theses at NTNU, 2020:355

Svenn Are Tutturen Værnø

Transient Performance in Dynamic Positioning of Ships: Investigation of Residual Load Models and Control Methods for Effective Compensation

Doctoral thesis

Svenn Are Tutturen Værnø

NTNU
Norwegian University of Science and Technology
Thesis for the degree of Philosophiae Doctor
Faculty of Engineering
Department of Marine Technology

ISBN 978-82-326-5056-9 (printed ver.)
ISBN 978-82-326-5057-6 (electronic ver.)
ISSN 1503-8181

Doctoral theses at NTNU, 2020:355

NTNU
Norwegian University of Science and Technology

NTNU

Svenn Are Tutturen Værnø

Transient Performance in Dynamic Positioning of Ships: Investigation of Residual Load Models and Control Methods for Effective Compensation

Thesis for the degree of Philosophiae Doctor

Trondheim, November 2020

Norwegian University of Science and Technology
Faculty of Engineering
Department of Marine Technology

NTNU
Norwegian University of
Science and Technology

NTNU
Norwegian University of Science and Technology

Thesis for the degree of Philosophiae Doctor

Faculty of Engineering
Department of Marine Technology

ISBN 978-82-326-5056-9 (printed ver.)
ISBN 978-82-326-5057-6 (electronic ver.)
ISSN 1503-8181

Doctoral theses at NTNU, 2020:355

Printed by Skipnes Kommunikasjon AS

November 18, 2020

To Victoria

"You only have to do a very few things right in life so long as you don't do too many things wrong.

Warren Buffet

Abstract

This thesis concerns how the dynamic positioning (DP) control system can better handle transient events, where the loads experienced by the vessel change significantly over a short time frame. The material is intended for DP systems controlling surface ships, but it is also relevant for other DP vessels, as well as other motion control applications for marine vessels. The thesis is a collection of papers, with some introductory chapters to set the context of the problem.

The thesis contains contributions on the fundamental level, where different load models and observer algorithms are fairly compared and analyzed. The study investigates the effect of including nonlinear damping in the model. The results show that when using models where the residual loads are modeled as a current, then nonlinear damping improves performance. For the models where the residual loads are modeled as a superimposed load vector, then the effect of nonlinear damping is less apparent. The different observer algorithms show surprisingly similar performance, which indicate that DP is dominantly a linear process.

Two different augmentations of existing observer design have been proposed for better transient performance, while maintaining good steady-state performance. A time-varying model-based observer is presented and analyzed, where aggressive gains are used during transient for responsiveness, and relaxed gains are used in steady state for lower oscillations in the state estimates. The performance is verified through high-fidelity closed-loop simulations and on experimental full-scale data from a cruise with the research vessel R/V Gunnerus. In addition, on the cruise with R/V Gunnerus, a partial closed-loop validation with integrated DP observer and controller was performed. The other design is a hybrid observer combining model-based and kinematic observers. The hybrid observer switches to the kinematic observer in transient conditions, and to the model-based observer in steady conditions. The observer performance is verified through model-scale closed-loop experiments, and on full-scale experimental data from R/V Gunnerus.

For the control design, integral action is compared to other ways of compensating the environmental and unmodeled loads, with special focus on transient conditions. The results show that the best solution is to use the estimate of the environmental and unmodeled loads from an observer with tuning optimized to estimate these loads. This method outperforms the other methods in transients, and has equal performance to integral action in steady state. In addition, using an observer to find the estimate alleviates anti windup

issues, and contrary to tuning integral action, an observer can be tuned open loop – which is a large benefit. Hybrid integral action is proposed to improve performance in transient conditions and still keep relaxed and satisfactory performance in steady conditions. This is achieved by high gains in the integrator in transients to better compensate the loads in transients, and relaxed gains in steady conditions to not induce unnecessary oscillations. Pseudo-derivative control (PDF) is proposed as an alternative to traditional proportional-integral-derivative (PID) control. The PDF control algorithm does not need a reference filter as the PID does, as the references are generated internally, and the PDF control algorithms is better at mitigating integral windup, compared to the PID control algorithm. Performance of the PDF control law is shown through a simulation study, and through full-scale closed-loop trials with R/V Gunnerus.

Acknowledgements

The PhD study and the years the PhD lasted has been transformative. I would especially like to thank my main supervisor Professor Roger Skjetne for the encouragement, and his helpful and warm-hearted attitude during the PhD. My co-supervisor Professor Asgeir Sørensen has been very helpful in convincing me early on that a PhD was the right thing to pursue. In the course of the PhD Asgeir has given me many ideas, but I first and foremost appreciate the pleasant early morning conversations about research topics, work, and other non-work related interesting topics. I would also like to thank Vincenzo Calabrò for helpful input that I have implemented throughout a lot of the papers in the thesis, and I am surprised by how knowledgeable, modest, and helpful Vincenzo is. That combination is truly impressive.

My colleagues has been indispensable. I would like to thank Astrid Brodtkorb for an outstanding collaboration on joint projects and papers. Also, I would like to thanks my office mate from early on in my PhD and when I wrote my Masters, Øivind Kjerstad, for very interesting discussions, input, and collaboration. This was very helpful for my understanding of the topic, and I am grateful for all the input I received. As I would consider all aforementioned people my friends, there are other colleagues that also made my time at NTNU AMOS more enjoyable. I would like to thank everyone from my time at NTNU AMOS for interesting talks, coffee breaks, Technical Thursdays, and social events. In particular, I would like to thank Mauro Candeloro. I have never met a more helpful, friendly, interesting, and self-less man.

Finally, I would like to thank the love of my life and wife, Victoria. She is an integral part of all aspects of my life, including the PhD. She has truly helped me in finalizing the PhD. For that I am grateful.

Preface

This thesis is submitted to the Norwegian University of Science and Technology (NTNU) for partial fulfillment of the requirements for the degree of philosophiae doctor.

This doctoral work has been carried on at the Department of Marine Technology (NTNU), with Professor Roger Skjetne as main supervisor and Professor Asgeir Johan Sørensen as co-supervisor.

Abbreviations

ADPRC	AMOS DP Research Cruise
AFF	Acceleration FeedForward
AMOS	Centre for Autonomous Marine Operations and Systems
AUV	Autonomous Underwater Vehicle
CoE	Centre of Excellence
CL	Closed Loop
C/S	Cyber Ship
DFO	Derivative Free Optimization
DOF	Degree Of Freedom
DP	Dynamic Positioning
EKF	Extended Kalman Filter
GAS	Globally Asymptotically Stable
GNSS	Global Navigation Satellite System
GPS	Global Positioning System
IMO	International Maritime Organization
IMU	Inertial Measurement Unit
INS	Inertial Navigation System
KF	Kalman Filter
LKF	Linear Kalman Filter
LTI	Linear Time Invariant
LTV	Linear Time-Varying
MC-Lab	Marine Cybernetics Laboratory
MRU	Motion Reference Unit

NED	North East Down
NLO	Nonlinear Observer
NPO	Nonlinear Passive Observer
NTNU	Norges Teknisk-Naturvitenskapelige Universitet (Norwegian University of Science and Technology)
PD	Proportional Derivative
PDF	Pseudo-derivative Feedback
PID	Proportional Integral Derivative
ROV	Remote Operated Vehicle
R/V	Research Vessel
SPR	Strictly Positive Real
UKF	Uncented Kalman Filter
ULES	Uniformly Locally Exponentially Stable
UGES	Uniformly Globally Exponentially Stable

Contents

Part I

Dynamic Positioning and Transient Challenges

Chapter 1

Overview

The thesis concerns DP control systems for marine surface vessels. The main topic is the transient challenges experienced by a DP control system, when either the environment change, or there is an event causing a sudden load change. The transient problem for DP and DP control systems are introduced before the results of the thesis are discussed.

1.1 Objectives of Research

The research questions governing the topic of the papers in the thesis are:

1. In model-based observer and controller design for DP, how does different control design models compare, and how does different estimation algorithms compare?
2. How can we improve observer and controller design to better handle transient events in DP?
3. What is the best way of compensating the transient bias loads in the DP controller?

1.2 Target Audience

This thesis is intended for engineers, students, and academics working on one or more of the following applications:

- Dynamic positioning systems for vessels, especially in severe conditions.
- Control systems for autonomous vessels.

1.3 Main Contributions

The main contributions of the thesis include the following:

- Contribute to knowledge of how to use different control design models and observer algorithms for DP.
- Construct a time-varying model-based observer for DP that works well in both steady state and transient conditions, with experimental validation.
- Contribute to the design of a hybrid observer for DP, that switches automatically between a kinematic observer in transients, and a model-based observer in steady state, in order to optimize performance in both steady state and transient conditions.
- Compare different ways of compensating the bias loads by control action, and give a clear understanding of when to apply different methods and how they compare.
- Contribute to the design of a pseudo-derivative feedback control law for DP, with experimental validation of performance.

1.4 Thesis Outline

The thesis is divided in three parts, and outline of the thesis is as follows:

- Part I gives a brief presentation about dynamic positioning in general, its history, the background and motivation for the thesis topic and the published papers.
  - Chapter 1 presents the thesis outline, discussion of target audience, and outline of main contributions.
  - Chapter 2 describes the background and functionality of the DP system, introduces and discusses the transient problem for DP observer and controller design, and discusses solutions proposed in the literature not including the ones proposed in this thesis.
  - Chapter 3 gives a brief overview of the AMOS DP Research Cruise 2016.
  - Chapter 5 presents the scope of work, publication list, and discusses the common thread in the publications included in the thesis.
- Part II presents all the articles of the thesis, either published or sent for publication.
  - Chapter 6 presents all the journal papers.
  - Chapter 7 presents all the conference papers.
- Part III presents concluding remarks and further work for the thesis as a whole.

Chapter 2

Dynamic Positioning and the Transient Load Challenge

In this chapter, we provide a background and motivation for the research reported in this thesis. First, the theoretical background for Dynamic Positioning (DP) systems is briefly explained, with focus on the DP control system and its basic control mechanisms. In Section 2.3, a general description of conventional model-based DP is explained along with a description of the transient load challenge for DP, building on the DP basics from Section 2.1 and 2.2. In Section 2.4, existing solutions to the transient problem from the literature is discussed. This discussion excludes the works of this thesis, since these will be explained in Chapter 5 with a description of the common thread of the thesis. The reader is conferred to the publications presented in Part II for the detailed descriptions of our analysis, findings, and proposed solutions.

2.1 Dynamic Positioning for Marine Surface Vessels

Due to needs in the offshore and petroleum industries to perform marine operations in deep waters, where jackups and fixed installations are not viable options, the DP system was developed and has become an essential asset to accomplish increasingly more complex field developments. The first computer-controlled DP vessel was the drillship Eureka that came in 1961 (Fay, 1989). Today, oil and gas is a major user of DP systems, typically in platform supply vessels (PSVs), drilling vessels, pipe-laying, subsea construction, remote operated vehicle (ROV) support, diving support, and virtual anchoring. Other vessel types that use DP systems include cruise ships, fishing vessels, modern icebreakers, research vessels, and more and more underwater vehicles. In the recent developments of autonomous ships (MTEC/ICMASS, 2019), the DP control system is essential in order to safely and effectively achieve the desired autonomous operations of the vessel.

A DP vessel means a vessel that automatically maintains its position (fixed location or predetermined track) exclusively by means of thruster force (IMO, 1994). As presented by

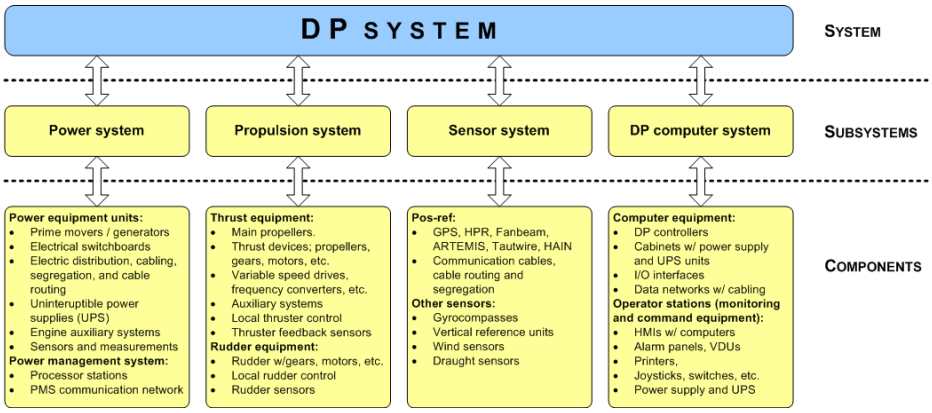

Figure 2.1: Subsystems and components of a DP system (Skjetne and Egeland, 2006).

Sørensen (2011), the main subsystems of a DP vessel include a power system, a thruster system, and a DP control system; see also (DNV GL, 2019).

Depending on the criticality of the operation, there are different requirements for the DP system in terms of redundancy and safety. These are called DP Equipment Classes (IMO, 1994) defined by the IMO, and verified through ship rules by the classification societies such as DNV GL, Lloyds Registry, ABS, and Buraeu Veritas. There are three DP classes. DP1 is the most relaxed, where loss of position or heading is acceptable in the case of a single failure. For DP2 and DP3, a single failure shall not lead to loss of position/heading, and the DP system must have redundancy in all active components to achieve this. For instance, there must be three position reference systems, three vertical motion sensors, three gyro compasses, and three wind sensor. The additional requirement for DP3 is that also passive components (electrical cables, piping, etc.) are considered in the single failure criterion, resulting in segregation requirements for the physical arrangement of the equipment, in order to ensure that fire and flooding in rooms and compartments do not cause loss of position/heading.

Figure 2.1 shows an overview of the subsystems and typical components of a DP system. The power system is responsible for the power supply to all components of the vessel. Especially important for DP2 and DP3 is the ability to reconfigure the power plant into two or more isolated electrical systems in order to avoid blackout on the vessel due to electrical failures. Also important is the uninterrupted power supply to sensor units and control equipment. The electrical system is governed by a power management system (PMS), whose objectives include preventing blackouts, starting/stopping gensets according to prevailing load conditions, and ensure load-sharing between the connected gensets. More recent developments have defined energy and emission management functionality by use of energy storage devices in a hybrid electric power plant for the DP vessel, to achieve reduced emissions to air and reduced fuel consumption (Sørensen et al., 2017; Reddy et al., 2019). The thruster system is the low-level actuator control system, respon-

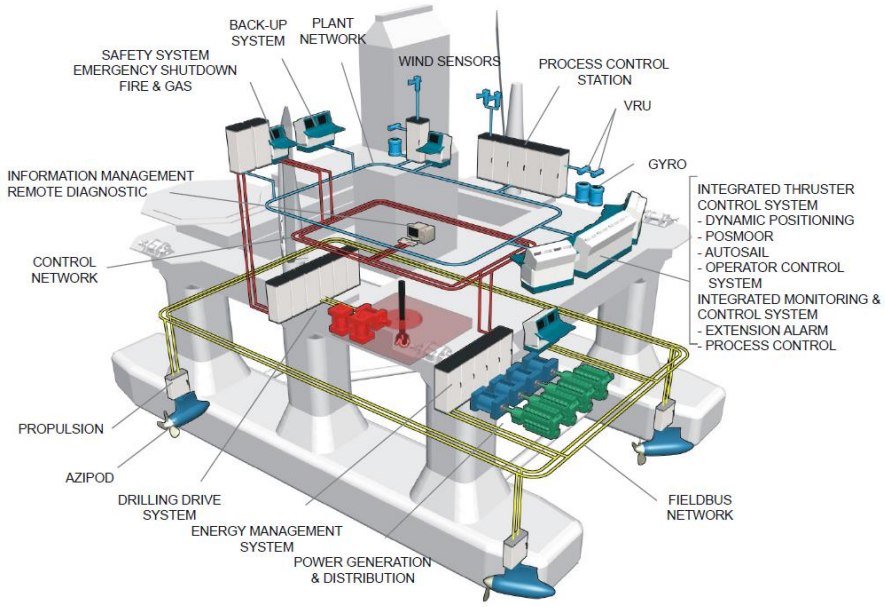

Figure 2.2: DP drill rig. Courtesy: Sørensen (2013) and ABB Marine.

sible for producing the required thrust forces and directions commanded by the DP control system. It includes the main propulsion units, fixed direction thrusters, azimuth thursters, and rudders, along with the drives and necessary auxiliary systems (Smogeli, 2006). The components of the DP control system include sensors, control computers, networks, and signal cabling (Skjetne and Egeland, 2006; Skjetne et al., 2017). Hence, the DP control system includes all the steps from receiving noisy and unprocessed measurements, such as the the position and attitude of the vessel, to the output by a demanded thrust force and moment to the thrust allocation that translates this into specific commands for each thruster. An illustration of the subsystems and components of a DP system, and their locations in a DP drilling rig, is shown in Figure 2.2. The DP control system, which will be outlined in more detail in Section 2.2, is the relevant subsystem for this thesis.

2.2 The DP Control System

The DP control system is the subsystem of a DP vessel relevant for this thesis. The first DP controllers from 1961 used a single-input-single-output proporional-derivative-integral (PID) controller along with lowpass and/or notch filters (Sørensen, 2011). Later, Kalman Filtering with wave-filtering and multivariable control was proposed for DP by Balchen et al. (1976), and later extended by Balchen et al. (1980), Jenssen (1981), Grimble et al. (1980), Saelid et al. (1983), Fung and Grimble (1983), Fossen (1994), Mandžuka

and Vukić (1995), Sørensen et al. (1996), Fossen et al. (1996), Katebi, Zhang and Grimble (1997); Katebi, Grimble and Zhang (1997), Tannuri and Donha (2000), and Katebi et al. (2001). The use of a nonlinear passive observer was presented by Fossen and Strand (1999), and their work was extended to include adaptive wave-filtering by Strand and Fossen (1999). Feedback of acceleration measurements for DP was studied by Lindegaard (2003), whereas extensions to slow speed tracking of a path, called maneuvering, was developed by Skjetne (2005). More recently, DP in heavy sea-ice conditions has been studied (Kjerstad, 2016), and inertial navigation systems with adaptive wave-filtering was presented by Bryne et al. (2017). See also Sørensen (2011) and Breivik (2010), and the references therein, for a comprehensive account of the DP development and literature.

In a state-of-the-art DP system, a *control design model* (often called a *control-oriented model*) is used for controller and observer design. This is usually a reduced model including the relevant dynamics for the mode of operation. For low-speed applications such as DP, this implies that Coriolis and centripetal loads are neglected, and typically nonlinear damping is neglected as well. For surface vessels, only the horizontal motions (planar motion and yaw rotation) are typically considered in the DP observer and control design, because the other degrees of freedom (DOF) are self-restoring and self-stabilizing. The motions are described in two main reference frames used for DP, the local Earth-fixed North-East-Down frame (NED) used for navigation, and the local body-fixed frame (B) in which the kinetics of the vessel is described. The NED-frame is a local tangent plane on the mean ocean surface, with origin placed at an arbitrary location. The x-axis points in the North direction, the y-axis points East, and the z-axis points down towards the centre of the Earth. The NED-frame is assumed to be inertial (non-accelerating) such that Newton's laws apply. The B-frame moves with the vessel. It typically has its origin midships in the waterline, referred to as CO (common origin), with the x-axis pointing in the direction of the bow, y-axis pointing starboard, and positive z-direction downwards (Fossen, 2011). A sketch of a DP vessel subject to waves, wind, and current, with the body coordinate axes highlighted, is shown in Figure 2.3.

The DP control system is a complex system with several modules. Explained briefly, the modules of the DP system are (Sørensen, 2011, 2013):

Sensor module: This module includes all the sensors systems, providing information about the vessel and its environment. The different systems includes:

- *Position reference systems:* The Global Navigation Satellite System (GNSS) provides position measurements in the NED-frame, and the most common GNSS system is the Global Positioning System (GPS). Other positioning systems include hydroacoustic positon reference (HPR) systems, taut wire system, and other relative reference systems based on radar, laser, or microwave technologies.
- *Motion reference systems:* The Inertial Measurement Unit (IMU) contains gyros and accelerometers in three axis and provides linear accelerations and angular velocities.

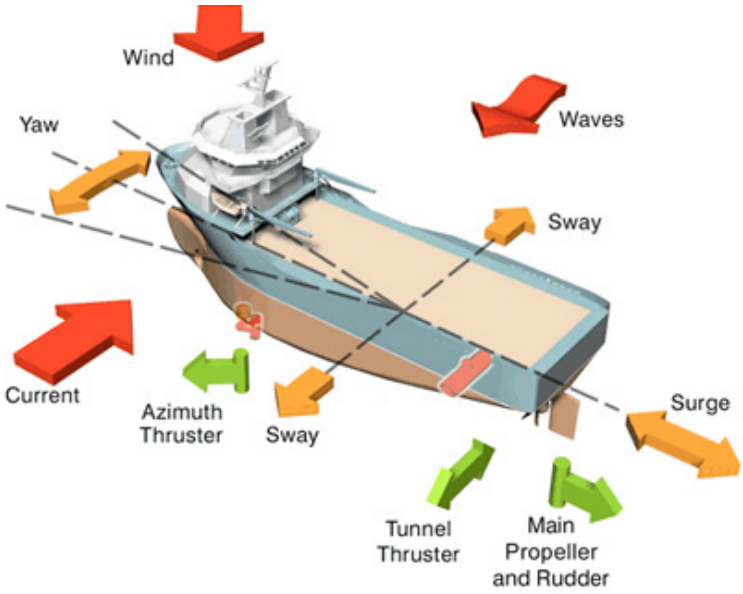

Figure 2.3: DP principle sketch. Courtesy: Kongsberg Maritime.

- *Attitude sensors:* For heading measurements there exists gyrocompasses and magnetic compasses, and the Vertical Measurement Unit (VRU) provides pitch and roll measurements.
- *Environmental sensors:* There are wind sensors (anemometer) that measure wind velocity and direction, wave radar, and draft sensors.

Signal Processing: Processes the raw measurements from the sensors and faulty signals are handled (e.g. by voting). This includes checking for wildpoints, signal freeze, and checking signal range and variance. The signals are also weighted when there are several sensors for the same sensory information.

Vessel Observer: Estimates low-frequency noise free vessel states based on the processed signals, where the first order wave motion is filtered out. In addition, low-frequency unmeasured states, such as the velocity and environmental loads are estimated. There exists both kinematic and model-based observers, where model-based observers are most common for DP – such as the nonlinear passive DP observer or by using an Extended Kalman Filter (EKF). The kinematic observer uses processed measurements of acceleration, angular velocities, heading, and position to estimate the states of the vessel, that is, the position, velocity, and also the acceleration. The model-based observer typically use processed measurements of heading and position in combination with a kinetic model of the vessel to estimate the position, velocity, and environmental loads. The vessel observer also provide dead reckoning in case of signal drop out, and for this the model-based

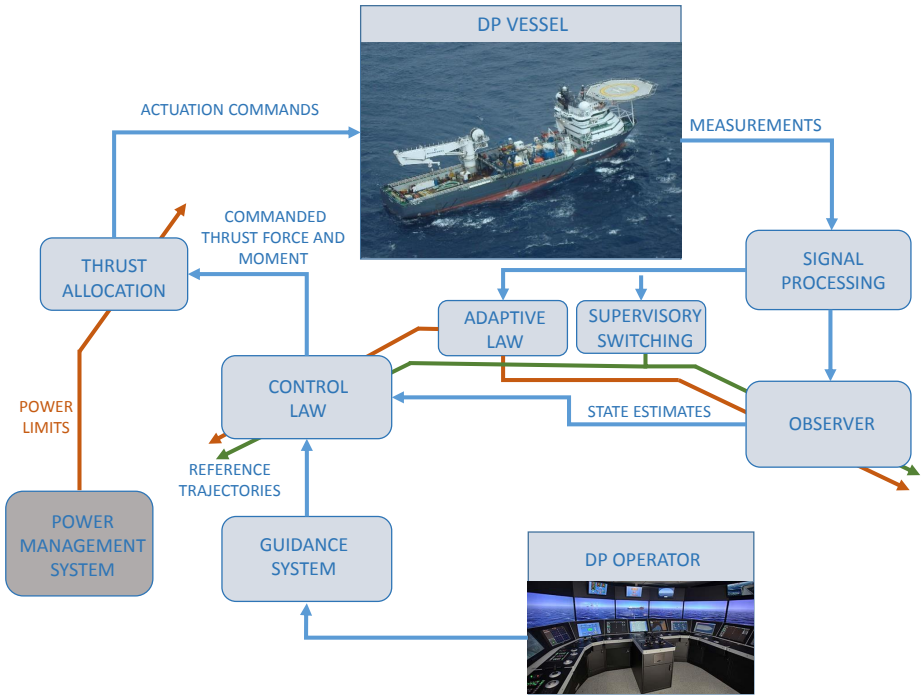

Figure 2.4: Block diagram of a DP control system integrated with the power management system. Adopted from Sørensen (2013).

observer is the best choice.

Guidance system: Produces desired trajectories and reference states for the vessel to follow in order to perform a maneuver, such as a setpoint change or low-speed tracking. The reference trajectory is sent to the controller.

Supervisory logic: Governs which observer and controller algorithms are to be used at any point in time, depending on the mode of operation, the sea state and the environment. The controller logic ensures a smooth transition when switching between the different controller and observer algorithms.

Control law: Controls the vessel states towards the reference by using state estimates from the vessel observer, the reference trajectories from guidance system, and environmental measurements. It calculates a command thrust load in the body-frame of the vessel. The control law has two parts:

- *Feedback control law:* Uses the deviation between the estimated states and the reference trajectories to calculate an appropriate force to correct for the deviation, and bring the vessel towards the trajectory.
- *Feedforward control law:* Directly cancels the wind forces, measured by a wind sensor. In addition, the desired trajectories from the guidance system are used as reference feedforward along with the model parameters such as mass and damping to better control the vessel through maneuvers and along trajectories.

Adaptive law: During operation, the environmental conditions, the sea state, and other conditions, such as the load conditions and draft, change. The adaptive law identifies these changes and sends this information as input to the observer, control law(s), and the supervisory logic block.

Thrust allocation: This module forms a layer below the control law in order to translate the commanded thrust load vector from the control law (in the vessel body-frame) into a commanded thrust force and direction (angle) for each of the thrusters of the vessel. It gives the thrusters a speed command (most common), or a torque or power command, and for azimuth thrusters also an angular command. The process of finding desired force and direction for each thruster is generally solved as a constrained optimization problem, where limits of the thruster forces, rate of turn of azimuth thrusters, forbidden zones, power limits, and other requirements are taken into consideration.

Together, all the components of the DP system described above produce commands to the thrusters so that the vessel can maintain the desired position or execute a guided maneuver.

2.3 The Transient Load Challenge

During DP operation, the vessel may keep the same position and heading for hours and days in row in very slowly varying environmental conditions. Hence, the DP control sys-

tem should inhibit a relaxed behavior, for the majority of time, to not induce unnecessary oscillations in the use of the thrusters. In steady conditions, the DP is able to accurately position the vessel by relaxed control actions, which also lowers the fuel consumption and reduces wear and tear on the thrusters. The DP control system normally compensates the low-frequency dynamics only. The vessel is subject to waves, wind, and current in open sea, where the first-order wave loads are large, but oscillatory, and on average do not push the vessel off position. The other loads are called low-frequency loads, including second-order wave-drift loads, slowly-varying current loads, and mean wind loads (Faltinsen, 1990), and these have to be rejected by the control system. A wave-filter is implemented in the observer to separate the vessel motion induced by the first-order wave loads, called the wave-frequency motion, from the low-frequency motion caused by the slowly-varying loads. Because of this separation into low-frequency and wave-frequency motion, the observer injection gains have to be tuned such that the wave-filtering capabilities are good. This implies a lower tuning than if the wave-filtering was not present.

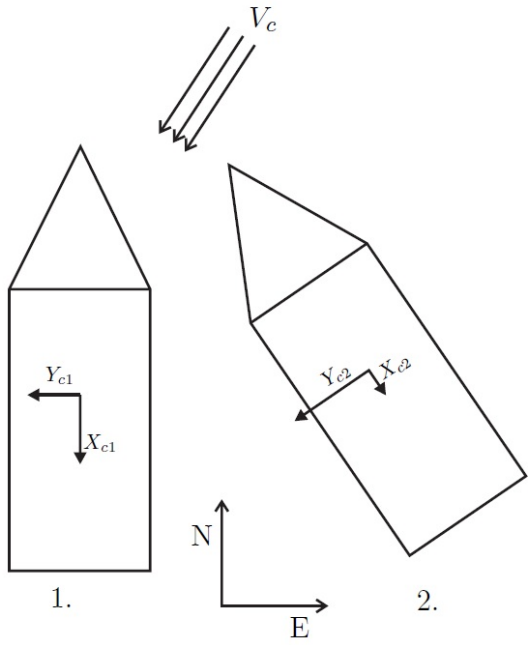

Figure 2.5: A ship with different heading subject to an ocean current V_c. Courtesy: Refsnes and Sørensen (2007).

As DP operations move into harsher environments, transient events pose a substantial challenge for the DP observer and control law. These are events where the loads acting on the vessel change significantly over a short time period. The transient events can be external – such as wave trains, rotational currents, and sea-ice loads (Kjerstad et al., 2015), they can be operation specific – such as structural forces from coil tubing in well interven-

tion, gangway connections, or jackup platform operations at touchdown or release of the legs, or they can be operator induced – such as mode changes or heading changes during operation of the DP system. A heading change will, for instance, induce a transient since the loads experienced by the vessel will vary due to ship hull geometry – as illustrated for a current load in Figure 2.5 and in the next example.

Example 2.3.1. Residual bias load vector. Assume a NED-fixed irrotational current velocity vector is given by $\nu_c^n := \text{col}(V_c \cos(\beta_c), V_c \sin(\beta_c), 0)$ where (V_c, β_c) are the current speed and direction, respectively. Let $\nu := (u, v, r) \in \mathbb{R}^3$ be the B-frame velocity vector of the vessel, let $\nu_c^b := R(\psi)^\top \nu_c^n \in \mathbb{R}^3$ be the B-frame velocity vector of the current, and let $\nu_r := \nu - \nu_c^b$ be the corresponding relative velocity vector. Suppose according to (Fossen, 2011, Eq. 8.147) that the actual 3DOF low-frequency dynamics of the vessel is described by

$$M\dot{\nu}_r + C(\nu_r)\nu_r + D(\nu_r)\nu_r = \tau \tag{2.1}$$

where wave loads, wind loads, and thruster dynamics are disregarded, τ is the thrust load, M is the mass matrix, $C(\cdot)$ models the Coriolis and centripetal loads, and $D(\cdot)$ models the linear and nonlinear damping loads. Consider the typical DP control design model, studied in (Værnø et al., 2019),

$$\hat{M}\dot{\nu} + d = \hat{\tau}, \tag{2.2}$$

where $\hat{M}$ and $\hat{\tau}$ are the estimated mass matrix and thrust load vector, used in the control, and d is a load vector to capture hydrodynamic effects and bias loads. Typically, the model of d is chosen as either of:

$$d = \begin{cases} \hat{D}_L\nu - b^b, & \dot{b}^b = 0; \quad \text{B-fixed bias load} \\ \hat{D}_L\nu - R(\psi)^\top b^n, & \dot{b}^n = 0; \quad \text{NED-fixed bias load.} \end{cases} \tag{2.3}$$

$\hat{D}_L$ is the estimated linear damping matrix, and $R(\psi)$ is the rotation matrix from B to NED. Comparing (2.2) with (2.1) gives the expressions for the respective bias loads based on the difference between the reduced model and the actual dynamics (2.1),

$$\begin{aligned} b^b &= \tilde{\tau} - \tilde{M}\dot{\nu} + M\dot{\nu}_c^b - C(\nu_r)\nu_r - D(\nu_r)\nu_r + \hat{D}_L\nu \\ b^n &= R(\psi)\left[\tilde{\tau} - \tilde{M}\dot{\nu} + M\dot{\nu}_c^b - C(\nu_r)\nu_r - D(\nu_r)\nu_r + \hat{D}_L\nu\right], \end{aligned} \tag{2.4}$$

where $\tilde{\tau} := \tau - \hat{\tau}$ is the error of the unmodeled thruster dynamics, and $\tilde{M} := M - \hat{M}$ is the error in the mass matrix. The residual load terms in (2.4) is related to both body-fixed and NED-fixed effects; the relative velocity terms (and current) are correlated to a current in the NED frame, whereas the uncertainties due to thruster dynamics and inertial loads are body-fixed errors.

As an example, we investigate the bias loads on the platform supply vessel simulation model that we used in (Værnø et al., 2019). The model includes current loads, Coriolis/-centripetal loads, and linear/nonlinear damping. In the simulation we exclude wind loads,

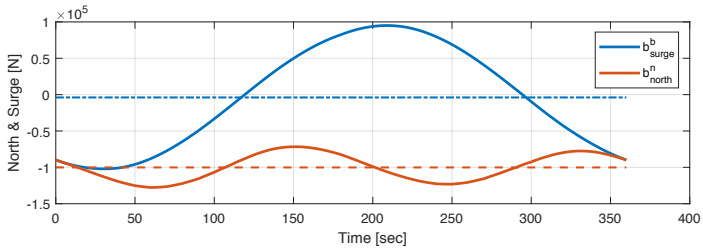

(a) North and Surge bias loads.

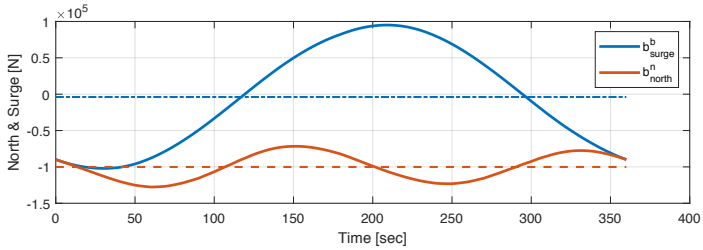

(b) East and Sway bias loads.

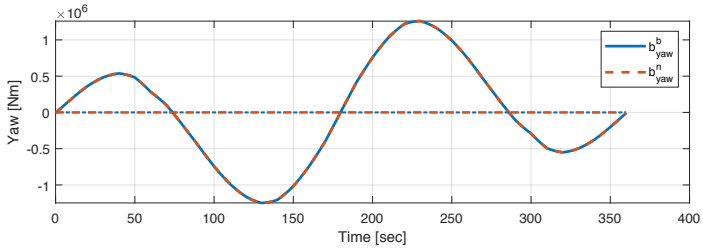

(c) Yaw bias loads.

Figure 2.6: Residual bias loads of supply vessel during a 360° *turn. The blue and red curves correspond, respectively, to the B- and NED-fixed bias vectors. The average values are shown as the constant curves.*

wavedrift loads, and uncertainties in thruster dynamics and mass/inertia. A forced yaw rotation $\psi(t) = \frac{\pi}{180}t$ so that $r = \frac{\pi}{180}$ rad/s $= 1$ deg/s is executed in a current field with $V_c = 0.5$ m/s and $\beta_c = 180$ deg, while we maintain $(u, v) = (0, 0)$. Figure 2.6 shows the evolution of the residual bias loads during the 360° turn of the vessel. It is very clear that the assumption of a constant bias load, either in NED or in body, is not valid during the heading change. The variation is significant, as seen by the varying difference from the average values. The faster the heading change is executed, the faster the bias load also changes. We also observe, in this case, that the NED-fixed bias has a larger average value but with less variation than the B-fixed bias. □

Transient events pose great challenges for the DP control system, partly because the typi-

cal sensor instrumentation and control design models do not capture the load changes well enough. There are umodeled dynamics from, for instance, errors in the mass and added mass, hydrodynamic damping, and errors in the thruster dynamics, and there are uncertain environmental loads from wind, waves, and current as mentioned earlier. The DP system must robustly compensate these uncertain loads in order to maintain acceptable positioning performance. However, with typical instrumentation where North/East position along with the heading angle are measured, it is not possible to separate between what is current, wind, wave loads, or unmodeled dynamics in the estimator or controller. Thus, the environmental loads and unmodeled dynamics are lumped into one vector, typically as a *residual* load vector or bias, b, as shown in Example 2.3.1. Most often, this is modeled as a constant load in the NED-frame (Fossen, 2011; Fossen and Strand, 1999). This has its background in the assumption that the bias load is dominated by environmental parameters like current and waves, which are represented in the NED-frame. Body-fixed bias models do also occur, typically in linearized models; see for instance the works by Fossen and Perez (2009) and Hassani et al. (2012). This is justified by the fact that much of the unmodelled loads and dynamics are body-related mechanisms that has no correlation to the North-East axes.

Another approach, assuming the bias loads are dominated by unmodeled hydrodynamic effects, is to model the damping loads based on the relative velocity vector ν_r between the hull and the fluid; see for instance (Fossen, 2011; Refsnes, 2007). Again, all loads are estimated in one vector, but now as dissipation loads represented by a bias velocity, for instance as $D(\nu)\nu_c^b$, where $D(\nu)$ is the damping matrix and ν_c^b is a DP-observed "current" velocity vector to be estimated by the observer. The estimated ν_c^b becomes, in reality, the sum of all the unmodeled dynamics and environmental forces captured as a bias velocity vector. This model should better capture current and wave loads, since it incorporates the dissipative damping of the vessel hull. Thus, it should also be less affected by heading changes. However, as the loads to be estimated in this vector still is a combination of body-fixed loads from the model errors in mass/inertia, damping, and thruster dynamics, and primarily NED-fixed loads from current, waves, and wind, this approach is not perfect either. Again, any discrepancies in the model will result in a transient load under various events, like heading changes, implying a need for mechanisms to more rapidly updating the bias estimates during such load variations.

Example 2.3.2. Residual bias velocity vector. Consider again the DP vessel in Example 2.3.1 and its dynamics (2.1) and reduced control design model (2.2). Let $\nu_b \in \mathbb{R}^3$ be a *velocity bias* vector (to estimate a DP current vector), with the relationship $\nu_b^b = R(\psi)^\top \nu_b^n$ between the B-fixed and NED-fixed vectors. Consider d selected among:

$$d = \begin{cases} \hat{D}_L(\nu - \nu_b^b), & \dot{\nu}_b^b = 0; \quad \text{B-fixed bias velocity} \\ \hat{D}_L(\nu - R(\psi)^\top \nu_b^n), & \dot{\nu}_b^n = 0; \quad \text{NED-fixed bias velocity.} \end{cases} \tag{2.5}$$

Inserting (2.5) into (2.2) and comparing with (2.1), gives the bias velocitiy vectors based

on the difference between the model and the "actual" dynamics,

$$\begin{aligned} \nu_b^b &= \nu + \hat{D}_L^{-1}\left[\tilde{\tau} - \tilde{M}\dot{\nu} + M\dot{\nu}_c^b - C(\nu_r)\nu_r - D(\nu_r)\nu_r\right] \\ \nu_b^n &= R(\psi)\nu + R(\psi)\hat{D}_L^{-1}\left[\tilde{\tau} - \tilde{M}\dot{\nu} + M\dot{\nu}_c^b - C(\nu_r)\nu_r - D(\nu_r)\nu_r\right]. \end{aligned} \tag{2.6}$$

Suppose $C(\nu_r)\nu_r \approx 0$, $D(\nu_r)\nu_r \approx \hat{D}_L(\nu - \nu_c)$, and $\tilde{\tau} - \tilde{M}\dot{\nu} + M\dot{\nu}_c \approx 0$ in (2.6). Then the velocity bias vectors will match $\nu_b^b = \nu_c^b$ and $\nu_b^n = R(\psi)\nu_c^b = \nu_c^n$. Assuming constant current velocity in the NED-frame, only the latter of these will validly conform to the constant bias model $\dot{\nu}_b^n = 0$.

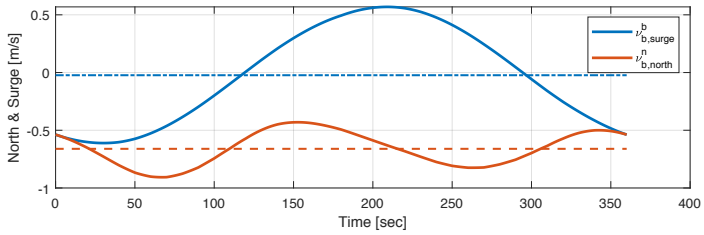

(a) Bias velocities North and Surge.

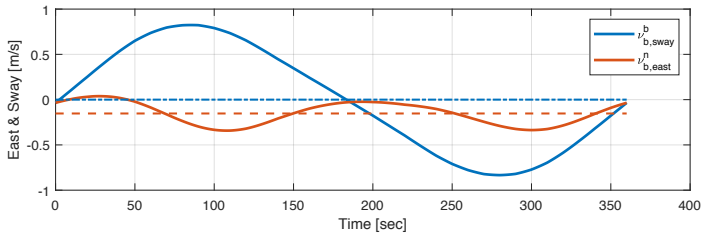

(b) Bias velocities East and Sway.

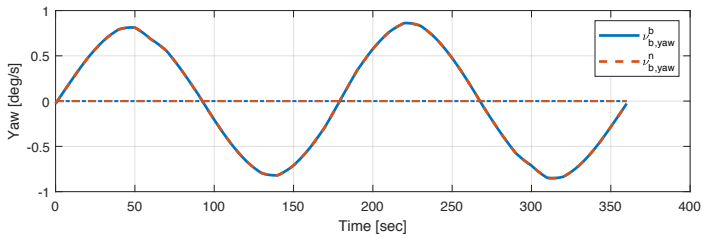

(c) Bias Yaw rates.

Figure 2.7: Residual bias velocities of supply vessel during a 360° turn. The blue and red curves correspond, respectively, to the B- and NED-fixed velocity vectors. The average values are shown as the constant curves.

Figure 2.7 shows the evolution of the bias velocities during a 360° turn of the platform supply vessel simulation model used in (Værnø et al., 2019), by again inducing a forced yaw rotation while keeping $(u, v) = (0, 0)$, with the same data as in Example 2.3.1. It is

clear that the assumption of a constant bias velocity, either in NED or in body, is again not valid during the heading change due to the various unmodeled loads and dynamics. The variations in the bias velocities are similar as in Example 2.3.1, but note that the size of the bias velocities are in the order of 1 while being in order of 10^5 for the bias loads.

Figure 2.8 better illustrates the evolution of the bias velocity vector (u_b, v_b) and yaw rate r_b, both for ν_b^b and ν_b^n. In the left plot, it is seen that (u_b^n, v_b^n) has a smaller footprint, but larger mean value, than (u_b^b, v_b^b). □

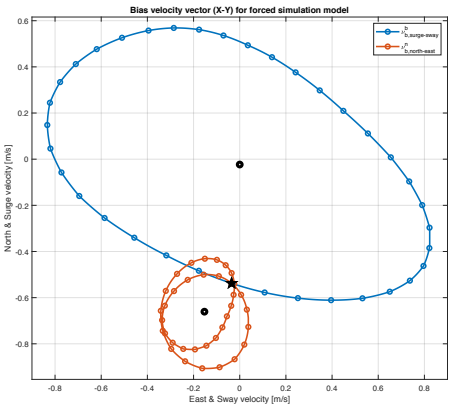

(a) Bias velocities North/Surge vs East/Sway.

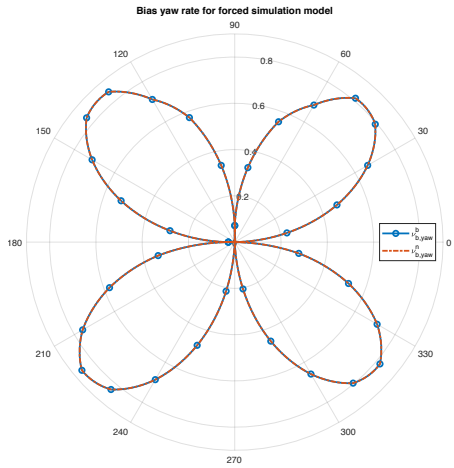

(b) Bias Yaw rate for each heading angle.

Figure 2.8: Residual bias velocity components for the supply vessel during the 360° turn, corresponding to Figure 2.7. Left plot (a) shows u_b vs. v_b for the B-fixed (blue curve; surge vs. sway) and NED-fixed (red curve; North vs. East) vectors, where the dots indicate every 10° heading angle. The black star indicates the initial heading $\psi = 0°$, for both curves, and the black circles indicate the respective average values. Right plot (b) shows the bias yaw rate r_b as a polar plot with respect to heading angle ψ.

Remark 1. A higher fidelity bias velocity model than (2.5) may be used with respect to relative velocity in an observer (Værnø et al., 2019). By incorporating the full nonlinear damping and Coriolis, the bias velocity may be modeled as

$$\begin{aligned} \dot{\nu}_b^n &= 0 \\ d &= C(\nu_r)\nu_r + D(\nu_r)\nu_r, \qquad \nu_r = \nu - R(\psi)^\top \nu_b^n. \end{aligned} \tag{2.7}$$

Then this dynamics is included in the nonlinear observer, such as an EKF or UKF. Including nonlinear damping in the bias velocity model showed a slight positive effect on performance in our study in (Værnø et al., 2019). □

The bias load/velocity vector is slowly-varying in steady conditions, while it can change rapidly during transient events, as explained above. To better capture these transient variations in the bias, one may attempt to improve the fidelity of the control design model

by including more precise hydrodynamic descriptions of the loads. However, this will require more complex hydrodynamic parameters to be identified, which is a costly process, and it will give a more complex control algorithm that may be more difficult to qualify with regards to stability and robustness. In addition, there will still be uncertainties in the more complex model, so that other transient problems and new safety issues may be the outcome. Because of this, the preferred method in conventional model-based observer design for DP, is for the residual load to be modeled as a constant bias load or through a constant bias velocity. This assumption has been shown to work well in normal practice, as well as in the experimental results by Fossen and Strand (1999) and Loría and Panteley (1999). However, we highlight that these practices are related to operations where the bias loads are constant or slowly-varying, and not on the more rapidly varying conditions that motivates this thesis.

Accurate estimation of the environmental loads and unmodeled dynamics is crucial for the performance of a model-based observer. When this estimate is inaccurate, the error propagates especially to the velocity estimate, and further to the position estimate – making them biased. Ideally both a current velocity model and a bias model should be included in the control design model to better capture the total variations. However, that causes observability issues to be overcome. We illustrate this in the next example.

Example 2.3.3. Observability of 1DOF DP model. Consider a 1DOF hydrodynamic model that, say, resemble the surge dynamics of a DP vessel. Let $x \in \mathbb{R}$ be a position and $u := \dot{x}$ be its velocity. Further, let u_c be a constant current velocity, and define $u_r := u - u_c$ as the relative velocity. Suppose the rigid-body and hydrodynamic model, with linear and nonlinear damping, is expressed as the 1DOF mass-damper system

$$m_{rb}\dot{u} + m_a\dot{u}_r + d_{nl}\left|u_r\right|u_r + d_l u_r = \tau + \delta \tag{2.8}$$

where m_{rb} and m_a are rigid-body and added mass, d_l and d_{nl} are linear and nonlinear damping coefficients, τ is the control input, and δ is a disturbance force. Since $\dot{u}_c = 0$ implies $\dot{u}_r = \dot{u}$, we can write the dynamics both in terms of absolute and relative velocity, that is,

$$m\dot{u} + d_{nl}\left|u - u_c\right|(u - u_c) + d_l(u - u_c) = \tau + \delta \tag{2.9a}$$

$$m\dot{u}_r + d_{nl}\left|u_r\right|u_r + d_l u_r = \tau + \delta \tag{2.9b}$$

where $m := m_{rb} + m_a$.

Letting b be a bias state and choosing the state vector $\xi := \mathrm{col}(b, x, u)$, with absolute velocity u, we can reduce the system into the simplified control design model

$$\dot{\xi} = \begin{bmatrix} 0 & 0 & 0 \\ 0 & 0 & 1 \\ \frac{1}{m} & 0 & -\frac{d_l}{m} \end{bmatrix}\xi + \begin{bmatrix} 0 \\ 0 \\ \frac{1}{m} \end{bmatrix}\tau \tag{2.10a}$$

$$y = \begin{bmatrix} 0 & 1 & 0 \end{bmatrix}\xi. \tag{2.10b}$$

We recognize here the bias, to match the uncertain terms, as

$$b = -d_{nl} \left| u_r \right| u_r + d_l u_c + \delta,$$

which depends on u through the nonlinear damping. The observability matrix and its determinant for this system are

$$O = \begin{bmatrix} 0 & 1 & 0 \\ 0 & 0 & 1 \\ \frac{1}{m} & 0 & -\frac{d_l}{m} \end{bmatrix} \quad \text{and} \quad \det O = \frac{1}{m} \neq 0. \tag{2.11}$$

It follows that the system state ξ is uniformly completely observable; however, this is based on the assumption that $\dot{b} = 0$ which is valid only for constant u.

Letting both b and u_c be states, and choosing the state vector $\zeta := \mathrm{col}(b, x, u_c, u_r)$, with relative velocity u_r, we can alternatively express the system by the simplified control design model

$$\dot{\zeta} = \begin{bmatrix} 0 & 0 & 0 & 0 \\ 0 & 0 & 1 & 1 \\ 0 & 0 & 0 & 0 \\ \frac{1}{m} & 0 & 0 & -\frac{d_l}{m} - \frac{d_{nl}}{m} \left| u_r \right| \end{bmatrix} \zeta + \begin{bmatrix} 0 \\ 0 \\ 0 \\ \frac{1}{m} \end{bmatrix} \tau \tag{2.12a}$$

$$y = \begin{bmatrix} 0 & 1 & 0 & 0 \end{bmatrix} \zeta \tag{2.12b}$$

where b is recognized as $b = \delta$. Hence, in this case the assumptions $\dot{b} = 0$ and $\dot{u}_c = 0$ are both valid. Disregarding the nonlinear damping, by setting $d_{nl} = 0$, the observability matrix and its determinant for this system becomes

$$O = \begin{bmatrix} 0 & 1 & 0 & 0 \\ 0 & 0 & 1 & 1 \\ \frac{1}{m} & 0 & 0 & -\frac{d_l}{m} \\ -\frac{d_l}{m^2} & 0 & 0 & \frac{d_l^2}{m^2} \end{bmatrix} \quad \text{and} \quad \det O = 0. \tag{2.13}$$

It follows that this system, now having a valid bias model, instead struggle from lack of observability, meaning that the states b and u_c may not be distinguishable and estimated individually. □

Remark 2. One may consider to use the relative velocity vector ν_r in the DP observer. However, one should then note that the DP control law requires a precise estimate of the absolute velocity ν and not ν_r. Hence, if ν_r is used as a state in the observer, as in Example 2.3.3, then accurate estimation of ν_c is also necessary so that $\nu = \nu_r + \nu_c^b$ can be output from the observer.

When sticking to the approach of using a bias load or velocity model, more aggressive tuning during the transients seems necessary for satisfactory performance of the observer, whereas relaxed tuning is beneficial in steady conditions to reduce oscillations in the state estimates. During transient events, a prompt and responsive control action is necessary

for good DP performance, which implies using higher gains in the control law. However, since transient events occur infrequently, a controller optimized only for transient conditions will cause unnecessary oscillations in the longer periods of steady conditions. This will in overall lead to worse positioning performance, higher wear and tear on the thrusters, and higher fuel consumption compared to using more relaxed control gains that are optimized for the steady conditions.

2.4 Towards Better Transient Performance

There are several designs in the literature to improve transient performance of DP operation. Hybrid control for switching between different controller/observer pairs for DP has been proposed by Nguyen et al. (2007), where the appropriate pairs were selected based on the sea state. This was also analyzed by Brodtkorb et al. (2014), and it is a part of the "controller logic" block described in Section 2.2. This allows for performance optimized for the condition the vessel is operating in, from calm to severe sea states. Hybrid control in general (Hespanha, 2001; Goebel et al., 2009) gives great flexibility in designing observers and controllers that by discrete switching or updates can handle a changing environment and transient events. Another work on hybrid control for DP was proposed by Nguyen et al. (2008), where a supervisory control method is applied for control transfer between different modes; stationkeeping, low-speed maneuvering, and transit. Different observer/controller pairs are selected based on the desired mode of operation, and controllers that automatically switch between the different modes are also included. This allows for a holistic control system, not just optimized for one mode of operation. See Figure 2.9 by Nguyen et al. (2007) for an illustration of the switching logic for the observer/controller pairs.

Kinematic observers avoid the bias transient problems, and is a viable solution to the observer side of the transient problem. The bias problem of the model-based observer is avoided by using a purely kinematic model, and thus no bias load is part of the model. Using a kinematic observer, at least in transients, is beneficial, and a comparison of the methods in both steady conditions and transients should be performed. The kinematic observers, often called navigation filters, combine an inertial nagivation system (INS) with GNSS measurements. This has been proposed used for DP by Bryne et al. (2014) and Bryne et al. (2017) based on work by Grip et al. (2015) and Grip et al. (2012). This further build on, among others, the works by Salcudean (1991), Thienel and Sanner (2003), Vik and Fossen (2001), Mahony et al. (2008), Mahony et al. (2008), Hamel and Mahony (2006), and Vasconcelos et al. (2008). In (Bryne et al., 2017), a wave-filtering capability is added to a kinematic observer making it suitable as an observer in waves. Since kinematic observers do not estimate loads, some kind of integral action is needed in the control law. Either a model-based observer could be used to estimate the loads, or integral action on the tracking errors in the controller should be used. Hence, the load transient problems will still be present in the closed-loop system, but it will not propagate to the position and velocity state estimates in this case. Hence, the kinematic observer seems to be a promising option.

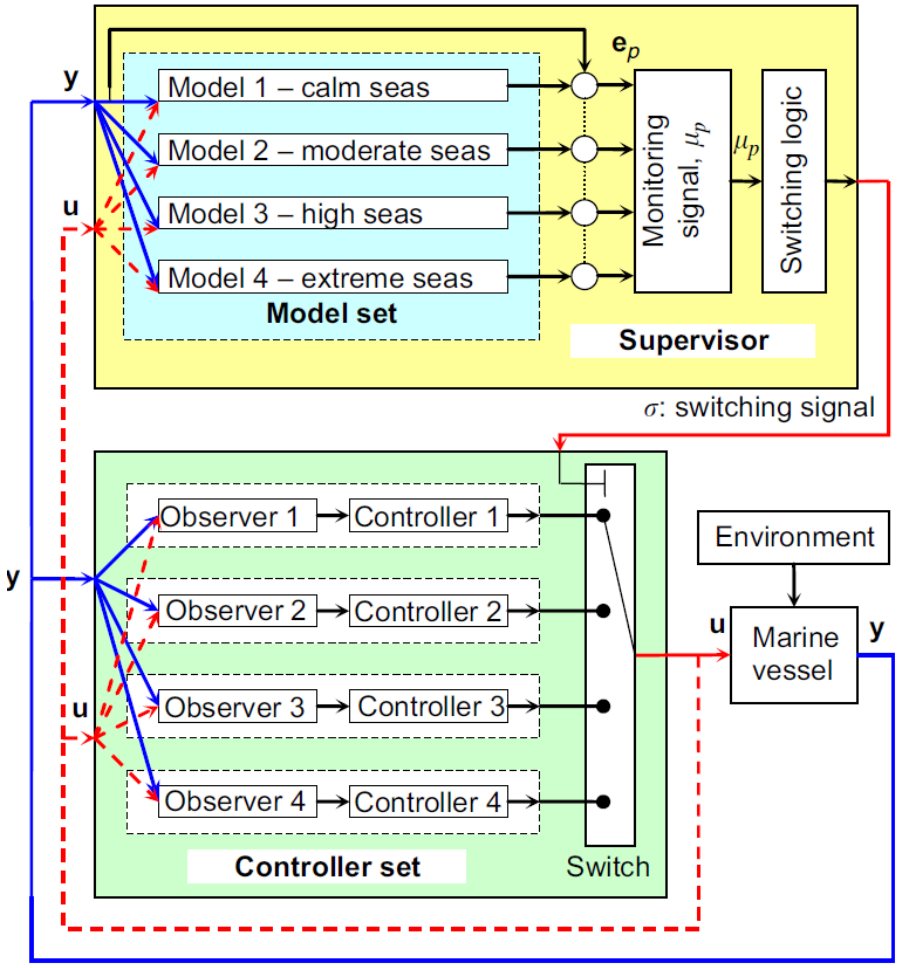

Figure 2.9: Switching logic for the calm to extreme sea hybrid controller, as presented by Nguyen et al. (2007).

Figure 2.10: Platform and offshore supply vessel in extreme conditions.

Lindegaard (2003) and Kjerstad and Skjetne (2016) proposed the use of acceleration sensors and kinematic models to improve control in harsh environment. In Lindegaard (2003), acceleration feedback is proposed to virtually increase the mass of the vessel. This is used to make the vessel "more inertial" and less sensitive to external load variations. Kjerstad and Skjetne (2016), on the other hand, proposed a mechanism for direct cancellation of the residual loads, denoted *acceleration feedforward* and primarily directed towards ice loads. The estimated acceleration is, in this case, used to directly calculate the loads acting on the vessel using Newton's second law. This method is promising, and it is shown by Kjerstad and Skjetne (2016) to work well against ice loads that are large, fast, and require responsive control actions. The approaches by Lindegaard (2003) and Kjerstad and Skjetne (2016) to load rejection, are fundamentally different from the bias estimation or integral action approaches. They are based on extra instrumentation to better sense the loads (through accelerations) and thereby compensate load variations more directly from measurements. The challenge of using acceleration feedback or feedforward for open seas is the wave-filtering of the acceleration measurements or the estimated loads. The first order wave accelerations are much larger than the low-frequency aceleration, and the oscillation period of the waves are in the range of $5 - 15$ seconds. Therefore, good wave-filtering of the accelerations or the load estimates is difficult. In case the wave-filtering is out of phase, the loads can easily dominate the other low-frequency loads. Another option for some applications, using acceleration feedforward, is to cancel all the external loads acting on the vessel, provided the thruster system is dimensioned for it. This will provide aggressive control and should probably only be used in conditions that absolutely require it, since this will increase fuel consumption and cause extra wear and tear on the thrusters. In the case of DP in sea ice, such aggressive control is necessary, since the thrusters must respond directly to the agile sea ice loads to avoid loss of position.

Chapter 3

NTNU AMOS DP Research Cruise 2016

In the fall of 2016, NTNU AMOS in collaboration with Kongberg Maritime conducted a two week long full-scale DP test campaign. The campaign, NTNU AMOS DP Research Cruise 2016 (ADPRC'16), was conducted with the research vessel (R/V) Gunnerus shown in Figure 3.2. To the author's knowledge, this is the first time DP algorithms has been implemented and tested closed-loop on a vessel of this size in an academic research context (Skjetne et al., 2017). Several papers of this thesis either present closed-loop results or use data from the cruise, and thus a brief presentation of the cruise follows.

R/V Gunnerus is owned and operated by NTNU. It has been used as a university reasearch vessel since 2006, within marine biology, marine archeology, oceanography, subsea geology, fisheries, and marine technology. R/V Gunnerus has a K-Pos DP-11 system from Kongsberg Maritime, is equipped with two main azimuth thrusters by Rolls-Royce Marine (now Kongsberg Maritime), and a Brunvoll tunnel thruster in the bow. During the ADPRC'16 campaign, the vessel was of length overall $Loa = 31.25$ meters and dead weight of 107 tons. Note however, that after these sea trials, in the winter 2018-2019, R/V Gunnerus was retrofitted and elongated by 5 meters, now with $Loa = 36.25$ meters

Figure 3.1: The research team on ADPRC'16.

Figure 3.2: The NTNU-owned research vessel R/V Gunnerus.

and dead weight of 165 tons.

When testing algorithms, a simulation study is the first step, starting at a low-fidelity model, and moving over to a higher fidelity model. Thereafter, experimental tests are preferred for performance verification in "real conditions". At NTNU, up to ADPRC'16 this has been limited to model-scale tests in the basin at MC-Lab; see for instance Lindegaard (2003), Nguyen et al. (2007) and Bjørnø et al. (2017) for details about the lab and model scale vessels. Model tests are a great way of testing the algorithms. However, full-scale tests have the benefit of a more realistic environment, real machinery and propulsion systems, and a real sensor suite compared to the lab. Thanks to the DP Development and Cybernetics department in Kongberg Maritime, implementation of our (NTNU AMOS) control algorithms was possible. Figure 3.3 shows the topology of the DP system for R/V Gunnerus, where the "NTNU algorithm" block is where our algorithms were implemented, taking the processed measurements as input, and commanded thrust as output. Safety functions were built around this block, so that we could test new algorihtms with minimum risk. Safety fallback was provided by a switch back to the commercial DP control functions installed in the vessel.

The test objectives from the ADPRC'16 cruise were (Skjetne et al., 2017):

- *Establish a test interface and a method for the academic reasearchers to test their control-related algorithms on the industrial DP control system onboard R/V Gunnerus.*
- *Test relevant DP state observer algorithms in full-scale.*
- *Test relevant DP feedback control algorithms in full-scale.*

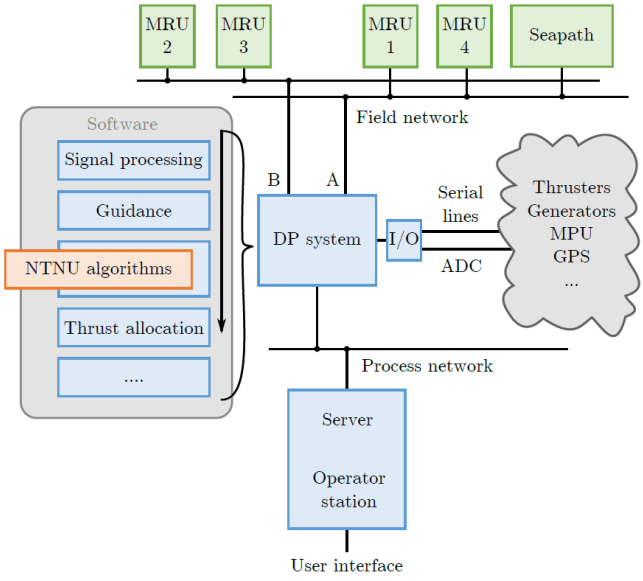

Figure 3.3: Topology of DP test interface on R/V Gunnerus for ADPRC'16 (Skjetne et al., 2017).

- *Test experimental adaptive autopilot control algorithms in full-scale.*
- *Evaluate the test methodology and results from testing, and learn from both successes and failures.*

Our algorithms were tested as either closed-loop tests in real time at the DP operation, or offline based on collected data from the campaign. For the closed-loop test, the objectives were to test and verify performance of 1) DP control laws in feedback with a selected observer algorithm (often the industrial DP observer), or 2) DP observer algorithms in feedback with a selected control law (possibly the industrial DP algorithm). Otherwise, performance of the observer algorithms have been verified offline by the collected data in the office later. Which papers of this thesis that consider closed-loop tests, and which later used data from the ADPRC'16, are highligheted in Chapter 5.2. See otherwise (Skjetne et al., 2017) for more detailed descriptions of other tests, and for more details about the campaign itself.

Chapter 4

Tuning by Derivative Free Optimization

In several papers of the thesis ((J.1),(J.2),(J.4)) optimization is applied to find gains of observers and controllers. Optimal tuning based on a common cost function is applied in order to get comparable gains and performance and, thus, be able to fairly compare the different algorithms. In addition, in one of the papers, optimization is applied to identify hydrodynamic parameters. We have chosen to use *derivative free optimization* (DFO), defined as *"the mathematical study of optimization algorithms that do not use derivatives"* (Audet and Hare, 2017). Hence, the benefit of DFO that it does not require any information about derivatives or gradients, is what we have exploited in our studies. This is useful for computer simulations and experimental data since accurate and explicit information about the derivatives is not readily available. Note also, as stated by Audet and Hare (2017), that if *"gradient information is available, reliable, and obtainable at a reasonable cost, then DFO ... will almost never outperform modern gradient-based methods."* The reader is referred to Audet and Hare (2017), and references therein, for presentation of several advanced algorithms for solving DFO and blackbox optimization problems as well as relevant background information.

In the recent M.Sc. thesis by Løvås (2019), several methods for DFO-based autotuning of the DP control law has been investigated – as a follow-up of relevant papers in this thesis. This included parametrization of the control law, discussion and evaluation of different performance functions, and comparison of different DFO algorithms such as *particle swarm* optimization (PSO), *surrogate model* optimization, and the Nelder-Mead *simplex* search method (Lagarias et al., 1998) as implemented in the MATLAB function $fminsearch$. In the development work by Løvås (2019), the PSO was chosen as the preferred algorithm, and the cost function was chosen simply as the integral of absolute error (IAE) on the DP output tracking error. An experimental setup was implemented in the MC-Lab at NTNU, where a model ship was running automated DP maneuvers in a repeated manner while executing the DFO-based tuning of the control gains. See (Løvås, 2019) for further details of this investigation.

In the following, a short description of how to apply the optimization for tuning an observer is outlined. This is similar to what was done in the papers (J.1), (J.2), and (J.4). In the studies leading to these papers, the objective of the DFO-based tuning was on finding observer gains that gave fair comparison between different observer algorithms. Towards this goal, the MATLAB function $fminsearch$ (MATLAB, 2016) was found adequate and implemented similarly as in the following setup.

We consider finding optimal gains for an observer based on a dataset consisting of sampled time evolutions of the state, (control) input, and (measurement) output values. Let $\mathcal{X} = \{x_0, x_1, x_2, \dots, x_n\}$ be the set of $n+1$ samples of the state, $\mathcal{U} = \{u_0, u_1, u_2, \dots, u_n\}$ be the set of control inputs, and $\mathcal{Y} = \{y_0, y_1, y_2, \dots, y_n\}$ be the set of measurement outputs. Accordingly, let $\hat{\mathcal{X}} = \{\hat{x}_0, \hat{x}_1, \hat{x}_2, \dots, \hat{x}_n\}$ be the state estimates from the observer, where the observer algorithm is represented by the overall difference equation

$$\hat{x}_k = \Gamma_{k-1}(\hat{x}_{k-1}, u_{k-1}, y_k, K), \qquad k = 1, 2, \dots, n. \tag{4.1}$$

K is the tunable observer gain that the state estimates then depend upon, that is, $\hat{\mathcal{X}} = \hat{\mathcal{X}}(K)$. The optimization problem can now be formulated as

$$\underset{K}{\text{minimize}} \qquad J(\mathcal{X}, \hat{\mathcal{X}}(K)) \tag{4.2a}$$

$$\text{subject to} \qquad y_k \in \mathcal{Y}, u_k \in \mathcal{U}, x_k \in \mathcal{X}, \text{ and } (4.1), \tag{4.2b}$$

where $J(\mathcal{X}, \hat{\mathcal{X}}(K))$ is the cost function. DFO is then used to solve this problem.

An obvious example of a cost function, is the sum (integral) of absolute errors in the state estimate, that is,

$$J(\mathcal{X}, \hat{\mathcal{X}}(K)) = \sum_{k=0}^{n} |x_k - \hat{x}_k|. \tag{4.3}$$

For high-fidelity computer simulations of a DP vessel and control system, the data to evaluate the cost function on is directly available from the simulation data, that is, the full state dataset $\mathcal{X}$ and its estimate dataset $\hat{\mathcal{X}}$. For the full-scale experimental data, on the other hand, the available values to evaluate the cost function on are the post-processed measurement data. It is therefore a question if the complete state data $\mathcal{X}$, or the most important subset of this, can be made available through post-processing. For DP, the measured data correspond to the pose η, and from this the actual velocity ν may be found in post-processing by differentiating the resulting positions and heading using a finite impulse response (FIR) filter. Therefore, as long as the study is conducted offline on the sampled data, the state (η, ν) may be accurately reconstructed in order to evaluate the cost function J in each iteration of the DFO. The alternative, available for online execution of DFO, is to design the cost function based only on measured data or based on a surrogate model (Audet and Hare, 2017).

To run the optimization, first an initial value for the observer gain, K_0, is selected. Then the MATLAB function $fminsearch$ is used, where the function $findgains$ supplies $fminsearch$ with the cost.

Algorithm 1 findgains.m (pseudocode)

function J = FINDGAINS($\mathcal{X}, \mathcal{U}, \mathcal{Y}$, K)
  for k **do** = 1:n
    $\hat{x}_k = \Gamma_{k-1}(\hat{x}_{k-1}, u_{k-1}, y_k, K)$
  end for
  J = norm($\hat{\mathcal{X}} - \mathcal{X}$);
end function

This is executed according to

$$K = \text{fminsearch}(@findgains, \mathcal{X}, \mathcal{U}, \mathcal{Y}, K_0) \tag{4.4}$$

Finally, because the DFO finds a local optimum, the optimization is run several times with different initial K_0 values, either using a grid search or some other technique to select random variations of K_0.

Chapter 5

Research Overview

Section 5.1 presents an overview of the publications, and in Section 5.2 the context of the thesis and papers is outlined. The research questions from Section 1.1 define the scope of work of the thesis, and Section 5.2 discuss how the papers address the research questions.

5.1 List of Publications

The papers published and submitted in the time 2014-2018 are listed below.

International Refereed Journal papers

(J.1) **Værnø, S. A.**, Skjetne, R., Kjerstad, Ø. K., Calabrò, V. (2019). Comparison of control design models and observers for dynamic positioning of surface vessels. *Control Engineering Practice, DOI: 10.1016/j.conengprac.2019.01.015*.

(J.2) **Værnø, S. A.**, Brodtkorb, A. H., Skjetne, R., Calabrò, V. (2017). Time-varying Model-based Observer for Marine Surface Vessels in Dynamic Positioning. *IEEE Access, DOI: 10.1109/ACCESS.2017.2731998* .

(J.3) Brodtkorb, A. H., **Værnø, S. A.**, Teel, A. R., Sørensen, A. J., Skjetne, R. (2018). Hybrid controller concept for dynamic positioning of marine vessels with experimental results. *Automatica, DOI: 10.1016/j.automatica.2018.03.047*.

(J.4) **Værnø, S. A.**, Brodtkorb, A. H., Skjetne, R. (2019). Compensation of bias loads in dynamic positioning of marine surface vessels. *Ocean Engineering, DOI: 10.1016/j.oceaneng.2019.03.010*.

International Refereed Conference papers

(C.1) **Værnø, S. A.**, Brodtkorb, A. H., Skjetne, R., Sørensen, A. J. (2016). An Output

Feedback Controller with Improved Transient Response of Marine Vessels in Dynamic Positioning. In *Proceedings of IFAC CAMS*.

(C.2) Brodtkorb, A. H., **Værnø, S. A.**, Teel, A. R., Sørensen, A. J., Skjetne, R. (2016). Hybrid observer for improved transient performance of a marine vessel in dynamic positioning. In *Proceedings of IFAC NOLCOS*.

(C.3) **Værnø, S. A.**, Skjetne, R. (2015). Hybrid Control to Improve Transient Response of Integral Action in Dynamic Positioning of Marine Vessels. In *Proceedings of IFAC MCMC*.

(C.4) Kjerstad, Ø. K., **Værnø, S. A.** , Skjetne, R. (2016). A Robust Dynamic Positioning Tracking Control Law Mitigating Integral Windup. In *Proceedings of IFAC CAMS*.

(C.5) Skjetne, R., Sørensen, M. E. N., Breivik, M., **Værnø, S. A.**, Brodtkorb, A. H., Sørensen, A. J., Kjerstad, Ø. K., Calabrò, V., Vinje, B. O. (2017). AMOS DP Research Cruise 2016: Academic Full-scale Testing of Experimental Dynamic Positioning Control Algorithms Onboard R/V Gunnerus. In *Proceedings of ASME OMAE*.

5.2 Context of Thesis and Papers

The common theme in this thesis is on understanding DP systems experiencing transient events and on improving the performance of the DP system. All the publications presented in Part II are stand-alone. However, the thesis can be read as a whole, and the relationships between the papers are summed up in Figure 5.1.

The papers address the three research questions presented in Section 1.1. Research question 1 is answered by paper (J.1) that compares and contrasts different models and observer algorithms for DP, with special focus on transient events. This information can support selection of a good model and corresponding observer algorithm. The observer part of research question 2 is addressed by the papers (J.2), (C.1), (J.3), and (C.2). They present solutions to extend existing observer designs to work well in both transient and steady state conditions. Even though specific models and observer algorithms are chosen for these four papers, the methods can be applied for different models and algorithms. Finally, to close to loop, control action is addressed in (J.4), (C.3), and (C.4), with special focus on transient performance, especially in (J.4) and (C.3). The papers (C.3) and (C.4) address the control action part of research question 2, whereas research question 3 is addressed in (J.4), where different methods to compensate the bias loads in DP are analyzed. The discussion below is separated into the observer and control problem.

5.2.1 Observer Problem

The aim of (J.1) is to aid in model selection for observer and control design for DP. Different control design models are investigated, where some are bias load models and some are

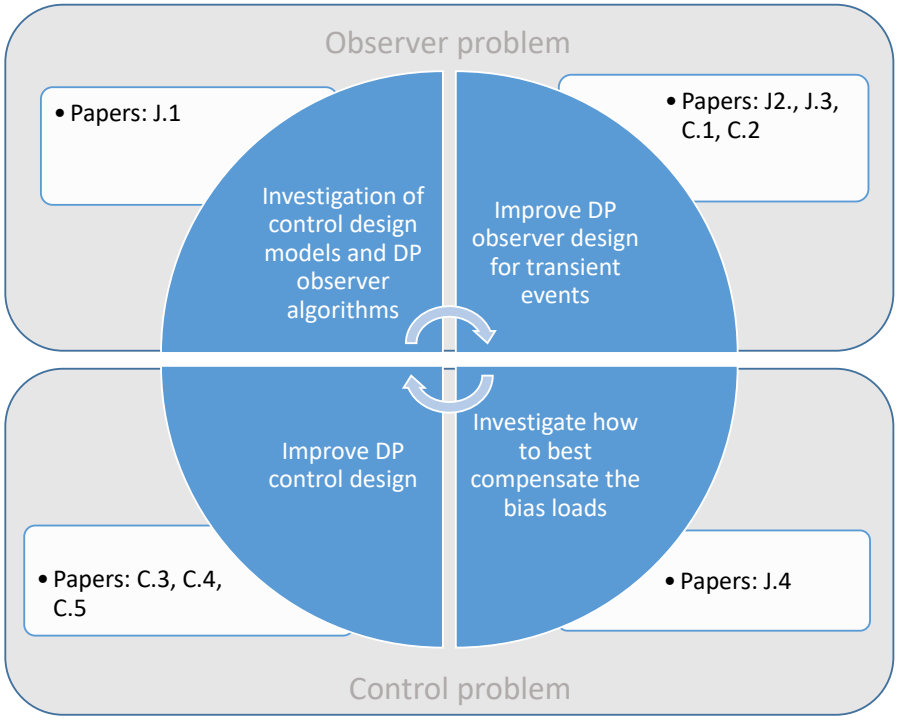

Figure 5.1: Illustration of the connection between different papers of the thesis.

current models, as described in Section 2.3. As discussed in Section 2.3, the residual loads are more precisely modeled as a combination of a bias load model and a current model; however, with standard instrumentation for DP it is not possible to separate the two in the observer. Therefore, each control design model is either a bias load model or a current model. The paper also investigates the effect of including nonlinear damping in the models. In addition, the paper compares common observer algorithms for DP. Three observer algorithms are compared; the Extended Kalman Filter (EKF) (Saelid et al., 1983) (Tannuri and Morishita, 2006), the Uncented Kalman Filter (UKF) (Simon, 2006), and the linear time-varying Kalman Filter (LTV-KF). The comparisons are made fair through derivative free optimization used to tune the observers based on a common cost function. An interesting observer to include in the comparison is the nonlinear passive observer (Fossen and Strand, 1999), which is common in the DP literature. However, to achieve a more structurally fair comparison, only Kalman Filters were studied. One should note, though, that the LTV-KF is the Kalman Filter-equivalent to the nonlinear passive observer when only linear damping is used. Therefore, this gives a good indication of the achievable performance of the nonlinear passive observer. All the maneuvers used are rich on transient events. Both high-fidelity simulation data and experimental data is used, where the experimental data was collected on a cruise with R/V Gunnerus, as described in Chapter 3 and (C.5).

The paper (J.2) seeks to modify existing model-based observer design to better handle transient events by using time-varying injection gains. The presented design gives both good transient performance, as well as good steady state performance. The journal paper (J.2) is an extension of the observer design in (C.1), where the whole output-feedback system was the focus. The observer part from (C.1) has been extended to include the velocity injection gains, and not just the bias injection gains as in (C.1). In addition, experimental full-scale data from R/V Gunnerus is used in (J.2), and experimental validation of (C.1) is briefly presented in (C.5), and in more detail in (J.2). A state of the art fixed-gain observer is used as the basis for the time-varying design. Even though it is not discussed in the paper, the same time-varying gain method would work for Kalman Filters, where instead of time-varying gains, the state covariance matrix Q could be time-varying.

The paper (J.3) has the same objective as (J.2), to achieve both good steady-state and transient performance of the DP observer. It applies a hybrid design with a model-based observer including a wave filter to be used in steady-state conditions, and a kinematic observer with IMU/GNSS integration for use in transient conditions. The kinematic observer does not include bias estimation, and therefore works well in transients. The kinematic observer does not include a wave-filter, rendering the control action in transients more aggressive. The journal version (J.3) is an extension of (C.2), where the journal paper includes a deeper analysis, as well as model-scale experimental results and full-scale experimental results with R/V Gunnerus from the ADPRC' 16 cruise.

5.2.2 Control Problem

The paper (J.4) investigates how to best compensate the bias loads in the controller, and thereby closing the loop. Traditional integral action is compared to different variations of using the bias estimate from observer designs. The performance of the methods is made comparable through derivative-free optimization methods, giving a fair comparison in order to find the best way to effectively compensate the bias loads. The journal paper (J.4) is an extension of the controller part of (C.1). In (C.1) a filtered version of the bias load estimate was proposed to be used instead of traditional integral action. This was merely argued for in (C.1), but in (J.4) these claims are made rigorous. The conference paper (C.3) addresses hybrid integral action, and applies much of the same design philosophy as in (J.2) and (C.1), where different gains for the integral action is applied to achieve good steady state and transient performance of the control system. Finally, the paper (C.4) proposes a viable alternative to using a traditional PID-controller in conjunction with a reference filter. The benefit of this approach is both a simpler design, with easy implementation of both rate constraints in the integral action, and an easier way to handle wind-up issues in the integral action of the controller.

Part II

Publications

Chapter 6

International Refereed Journal Papers

J.1

Comparison of control design models and observers for dynamic positioning of surface vessels

---

Værnø, S. A., Skjetne, R., Kjerstad, Ø. K., Calabrò, V.

Control Engineering Practice 85 (2019) 235–245

Contents lists available at ScienceDirect

Control Engineering Practice

journal homepage: www.elsevier.com/locate/conengprac

Comparison of control design models and observers for dynamic positioning of surface vessels

Svenn A. Værnø [a,*], Roger Skjetne [a], Øivind K. Kjerstad [b], Vincenzo Calabrò [c]

[a] Department of Marine Technology, Norwegian University of Science and Technology, 7491 Trondheim, Norway
[b] University Centre in Svalbard, Norway
[c] Kongsberg Maritime AS, Norway

ARTICLE INFO

Keywords:
Dynamic positioning
Marine vessels
Observers
Modeling
Optimization

ABSTRACT

This paper investigates some fundamental aspects of control system design for dynamic positioning of marine surface vessels. Different control design models are compared. The impact of applying linear and nonlinear models to describe the hydrodynamic damping loads are investigated, and common observer algorithms for DP are compared. The comparison includes a linear time-varying Kalman filter, an extended Kalman filter, and an unscented Kalman filter. To make the comparisons rigorous, optimization is employed to find optimal observer gains, and high-fidelity simulation data and full-scale experimental data are used to test the performance under operations/conditions with significant transient effects.

1. Introduction

In a model-based control and observer design, the performance of the control and observer algorithms strongly depends on how well the underlying model captures the dynamics of the system. The modeling of marine surface vessels performing dynamic positioning (DP) has an extensive literature; see for instance Fossen (2011) and Sørensen (2011) where high-fidelity models are described in detail, along with different models for controller and model-based observer design. However, there are few rigorous comparisons of control design models in the literature. There are papers where observers and controllers based on control design models have been shown to work well, as for instance by Fossen and Strand (1999), and Tannuri and Morishita (2006), where experimental validations were presented. In the work by Refsnes and Sørensen (2007) two control design models were compared for a linear system subject to an ocean current. A similar study is done by Refsnes (2007) where different control design models were compared for autonomous underwater vehicles (AUV's) subject to ocean currents. The study reported by Refsnes (2007) used a number of injection gains for each observer. However, the simulation model used to simulate the plant dynamics matches one of the control design models, giving the observers based on this model a clear advantage in their simulation study.

There exist a number of papers where different observer algorithms are presented and tested for DP. Early work on using the Kalman filter for DP was presented by Grimble, Patton, and Wise (1980) and Fung and Grimble (1983), and the Extended Kalman Filter (EKF) by Balchen, Jenssen, and Sælid (1976) and Saelid, Jenssen, and Balchen (1983). In the work by Fossen and Strand (1999) the authors presented a nonlinear (passive) observer (NLO) with full-scale experimental results, and in Tannuri and Morishita (2006) experimental results of a typical DP system using an EKF was presented. However, to the authors' knowledge, there are no papers with a rigorous comparison of the different algorithms applied to DP. In Fossen and Strand (1999), the authors argued that the NLO has some benefits compared to the EKF. The NLO has fewer tuning parameters and is shown to be UGES, whereas there is no global stability guarantee for the EKF. In terms of performance, the EKF has time-varying gains initially, whereas the NLO is a fixed-gain observer. Additionally, the NLO assumes that the rotation matrix is a signal, using the measured heading angle, whereas the EKF uses the low-frequency (LF) heading as a state in the rotation matrix. Especially in moderate to high sea states, this EKF mechanism should be beneficial. In Candeloro, Sørensen, Longhi, and Dukan (2012) different observer algorithms were compared for remotely operated vehicles (ROVs), but the tuning of the observers is found in an ad hoc manner, so a definite conclusion on performance is difficult.

In this work a rigorous analysis of the performance of both the models and observer algorithms for DP is reported, using derivative-free optimization (DFO). Different model structures to capture the environmental loads and unmodeled dynamics are analyzed. This includes a comparison of using nonlinear damping as opposed to just linear damping. For each such model, different observer algorithms are then quantitatively compared using a high-fidelity simulation model of a

* Corresponding author.
E-mail addresses: svenn.are.varno@ntnu.no (S.A. Værnø), roger.skjetne@ntnu.no (R. Skjetne), oivind.kjerstad@unis.no (Ø.K. Kjerstad), v.calabro@ieee.org (V. Calabrò).

https://doi.org/10.1016/j.conengprac.2019.01.015
Received 8 May 2018; Received in revised form 24 January 2019; Accepted 24 January 2019
Available online 19 February 2019
0967-0661/

supply vessel and full-scale data from DP operations of R/V Gunnerus. The observers are an EKF, an Unscented Kalman Filter (UKF), and a Linear Time-Varying Kalman-Filter (LTV-KF). The natural comparison is to compare the EKF with the NLO, the two most applied DP observers. However, it is easier to rigorously compare Kalman filters, since they have the same structure and the DFO can optimize on the same parameters. The LTV-KF is the Kalman filter equivalent of the NLO, provided only linear damping is included. Typically when the NLO is implemented for DP in the literature (Fossen & Strand, 1999; Loria, Fossen, & Panteley, 2000), only the linear damping is included. Since the yaw angle is assumed to be a signal, the rotation matrix can be assumed to be a known time-varying matrix, and the system is linear time-varying. Thus, a linear Kalman filter can be applied. When the LTV-KF reaches steady state Kalman gains, the LTV-KF and the NLO are identical in structure.

The last observer algorithm that is included in the comparison is the UKF. This is a nonlinear filter that does not rely on linearized dynamics as the EKF, thus being interesting for the comparison. The UKF is better at handling nonlinearities than the EKF (Simon, 2006), and it also has the benefit of using the low-frequency heading angle as a state (and not a signal) in the rotation matrix.

The main contribution of this paper is a systematic comparison of residual load models and Kalman filter algorithms for DP of marine surface vessels, using derivative-free optimization on test data that holds significant transient effects. The effect of using nonlinear damping versus only linear damping is tested. Both high-fidelity simulation data and full-scale experimental data from the AMOS DP Cruise 2016 (Skjetne et al., 2017) are used.

Nomenclature

Notation

A column vector is stated as $\mathrm{col}(\boldsymbol{x},\boldsymbol{y},\boldsymbol{z}) := \left[\boldsymbol{x}^\top,\boldsymbol{y}^\top,\boldsymbol{z}^\top\right]^\top$, $\mathbb{R}_{>0}$ denotes positive real numbers, and $\mathbb{S}$ represents the angle defined on the interval $[-\pi,\pi)$.

Abbreviations

AUV Autonomous underwater vehicle

CDM Control design model

DFO Derivative free optimization

DOF Degrees of freedom

EKF Dynamic positioning

LF Low frequency

LTV-KF Linear time-varying Kalman filter

NED North-East-Down

NLO Nonlinear observer

SVM Simulation verification model

UGES Uniformly globally exponentially stable

UKF Unscented Kalman filter

2. Problem formulation

The two reference frames used in DP are the North-East-Down (NED) frame, which is a local Earth-fixed frame assumed inertial (with x-axis pointing North, y-axis pointing East, and z-axis pointing down), and the body-fixed frame, which typically has the origin in the waterline along the centerline of the vessel(with x-axis pointing in the direction of the bow, y-axis pointing starboard, and z pointing down).

In the following there is a distinction between the *simulation verification model (SVM)* and the *control design model* (CDM). The former is a higher fidelity model used for controller and observer verification, whereas the latter is used for observer and controller design. The CDM captures the main dynamics, and for DP this includes the part of the model relevant for low-speed maneuvers, that is, Coriolis and centripetal terms are often omitted, and typically the nonlinear damping effects as well (Fossen, 2011). A bias load model is then typically applied to capture the residual loads in the CDM. These are uncertainties related to ocean current loads, slowly-varying wave drift loads, differences between actual wind loads and the estimated wind loads from the wind sensor measurements, unmodeled dynamics in the thruster system, and parametric uncertainties in the mass/inertia and damping terms.

2.1. Overall control design model

The CDM used in this study is the 3 DOF model (Fossen, 2011; Fossen & Perez, 2009; Sørensen, 2011)

$$\dot{\boldsymbol{\xi}} = \boldsymbol{A}_{\boldsymbol{w}}\boldsymbol{\xi} + \boldsymbol{E}_{\boldsymbol{w}}\boldsymbol{w}_{\boldsymbol{w}} \tag{1a}$$

$$\dot{\boldsymbol{\eta}} = \boldsymbol{R}(\psi)\boldsymbol{\nu} \tag{1b}$$

$$\boldsymbol{M}\dot{\boldsymbol{\nu}} + \boldsymbol{d} = \boldsymbol{\tau} + \boldsymbol{w}_{\boldsymbol{\nu}} \tag{1c}$$

$$\boldsymbol{y} = \boldsymbol{\eta} + \boldsymbol{C}_{\boldsymbol{w}}\boldsymbol{\xi} + \boldsymbol{v}_{\boldsymbol{y}}, \tag{1d}$$

where $\boldsymbol{\xi} \in \mathbb{R}^6$ models the wave-frequency motion by a damped oscillation model. $\boldsymbol{A}_{\boldsymbol{w}}$ is a Hurwitz matrix that contains the damping ratio of the wave motion model and the peak frequency of the sea state, and $\boldsymbol{w}_{\boldsymbol{w}} \in \mathbb{R}^3$ is white noise; see Fossen (2011) for details. There is a separation between the wave-frequency motion in (1a) and the low-frequency motion of the vessel in (1b)–(1c). In low-speed applications such as DP, it is typically only interesting to control the low-frequency motion of the vessel, since compensating the first-order wave motion causes extra wear and tear on the thrusters, and in most cases it is not possible to compensate this motion. The vector $\boldsymbol{\eta} = \mathrm{col}\left(\eta_N,\eta_E,\psi\right) \in \mathbb{R}^2 \times \mathbb{S}$ is the low-frequency North/East position and heading angle of the vessel, and $\boldsymbol{\nu} = \mathrm{col}\left(u,v,r\right) \in \mathbb{R}^3$ is the low-frequency surge/sway velocity in the body-frame, and the yaw rate, respectively. The matrix $\boldsymbol{R}(\psi)$ rotates a 3 DOF vector from body to NED according to

$$\boldsymbol{R}(\psi) = \begin{bmatrix} \cos(\psi) & -\sin(\psi) & 0 \\ \sin(\psi) & \cos(\psi) & 0 \\ 0 & 0 & 1 \end{bmatrix}. \tag{2}$$

The mass matrix contains the inertia and added mass parameters of the vessel, and $\boldsymbol{\tau} \in \mathbb{R}^3$ is the control vector formed by propulsion loads.

The measurement $\boldsymbol{y} \in \mathbb{R}^2 \times \mathbb{S}$ is the sum of the low-frequency North/East position and heading vector η, the wave-frequency North/East position and heading vector $\boldsymbol{\eta}_{\boldsymbol{w}} = \boldsymbol{C}_{\boldsymbol{w}}\boldsymbol{\xi}$, where $\boldsymbol{C}_{\boldsymbol{w}} = \begin{bmatrix}\boldsymbol{0}_{3\times3} & \boldsymbol{I}_{3\times3}\end{bmatrix}$, and the measurement noise $\boldsymbol{v}_{\boldsymbol{y}} \in \mathbb{R}^3$.

Remark 1. It is assumed that only the vector $\boldsymbol{\eta}$ is measured through $\boldsymbol{y}$ in (1d). If, however, also the velocity $\boldsymbol{\nu}$ is accurately measured, for example through a measurement equation $\boldsymbol{y}_{\boldsymbol{\nu}} = \boldsymbol{R}(\boldsymbol{\psi})\boldsymbol{\nu} + \boldsymbol{C}_{\boldsymbol{w}}\boldsymbol{A}_{\boldsymbol{w}}\boldsymbol{\xi} + \boldsymbol{v}_{\boldsymbol{\nu}}$ from a sophisticated navigation system, then this can with ease be included in the measurement equations of the observer, typically resulting in improved estimation accuracy of the overall state vector.

The load vector $\boldsymbol{d} \in \mathbb{R}^3$ contains hydrodynamic damping loads, slowly-varying second order wave drift loads, and other unmodeled dynamics such as parametric uncertainties in the mass/inertia and damping terms, and errors in thrust modeling. Different choices for $\boldsymbol{d}$ are outlined in the next section.

2.2. Damping and bias load models

Control design models for DP can differ in their complexity, but they also differ in how the residual loads such as current, second order wave loads, and unmodeled dynamics are accounted for in the model. In the state estimator, using only GNSS and compass measurements, it is not possible to separate the different environmental loads and unmodeled dynamics, so they are lumped together and estimated as one bias load vector. The most common assumption is that these loads are slowly-varying (or even constant) in the NED-frame so that they can be compensated by a type of integral action. However, even if the environmental loads are constant in the NED-frame, they will not be constant as experienced by the vessel, due to vessel hull geometry. Another method is to model the unknowns as a current vector, which should be more accurate in terms of estimating environmental disturbances, such as current and second order wave loads. This model, contrary to the bias vector model, takes the vessel hull into account by including the damping matrix. In addition, if the current is irrotational and constant, this load is accurately described as a NED-fixed current. However, there are other loads that has to be accounted for as well. Errors in the damping parameters become a body-fixed bias load, and so do errors in the thrust modeling and mapping. Therefore, the choice of the most accurate model is not obvious.

Another motivation for model choice in the literature concerns the stability proofs of the observer and controller designs. These typically require an assumption on the external and unmodeled loads, either that they are constant in the NED- or the body-frame. Neither is 100% correct.

Next, the different models for $\boldsymbol{d}$ in (1c) are presented.

Residual load modeling. CDMs 1 and 2 capture the environment and unmodeled dynamics as a load vector assumed constant in the NED-frame and body-frame, respectively.

CDM 1 (NED-fixed):

$$\boldsymbol{d} := \boldsymbol{D}(\boldsymbol{\nu})\boldsymbol{\nu} - \boldsymbol{R}(\psi)^\top \boldsymbol{b}^n \tag{3a}$$

$$\dot{\boldsymbol{b}}^n = \boldsymbol{w}_b, \tag{3b}$$

where $\boldsymbol{b}^n \in \mathbb{R}^3$ is a NED-fixed bias load vector, $\boldsymbol{w}_b \in \mathbb{R}^3$ is white noise, and the damping matrix $\boldsymbol{D}(\boldsymbol{\nu})\boldsymbol{\nu}$ is given as

$$\boldsymbol{D}(\boldsymbol{\nu})\boldsymbol{\nu} := \boldsymbol{D}_L\boldsymbol{\nu} + \boldsymbol{D}_{NL}(\boldsymbol{\nu})\boldsymbol{\nu} \tag{4}$$

where $\boldsymbol{D}_L, \boldsymbol{D}_{NL}(\boldsymbol{\nu}) \in \mathbb{R}^{3\times3}$ are the linear and nonlinear damping matrices, respectively. The bias model (3b) is the common random walk model used in the literature; see for instance Kjerstad and Skjetne (2016). Another common version of (3b) is the Markov model (Sørensen, 2011). However, typically the time constant is very large, essentially making it a random walk model as in (3b).

CDM 2 (body-fixed):

$$\boldsymbol{d} := \boldsymbol{D}(\boldsymbol{\nu})\boldsymbol{\nu} - \boldsymbol{b}^b \tag{5a}$$

$$\dot{\boldsymbol{b}}^b = \boldsymbol{w}_b, \tag{5b}$$

where $\boldsymbol{b}^b \in \mathbb{R}^3$ is a body-fixed bias load vector. Since unmodeled dynamics and other load effects often are body-fixed, it makes good sense to include the bias $\boldsymbol{b}$ as a body-fixed vector. In addition, this model is typically used in linearized models; see for instance Fossen and Perez (2009) and Hassani, Pascoal, Aguiar, et al. (2012).

Current estimation. CDMs 3 and 4 are current models with ocean currents assumed constant in the NED-frame and the body-frame, respectively.

CDM 3 (NED-fixed):

$$\boldsymbol{d} := \boldsymbol{D}(\boldsymbol{\nu}_r)\boldsymbol{\nu}_r \tag{6a}$$

$$\dot{\boldsymbol{\nu}}_c^n = \boldsymbol{w}_c \tag{6b}$$

$$\boldsymbol{\nu}_r = \boldsymbol{\nu} - \boldsymbol{R}(\psi)^\top \begin{bmatrix} \boldsymbol{\nu}_c^n \\ 0 \end{bmatrix}, \tag{6c}$$

where $\boldsymbol{\nu}_c^n \in \mathbb{R}^2$ is an unknown NED-fixed current vector, and $\boldsymbol{w}_c \in \mathbb{R}^2$ is white noise.

CDM 4 (body-fixed):

$$\boldsymbol{d} := \boldsymbol{D}(\boldsymbol{\nu}_r)\boldsymbol{\nu}_r \tag{7a}$$

$$\dot{\boldsymbol{\nu}}_c^b = \boldsymbol{w}_c \tag{7b}$$

$$\boldsymbol{\nu}_r = \boldsymbol{\nu} - \begin{bmatrix} \boldsymbol{\nu}_c^b \\ 0 \end{bmatrix}, \tag{7c}$$

$\boldsymbol{\nu}_c^b \in \mathbb{R}^2$ is an unknown body-fixed current vector.

The different CDMs are summarized in Table 1.

Table 1
The control design models.

CDM	Description
1	Bias load model, NED-fixed
2	Bias load model, body-fixed
3	Current model, NED-fixed
4	Current model, body-fixed

2.3. Observer realizations

For all implementations, the models are discretized and discrete-time observers are used. The following continuous dynamics covers all models in this paper,

$$\dot{\boldsymbol{x}} = \boldsymbol{A}(t,\boldsymbol{x})\boldsymbol{x} + \boldsymbol{B}\boldsymbol{u} + \boldsymbol{E}\boldsymbol{w} \tag{8a}$$

$$\boldsymbol{y} = \boldsymbol{C}\boldsymbol{x} + \boldsymbol{v}, \tag{8b}$$

and the discretized system becomes

$$\boldsymbol{x}_k = \boldsymbol{f}_{k-1}(\boldsymbol{x}_{k-1}, t_{k-1}, \boldsymbol{u}_{k-1}, \boldsymbol{w}_{k-1}) \tag{9a}$$

$$= \boldsymbol{\Phi}_{k-1}(\boldsymbol{x}_{k-1}, t_{k-1})\boldsymbol{x}_{k-1} + \boldsymbol{\Delta}_{k-1}(\boldsymbol{x}_{k-1}, t_{k-1})\boldsymbol{u}_{k-1} + \boldsymbol{\Gamma}_{k-1}(\boldsymbol{x}_{k-1}, t_{k-1})\boldsymbol{w}_{k-1} \tag{9b}$$

$$\boldsymbol{y}_k = \boldsymbol{H}_k\boldsymbol{x}_k + \boldsymbol{v}_k \tag{9c}$$

$$\boldsymbol{w}_k \sim (\boldsymbol{0}, \boldsymbol{Q}_k) \tag{9d}$$

$$\boldsymbol{v}_k \sim (\boldsymbol{0}, \boldsymbol{R}_k), \tag{9e}$$

where, using Taylor expansion (Chen, 2009; Fossen, 2011) and sampling time $h = 0.1$ s gives

$$\boldsymbol{\Phi}_k = \mathrm{e}^{\boldsymbol{A}(t_k,\boldsymbol{x}_k)h} \approx \boldsymbol{I} + \boldsymbol{A}(t_k,\boldsymbol{x}_k)h + \frac{1}{2}(\boldsymbol{A}(t_k,\boldsymbol{x}_k)h)^2 \tag{10a}$$

$$\boldsymbol{\Delta}_k = \left(\int_0^h \mathrm{e}^{\boldsymbol{A}h}d\sigma\right)\boldsymbol{B} \approx \left(\boldsymbol{I}h + \frac{1}{2}\boldsymbol{A}(t_k,\boldsymbol{x}_k)h^2 + \frac{1}{6}\boldsymbol{A}(t_k,\boldsymbol{x}_k)^2h^3\right)\boldsymbol{B} \tag{10b}$$

$$\boldsymbol{\Gamma}_k = \left(\int_0^h \mathrm{e}^{\boldsymbol{A}(t_k,\boldsymbol{x}_k)h}d\sigma\right)\boldsymbol{E} \approx \left(\boldsymbol{I}h + \frac{1}{2}\boldsymbol{A}(t_k,\boldsymbol{x}_k)h^2 + \frac{1}{6}\boldsymbol{A}(t_k,\boldsymbol{x}_k)^2h^3\right)\boldsymbol{E} \tag{10c}$$

$$\boldsymbol{H}_k = \boldsymbol{C}. \tag{10d}$$

The goal is not to obtain the best and most accurate observer, but to have a fair comparison between the models and observers being investigated. Because of this, the sample time is set quite high to keep the run-time of the DFOs low.

Kalman filters

The Kalman filters have been implemented as in Simon (2006). The implementation for the LTV-KF and the EKF are given below, and the UKF implementation is shown in Appendix A.

- Initialization:

$$\hat{\boldsymbol{x}}_0^+ = E(\boldsymbol{x}_0) \tag{11a}$$

$$\boldsymbol{P}_{\boldsymbol{0}}^+ = E[(\boldsymbol{x}_0 - \hat{\boldsymbol{x}}_0^+)(\boldsymbol{x}_{\boldsymbol{0}} - \hat{\boldsymbol{x}}_0^+)^\top] \tag{11b}$$

- Kalman Filter equations LTV-KF and EKF (Simon, 2006):

$$\boldsymbol{P}_{\boldsymbol{k}}^- = \boldsymbol{F}_{\boldsymbol{k-1}}\boldsymbol{P}_{\boldsymbol{k-1}}^+\boldsymbol{F}_{\boldsymbol{k-1}}^\top + \boldsymbol{\Gamma}_{\boldsymbol{k-1}}\boldsymbol{Q}_{\boldsymbol{k-1}}\boldsymbol{\Gamma}_{\boldsymbol{k-1}}^\top \tag{12a}$$

$$\boldsymbol{K}_{\boldsymbol{k}} = \boldsymbol{P}_{\boldsymbol{k}}^-\boldsymbol{H}_{\boldsymbol{k}}^\top(\boldsymbol{H}_{\boldsymbol{k}}\boldsymbol{P}_{\boldsymbol{k}}^-\boldsymbol{H}_{\boldsymbol{k}}^\top + \boldsymbol{R}_{\boldsymbol{k}})^{-\boldsymbol{1}} \tag{12b}$$

$$\hat{\boldsymbol{x}}_{\boldsymbol{k}}^- = \boldsymbol{\Phi}_{\boldsymbol{k-1}}(t_{k-1})\hat{\boldsymbol{x}}_{\boldsymbol{k}}^+ + \boldsymbol{\Delta}_{\boldsymbol{k-1}}(t_{k-1})\boldsymbol{u}_{\boldsymbol{k-1}} \quad \text{(LTV-KF)} \tag{12c}$$

$$\hat{\boldsymbol{x}}_{\boldsymbol{k}}^- = \boldsymbol{f}_{\boldsymbol{k-1}}(\hat{\boldsymbol{x}}_{\boldsymbol{k-1}}^+, \boldsymbol{u}_{\boldsymbol{k-1}}) \quad \text{(EKF)} \tag{12d}$$

$$\hat{\boldsymbol{x}}_{\boldsymbol{k}^+} = \hat{\boldsymbol{x}}_{\boldsymbol{k}}^- + \boldsymbol{K}_{\boldsymbol{k}}(\boldsymbol{y}(k) - \boldsymbol{H}_{\boldsymbol{k}}\hat{\boldsymbol{x}}_{\boldsymbol{k}}^-) \tag{12e}$$

$$\boldsymbol{P}_{\boldsymbol{k}}^+ = (\boldsymbol{I} - \boldsymbol{K}_{\boldsymbol{k}}\boldsymbol{H}_{\boldsymbol{k}})\boldsymbol{P}_{\boldsymbol{k}}^-(\boldsymbol{I} - \boldsymbol{K}_{\boldsymbol{k}}\boldsymbol{H}_{\boldsymbol{k}})^\top + \boldsymbol{K}_{\boldsymbol{k}}\boldsymbol{R}_{\boldsymbol{k}}\boldsymbol{K}_{\boldsymbol{k}}^\top \tag{12f}$$

where $\boldsymbol{F}_{\boldsymbol{k}}$ is

$$\boldsymbol{F}_{k-1} = \boldsymbol{\Phi}_k(t_{k-1}) = \boldsymbol{\Phi}_{k-1}(\boldsymbol{\psi}_{k-1}^{\boldsymbol{m}}) \quad \text{(LTV-KF)}$$

$$\boldsymbol{F}_{k-1} = \frac{\partial \boldsymbol{f}_{k-1}}{\partial \boldsymbol{x}}\Big|_{\hat{\boldsymbol{x}}_{k-1}^+} \quad \text{(EKF)},$$

and $\boldsymbol{\psi}_{\boldsymbol{k}}^{\boldsymbol{m}}$ is the measured yaw angle at time step k.

2.4. Feedback control law

The controller $\boldsymbol{\tau}$ in (1c) has a feedforward and feedback component,

$$\boldsymbol{\tau} = \boldsymbol{\tau}_{FF} + \boldsymbol{\tau}_{FB}, \tag{13a}$$

where $\boldsymbol{\tau}_{FF}$ helps track the reference trajectory, and τ_{FB} is a PID (proportional–integral–derivative) tracking controller using state feedback,

$$\boldsymbol{\tau}_{FF} = \boldsymbol{D}\boldsymbol{\nu}_d(t) + \boldsymbol{M}\dot{\boldsymbol{\nu}}_d(t) \tag{13b}$$

$$\boldsymbol{\tau}_{FB} = -\boldsymbol{K}_{\boldsymbol{p}}\boldsymbol{R}(\psi)^\top(\hat{\boldsymbol{\eta}} - \boldsymbol{\eta}_d(t)) - \boldsymbol{K}_{\boldsymbol{d}}(\hat{\boldsymbol{\nu}} - \boldsymbol{\nu}_d(t)) - \boldsymbol{K}_{\boldsymbol{i}}\boldsymbol{R}(\psi)^\top\boldsymbol{\zeta} \tag{13c}$$

$$\dot{\boldsymbol{\zeta}} = \hat{\boldsymbol{\eta}} - \boldsymbol{\eta}_{\boldsymbol{d}}(t), \tag{13d}$$

where $\boldsymbol{\eta}_{\boldsymbol{d}}$, $\boldsymbol{\nu}_{\boldsymbol{d}}$, and $\dot{\boldsymbol{\nu}}_{\boldsymbol{d}(t)}$ are references generated by a guidance system and $\boldsymbol{K}_{\boldsymbol{p}}$, $\boldsymbol{K}_{\boldsymbol{d}}$ and $\boldsymbol{K}_{\boldsymbol{i}}$ are positive definite gain matrices, and $\hat{\boldsymbol{\eta}}$, $\hat{\boldsymbol{\nu}}$ are state estimates; for details see Sørensen (2013).

Remark 2. In a DP control law, the states $\hat{\boldsymbol{\eta}}$ and $\hat{\boldsymbol{\nu}}$ in (13) will be state estimates from the DP observer used in the loop. To generate the simulated dataset in this work, the LF state estimates $\hat{\boldsymbol{\eta}}$, $\hat{\boldsymbol{\nu}}$ from one well-tuned observer were used in the control law to track the reference trajectories. The different observers will then be tested and evaluated on this dataset. For the experimental data, the control input was given and the corresponding dataset will be used directly after some post-processing.

2.5. Derivative free optimization for comparison

To compare performance in the model and the observer investigation, optimization is used. A classic gradient decent-like method is not applicable, since information about the gradient, Hessian, or higher order derivatives are not available. Therefore, DFO is used.

The cost function used for the DFO in the paper is

$$J(\tilde{\boldsymbol{\eta}}, \tilde{\boldsymbol{\nu}}) = J_\eta(\tilde{\boldsymbol{\eta}}) + c_\nu J_\nu(\tilde{\boldsymbol{\nu}}) \tag{14a}$$

where

$$J_\eta(\tilde{\boldsymbol{\eta}}) = \sum_{k=0}^{n}(|\eta_{N,k} - \hat{\eta}_{N,k}| + |\eta_{E,k} - \hat{\eta}_{E,k}| + \frac{180}{\pi}|\psi_k - \hat{\psi}_k|) \tag{14b}$$

$$J_\nu(\tilde{\boldsymbol{\nu}}) = \sum_{k=0}^{n}(|u_k - \hat{u}_k| + |v_k - \hat{v}_k| + \frac{180}{\pi}|r_k - \hat{r}_k|). \tag{14c}$$

Here, $\tilde{\boldsymbol{\eta}} = \boldsymbol{\eta} - \boldsymbol{\eta}_{\boldsymbol{d}}$, $\tilde{\boldsymbol{\nu}} = \boldsymbol{\nu} - \boldsymbol{\nu}_{\boldsymbol{d}}$, $k = n$ is the final time step of the interval, and $c_\nu \in \mathbb{R}_{>0}$ is a scaling constant to weight the respective contributions from the estimation error in position and velocity. This scaling function is found iteratively and set such that the size of (14b) and (14c) are similar. Typical operating limits for DP is 3 m and 3 degrees (Veritas, 2011). The weighting in (14) is chosen to be close to this. In (14b), the cost on 1 m position error is chosen to be equivalent to 1 deg in heading. Similarly, 1 m/s error in linear velocity is equivalent to 1 deg/s angular velocity in (14c).

For a given dataset of n state, input, and output values according to the model (1), let $\boldsymbol{\mathcal{Y}} = \{\boldsymbol{y}_0, \boldsymbol{y}_1, \boldsymbol{y}_2, \dots, \boldsymbol{y}_n\}$ be the set of measurement data according to (1d), $\boldsymbol{\mathcal{U}} = \{\boldsymbol{u}_0, \boldsymbol{u}_1, \boldsymbol{u}_2, \dots, \boldsymbol{u}_n\}$ be the set of control input data according to (13), $\boldsymbol{\mathcal{H}} = \{\boldsymbol{\eta}_0, \boldsymbol{\eta}_1, \boldsymbol{\eta}_2, \dots, \boldsymbol{\eta}_n\}$ be the set of low-frequency position/heading data according to (1b), and $\boldsymbol{\mathcal{V}} = \{\boldsymbol{\nu}_0, \boldsymbol{\nu}_1, \boldsymbol{\nu}_2, \dots, \boldsymbol{\nu}_n\}$ be the set of low-frequency velocity data according to (1c). Let the selected observer algorithm be represented by the overall difference equation

$$\hat{\boldsymbol{X}}_{\boldsymbol{k}} = \boldsymbol{\Gamma}_{\boldsymbol{k-1}}(\hat{\boldsymbol{X}}_{\boldsymbol{k-1}}, \boldsymbol{u}_{\boldsymbol{k-1}}, \boldsymbol{y}_{\boldsymbol{k}}, \boldsymbol{K}) \tag{15}$$

where $\hat{\boldsymbol{X}}$ collects the overall state vector of the observer, and $\boldsymbol{K}$ represent the tunable observer gain vector. The optimization problem can then be formulated as

$$\underset{\boldsymbol{K}}{\text{minimize}} \qquad J(\tilde{\boldsymbol{\eta}}, \tilde{\boldsymbol{\nu}}) \tag{16a}$$

$$\text{subject to} \qquad \boldsymbol{y}_{\boldsymbol{k}} \in \boldsymbol{\mathcal{Y}}, \boldsymbol{u}_{\boldsymbol{k}} \in \boldsymbol{\mathcal{U}}, \boldsymbol{\eta}_{\boldsymbol{k}} \in \boldsymbol{\mathcal{H}}, \boldsymbol{\nu}_{\boldsymbol{k}} \in \boldsymbol{\mathcal{V}}, \text{ and (15)} \tag{16b}$$

with $J(\tilde{\boldsymbol{\eta}}, \tilde{\boldsymbol{\nu}})$ according to (14). Derivative-free optimization is then used to solve this optimization problem. For the high-fidelity simulation data, the data to evaluate the cost function are directly available from the simulation data. For the full-scale experimental data, on the other hand, the values used to evaluate the cost function (14) are the post-processed position/heading data, and from this the actual velocities are found by differentiating the resulting position/heading using a finite impulse response (FIR) filter.

2.6. Assumptions

For the linear LTV-KF, the heading angle in the rotation matrix is a measured signal. Thus $t \mapsto R(\psi(t))$ is seen as a measured time-varying signal $\hat{R}(t)$. The assumption according to Fossen and Strand (1999) is made:

(A1) $R(\psi + \psi_w) \approx R(\psi)$; that is, the heading angle due to wave-induced motion, ψ_w, is negligible, since the wave-induced heading angle is typically less than 1° for normal sea states and less than 5° for extreme sea states (Price & Bishop, 1974),

and by (A1), the matrix signal $\hat{R}(t)$ approximates the low-frequency rotation matrix, $R(\psi)$.

2.7. Problem objective

The objective is to quantitatively compare the performance of the LTV-KF, EKF, and UKF observer algorithms over the four different residual load models (CDM1–CDM4) on several realistic (simulated and experimental) datasets containing transient operating and environmental conditions. Additionally, the effect of including nonlinear damping on the observer performance shall be particularly analyzed. The intended outcome is to gain deeper insight on the differences in performance for the investigated observers and models.

3. Setup

3.1. DP simulation verification model

The SVM is a 6 DOF high-fidelity model of a platform supply vessel with the main parameters listed in Table 2. The model includes waves, Coriolis, centripetal loads, linear damping, and nonlinear damping. The benefit of this model is the use of lookup tables for environmental forces, creating realistic variations of the environmental loads with

Table 2
Simulation, platform supply vessel, main parameters.

Parameters	Value
Length between perp.	80 m
Breadth	17.4 m
Draft	5.6 m
Displacement	6150 tons

Table 3
R/V Gunnerus, main parameters.

Parameters	Value
Length over all	31.3 m
Length between perp.	28.9 m
Breadth middle	9.6 m
Draft	2.7 m
Dead weight	107 tons

vessel heading, allowing for a fair comparison of the different control design models. The sea state has a significant wave height of 6 m, with a peak frequency of 0.53 rad/s taken from the JONSWAP[1] spectrum. The mean incident wave heading is 190° (head waves) in the North/East frame (Price & Bishop, 1974). The current has an initial velocity of 0.5 m/s and direction of 160° (bow). The SVM has realistic noise on the sensors, and the measurements are discretely updated at 1 Hz for the GPS and 10 Hz for the compass. The control action is implemented in discrete time with an update rate of 1 Hz. In addition, a first order filter (with time constant 5 s) is included to account for the actuator dynamics.

For the SVM, the linear damping is known from the model. The nonlinear damping was identified through several maneuvers with no waves or current. Maneuvers with pure surge, pure sway, and pure yaw were used to find the diagonal terms, and a maneuver with coupled sway and yaw motion was then used to find the cross-terms. The damping was identified also using DFO as described in Section 2.5. For details about the mass and damping parameters for the SVM, see Appendix B.

3.2. AMOS DP research cruise 2016

R/V Gunnerus is a 31 m long NTNU-owned research vessel, shown in Fig. 1, with main parameters in Table 3. Experimental full-scale data of R/V Gunnerus was collected during the AMOS DP Research Cruise (ADPRC) 2016. Kongsberg Maritime made available a test interface in the onboard commercial DP system, for the NTNU researchers to test different control and observer algorithms in real time and to log all necessary data during the trials (Skjetne et al., 2017).

On the sea trials for ADPRC, the DP 4-corner maneuver shown in Fig. 2 was performed. The waves were negligible, but there were current and wind during the sea trials. Three datasets are used, where dataset 1 had a current of velocity 0.6 m/s with direction 170°, and wind velocity of 5 m/s and direction 150°. Datasets 2 and 3 had similar environmental conditions, with a current of velocity 0.3 m/s with direction 300°, and wind velocity of 6 m/s and direction 250°.

The damping identification for the experimental data followed almost the same procedure as described for the SVM in Section 3.1, except for the identification of the linear damping matrix. For the simulation model, the linear damping matrix was known from the model. However, for the experimental data, the linear damping matrix was first identified as a standalone linear damping matrix, that is, for the case where only linear damping was used in the observer. For the identification of the nonlinear damping, the linear damping matrix as identified above was fixed and the model was further fit to the nonlinear terms. Thus, the same linear damping matrix is used when nonlinear damping is included. This makes the experimental data case similar to that of the simulation data case study. For details about the mass and damping parameters for R/V Gunnerus, see Appendix C.

[1] Joint North Sea Wave Project.

3.3. Application of the DFO

The MATLAB® function *fminsearch* has been adopted to run the DFO optimization according to (16). The DFO searches the points around the current value of the tunable observer gain $\boldsymbol{K}$ to see if any values give a lower cost for $J(\tilde{\boldsymbol{\eta}}, \tilde{\boldsymbol{\nu}})$. However, the DFO does only provide a local minimum, so it is therefore important to run simulations with several different initial conditions.

When DFO is used to find the optimal tuning for the Kalman filters, the Q-matrices (process noise) are restricted to be diagonal, and so is the initial covariance matrix. The constraint that the Kalman filters must start with a diagonal covariance matrix is not optimal for performance, but is in practice necessary for finding the minimum of the DFO cost function within a reasonable time. If all non-diagonal terms are to be included in the DFO, the problem becomes too large to solve, especially since several initial conditions have to be tested.

3.4. DP test cases

Two test cases of different characteristics are used to compare the models and observers, as described next.

Dp 4-corner test

The maneuver here called *DP 4-corner* is a box maneuver as shown in Fig. 2, where the vessel starts at $\boldsymbol{\eta} = \mathrm{col}(0m, 0m, 0°)$ with the following setpoint changes:

1. $\boldsymbol{\eta} = \mathrm{col}(40\mathrm{m}, 0m, 0°)$ (pure surge motion)
2. $\boldsymbol{\eta} = \mathrm{col}(40m, -40m, 0°)$ (pure sway motion)
3. $\boldsymbol{\eta} = \mathrm{col}(40m, -40m, -45°)$ (pure rotation)
4. $\boldsymbol{\eta} = \mathrm{col}(0m, -40m, -45°)$ (coupled surge/sway)
5. $\boldsymbol{\eta} = \mathrm{col}(0m, 0m, 0°)$ (coupled, all DOFs)

For each setpoint change above, the vessel follows a reference filter trajectory.

Transient test

Especially when comparing the control design models, a lot of transients are beneficial to trigger the potential differences in the models. The vessel is exposed to current and waves, and there is a setpoint change in both North/East and heading, that is, a coupled maneuver with a transient due to the heading change. For the setpoint change, the vessel follows a reference filter trajectory. Shortly thereafter there is a current direction change of 60°, and a slight change in current velocity, to simulate an unknown transient event. These changes are filtered through a first order filter with time constant of 30 s. The time frame between the two transients is short, which is deliberate to have three transient bias events (including initialization) in a short maneuver. The reference filter trajectories are shown in Fig. 3. Note that the reference trajectories are intentionally made fast compared to the size of the vessel (as seen in Table 2).

4. Results and discussion

Three different Kalman filters are compared; LTV-KF, EKF, and UKF for the four different control design models presented in Section 2.2. In addition, results for including nonlinear damping versus only linear damping are shown for the EKF and UKF. Results from the simulation cases as well as the experimental data are presented, before overall conclusions on the different observers and models are provided.

The tuning of the observers was found through DFO. First, several initial conditions was used to find minimum tuning of the LTV-KF algorithm. Then, variations around the minimum tuning for the LTV-KF was used as initial conditions to search for the minimum tuning of the EKF and the UKF.

Fig. 1. The R/V Gunnerus. Photo: Helge Sunde/Samfoto.

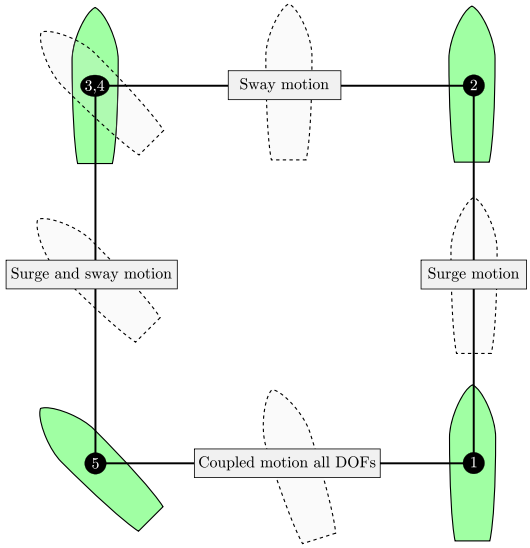

Fig. 2. The 4-corner DP test.

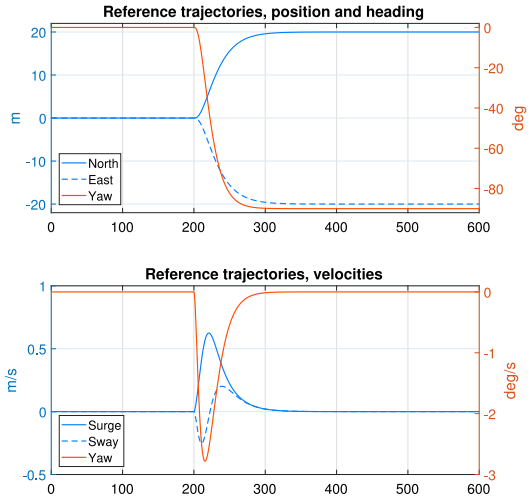

Fig. 3. Reference trajectories for the transient dataset.

4.1. Simulation results

For the simulation results, the high-fidelity model described in Section 3.1 was used with the transient dataset and the DP 4-corner dataset described in Section 3.4. At the beginning of the simulation, the position $\boldsymbol{\eta}$ and all observer states were initialized at zero, except the observer states for $\boldsymbol{\eta}_w$ from (1d) that was initialized at the measured position. The scaling factor in (14) was $c_v = 7$ for the simulation runs. The tuning was optimized for the transient dataset, and the same tuning was used for the DP 4-corner dataset. The environmental conditions in the two maneuvers were the same. Thus, by applying the tuning found through DFO for the transient dataset, the results for the DP 4-corner reveal how applicable the tuning was across the different maneuvers.

The results for the transient dataset are shown in Table 4 where the cost function $J(\tilde{\boldsymbol{\eta}}, \tilde{\boldsymbol{\nu}})$ from (14) is given for all the different combinations, and the results are normalized such that the worst performing $J(\tilde{\boldsymbol{\eta}}, \tilde{\boldsymbol{\nu}})$ has a score of 100. Fig. 4 shows time plots of how the cost function $J(\tilde{\boldsymbol{\eta}}, \tilde{\boldsymbol{\nu}})$ evolves for some of the CDM/observer combinations from Table 4. The plots show the best performing combination; the EKF using CDM 3 and nonlinear damping included, against the worst performing; the EKF using CDM 4 with only linear damping. Finally, the best performing LTV-KF version is plotted (using CDM 1). Note that the deviations mainly occur at the transients, that is, in the beginning, at 200 s, and at 400 s; see Section 3.4 for details about the transients.

From the results of the transient dataset, it is observed that the differences between the performance of the Kalman filters are small. The nonlinear damping significantly improves performance for CDMs 3 and 4, but only slightly for the CDMs 1 and 2. The differences between the CDMs are notable, but not significant.

The results for the DP 4-corner dataset are shown in Table 5, where it is observed that the differences between the observer algorithms are small also here. It is noted that the benefit of nonlinear damping is not as explicit as for the transient dataset. This is especially notable for CDMs 3 and 4. The differences between the four CDMs are smaller than for the transient dataset, and the best performing CDMs are different for the two datasets. That is true also when just linear damping is included.

For both the transient dataset and the DP 4-corner, the LTV-KF performs similarly to the EKF and UKF that use linear damping. In other words, there is no significant performance deterioration by using the measured yaw angle in the rotation matrix as a signal.

Table 4
Results on high fidelity simulation data: The transient dataset. The table shows the cost (14), where the results are normalized such that the worst performing J has a score of 100.

	EKF	UKF	LTV-KF	EKF(Lin.)	UKF(Lin.)
CDM 1	88.2	88.1	90.1	90.1	90.1
CDM 2	90.2	90.2	91.9	92.0	92.0
CDM 3	83.4	83.5	94.8	94.8	95.8
CDM 4	87.5	87.5	99.2	100.	100.

Table 5
Results on high fidelity simulation data: DP 4-corner dataset using the optimal tuning for the transient dataset. The table shows the cost (14), where the results are normalized such that the worst performing J has a score of 100.

	EKF	UKF	LTV-KF	EKF(Lin.)	UKF(Lin.)
CDM 1	94.9	94.9	97.0	96.9	96.9
CDM 2	100.	100.	98.0	98.0	98.0
CDM 3	91.8	91.8	92.4	92.4	92.4
CDM 4	90.5	90.5	91.9	92.0	92.0

4.2. Results from sea trials

The sea trial results are given for the three datasets described in Section 3.2, with the DP 4-corner test described in Section 3.4. The scaling factor in (14) was $c_v = 1.1$ for the experimental results. The resulting maneuver for dataset 1 is shown in Fig. 5. The tuning is optimized for dataset 1, and that tuning is thereafter applied for dataset 2 and dataset 3. This is to verify how well the tuning performs for maneuvers with different environmental conditions. Datasets 2 and 3 are performed in similar environmental conditions. The results are shown in Tables 6–8 for datasets 1, 2, and 3, respectively. The tables show the cost function $J(\tilde{\eta}, \tilde{\nu})$ from (14) where the results are normalized such that the worst performing J has a score of 100.

As found on the simulation data, the experimental results show that with the same CDM and damping matrix, the KFs have similar performance. This is a surprising results, especially considering that the UKF should be better at handling nonlinearities than the EKF. However, this indicates that the DP process is dominantly linear, and that using the measured heading angle in the rotation matrix may be sufficient. The three datasets did, however, contain a limited amount of environmental disturbances, since the weather conditions for the sea trials were very nice, and in such conditions the linear dynamics is even more dominant. However, dataset 1 does reveal a performance improvement using nonlinear damping. Note that the environmental conditions are similar for datasets 2 and 3.

CDMs 3 and 4 are good only if the EKF or UKF with nonlinear damping is used. Then a performance improvement over just using linear damping is observed. If linear damping (and bias) is used in the KFs, then the data supports using CDMs 1 or 2 (see Table 7).

4.3. Overall conclusions

The performance of the CDMs conclude somewhat differently for the high-fidelity simulation data versus the R/V Gunnerus full-scale data.

- For the simulation data, the EKF and UKF including nonlinear damping with CDM 3 perform the best for the transient dataset. The EKF and UKF including nonlinear damping with CDMs 3 and 4 perform the best for the 4-corner dataset.
- For the full-scale experimental datasets, CDM 1 performs the best. The performance is only slightly better for the EKF and UKF including nonlinear damping than the KFs with linear damping.
- If only using linear damping is considered for the simulation data, then the bias models (CDMs 1 and 2) perform best for the transient dataset, while the current models CDMs 3 and 4 are better for the 4-corner dataset.
- Including nonlinear damping gives a positive effect for the current models (CDMs 3 and 4), both for the simulation and experimental results. For the bias load models (CDM 1 and 2) the effect is negligible, and even slightly negative for CDM 2 on the 4-corner dataset on the simulation data.

Table 6
Experimental results for dataset 1. The table shows the cost (14), where the results are normalized such that the worst performing J has a score of 100.

	EKF	UKF	LTV-KF	EKF(Lin.)	UKF(Lin.)
CDM 1	90.8	90.8	91.1	91.0	91.0
CDM 2	91.9	91.9	92.2	92.2	92.2
CDM 3	93.2	93.2	100.	100.	100.
CDM 4	94.6	96.0	99.3	99.3	99.3

Table 7
Experimental results for dataset 2 using the optimal tuning for dataset 1. The table shows the cost (14), where the results are normalized such that the worst performing J has a score of 100.

	EKF	UKF	LTV-KF	EKF(Lin.)	UKF(Lin.)
CDM 1	97.5	97.4	97.5	97.5	97.5
CDM 2	99.0	99.0	99.0	99.0	99.0
CDM 3	96.9	96.9	100.	100.	100.
CDM 4	96.8	97.5	99.1	99.1	99.1

Table 8
Experimental results for dataset 3 using the optimal tuning for dataset 1. The table shows the cost (14), where the results are normalized such that the worst performing J has a score of 100.

	EKF	UKF	LTV-KF	EKF(Lin.)	UKF(Lin.)
CDM 1	96.4	96.4	96.8	96.8	96.8
CDM 2	97.0	97.0	97.4	97.4	97.4
CDM 3	97.6	97.6	100.	100.	100.
CDM 4	97.1	97.5	99.4	99.3	99.3

- In all test cases, the best performance is obtained by the EKF and/or UKF with nonlinear damping.

The fact that the current models perform better for the simulation data can be explained by richer environmental disturbances in the simulation, less uncertain and unmodeled dynamics, and vice versa for the experimental full-scale data.

Both the simulation and experimental data show that the different Kalman filters all performed similarly, showing that DP is dominantly a

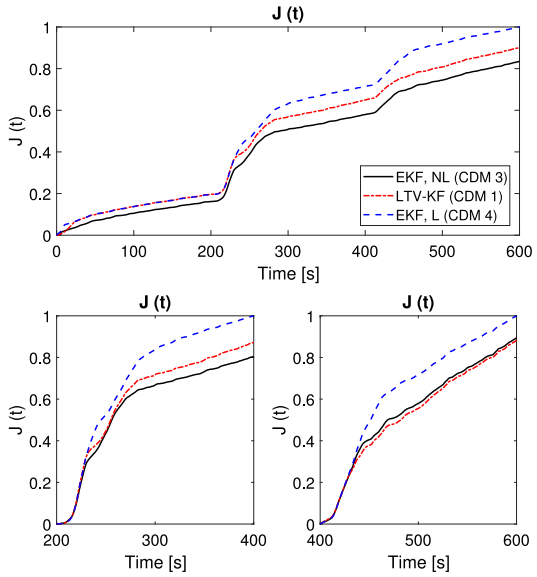

Fig. 4. Results from the simulation data using the transient dataset: The figures show the cost (14), where the results are normalized such that the worst performing J has a score of 1. In the figures, three of the combinations of observer algorithm and CDMs are shown. These are the EKF with CDM 3 and nonlinear damping (the best performing), the EKF with CDM 4 and linear damping (the worst performing), and the best performing version of the LTV-KF, that is, with CDM 1. The lower left plot starts at the setpoint change transient, and the lower right plot starts at the current direction transient; see Section 3.4 for details..

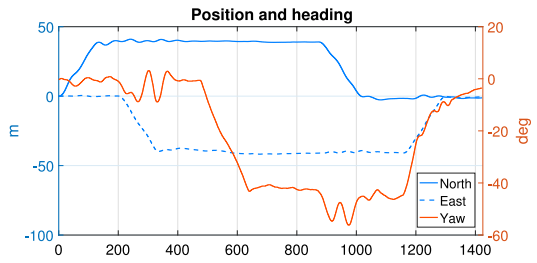

Fig. 5. Resulting position and heading for the experimental DP 4-corner test for dataset 1.

linear process. The nonlinear damping, however, gives a slight performance improvement. Both the simulation and experimental results show no significant performance deterioration when using the measured yaw angle in the rotation matrix with the LTV-KF instead of using the state estimate with the EKF/UKF. The LTV-KF performs similarly to the EKF and UKF when these use only linear damping.

Further work should put emphasis on the damping identification, especially for the experimental data. This could to a greater extent reveal what is achievable for the different control design models.

5. Conclusion

In this study different control design models and common Kalman filter algorithms for DP were compared for a high-fidelity simulation verification model of a supply vessel and for full-scale data from sea trials by R/V Gunnerus. In particular, the effect of including nonlinear damping in the observers was tested. The observer algorithms tested were the Linear Time-Varying Kalman Filter, the Extended Kalman Filter, and the Unscented Kalman Filter. The latter two were tested on both a linear damping model and a nonlinear damping model. The high-fidelity simulation data included waves, whereas the full-scale experimental data did not. The results indicated similar performance across the different design models and observers. The results justified that the DP process is dominantly linear, whereas a slight performance improvement can be obtained by using nonlinear damping (and consequently the EKF or UKF algorithms). However, the data from all the test cases did not show a clear indication of when to use the bias models, CDMs 1/2, over the current models, CDMs 3/4, or vice versa.

Acknowledgments

This work was supported by the Research Council of Norway (RCN) through the Center of Excellence "Autonomous Marine Operations and Systems" (NTNU AMOS), RCN project no. 223254.

The authors would like to thank the personnel from Kongsberg Maritime and the crew of R/V Gunnerus and for their help and support during the sea trials. A special thanks to Rune Skullestad and Øystein Lurås from Kongsberg Maritime for help with code implementation and the simulation platform to test the code. Also, the authors would like to thank the NTNU research team, Astrid H. Brodtkorb, Asgeir J. Sørensen, Mikkel E. N. Sørensen, Zhengru Ren, and Morten Breivik. Finally, MSc. Alexander Mykland deserves thanks for writing the test log. The authors would like to thank the anonymous reviewers for their constructive comments to improve the quality of this article.

Conflict of interest

None declared.

Appendix A. UKF-implementation

The implemented UKF is the discrete-time unscented Kalman Filter according to Simon (2006):

1. Discrete nonlinear system is given by

$$\boldsymbol{x}_{k+1} = \boldsymbol{f}(\boldsymbol{x}_k, \boldsymbol{u}_k, t_k) + \boldsymbol{\Gamma}(\boldsymbol{x}_k, t_k)\boldsymbol{w}_k \tag{17a}$$

$$\boldsymbol{y}_k = \boldsymbol{h}(\boldsymbol{x}_k, t_k) + \boldsymbol{v}_k \tag{17b}$$

$$\boldsymbol{w}_k \sim (0, \boldsymbol{Q}_k) \tag{17c}$$

$$\boldsymbol{v}_k \sim (0, \boldsymbol{R}_k), \tag{17d}$$

2. The UKF is initialized as

$$\hat{\boldsymbol{x}}_0^+ = E(\boldsymbol{x}_0) \tag{18a}$$

$$\boldsymbol{P}_0^+ = E[(\boldsymbol{x}_0 - \hat{\boldsymbol{x}}_0^+)(\boldsymbol{x}_0 - \hat{\boldsymbol{x}}_0^+)^\top] \tag{18b}$$

3. Time update equations:

$$\hat{\boldsymbol{x}}_{k-1} = \hat{\boldsymbol{x}}_{k-1}^+ + \tilde{\boldsymbol{x}}^{(i)}, \quad i = 1, \dots, 2n \tag{19a}$$

$$\tilde{\boldsymbol{x}}^{(i)} = \left(\sqrt{n\boldsymbol{P}_{k-1}^+}\right)_i^\top, \quad i = 1, \dots, n \tag{19b}$$

$$\tilde{\boldsymbol{x}}^{(n+i)} = -\left(\sqrt{n\boldsymbol{P}_{k-1}^+}\right)_i^\top, \quad i = 1, \dots, n \tag{19c}$$

$$\hat{\boldsymbol{x}}_k^{(i)} = \boldsymbol{f}(\hat{\boldsymbol{x}}_{k-1}^{(i)}, \boldsymbol{u}_k, t_k) \tag{19d}$$

$$\hat{\boldsymbol{x}}_k^- = \frac{1}{2n}\sum_{i=1}^{2n} \hat{\boldsymbol{x}}_k^{(i)} \tag{19e}$$

$$\boldsymbol{P}_k^- = \frac{1}{2n}\sum_{i=1}^{2n}\left(\hat{\boldsymbol{x}}_k^{(i)} - \hat{\boldsymbol{x}}_k^-\right)\left(\hat{\boldsymbol{x}}_k^{(i)} - \hat{\boldsymbol{x}}_k^-\right)^\top + \boldsymbol{\Gamma}(\boldsymbol{x}_k, t_k)\boldsymbol{Q}_{k-1}\boldsymbol{\Gamma}(\boldsymbol{x}_k, t_k)^\top \tag{19f}$$

Table 9
Mass and damping coefficients, control design model simulation verification model.

Coefficient	Value	Coefficient	Value
m_{11} [kg]	6 684 200	$Y_{\lvert v\rvert v}$ [$\frac{\text{kg}}{\text{m}}$]	−182 481
m_{22} [kg]	11 332 800	$Y_{\lvert r\rvert v}$ [$\frac{\text{kg}}{\text{rad}}$]	−1 922 557
m_{33} [$\frac{\text{kg m}^2}{\text{rad}}$]	3 193 127 000	$Y_{\lvert v\rvert r}$ [$\frac{\text{kg}}{\text{rad}}$]	−1 469 858
X_u [$\frac{\text{kg}}{\text{s}}$]	−167 105	$Y_{\lvert r\rvert r}$ [$\frac{\text{kg m}}{\text{rad}^2}$]	1 298 060
Y_v [$\frac{\text{kg}}{\text{s}}$]	−141 660	$N_{\lvert v\rvert v}$ [kg]	−702 742
Y_r [$\frac{\text{kg m}}{\text{rad s}}$]	650 440	$N_{\lvert r\rvert v}$ [$\frac{\text{kg m}}{\text{rad}}$]	2 383 317
N_v [$\frac{\text{kg m}}{\text{s}}$]	650 440	$N_{\lvert v\rvert r}$ [$\frac{\text{kg m}}{\text{rad}}$]	379 526
N_r [$\frac{\text{kg m}^2}{\text{rad s}}$]	−63 862 540	$N_{\lvert r\rvert r}$ [$\frac{\text{kg m}^2}{\text{rad}^2}$]	−10 683 000
$X_{\lvert u\rvert u}$ [$\frac{\text{kg}}{\text{m}}$]	−14 778	–	–

Table 10
Mass and damping coefficients, control design model R/V Gunnerus.

Coefficient	Value	Coefficient	Value
m_{11} [kg]	788 900	$Y_{\lvert v\rvert v}$ [$\frac{\text{kg}}{\text{m}}$]	−12 212
m_{22} [kg]	924 500	$Y_{\lvert r\rvert v}$ [$\frac{\text{kg}}{\text{rad}}$]	−131 673
m_{33} [$\frac{\text{kg m}^2}{\text{rad}}$]	51 240 000	$Y_{\lvert v\rvert r}$ [$\frac{\text{kg}}{\text{rad}}$]	2 224 318
X_u [$\frac{\text{kg}}{\text{s}}$]	−4949	$Y_{\lvert r\rvert r}$ [$\frac{\text{kg m}}{\text{rad}^2}$]	1 234 186
Y_v [$\frac{\text{kg}}{\text{s}}$]	−34 890	$N_{\lvert v\rvert v}$ [kg]	−163 526
Y_r [$\frac{\text{kg m}}{\text{rad s}}$]	−1 292 126	$N_{\lvert r\rvert v}$ [$\frac{\text{kg m}}{\text{rad}}$]	3 568 858
N_v [$\frac{\text{kg m}}{\text{s}}$]	−1 292 126	$N_{\lvert v\rvert r}$ [$\frac{\text{kg m}}{\text{rad}}$]	−6 564 338
N_r [$\frac{\text{kg m}^2}{\text{rad s}}$]	−66 285 641	$N_{\lvert r\rvert r}$ [$\frac{\text{kg m}^2}{\text{rad}^2}$]	0
$X_{\lvert u\rvert u}$ [$\frac{\text{kg}}{\text{m}}$]	−2275	–	–

4. Measurement update equations:

$$\hat{\boldsymbol{x}}_k = \hat{\boldsymbol{x}}_k^- + \tilde{\boldsymbol{x}}^{(i)}, \quad i = 1, \dots, 2n \tag{20a}$$

$$\tilde{\boldsymbol{x}}^{(i)} = \left(\sqrt{n\boldsymbol{P}_{k-1}^+}\right)_i^\top, \quad i = 1, \dots, n \tag{20b}$$

$$\tilde{\boldsymbol{x}}^{(n+i)} = -\left(\sqrt{n\boldsymbol{P}_{k-1}^+}\right)_i^\top, \quad i = 1, \dots, n \tag{20c}$$

$$\hat{\boldsymbol{y}}_k^{(i)} = \boldsymbol{h}(\hat{\boldsymbol{x}}_k^{(i)}, t_k) \tag{20d}$$

$$\hat{\boldsymbol{y}}_k = \frac{1}{2n}\sum_{i=1}^{2n} \hat{\boldsymbol{y}}_k^{(i)} \tag{20e}$$

$$\boldsymbol{P}_{\boldsymbol{y}} = \frac{1}{2n}\sum_{i=1}^{2n} \left(\hat{\boldsymbol{y}}_k^{(i)} - \hat{\boldsymbol{y}}_k\right)\left(\hat{\boldsymbol{y}}_k^{(i)} - \hat{\boldsymbol{y}}_k\right)^\top + \boldsymbol{R}_k \tag{20f}$$

$$\boldsymbol{P}_{\boldsymbol{xy}} = \frac{1}{2n}\sum_{i=1}^{2n} \left(\hat{\boldsymbol{x}}_k^{(i)} - \hat{\boldsymbol{x}}_k^-\right)\left(\hat{\boldsymbol{y}}_k^{(i)} - \hat{\boldsymbol{y}}_k\right)^\top \tag{20g}$$

$$\boldsymbol{K}_k = \boldsymbol{P}_{\boldsymbol{xy}}\boldsymbol{P}_{\boldsymbol{y}}^{-1} \tag{20h}$$

$$\hat{\boldsymbol{x}}_k^+ = \hat{\boldsymbol{x}}_k^- + \boldsymbol{K}_k(\boldsymbol{y}_k - \hat{\boldsymbol{y}}_k) \tag{20i}$$

$$\boldsymbol{P}_k^+ = \boldsymbol{P}_k^- - \boldsymbol{K}_k\boldsymbol{P}_{\boldsymbol{y}}\boldsymbol{K}_k^\top. \tag{20j}$$

Appendix B. Control design model for the simulation verification model

The simulation verification model is a 6 DOF model of a supply ship, and is part of the MCSim repository based on the MSS GNC toolbox (Fossen & Perez, 2004). For its corresponding 3 DOF control design model, the linear damping and mass matrix are known from the simulation model, whereas the nonlinear damping matrix is identified as discussed in Section 4. The matrices are given below and the parameter values are given in Table 9.

$$\boldsymbol{M} = \text{diag}\{m_{11}, m_{22}, m_{33}\} \tag{21}$$

$$\boldsymbol{D}_L = \begin{bmatrix} -X_u & 0 & 0 \\ 0 & -Y_v & -Y_r \\ 0 & -N_v & -N_r \end{bmatrix} \tag{22}$$

$$\boldsymbol{D}_{NL}(\nu_r) = \begin{bmatrix} d_{11} & 0 & 0 \\ 0 & d_{22} & d_{23} \\ 0 & d_{32} & d_{33} \end{bmatrix}, \tag{23}$$

where $d_{11} = -X_{\lvert u\rvert u}\lvert u_r\rvert$, $d_{22} = -Y_{\lvert v\rvert v}\lvert v_r\rvert - Y_{\lvert r\rvert v}\lvert r\rvert$, $d_{23} = -Y_{\lvert v\rvert r}\lvert v_r\rvert - Y_{\lvert r\rvert r}\lvert r\rvert$, $d_{32} = -N_{\lvert v\rvert v}\lvert v_r\rvert - N_{\lvert r\rvert v}\lvert r\rvert$, $d_{33} = -N_{\lvert v\rvert r}\lvert v_r\rvert - N_{\lvert r\rvert r}\lvert r\rvert$.

Appendix C. R/V Gunnerus control design model

For the NTNU-owned vessel R/V Gunnerus, observers are tested on real data captured during DP operations at the AMOS DP Research Cruise 2016 (Skjetne et al., 2017). In the observers, the mass matrix applied has been calculated using ShipX VeRes (MARINTEK, 0000), whereas the damping matrices are identified as discussed in Section 4. The matrices are given below and the parameter values are given in Table 10.

$$\boldsymbol{M} = \text{diag}\{m_{11}, m_{22}, m_{33}\} \tag{24}$$

$$\boldsymbol{D}_L = \begin{bmatrix} -X_u & 0 & 0 \\ 0 & -Y_v & -Y_r \\ 0 & -N_v & -N_r \end{bmatrix} \tag{25}$$

$$\boldsymbol{D}_{NL}(\nu_r) = \begin{bmatrix} d_{11} & 0 & 0 \\ 0 & d_{22} & d_{23} \\ 0 & d_{32} & d_{33} \end{bmatrix}, \tag{26}$$

where $d_{11} = -X_{\lvert u\rvert u}\lvert u_r\rvert$, $d_{22} = -Y_{\lvert v\rvert v}\lvert v_r\rvert - Y_{\lvert r\rvert v}\lvert r\rvert$, $d_{23} = -Y_{\lvert v\rvert r}\lvert v_r\rvert - Y_{\lvert r\rvert r}\lvert r\rvert$, $d_{32} = -N_{\lvert v\rvert v}\lvert v_r\rvert - N_{\lvert r\rvert v}\lvert r\rvert$, $d_{33} = -N_{\lvert v\rvert r}\lvert v_r\rvert - N_{\lvert r\rvert r}\lvert r\rvert$.

$N_{\lvert r\rvert r}$ is zero because the identification results provided slightly negative and slightly positive values for the coefficient (for different data series). Therefore, it was set to zero.

References

Balchen, J. G., Jenssen, N. A., & Sælid, S. (1976). Dynamic positioning using Kalman filtering and optimal control theory. In *IFAC/IFIP symposium on automation in offshore oil field operation, Vol. 183* (p. 186).

Candeloro, M., Sørensen, A. J., Longhi, S., & Dukan, F. (2012). Observers for dynamic positioning of ROVs with experimental results. In *Proceedings of the IFAC conference on manoeuvring and control of marine craft 2012, Vol. 45(27)* (pp. 85–90).

Chen, C. -T. (2009). *Linear system theory and design* (3rd ed.). Oxford University Press, Inc..

Fossen, T. I. (2011). *Handbook of marine craft hydrodynamics and motion control*. John Wiley & Sons.

Fossen, T. I., & Perez, T. (2004). Marine Systems Simulator (MSS), https://github.com/cybergalactic/MSS Accessed: 2017-02-24.

Fossen, T. I., & Perez, T. (2009). Kalman filtering for positioning and heading control of ships and offshore rigs. *IEEE Control Systems*, *29*(6), 32–46.

Fossen, T. I., & Strand, J. P. (1999). Passive nonlinear observer design for ships using Lyapunov methods: full-scale experiments with a supply vessel. *Automatica*, *35*(1), 3–16.

Fung, P., & Grimble, M. (1983). Dynamic ship positioning using a self-tuning Kalman filter. *IEEE Transactions on Automatic Control*, *28*(3), 339–350.

Grimble, M. J., Patton, R., & Wise, D. (1980). Use of kalman filtering techniques in dynamic ship-positioning systems. In *IEE proceedings D-control theory and applications, Vol. 127* (p. 93). IET.

Hassani, V., Pascoal, A. M., Aguiar, A. P., et al. (2012). Multiple model adaptive wave filtering for dynamic positioning of marine vessels. In *American control conference (ACC), Vol. 2012* (pp. 6222–6228). IEEE.

Kjerstad, Ø. K., & Skjetne, R. (2016). Disturbance rejection by acceleration feedforward for marine surface vessels. *IEEE Access*, *4*, 2656–2669.

Loria, A., Fossen, T. I., & Panteley, E. (2000). A separation principle for dynamic positioning of ships: Theoretical and experimental results. *IEEE Transactions on Control Systems Technology*, *8*(2), 332–343.

MARINTEK (n.d.) ShipX VeRes, https://www.sintef.no/en/software/shipx/ Accessed: 2018-04-18.

Price, W. G., & Bishop, R. E. D. (1974). *Probabilistic theory of ship dynamics*. Halsted Press.

Refsnes, J. E. G. (2007). *Nonlinear model-based control of slender body AUVs* (PhD thesis), Norwegian University of Science and Technology, Trondheim, Norway.

Refsnes, J. E., & Sørensen, A. J. (2007). Comparison of two observers for marine vessels in ocean current. In *Proceedings of the IFAC conference on control applications in marine systems 2007, Vol. 40(17)* (pp. 32–37). Elsevier.

Saelid, S., Jenssen, N., & Balchen, J. (1983). Design and analysis of a dynamic positioning system based on Kalman filtering and optimal control. *IEEE Transactions on Automatic Control*, *28*(3), 331–339.

Simon, D. (2006). *Optimal state estimation: Kalman, H infinity, and nonlinear approaches*. John Wiley & Sons.

Skjetne, R., Sørensen, M. E. N., Breivik, M., Værnø, S. A., Brodtkorb, A. H., & Sørensen, A. J. (2017). AMOS DP Research cruise 2016: Academic full-scale testing of experimental dynamic positioning control algorithms onboard R/V Gunner us. In *ASME 2017 36th international conference on ocean, offshore and arctic engineering*. American Society of Mechanical Engineers.

Sørensen, A. J. (2011). A survey of dynamic positioning control systems. *Annual Reviews Control*, *35*(1), 123–136.

Sørensen, A. J. (2013). *Marine control systems - lecture notes*. Department of Marine Technology, Norwegian Univ. of Sci. and Tech..

Tannuri, E., & Morishita, H. (2006). Experimental and numerical evaluation of a typical dynamic positioning system. *Applied Ocean Research*, *28*(2), 133–146.

Veritas, D. N. (2011). Dynamic Positioning Systems-Operation Guidance.

J.2

Time-varying Model-based Observer for Marine Surface Vessels in Dynamic Positioning

---

Værnø, S. A., Brodtkorb, A. H., Skjetne, R., Calabrò, V.

IEEE Access
Multidisciplinary ⋮ Rapid Review ⋮ Open Access Journal

Received July 5, 2017, accepted July 13, 2017, date of publication July 26, 2017, date of current version August 14, 2017.

Digital Object Identifier 10.1109/ACCESS.2017.2731998

Time-Varying Model-Based Observer for Marine Surface Vessels in Dynamic Positioning

SVENN ARE VÆRNØ[1], ASTRID H. BRODTKORB[1], ROGER SKJETNE[1], AND VINCENZO CALABRÒ[2], (Member, IEEE)

[1]Centre of Autonomous Marine Operations and Systems, Department of Marine Technology, Norwegian University of Science and Technology, 7491 Trondheim, Norway
[2]Kongsberg Maritime AS, 3616 Kongsberg, Norway

Corresponding author: Svenn Are Værnø (svenn.are.varno@ntnu.no)

This work was supported in part by the Research Council of Norway, through the Centre of Excellence NTNU AMOS, under Project 223254, and through the Centre for Research-based Innovation MOVE, under Project 237929.

ABSTRACT This paper deals with the problem of transient events in model-based observers for dynamic positioning of marine surface vessels. Traditionally, model-based observers experience a deterioration of performance during transients, and there is a give or take relationship between transient and steady state performance. To remedy this problem, we propose to use time-varying gains for a model-based observer. The gains are aggressive during transients to improve transient performance, and relaxed in steady state to lower the oscillations of the estimates. The proposed observer is analyzed with regard to stability. Its performance is verified in both a high-fidelity simulation model, and on experimental data with the research vessel (R/V) Gunnerus. In addition, a partial closed-loop validation with R/V Gunnerus has been performed.

INDEX TERMS Dynamic positioning, Marine control systems, Observers.

I. INTRODUCTION

A dynamically positioned (DP) vessel means a unit or a vessel which automatically maintains its position (fixed location or predetermined track) exclusively by means of thruster force [1]. As dynamic positioning operations are moving into harsher conditions or doing more complex operations, better transient performance of the DP system is required. A bias term is used as integral action to model slowly-varying environmental loads and unmodeled dynamics, and for good model-based observer performance it is important to estimate this bias accurately. Integral action is typically based on the assumption that this bias is constant. The bias load is, however, slowly-varying in steady state, but can vary rapidly in transient events. A major obstacle in transient performance of DP is how to handle rapid changes in this bias load.

In model-based observers for DP, the environmental loads are typically modeled as a constant force vector in the North-East-Down-frame (NED), that is, the following kinetic equation is typically used, $M\dot{\nu} = -D\nu + R(\psi)^\top b + \tau$, where b is this constant load (bias) vector in the NED-frame and R(·) is a rotation matrix mapping into the body-frame of the vessel; see Section II-A for more details about the modeling, as well as [2], [3]. There are instances when the bias loads change significantly over a short time period, where this assumption does not hold. In Figure 1 we investigate, as an example, how the current and wave drift loads vary in the NED-frame over a heading change. The figure shows a high-fidelity simulation of a surface vessel performing two maneuvers; first, a position setpoint change, and afterwards, a combined setpoint change of position and heading. In the top plot of Figure 1 the low-frequency North position and heading angle are shown. In the bottom plot the combined current and wave-drift loads are shown in North and yaw. We observe that the loads experienced by the vessel in the NED-frame changes significantly, even though the current and wave parameters are constant in the NED-frame. This is because the forces experienced by the vessel vary due to ship hull geometry, which is not accounted for in the simple (but effective) bias model. Consequently, for some time after a transient event, the bias load estimate of a model-based observer will be off, leading to poor velocity and position estimates. This example clearly illustrates that if the vessel changes heading, the common slowly-varying assumption of the bias model in the NED-frame does not apply in transients; see also [4] for a discussion on this for AUVs (Autonomous Underwater Vehicles) exposed to currents. Other common occurrences of rapid bias load changes include wave trains, rotational currents, sea-ice loads, or during mode changes in the operation of the DP system.

Even with the knowledge that the slowly-varying bias assumption is not good in transients, it is difficult to device better ways of handling this. One non-model based option

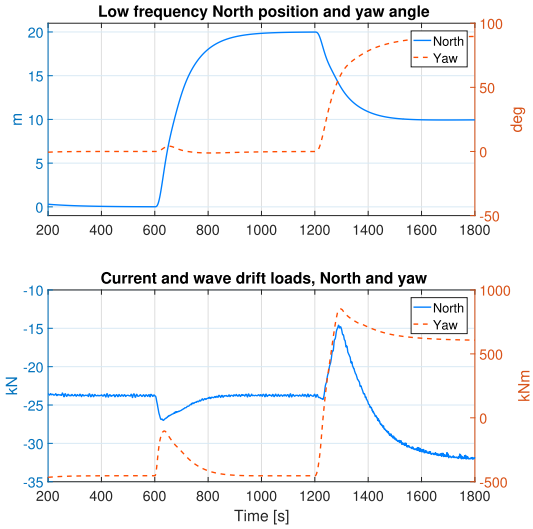

FIGURE 1. Low-frequency North position and heading angle (top), and current and wave-drift loads in North and yaw experienced by the vessel (bottom).

is to measure accelerations to estimate the forces in a direct fashion as suggested in [5]. Another option that does not require more instrumentation is to use a more complex model of the hydrodynamic loads, but this would also give a more complex control algorithm that could be more difficult to parameterize and analyze with respect to stability. Moreover, depending on the type of environment, there will always be uncertainty in such models.

There exists other time-varying observer schemes for DP in the literature. See for instance [6], where an inertial observer for DP is proposed that uses time-varying gains to improve convergence and suppress sensor noise. In [7] and [8] a wave encounter frequency observer is proposed, where time-varying gains are used in an adaption law, and in [9] hybrid gains are used in integral action for DP.

The main contribution of this paper is to construct a model-based observer with time-varying gains that performs well in transients as well as in steady state. In state-of-the-art fixed gain model-based observer design for DP [2], there is a tradeoff in tuning the observer for either good steady state performance or good transient performance, and in commercial systems there are typically three gain settings; low, medium, and high, which the DP operator can select from. As an extension of the observer design from [10], we propose in this paper to use time-varying bias and velocity injection gains. The paper includes a comprehensive analysis and thorough selection of gains, and an observer verification based on experimental data. Another contribution is a full-scale closed-loop validation of the observer when conducting a DP experiment on the AMOS DP Research Cruise 2016 [11]. Demonstration of the observer performance through full-scale closed-loop experiments on an academic research cruise is, to the author's knowledge, not done before.

Notation and Terminology: In UGES, G stands for Global, U for uniform, E for exponential, and S for Stable. The smallest and largest eigenvalues of a matrix $A \in \mathbb{R}^{n\times n}$ is $\lambda_{min}(A)$ and $\lambda_{max}(A)$, respectively, and $\mathbb{R}_{>0}$ denotes positive real numbers. The $\mathcal{L}_\infty$ signal norm is $\|x\|_\infty = \text{ess sup}\{|x(t)| : t \geq 0\}$.

II. PROBLEM FORMULATION

In the following we separate between the *simulation model*, which is a high-fidelity model used for control and observer verification, and the *control design model*, which is a simplified model intended for control and observer design. The control design model typically only includes the parts relevant for the operational regime of the observer or controller. For low-speed applications such as DP, this implies that the Coriolis and centripetal forces are neglected, and the nonlinear damping is typically neglected as well. See [3], and [2] for DP modeling details, and [12], [13], [14] for other insightful DP literature.

Two reference frames are used: The North-East-Down frame (NED) is a local Earth-fixed frame assumed non-rotating, with x-axis pointing North, y-axis pointing East, and z-axis pointing down to the center of the Earth. The body-frame is a local frame, centered along the center line and in the water plane of the vessel. The x-axis points in the direction of the the bow, y-axis starboard, and z-axis down.

A. CONTROL DESIGN MODEL

The control design model is a 3 degree of freedom (DOF) model,

$$\dot{\xi} = A_w\xi + E_w w_w \tag{1a}$$
$$\dot{\eta} = R(\psi)\nu \tag{1b}$$
$$\dot{b} = -T_b^{-1}b + w_b \tag{1c}$$
$$M\dot{\nu} = -D\nu + R(\psi)^\top b + \tau \tag{1d}$$
$$y = \eta + C_w\xi + v_y, \tag{1e}$$

where there is a separation between the first order wave-induced motion in (1a) and the low-frequency motion of the vessel in (1b) - (1d) [2]. When controlling the vessel, we are typically only interested in the low-frequency part of the motion. Controlling the total motion causes extra wear and tear on the thrusters, and in most cases it is not possible to counteract the first order wave-induced motion. The wave-induced motion $\xi \in \mathbb{R}^5 \times \mathbb{S}^1$ is modeled by a second order mass-spring-damper model, where A_w is a Hurwitz matrix that contains the peak frequency of the sea state and the damping ratio of the wave motion model, $w_w \in \mathbb{R}^3$ is zero mean white noise, and $E_w = \begin{bmatrix}0_{3\times3} & I_{3\times3}\end{bmatrix}^\top$. The vector $\eta := \text{col}\,(\eta_N, \eta_E, \psi) \in \mathbb{R}^2 \times \mathbb{S}$ contains the low-frequency North/East position and heading angle of the vessel, and the bias load $b := \text{col}\,(b_N, b_E, b_\psi) \in \mathbb{R}^3$ is a NED-fixed vector that contains the slowly-varying loads affecting the vessel due to wave drift, mean and slowly-varying currents, mean wind

loads, as well as unmodeled dynamics from inaccurate mass and added mass, unmodeled hydrodynamic effects, and errors in thrust modeling. The bias load dynamics are modeled by a Markov process, where T_b is a diagonal matrix of time constants, and $w_b \in \mathbb{R}^3$ is the white noise vector [2]. The vector $\nu = \text{col}\,(u, v, r) \in \mathbb{R}^3$ contains the low-frequency surge/sway velocity and yaw rate in the body frame of the vessel, $M \in \mathbb{R}^{3\times3}$ and $D \in \mathbb{R}^{3\times3}$ are the mass (inertia and added mass) and linear damping matrices, respectively. $\tau \in \mathbb{R}^3$ is the control vector. The measurement vector $y \in \mathbb{R}^3$ is a sum of the low-frequency North/East position and heading η, and the wave frequency North/East and heading $C_\omega \xi$, where $C_\omega = \begin{bmatrix}0_{3\times3} & I_{3\times3}\end{bmatrix}$, and the measurement noise vector $v_y \in \mathbb{R}^3$. The rotation matrix $R(\psi)$ rotates a 3 DOF vector from the body to the NED frame. It satisfies $R(\psi)R(\psi)^\top = I$ and $\det(R(\psi)) = 1$, and its time derivative is $\dot{R} = R(\psi)Sr$, where

$$R(\psi) = \begin{bmatrix}\cos(\psi) & -\sin(\psi) & 0\\ \sin(\psi) & \cos(\psi) & 0\\ 0 & 0 & 1\end{bmatrix},$$
$$S = \begin{bmatrix}0 & -1 & 0\\ 1 & 0 & 0\\ 0 & 0 & 0\end{bmatrix}; \tag{2}$$

see [2] and [15] for details.

B. ASSUMPTIONS

Since the wave-induced heading angle is typically less than 1° for normal sea states and less than 5° for extreme sea states, we assume as in [16] that:

(A1) $R(\psi + \psi_w) \approx R(\psi)$, that is, the heading angle due to wave-induced motion, ψ_w, is small.

We also make the following assumptions:

(A2) The added mass part of M and the wave-induced damping of D are set to the values when the wave frequency approaches infinity, and therefore they are constant. In addition, starboard/port symmetry is assumed, $M = M^\top > 0$, and that the damping matrix satisfies $D + D^\top > 0$.

(A3) $w_w = w_b = 0$. Since the presented observers are deterministic, both the wave and the bias estimates in the observers are driven by the estimation error [16].

(A4) In the stability analysis, no measurement noise is considered, $v_y = 0$. However, simulation and experimental data include it.

The last two assumptions are common for a deterministic observer design, but in practice we will see that the resulting observer has good filtering properties of these noise inputs.

C. PROBLEM STATEMENT

We consider the case where the bias b is constant or slowly varying in long periods of time, but then sporadically experiences rapid changes due to some transient condition. The problem is thus to design an observer for (1) that accurately estimates the states during both steady and transient conditions. The performance of the observer shall be compared to a conventional design basis through a performance index.

III. OBSERVER DESIGN

The proposed observer is based upon the "nonlinear passive observer" initially presented in [16]. Time-varying injection gains for the velocity and the bias dynamics are proposed to capture slowly-varying dynamics in steady state, and fast dynamics during transients. The observer is designed by copying the control design model (1) and adding injection terms, that is,

$$\dot{\hat{\xi}} = A_w\hat{\xi} + K_1\tilde{y} \tag{3a}$$
$$\dot{\hat{\eta}} = R(\psi)\hat{\nu} + K_2\tilde{y} \tag{3b}$$
$$\dot{\hat{b}} = -T_b^{-1}\hat{b} + K_3(t)\tilde{y} \tag{3c}$$
$$M\dot{\hat{\nu}} = -D\hat{\nu} + R(\psi)^\top\hat{b} + \tau + K_4(t)R(\psi)^\top\tilde{y} \tag{3d}$$
$$\hat{y} = \hat{\eta} + C_w\hat{\xi}, \tag{3e}$$

where $\hat{\xi} \in \mathbb{R}^5 \times \mathbb{S}^1$, $\hat{\eta} \in \mathbb{R}^2 \times \mathbb{S}$, $\hat{b} \in \mathbb{R}^3$, and $\hat{\nu} \in \mathbb{R}^3$ are the state estimates, $K_1 \in \mathbb{R}^{6\times3}$, K_2, $K_3(t)$, $K_4(t) \in \mathbb{R}^{3\times3}$ are non-negative gain matrices, and $\tilde{y} = y - \hat{y}$ is the measurement error. The gains K_1 and K_2 depend on the peak frequency of the wave spectrum as in [16]. The observer in (3) was preliminarily presented in [10] with only $K_3(t)$ varying with time. Further analysis shows that an appropriate choice of values for K_3 and K_4 are important for good transient observer performance, so here a scheme for time-varying K_3 and K_4 is proposed.

As discussed in Section I, the transient changes of the bias load experienced by the vessel pose challenges for the model-based observer in (3). To illustrate this, consider the following case: When the vessel is pushed off setpoint due to a rapid external load b, the DP controller will try to decelerate and stop the movement, and bring the vessel back to setpoint. The observer has information about this control action τ and position deviation $\tilde{y}$, whereas the bias observer state $\hat{b}$ underestimates the actual bias load. While the position deviation is helpful for the observer, the control action's "push back" to position is seen as an indication that the vessel is moving in the direction of the control action, which initially is opposite of the actual motion of the vessel. Therefore, including feedback control action deteriorates the observer performance in the initial phase of a transient.

Therefore, in order to achieve good transient observer performance, the injection gain $K_4(t)$ in the velocity dynamics (3d) must be high enough to dominate the feedback control action. In addition, the injection gain $K_3(t)$ in (3c) must be high enough in order for the bias estimate to more accurately track the bias load value during the transient. Keeping these gains high all the time will, however, result in oscillatory estimates of the bias and velocity in steady state.

$K_3(t)$ and $K_4(t)$ are proposed to stay within the range

$$K_i(t) \in [K_{i,min}, K_{i,max}], \quad i = 3, 4\ \forall t \geq t_0.$$

The values of $K_{i,max}$ should be set such that they give a good transient performance of the observer, and $K_{i,min}$ such that the observer performs well in steady state. The steady state tuning is purposely set low, providing calmer estimates to the controller, as is normal tuning practice for conventional DP observers. The time-varying gains should react quickly to transient events by approaching their maximum values rapidly.

The equation for $K_3(t)$ and $K_4(t)$ is thus proposed as

$$K_i(t) = \kappa(t)K_{i,max} + (1-\kappa(t))K_{i,min}, \quad i = 3, 4, \tag{4}$$

where $\kappa(t) \in [0, 1]$, $\forall t \geq 0$. Whenever there is a transient event, κ should approach 1, and whenever the vessel is in steady state, κ should stay close to 0.

Three transient events are considered. The first is an operator-executed heading change, which is easily detected through the desired yaw rate from the guidance system. The second is a change in the environmental disturbances. This is detected through a deterioration of the observer performance. The final transient is the error due to initialization of the observer. The proposed dynamics for κ is

$$\kappa(t) = \max\{0, \beta(t) - 1\}\} \tag{5a}$$
$$\beta(t) = \min\{\varepsilon_{r_d}|r_d(t)| + \varepsilon_\eta|\tilde{\eta}_f(t)|, 2\} \tag{5b}$$
$$\dot{\tilde{\eta}}_f = -T_{\eta_f}^{-1}\{\tilde{\eta}_f - \tilde{y}\}, \tag{5c}$$

where $\varepsilon_{r_d} \in \mathbb{R}_{>0}$ and the desired yaw rate $r_d(t) \in \mathbb{R}$ are related to a heading change. The second term $\tilde{\eta}_f$ in (5b) is the lowpass filter (5c) that tracks the observer output error performance, where $T_{\eta_f} \in \mathbb{R}^{3\times3}$ is a diagonal matrix of filter time constants. If the observer performance deteriorate, $|\tilde{\eta}_f|$ will grow. The time constants and $\varepsilon_\eta \in \mathbb{R}_{>0}$ are tuned such that κ approaches zero at steady state. To incorporate the effect of a transient at observer startup, $\tilde{\eta}_f$ is initialized with non-zero values. The value of β in (5b) takes a value between zero and two. The maximum function in (5a) defines a threshold such that κ will not go above zero before β is larger than one. This will reduce the amount of switching back and forth.

IV. STABILITY ANALYSIS

By defining the estimation error states $\tilde{\xi} := \xi - \hat{\xi}$, $\tilde{\eta} := \eta - \hat{\eta}$, $\tilde{\nu} := \nu - \hat{\nu}$, and $\tilde{b} := b - \hat{b}$, and subtracting the observer equations (3) from the control design model (1), we get the observer error dynamics,

$$\dot{\tilde{\xi}} = A_w\tilde{\xi} - K_1\tilde{y} \tag{6a}$$
$$\dot{\tilde{\eta}} = R(\psi)\tilde{\nu} - K_2\tilde{y} \tag{6b}$$
$$\dot{\tilde{b}} = -T_b^{-1}\tilde{b} - K_3(t)\tilde{y} \tag{6c}$$
$$M\dot{\tilde{\nu}} = -D\tilde{\nu} + R(\psi)^\top\tilde{b} - K_4(t)R(\psi)^\top\tilde{y}. \tag{6d}$$

The stability analysis follows the same structure as in [10]. However, the following proof removes the assumption of a maximum yaw rate. We collect all the observer error states from (6) in a vector $x := \text{col}(\tilde{\xi}, \tilde{\eta}, \tilde{b}, \tilde{\nu}) \in \mathbb{R}^{15}$ and write the observer error dynamics from (6) compactly as

$$\dot{x} = A(\psi, t)x, \tag{7}$$

where the equation can be derived, as shown at the bottom of this page.

The dynamics (7) can be written as [17],

$$\dot{x} = T(\psi)^\top A(0, t)T(\psi)x, \tag{8}$$

where

$$T(\psi) = \text{diag}\{R(\psi)^\top, R(\psi)^\top, R(\psi)^\top, R(\psi)^\top, I\}, \tag{9}$$

if the matrices K_2, $K_3(t)$, and T_b commute with $R(\psi)$, and $K_1 R = \text{diag}\{R, R\}K_1$. Note that the nonlinearity $R(\psi)$ is replaced by $R(0) = I$ in $A(0, t)$. Moreover, it can be shown that we can write $A(0, t)$ as

$$A(0, t) = \kappa(t)A_{max} + (1-\kappa(t))A_{min}, \quad \kappa(t) \in [0, 1]. \tag{10}$$

where $A_{min} = A(0, 0)$ and $A_{max} = A(0, 1)$.

Proposition 1: The equilibrium $x = 0$ of (7) where $K_i(t)$, $i = 3, 4$, is given by (4), and

$$\kappa(t) \in [0, 1] \quad \forall t \geq 0,$$

is uniformly globally exponentially stable (UGES) if the following holds:

(1) The matrices K_2, $K_3(t)$, and T_b commute with the rotation matrix $R(\psi)$, and $K_1 R = \text{diag}\{R, R\}K_1$.
(2) The linear matrix inequalities (LMIs) below are satisfied,

$$A_{min}^\top P + PA_{min} < -Q \tag{11a}$$
$$A_{max}^\top P + PA_{max} < -Q \tag{11b}$$
$$PS_T - S_T P \text{ is skew-symmetric}, \tag{11c}$$

where $S_T = \text{diag}\{S, S, S, 0\}$, and $P \in \mathbb{R}^{15\times15}$ and $Q \in \mathbb{R}^{15\times15}$ are symmetric positive definite matrices. □

Proof 1: Consider the transformation $z = T(\psi)x$ given by (9), and notice that $T(\psi)^{-1} = T(\psi)^\top$. From (8) we get

$$\begin{aligned}\dot{z} &= T(\psi)T(\psi)^\top A(0, t)z + \dot{T}(\psi)T(\psi)^\top z \\ &= A(0, t)z - rS_T z,\end{aligned} \tag{12}$$

$$A(\psi, t) := \begin{bmatrix} A_w - K_1C_w & -K_1 & 0 & 0 \\ -K_2C_w & -K_2 & 0 & R(\psi) \\ -K_3(t)R(\psi)^\top C_w & -K_3(t)R(\psi)^\top & -T_b^{-1} & 0 \\ -M^{-1}K_4(t)R(\psi)^\top C_w & -M^{-1}K_4(t)R(\psi)^\top & -M^{-1}R(\psi)^\top & -M^{-1}D \end{bmatrix}.$$

where r is the yaw rate. We introduce a quadratic Lyapunov function $V(z) = z^\top Pz$ with P from (11), and take the time derivative of V along (12), which gives

$$\begin{aligned}\dot{V} &= z^\top\{PA(0,t) + A(0,t)^\top P - r(PS_T - S_T P)\}z \\ &= 0.85z^\top\{\kappa(t)(PA_{max} + A_{max}^\top P) \\ &\quad + (1-\kappa(t))(PA_{min} + A_{min}^\top P)\}z \\ &\leq -q_m|z|^2 \end{aligned} \tag{13}$$

where q_m is the smallest eigenvalue of Q from (11).

V. SETUP, RESULTS, AND DISCUSSION

The observer in (3) has been tested on the high-fidelity simulation model and on full-scale experimental data, described in sections V-A and V-B, respectively. For the experimental data we only have data sets with negligible waves, so the observer tested does not apply the wave filter. Hence, the observer used is (3b)-(3d) with $\hat{y} = \hat{\eta}$. In addition, the data series for the full-scale experiments contain a lot of transients, but little steady state. Therefore, the simulation study has a wider discussion of performance than the observer results on the experimental data.

After a presentation of the setup, we start with presenting a closed-loop verification of the observer from [10] onboard the R/V Gunnerus. This serves as a verification of the time-varying observer design, which is relevant for the observer presented in this paper, as the observers have similar structure and scheme for selecting the time-varying gains.

A. DP SIMULATION MODEL

The simulation model is a 6 DOF high-fidelity model of a platform supply vessel with main parameters shown in Table 1. The model includes nonlinear damping, Coriolis, centripetal forces, and linear damping, based on building blocks from the MSS Toolbox [18]. Wave drift and current forces are calculated using lookup tables, which give a realistic variation of the bias loads with vessel heading. Realistic noise is added to the measurement signals from the GPS and compass, with sampling rates of 1 Hz and 10 Hz, respectively.

TABLE 1. Simulation, platform supply vessel, and main parameters.

Parameters	Value
Length between perp.	80 m
Breadth	17.4 m
Draft	5.6 m
Displacment	6150 tons

The simulated sea state is very rough with significant wave height of 6 meters, and a peak frequency of 0.53 rad/s taken from the JONSWAP[1] spectrum. The mean incident wave heading is 190° (head waves) in the North/East frame [19]. The simulation also includes current with a speed of 0.5 m/s with direction of 160° (bow).

[1] Joint North Sea Wave Project

FIGURE 2. The NTNU-owned research vessel R/V Gunnerus.

TABLE 2. R/V Gunnerus, main parameters.

Parameters	Value
Length over all	31.3 m
Length between perp.	28.9 m
Breadth middle	9.6 m
Draft	2.7 m
Dead weight	107 tons

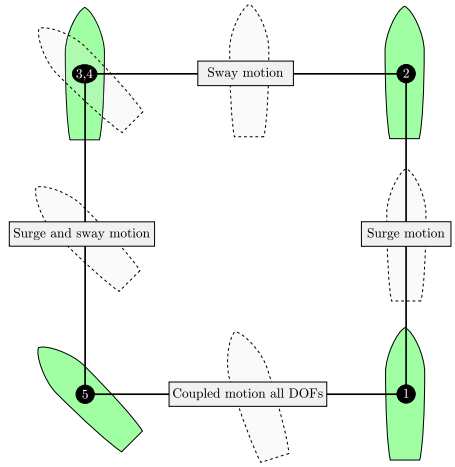

FIGURE 3. The 4-corner DP test. Courtesy: Øivind K. Kjerstad.

B. AMOS DP RESEARCH CRUISE 2016

Full-scale experimental data were collected during the AMOS DP Research Cruise (ADPRC) 2016 [11] with R/V Gunnerus, a 31-meter long research vessel owned and operated by NTNU, as seen in Figure 2, and with main parameters in Table 2. In addition, a closed-loop verification of the observer from [10] onboard the R/V Gunnerus was tested on the cruise. For the experimental data we only have data sets with negligible waves.

The data sets from the full-scale experiment with R/V Gunnerus are all from the vessel performing a box maneuver,

here called *DP 4-corner test*, as shown in Figure 3. The vessel starts at North and East position $(N, E) = (0, 0)$ with heading zero degrees, and the test steps are:

1) Position change to $(N, E) = (40m, 0)$ with zero heading (pure surge motion).
2) Position change 40 meter to $(N, E) = (40m, -40m)$ with zero heading (pure sway motion).
3) Heading change to $\psi = -45$ degrees (pure rotation).
4) Position change to $(N, E) = (0, -40m)$ keeping heading at -45 degrees (combined surge and sway motion).
5) Position change to $(N, E) = (0, 0)$ and heading $\psi = 0$ degrees (coupled motion with all DOFs).

C. PERFORMANCE EVALUATION

To compare performance of the different observer algorithms, we will apply the following cost functions as performance indicators,

$$J_\eta = \int_{t_0}^{t_f} \{|\eta_N - \hat{\eta}_N| + |\eta_E - \hat{\eta}_E| + \frac{180}{\pi}|\psi - \hat{\psi}|\}dt \quad (14a)$$

$$J_v = \int_{t_0}^{t_f} \{|u - \hat{u}| + |v - \hat{v}| + \frac{180}{\pi}|r - \hat{r}|\}dt \quad (14b)$$

$$J_b = \int_{t_0}^{t_f} \{\frac{|b_N - \hat{b}_N|}{\|b_N\|_\infty} + \frac{|b_E - \hat{b}_E|}{\|b_E\|_\infty} + \frac{|b_\psi - \hat{b}_\psi|}{\|b_\psi\|_\infty}\}dt, \quad (14c)$$

where t_0 and t_f are the initial and final time of the interval.

D. DERIVATIVE FREE OPTIMIZATION FOR TUNING

When comparing observers, a fair tuning is important. We would like to find the tuning based on optimization. Due to the absence of information about the gradient, Hessian, or higher derivatives of a typical cost function, a classic gradient descent-like method is not applicable. Therefore, derivative free optimization (DFO) will be used as a guide to tune the observers, and the MATLAB® function *fminsearch* has been adopted.

To illustrate how derivative free optimization works, let us consider a variable of interest, $x \in \mathbb{R}$. The goal is to establish a cost function to minimize the error $\tilde{x} = x - \hat{x}$ given a certain parameter $K \in \mathbb{R}$ and a simulation time of t_f seconds. We consider a cost function $J(K, t_f)$, where for each value of K a new simulation is performed and the cost function is evaluated. The derivative free optimization method explores the solution set around the current iteration result to compute a new solution point which minimizes the cost function. In our case this means to find a new value for K that gives a lower cost for J than the one before. There is a chance of getting stuck in a local minimum, and therefore several initial conditions for K are needed.

E. OBSERVER OF [10]: TIME-VARYING $K_3(t)$ ONLY, WITH FULL-SCALE CLOSED-LOOP VERIFICATION

The time-varying observer from [10] was tested in closed loop on the ADPRC 2016. The observer is similar to (3), with a time-varying bias injection gain $K_3(t)$, but K_4 was kept constant. However, since the waves were negligible while performing the closed-loop trials, the observer used in closed-loop was (3b)-(3d) with $\hat{y} = \hat{\eta}$.

The control law τ used for the full-scale experiments had a feedback term τ_{FB}, and a reference feedforward term τ_{FF}, where the feedback term consisted of a nonlinear PD (proportional, derivative) tracking term and a bias load rejection term,

$$\tau = \tau_{FB} + \tau_{FF} \quad (15a)$$

$$\tau_{FF} = M\dot{v}_d(t) + Dv_d(t) \quad (15b)$$

$$\tau_{FB} = -K_p R(\psi)^\top(\hat{\eta} - \eta_d(t)) - K_d(\hat{v} - v_d(t)) - R(\psi)^\top \hat{b}_f, \quad (15c)$$

where K_p and K_d are positive definite gain matrices, and $\eta_d(t)$, $v_d(t)$, $\dot{v}_d(t)$ are the desired references generated by a guidance system. The state $\hat{b}_f$ is a lowpass-filtered state of the bias estimate $\hat{b}$,

$$\dot{\hat{b}}_f = -T_f^{-1}(\hat{b}_f - \hat{b}), \quad (16)$$

where T_f is a diagonal matrix of the filter time constants. This filter was used instead of the bias estimate directly, to achieve a calmer control signal; see [10] for more details. The tuning for the observer and controller gains were found through trial and error.

1) EXPERIMENTAL CLOSED-LOOP RESULTS

The vessel followed the DP 4-corner maneuver described in Section V-B, and Figure 4 shows the response of the vessel for two different runs. The left side of the figure shows the North/East position of the target and the two runs, and the right side of Figure 4 shows the heading setpoint and the vessel heading for the two runs. The figure indicates that the observer worked well in closed loop, and vessel followed the maneuver well. The best performance was in surge, and when the degree of coupling between surge, sway, and yaw increased, tracking the reference was harder.

The two runs had similar environmental conditions, with current of velocity 0.3 m/s and direction 300°, and with wind speed of 6 m/s and direction 250°. For both runs the observer gains were the same, but the filter time constant for the bias was four times higher for run 2. As seen from Figure 4, both runs were quite similar in performance, but run 2 was more oscillatory, at least on the last part of the maneuver. This is probably due to the higher bias filter time constant. The closed-loop results indicate that the observer worked well in closed loop, and managed to control the vessel to a satisfactory degree.

F. OBSERVER WITH TIME-VARYING BIAS AND VELOCITY INJECTION GAINS

We now present the results for the time-varying observer in (3), where both $K_3(t)$ and $K_4(t)$ are time-varying. In addition, the results of the observer in [10] with only $K_3(t)$ time-varying is presented, with $K_4 = K_{4,min}$. Two benchmarks are included to compare the performance of the observers. The first benchmark is an observer that always uses $K_{3,min}$

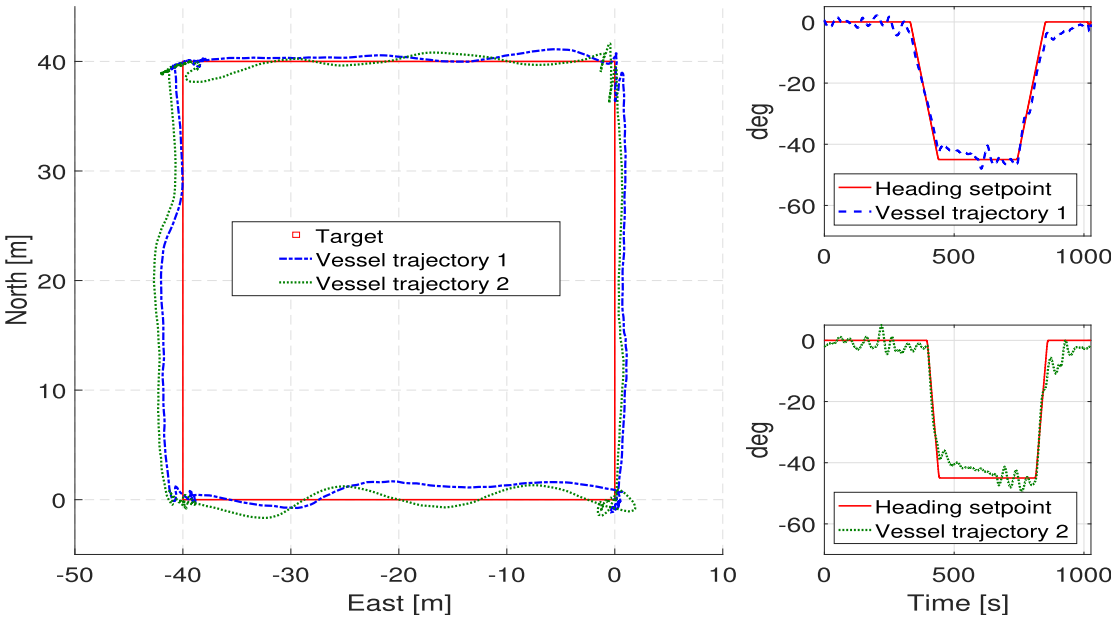

FIGURE 4. Full-scale experimental verification on R/V Gunnerus of the algorithm from [10]. The left plot shows the four corner target and results of two different runs. The right side shows the heading setpoint and the response of the two different runs.

and $K_{4,min}$ in (4), named the *baseline* observer, working well in steady state. This is the "nonlinear passive observer" presented in [16], with normal tuning, and is typical in the literature. The second benchmark is an observer called the *aggressive* observer that always uses $K_{3,max}$ and $K_{4,max}$, working well in transients.

1) TUNING

To find the tuning for the observers, derivative free optimization, as discussed in Section V-D, was used with the cost function

$$J = J_\eta + c_v J_v, \tag{17}$$

where J_η and J_v are defined in (14a) and (14b), and c_v is a scaling factor to weight the relative contributions for position and velocity.

For the simulated data in Section V-F.2, a maneuver with many transients has been used. The data set has both a change of the current direction and a heading change combined with a North/East position change, with short time intervals between the transients. The resulting tuning was adjusted to accommodate the stability requirements in (11), and this was used as a guide to tune the transient observer gains, that is, the maximum values of $K_3(t)$ and $K_4(t)$.

In order to find values for $K_{3,min}$ and $K_{4,min}$, several tests have been conducted. We tried to select maximum gains higher than the gains from the tuning found from DFO and combined this with a low minimum tuning, but this did not yield good results. This makes sense as the DFO tuning is found over a lot of transients, and thus is very aggressive already.

Thereafter, using the DFO tuning as the maximum values, we searched though several variations for the minimum tuning. Setting the minimum gains to $60-70\%$ of the maximum gains yielded the best results. However, since we needed to adjust $K_{3,max}$ to satisfy the stability requirements in (11), we selected the highest feasible $K_{3,max}$ that in combination with minimum gains $K_{i,min} = 0.7\ K_{i,max}$ that satisfied (11). This gave $K_{3,max} = 0.5\ K_{3,max}^{DFO}$.

For the full-scale experimental data, a similar approach was used where the DP 4-corner maneuver seen in Figure 3 was used to find the transient tuning. To find the gains by using DFO, the post-processed position measurement and velocities were used. The velocities were found by differentiating the North/East position and heading using a finite impulse response (FIR) filter. A search over possible ratios between the maximum and minimum tuning was performed, where 0.7 performed well, satisfying (11) with $K_{3,max} = 0.5\ K_{3,max}^{DFO}$.

2) ESTIMATION BASED ON SIMULATED DATA

For the simulated data the vessel is controlled by (15) and (16) that operate on the estimated states, i.e. the observers operate in closed loop.

In the data series, the current changes direction at $t = 500$ seconds, and at $t = 1000$ seconds there is

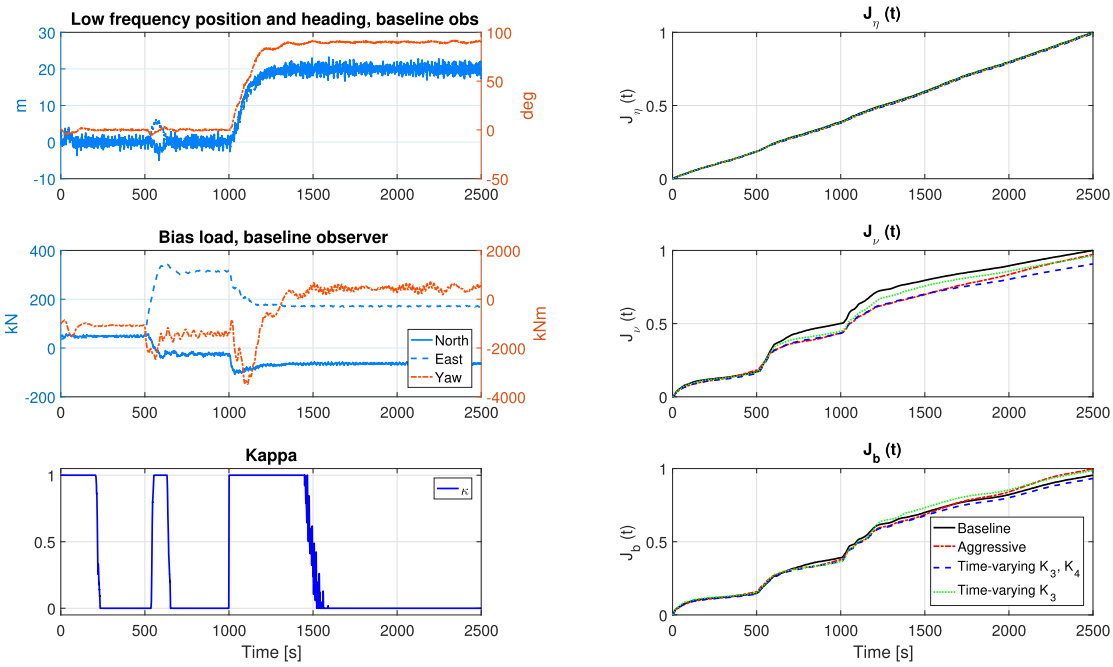

FIGURE 5. Simulation results of observer in closed-loop.

TABLE 3. Performance indices for the estimation error, simulation data.

Time:	0-1500 s			2000-3500 s		
Observer	J_η	J_ν	J_b	J_η	J_ν	J_b
Baseline	2125.2	96.4	666.8	2125.6	36.3	355.0
Aggressive	2098.8	84.7	653.2	2141.8	50.0	446.9
Time-varying K_3 and K_4	2099.3	85.1	646.2	2125.6	36.3	351.3
Time-varying K_3	2117.2	91.7	697.1	2125.6	36.4	352.4

a setpoint change of both North/East position and heading. Figure 5 shows the results of the four observers. The left side shows the low-frequency North/East position and heading of the baseline observer in the top plot, the middle plot shows the bias load of the baseline observer, found by solving (1d) for b, and the lower left plot shows the κ variable of the observer with time-varying $K_3(t)$ and $K_4(t)$ from (4). The right side shows the performance indices J_η, J_ν, and J_b in (14) from top to bottom, respectively. The same performance index values for 0 to 1500 seconds and for the steady-state time interval 2000 to 3500 are listed in Table 3. Note that the steady-state time interval 2500 to 3500 seconds is not shown in Figure 5.

Looking at the left side of Figure 5 we see that the bias loads change a lot, both at the current direction change at 500 seconds, and at the setpoint change at 1000 seconds. The κ-value starts at 1 due to high initialization of $\tilde{\eta}_f(t)$ in (5b) in order to handle initial transients before settling at $\kappa = 0$. At the heading change at 1000 seconds, κ reacts quickly and jumps to 1 due to the non-zero desired yaw rate. The current direction change at 500 seconds has to be detected through deterioration of the observer performance and the subsequent rise in $|\tilde{\eta}_f(t)|$. Therefore it takes κ longer to reach 1 during the current direction change.

On the right side of Figure 5 and in Table 3 we see that all observers perform similarly for J_η. In both the estimation of the velocity and bias loads, the time-varying observer proposed in this paper performs the best, especially in velocity. It outperforms the aggressive observer due to effect of lower oscillations in steady state, and it outperforms the baseline due to faster reaction over the transients. The time-varying observer with only K_3 time varying performs worse than the observer with both K_4 and K_3 time varying, but it performs better than the baseline observer in transients. As seen from Table 3, the baseline and time-varying observers are slightly better than the aggressive observer in steady state for position estimation, and considerable better for bias and velocity estimation.

If the noise variance of the measurements is increased, the time-varying observer performs better relative to the aggressive, due to lower tuning in steady state. To make the time-varying setup better handle large measurement noise, we could make ε_η in (5) depend on the variance of the noise. In this way the time-varying observer could adopt lower gains if the measurement noise increases.

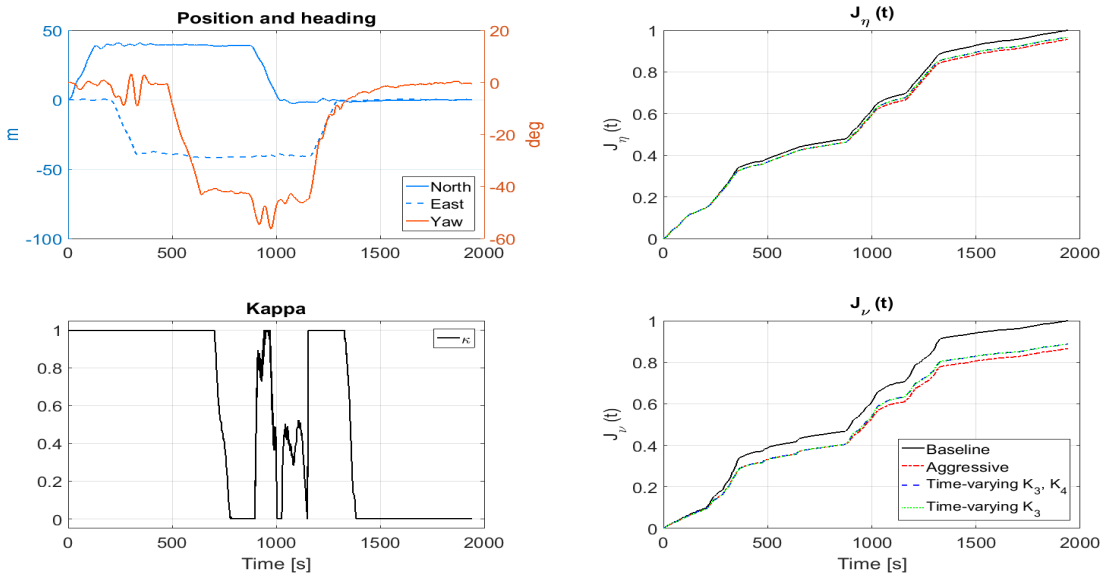

FIGURE 6. Observer results on full-scale experimental data from a DP 4-corner maneuver with R/V Gunnerus.

TABLE 4. Performance indices for the estimation error, full-scale exp. data.

Time:	0-1500 s		1500-1940 s	
Observer	J_η	J_ν	J_η	J_ν
Baseline	142.09	144.02	10.97	8.95
Aggressive	135.27	123.35	11.02	9.05
Time-varying K_3 and K_4	137.00	126.94	10.97	8.95
Time-varying K_3	138.83	126.97	10.97	8.95

3) ESTIMATION BASED ON FULL-SCALE MEASUREMENTS

Figure 6 shows the results of the four observers on data from R/V Gunnerus from ADPRC 2016. In the data set presented, the vessel is exposed to a current roughly estimated to 0.6 m/s and direction 170°, and with wind speed 5 m/s and direction 150°. The left side of the plot shows the measured North/East position, and heading in the top plot. The bottom left plot shows the κ variable. Notice that κ is 1 for most of the four corner maneuver, and after 1500 a steady state is reached.

Since the four corner maneuver has a lot of transients, and not too much steady state, it is harder to show a difference between the different observers. The right side of Figure 6 shows the performance indices J_η and J_ν in (14), and all four observers perform similarly for J_η, but for J_ν the baseline observer is significantly worse than the other three, due to all the transients. However, the performance between the observer with only time-varying K_3 to that of the other time-varying observer is smaller than for the closed-loop simulation results. The values for J_η and J_ν for the transient and steady state periods are given in Table 4, and the trend is similar to that of the closed-loop simulation results, although the differences in steady state are smaller. This is natural as the steady state in simulation is actually steady, and here the environment is changing, and there is less time to settle into steady state conditions.

VI. CONCLUSION

A time-varying model-based observer with good performance in both transients as well as steady state has been proposed. The observer is shown to be UGES, and performance is shown through a simulation study and on full-scale experimental data. In addition, a full-scale closed-loop verification is presented, and this shows that the observer works to a satisfactory degree in closed loop. Satisfactory transient tuning for the observer is found through derivative free optimization. The time-varying observer shows a marginal benefit over a well-tuned transient observer, depending on variations in measurement noise and environmental conditions. Especially, if there are large periods of steady state in between transients the time-varying observer is a tractable solution over the conventional DP observer. In addition, the added complexity of implementation for the time-varying gains is very small.

ACKNOWLEDGEMENTS

The authors would like to thank the crew of R/V Gunnerus and the personel from Kongsberg Maritime for their help and support during the sea trials. Especially, they would like to thank Rune Skullestad and Øystein Lurås from Kongsberg Maritime for help with code implementation and the simulation platform to test our code. Also, they would like to thank the NTNU research team, Øivind K. Kjerstad, Asgeir J. Sørensen, Mikkel E. N. Sørensen, Zhengru Ren, and

Morten Breivik. Finally, MSc. student Alexander Mykland deserves a thanks for writing the test log.

REFERENCES

[1] International Maritime Organization. "Guidelines for vessels with dynamic positioning systems," International Maritime Organization, London, U.K., Tech. Rep. MSC/circ.645, 1994.
[2] T. I. Fossen, *Handbook Marine Craft Hydrodynamics Motion Control*. Hoboken, NJ, USA: Wiley, 2011.
[3] A. J. Sørensen, "A survey of dynamic positioning control systems," *Annu. Rev. Control*, vol. 35, no. 1, pp. 123–136, Apr. 2011.
[4] J. E. G. Refsnes, "Nonlinear model-based control slender body AUVs," Ph.D. dissertation, Dept. Marine Technol., Norwegian Univ. Sci. Technol., Trondheim, Norway, 2007.
[5] O. K. Kjerstad and R. Skjetne, "Disturbance rejection by acceleration feedforward for marine surface vessels," *IEEE Access*, vol. 4, pp. 2656–2669, 2016.
[6] T. H. Bryne, T. I. Fossen, and T. A. Johansen, "Nonlinear observer with time-varying gains for inertial navigation aided by satellite reference systems in dynamic positioning," in *Proc. 22nd Medit. Conf. Control Autom. (MED)*, Jun. 2014, pp. 1353–1360.
[7] D. J. Belleter, D. A. Breu, T. I. Fossen, and H. Nijmeijer, "A globally k-exponentially stable nonlinear observer for the wave encounter frequency," in *Proc. IFAC Conf. Control Appl. Marine Syst.*, 2013, vol. 46. no. 33, pp. 209–214.
[8] D. J. W. Belleter, R. Galeazzi, and T. I. Fossen, "Experimental verification of a global exponential stable nonlinear wave encounter frequency estimator," *Ocean Eng.*, vol. 97, pp. 48–56, Mar. 2015.
[9] S. A. Værnø and R. Skjetne, "Hybrid control to improve transient response of integral action in dynamic positioning of marine vessels," in *Proc. IFAC Conf. Manoeuvring Control Marine Craft*, 2015, vol. 48. no. 16, pp. 166–171.
[10] S. A. Værnø, A. H. Brodtkorb, R. Skjetne, and A. J. Sørensen, "An output feedback controller with improved transient response of marine vessels in dynamic positioning," in *Proc. IFAC Conf. Control Appl. Marine Syst.*, 2016, vol. 49. no. 23, pp. 133–138.
[11] R. Skjetne *et al.*, "Amos dp research cruise 2016: Academic full-scale testing of experimental dynamic positioning control algorithms onboard RV gunnerus," in *Proc. ASME 36th Int. Conf. Ocean, Offshore Arctic Eng.*, 2017, pp. 1–4.
[12] P. Fung and M. J. Grimble, "Dynamic ship positioning using a self-tuning Kalman filter," *IEEE Trans. Autom. Control*, vol. 28, no. 3, pp. 339–350, Mar. 1983.
[13] M. Katebi, I. Yamamoto, M. Matsuura, M. Grimble, H. Hirayama, and N. Okamoto, "Robust dynamic ship positioning control system design and applications," *Int. J. Robust Nonlinear Control*, vol. 11, no. 13, pp. 1257–1284, 2001.
[14] E. Tannuri and H. Morishita, "Experimental and numerical evaluation of a typical dynamic positioning system," *Appl. Ocean Res.*, vol. 28, no. 2, pp. 133–146, 2006.
[15] A. J. Sørensen, "Marine control systems—Lecture notes," Dept. Marine Technol., Dept. Marine Technol., Norwegian Univ. Sci. Tech., Trondheim, Norway, 2013.
[16] T. I. Fossen and J. P. Strand, "Passive nonlinear observer design for ships using Lyapunov methods: Full-scale experiments with a supply vessel," *Automatica*, vol. 35, no. 1, pp. 3–16, Jan. 1999.
[17] K.-P. Lindegaard, "Acceleration feedback dynamic positioning," Ph.D. dissertation, Dept. Eng. Cybern., Norwegian Univ. Sci. Technol., Trondheim, Norway, 2003.
[18] T. I. Fossen and T. Perez. (2010). *Mss. Marine Systems Simulator*, accessed on Feb. 2015. [Online]. Available: http://www.marinecontrol.org
[19] W. G. Price and R. E. D. Bishop, *Probabilistic Theory of Ship Dynamics*. New York, NY, USA: Halsted, 1974.

SVENN ARE VÆRNØ was born in Norway in 1990. He received the M.Sc. degree in marine technology from the Norwegian University of Science and Technology, Trondheim, Norway, in 2014, where he is currently pursuing the Ph.D. degree with the Centre of Excellence Autonomous Marine Operations and Systems. His research include marine motion control systems and dynamic positioning.

ASTRID H. BRODTKORB received the M.Sc. degree in marine technology from the Norwegian University of Science and Technology, Trondheim, in 2014, where she is currently pursuing the Ph.D. degree in marine control systems with the Norwegian Centre of Excellence Autonomous Marine Operations and Systems. Her main research interests are hybrid control theory, observers, and sea state estimation applied to dynamic positioning systems for marine vessels.

ROGER SKJETNE received the M.Sc. degree in control engineering from the University of California at Santa Barbara in 2000, and the Ph.D. degree from the Norwegian University of Science and Technology (NTNU), in 2005. Prior to his studies, he was an Electrician with Aker Elektro AS on numerous oil installations for the North Sea. From 2004 to 2009, he was with Marine Cybernetics AS, where he was involved in hardware-in-the-loop simulation for testing safety-critical marine control systems. He was the Project Manager for the KMB Arctic DP Research Project. Since 2009, he has held the Kongsberg Maritime Chair of Professor in marine control engineering with the Department of Marine Technology, NTNU, where he is currently the Leader of the Research Group on Marine Structures. He is the Leader of the Ice Management Work Package with the CRI Sustainable Arctic Marine and Coastal Technology, an Associated Researcher with the CoE Center for Ships and Ocean Structures and CoE Autonomous Marine Operations and Systems, and a Principal Researcher with the CRI on Marine Operations. He is also a Co-Founder of the two companies BluEye Robotics and ArcISo. His research interests are within Arctic station keeping operations and ice management systems for ships and rigs, environmentally robust control of shipboard electric power systems, and nonlinear control theory for motion control of single and groups of marine vessels. He received the Exxon Mobil Prize for best Ph.D. thesis in applied research for his Ph.D. thesis at NTNU.

VINCENZO CALABRÒ (M'10) was born in Messina, Italy, in 1982. He received the Ph.D. degree in robotics automation and bioengineering from the University of Pisa, Italy, in 2012. In 2012, he joined the Cybernetics Research and Development Group, Kongsberg Maritime, where he developed and improved industrial solutions for Dynamic Positioning systems and related applications. Since 2017, he has been the Research and Development Manager with Norwegian Subsea AS company, developing inertial-based systems and applications. His current research interests include state observer design, neural networks, model predictive control, non-linear control, and fuzzy logic.

Errata (J.2)

- For Eq. (8) to be valid, there should be an assumption on A_w that $\text{diag}\{R(\psi), R(\psi)\}A_w\text{diag}\{R(\psi)^\top, R(\psi)^\top\} = A_w$. A typical wave-filter (used in this paper) is a second order filter (Sørensen, 2013), where

$$A_w = \begin{bmatrix} 0 & I \\ -\Omega^2 & -2\Lambda\Omega \end{bmatrix} \in \mathbb{R}^{6\times 6},$$

  where $\Omega = \text{diag}\{\omega_1, \omega_2, \omega_3\} \in \mathbb{R}^{3\times 3}$ and $\Lambda = \text{diag}\{\lambda_1, \lambda_2, \lambda_3\} \in \mathbb{R}^{3\times 3}$. The assumption above imples that $\omega_1 = \omega_2$ and $\lambda_1 = \lambda_2$, which means that the East and North components are treated the same. Typically, all elements of Ω are set to the same value; the peak frequency of the sea state. In practice, the values of Λ are often set to be the same as well. It makes sense to set $\lambda_1 = \lambda_2$, because it is hard to justify different damping factors in North and East, since these components are not linked to the vessel, but to arbitray directions (seen from the vessel). In the paper, all components of Ω were the same, and similarly for Λ.

- The matrix $A(\psi, t)$ at the bottom of page 4, below Eq. (12) has two typos in row 3, for element (3,1) and (3,2). Element (3,1) should write $-K_3(t)C_w$ and element (3,2) should write $-K_3(t)$

- In Eq. (13) the factor 0.85 is a typo and should not be there.

Additional comments (J.2)

The tuning of this paper relies on the LMI-constraints in Eq. (11) being satisfied. This is similar to the LMI-constraints in Eq. (18) of (C.1), where the notion of a maximum yaw rate, r_{max}, is used. The idea of Eq. (18) in (C.1) is that if the LMIs are satisfied for a very large and unattainable yaw rate the system is stable. In (J.2), the maximum yaw rate requirement is removed. However, the solution found in Eq. (11) of (J.2) is a subset of the solutions from Eq. (18) of (C.1). The stability analysis of (J.2) is thus more conservative than in (C.1). To illustrate this, let us consider the stability proof of the simulation model in (J.2). As mentioned in (J.2), the allowed minimum tuning of $K_{3,min}$ and $K_{4,min}$ is 0.7 (0.68) of the maximum tuning. However, if we instead apply the tuning rules of Eq. (18) of (C.1) the minimum tuning of $K_{3,min}$ and $K_{3.min}$ is allowed to be 0.55 of the maximum. This is using an r_{max} of $10^\circ/s$, which is reasonable. For a vessel of this size obtaining a yaw rate $10^\circ/s$ is unrealistic.

J.3

Hybrid controller concept for dynamic positioning of marine vessels with experimental results

---

Brodtkorb, A. H., **Værnø, S. A.**, Teel, A. R., Sørensen, A. J., Skjetne, R.

Automatica 93 (2018) 489–497

Contents lists available at ScienceDirect

Automatica

journal homepage: www.elsevier.com/locate/automatica

Brief paper

Hybrid controller concept for dynamic positioning of marine vessels with experimental results☆

Astrid H. Brodtkorb [a,*], Svenn Are Værnø [a], Andrew R. Teel [b], Asgeir J. Sørensen [a], Roger Skjetne [a]

[a] Centre for Autonomous Marine Operations and Systems, Department of Marine Technology, Norwegian University of Science and Technology (NTNU AMOS), 7491 Trondheim, Norway

[b] Department of Electrical and Computational Engineering, University of California Santa Barbara, CA 93106-9560, USA

ARTICLE INFO

Article history:
Received 15 March 2017
Received in revised form 15 January 2018
Accepted 27 January 2018
Available online 12 April 2018

Keywords:
Marine control systems
Hybrid systems
Dynamic positioning
Observers
Output feedback control

ABSTRACT

The next generation marine control systems will, as a step towards increased autonomy, have more automatic functionality in order to cope with a set of complex operations in unknown, challenging and varying environments while maintaining safety and keeping operational costs low. In this paper a hybrid control strategy for stationkeeping and maneuvering of marine vessels is proposed. The hybrid concept allows a structured way to develop a control system with a bank of controllers and observers improving dynamic positioning (DP) performance in stationary dynamics, changing dynamics including enhancing transient performance, and giving robustness to measurement errors. DP systems are used on marine vessels for automatic stationkeeping and tracking operations solely by use of the thrusters. In this paper a novel method improving the transient response of a vessel in DP is developed. The performance of the hybrid control system, including two observer candidates and one controller candidate, is demonstrated in model-scale experiments and on full-scale field data. The hybrid system has global stability properties.

1. Introduction

Marine operations are moving into harsher environments, and as a consequence, requirements for the vessel's operational window, safety functions, and energy-efficiency become stricter (Sørensen, 2011). As a result, the level of autonomy in marine control systems is increasing, with automatic performance monitoring and switching. During marine operations, both variations in stationary dynamics and transient behavior are important to account for in an all-year operation philosophy subject to changing weather, sea loads, and modes of operation (Perez, Sørensen, & Blanke, 2006). There are many unknown factors that may cause transients in the vessel response, both from the environment (e.g., wave trains and wind gusts) and triggered by the operation taking place (e.g., heading changes or crane operations of heavy goods). Fig. 1 shows a marine vessel with its operational conditions and a block diagram of a general hybrid marine control system. The vessel operational conditions with *use mode, speed*, and *environment* indicate how the vessel performs different tasks with varying speed in an unknown and changing environment. The use mode includes algorithms that satisfy different control objectives such as stationkeeping, maneuvering, and target tracking, which is closely linked with the vessel speed. Environment refers to the state of the environment consisting of wind, waves and current. Naturally, certain operations can only be performed in calm conditions. Because different physical effects matter for the various vessel operational conditions, there are distinct models and control strategies which are designed specifically for each operational condition. Nguyen, Sørensen, and Quek (2007) proposed to use supervisory switched control based on the methodology of Hespanha, Liberzon, and Morse (2003) and Hespanha and Morse (2002). In addition to handling different speed regimes, use modes and changing sea states, the proposed setup ensures redundancy in the (software) *design methodology* so that faults (Blanke, Kinnaert, Lunze, & Staroswiecki, 2003) may be detected early and alarms may be raised to operators, who are either on-site or remote. The performance monitoring and switching logic block includes monitoring of the environment, power system, observer performance, position precision, signal health, and more. In order to ensure

☆ This work was supported by the Research Council of Norway through the Centres of Excellence funding scheme, project number 223254-NTNU AMOS, and in part by NSF grant number ECCS-1508757 and AFOSR grant number FA9550-15-1-0155. The material in this paper was partially presented at the 10th IFAC Symposium on Nonlinear Control Systems, August 23–25, 2016, Monterey, CA, USA. This paper was recommended for publication in revised form by Associate Editor Jun-ichi Imura under the direction of Editor Thomas Parisini.
* Corresponding author.
E-mail addresses: astrid.h.brodtkorb@ntnu.no (A.H. Brodtkorb), svenn.are.varno@ntnu.no (S.A. Værnø), teel@ece.ucsb.edu (A.R. Teel), asgeir.sorensen@ntnu.no (A.J. Sørensen), roger.skjetne@ntnu.no (R. Skjetne).

https://doi.org/10.1016/j.automatica.2018.03.047
0005-1098/

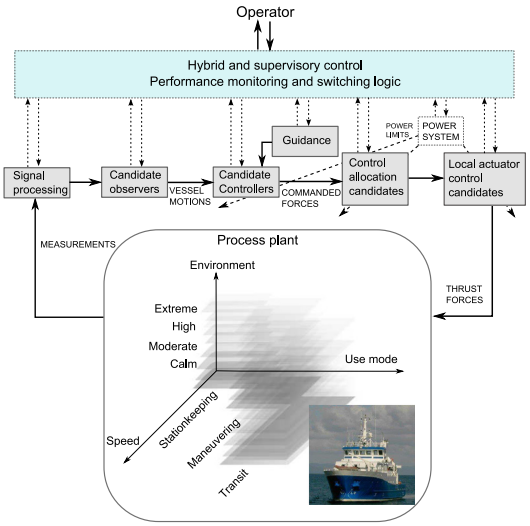

Fig. 1. Block diagram of a hybrid control system for a marine vessel in an unknown environment consisting of wind, waves and current. Sensors measure the operational status and vessel motions, and signal processing software filters, weights and votes between redundant measurements. The performance monitoring monitors the performance of the different blocks, and the switching logic chooses which algorithms to use in closed-loop control from the candidates. Here two observers and one controller are used.

safety, there are high requirements for system reconfiguration, fault tolerance and redundancy, and for testing and verification of performance (DNV-GL, 2014). Testing and verification of marine control systems with higher levels of autonomy are faced with a large (when not infinite) number of failure modes (Smogeli, Vik, Haugen, & Pivano, 2014); exhaustive testing is rarely possible. Therefore having modular design and proofs of subsystem properties may play a larger role in assuring safety (Kapinski, Deshmukh, Jin, Ito, & Butts, 2016). Systems with a wide range of dynamics and different modes that also use hybrid control approaches are for instance air traffic control (Hu, Prandini, & Sastry, 2005; Sastry et al., 1995), adaptive cruise control for the automotive industry (Girard, Howell, & Hedrick, 2005), autonomous docking operations of spacecraft (Malladi, Sanfelice, Butcher, & Wang, 2016), and in the marine industry hybrid power plants (Miyazaki, Sørensen, & Vartdal, 2016). The focus of this paper is on detecting and improving the transient performance of the DP control system using the hybrid system framework as proposed in Goebel, Sanfelice, and Teel (2012). As shown in Fig. 1, it is believed that the concept of hybrid control can provide a scalable and stringent methodology for the design of real industrial control applications dealing with several control objectives and changing environmental and operational conditions. A similar, or alternative, method may be to consider robust control by multiple model adaptive controllers as proposed by Hassani, Sørensen, Pascoal, and Athans (2017) and Hassani, Sørensen, Pascoal, and Dong (2012).

The main scientific contribution of this paper is the development of a hybrid control concept for proper switching of candidate observers and controllers, customized for transient and steady-state behavior of DP vessels. For particular observer candidates, this work combines a model-based observer (Fossen & Strand, 1999), a signal-based observer (Grip, Fossen, Johansen, & Saberi, 2015), a controller, and switching logic into a hybrid system with the goal of improving the transient response. The model-based observer, including wave filtering and bias force estimation, is especially suited in steady state, while the signal-based observer is more reactive during transients, even though it is more sensitive to signal noise. Stability analysis of the hybrid system applies results from Goebel, Sanfelice, and Teel (2009). Performance of the proposed concept is demonstrated experimentally through model-scale experiments with the hybrid observer estimates used in closed-loop output feedback control, and through estimation on full-scale field data. The paper is a continuation of Brodtkorb, Værnø, Teel, Sørensen, and Skjetne (2016), with the signal-based observer exchanged with one that has global stability properties, enhanced performance monitoring and switching logic, and new hybrid stability analysis.

The paper is organized as follows: The measurements and notation are introduced in Section 2, and the candidate observers and control algorithms are presented in Section 3. The hybrid system is assembled in Section 4, and stability is discussed in Section 5. The experimental setup and results are shown in Section 6. Section 7 concludes the paper.

2. Preliminaries

Common instrumentation in DP vessels includes position reference systems (typically GNSS[1]), compass, and inertial measurement units (IMU). The measurements, denoted with subscript m, are in this paper assumed to be of the form

$$p_m^n = [N, E]^\top \tag{1a}$$
$$\psi_m^n = \psi \tag{1b}$$
$$\omega_m^b = \omega^b + b_g \tag{1c}$$
$$f_m^b = R_\Theta^\top(\dot{v}^n - g^n), \tag{1d}$$

where the measurements in the North-East-Down (NED) frame (an Earth-fixed local reference frame assumed to be inertial) have superscript n, and measurements in the body-fixed frame have superscript b. For the purpose of stability analysis, the system is assumed to be deterministic such that noise is disregarded. This follows similar approaches as Fossen and Strand (1999) and Nguyen et al. (2007). The vector $p_m^n \in \mathbb{R}^2$ is the measured position in North and East. A vertical measurement may also be obtained through GNSS, but it is typically of low quality, and is not used here; see Section 3.2. The measured angle $\psi_m^n \in \mathbb{R}$ includes the low frequency yaw angle ψ and the wave-induced heading oscillations ψ_w, which are assumed to be small (Fossen & Strand, 1999). The angular velocity ω^b, which takes values in $\mathbb{R}^3$, is continuous and bounded, and the gyro bias is constant with a known bound $\|b_g\| \leq M_b$. The vector $f_m^b \in \mathbb{R}^3$ is the measured specific force,[2] including the acceleration of the vessel $\dot{v}^n$ and the acceleration due to gravity $g^n \in \mathbb{R}^3$. $R_\Theta \in \mathbb{R}^{3\times3}$ is the rotation matrix about the z, y, x-axes (Fossen, 2011, Ch. 2). We assume f_m^b is non-biased, bounded $\|f_m^b\| \leq M_f$, and the derivative of the actual specific force $\dot{f}^b$ is continuous and bounded. Furthermore, there exists a constant $c_{obs} > 0$ such that $\|c^b \times f_m^b\| > c_{obs}$, $c^b = [\cos(\psi_m^n), -\sin(\psi_m^n), 0]^\top$.

3. Candidate observers and controller

Two observers based on two philosophically different models of the same vessel are presented in the next sections. The relationship between the models is as follows:

$$\eta + \eta_w \equiv [p_{(1,1)}^n, p_{(2,1)}^n, \Theta_{(3,1)}]^\top \tag{2a}$$
$$\nu + \nu_w \equiv [v_{(1,1)}^b, v_{(2,1)}^b, \omega_{(3,1)}^b]^\top, \tag{2b}$$

[1] Global Navigation Satellite System.

[2] Specific force is the physical acceleration experienced by an object, consisting of the acceleration of the object and the acceleration due to gravity, i.e., it is the *measurable* acceleration, with unit [m/s^2].

with the subscript (i, j) denoting the elements of the corresponding vectors. On the left-hand side we have the position vector $\eta + \eta_w \in \mathbb{R}^3$ (North, East, yaw) and velocity vector $\nu + \nu_w \in \mathbb{R}^3$ (surge, sway, yaw) split into low-frequency and wave-frequency components. η and ν will later be estimated in the model-based observer and marked with a hat. On the right-hand side we have the low-frequency and wave-frequency position $p^n_{(1:2)} \in \mathbb{R}^2$ (North, East) and yaw $\Theta_{(3,1)}$, and velocity $v^b_{(1:2)} \in \mathbb{R}^2$ (surge, sway) and yaw $\omega^b_{(3,1)}$. Two consecutive elements of a vector are denoted with subscript $(1 : 2)$. p^n and $v^n := R_\Theta v^b$ are estimated in the signal-based observer and marked with a hat. Note that $\Theta_{(3,1)} \equiv \psi + \psi_w \approx \psi$.

3.1. Model-based observer

We have chosen to work with the nonlinear passive observer (Fossen & Strand, 1999) since it is an intuitive observer to tune, and it has global stability properties. This observer is based on the DP control plant model (Sørensen, 2011), which is a simplification of the real vessel dynamics. The inputs to the observer are the measurement $y = [p^{n\top}_m, \psi^n_m]^\top \in \mathbb{R}^3$ and the control input $\tau \in \mathbb{R}^3$. The 3 degree of freedom (DOF) model-based observer algorithm for a ship-shaped vessel in DP can be written as (Fossen & Strand, 1999)

$$\dot{\hat{\xi}} = A_\omega \hat{\xi} + K_{1,\omega}\tilde{y} \tag{3a}$$

$$\dot{\hat{\eta}} = R(\psi^n_m)\hat{\nu} + K_2\tilde{y} \tag{3b}$$

$$\dot{\hat{b}} = -T_b^{-1}\hat{b} + K_3\tilde{y} \tag{3c}$$

$$M\dot{\hat{\nu}} = -D_L\hat{\nu} + R^\top(\psi^n_m)\hat{b} + \tau + R^\top(\psi^n_m)K_4\tilde{y} \tag{3d}$$

$$\hat{y} = \hat{\eta} + W\hat{\xi}, \tag{3e}$$

where $\hat{\xi} \in \mathbb{R}^6$, $\hat{\eta}$, $\hat{\nu}$, $\hat{b} \in \mathbb{R}^3$ are the state estimates. The wave states $\xi \in \mathbb{R}^6$, low frequency position vector η and velocity vector ν, and the bias force vector $b \in \mathbb{R}^3$. $\tilde{y} := y - \hat{y}$ is the measurement estimation error, and $K_{1,\omega} \in \mathbb{R}^{6\times3}$, $K_2, K_3, K_4 \in \mathbb{R}^{3\times3}_{>0}$ are the observer gain-matrices. $A_\omega \in \mathbb{R}^{6\times6}$ is a Hurwitz matrix containing wave parameters, $R(\psi) \in \mathbb{R}^{3\times3}$ is the rotation matrix about the z-axis (Fossen, 2011, Ch. 2), $M = M^\top \in \mathbb{R}^{3\times3}$ is the inertia matrix including added mass, $D_L \in \mathbb{R}^{3\times3}$ is the linear damping coefficient matrix including second-order wave-induced damping, and $T_b \in \mathbb{R}^{3\times3}$ is a diagonal matrix of bias time constants. The first-order model (3c) accounts for *slowly-varying* environmental disturbances from mean wind, current, and second-order wave loads, as well as unmodeled vessel dynamics.

(A1) The bias force dynamics (3c) are assumed to account for only slowly-varying loads (Fossen & Strand, 1999).

This is a good assumption in steady state, but does not capture rapid variations in the bias force due to transients, e.g., heading changes or wave trains. Wave filtering is achieved by separating the wave-frequency motion estimate $\hat{\eta}_w = W\hat{\xi}$, $W = [0_{3\times3}, I_{3\times3}]$ from the low frequency estimate $\hat{\eta}$, giving the output from the model-based observer $\hat{\eta}_1 := \hat{\eta}$ and $\hat{\nu}_1 := \hat{\nu}$. The model-based estimation error dynamics, can be written compactly as

$$\dot{e}_1 = F_1(e_1), \tag{4}$$

with state vector

$$e_1 := x_1 - \hat{x}_1 = [(\xi - \hat{\xi})^\top, (b - \hat{b})^\top, (\eta - \hat{\eta})^\top, (\nu - \hat{\nu})^\top]^\top \in \mathbb{R}^{15}.$$

Claim 1. *Under Assumption (A1), the origin of the estimation error dynamics (4) is uniformly globally exponentially stable (UGES).* □

Proof. See Fossen and Strand (1999). □

3.2. Signal-based observer

Grip et al. (2015) propose a nonlinear observer, for GNSS-aided inertial navigation with biased gyro measurements. It is based on the kinematic model (Fossen, 2011) with an angular and a translational part, relating the position, velocity, and acceleration of the vessel in 6 DOF. The inputs to the signal-based observer are p^n_m, ψ^n_m, ω^b_m, and f^b_m from (1). The rotation matrix R_Θ (about the z, y, x-axis) is estimated directly, giving

$$\dot{\hat{R}}_\Theta = \hat{R}_\Theta S(\omega^b_m - \hat{b}_g) + \sigma L_p\hat{J} \tag{5a}$$

$$\dot{\hat{b}}_g = \mathrm{Proj}_{M_b}(\hat{b}_g, -L_I \mathrm{vex}(\mathbb{P}_a(\hat{R}^\top_{\Theta s} L_P \hat{J}))), \tag{5b}$$

where $\hat{R}_\Theta$ is the rotation matrix estimate, $\hat{b}_g$ is the gyro bias estimate, and the angular rate estimate is $\hat{\omega}^b := \omega^b_m - \hat{b}_g$. The projection function $\mathrm{Proj}_{M_b}(\cdot,\cdot)$ (Grip et al., 2015, Appendix) ensures that $\|\hat{b}_g\| \le M_{\hat{b}}$, and the $S(\cdot)$, $\mathrm{vex}(\cdot)$, and $\mathbb{P}_a(\cdot)$ operators are defined in the footnote.[3] $\hat{R}_{\Theta s}$, appearing in (5b), is saturated elementwise with bound 1; $\hat{R}_{\Theta s} := \mathrm{sat}_1(\hat{R}_\Theta)$. The gain-matrices are $L_P \in \mathbb{R}^{3\times3}_{>0}$, $L_I \in \mathbb{R}^{3\times3}_{>0}$, and $\sigma \ge 1$ is a scaling factor that is tuned to achieve stability. $\hat{J}$ is a stabilizing term (Grip et al., 2015, (3) and (5)) that takes ψ^n_m measured by the compass, and the specific force measurement f^b_m as input. The translational observer algorithm is

$$\dot{\hat{p}}_I = \hat{p}^n_{(3,1)} + k_{pipi}\tilde{p}_I \tag{6a}$$

$$\dot{\hat{p}}^n = \hat{v}^n + C_p e \tag{6b}$$

$$\dot{\hat{v}}^n = \hat{f}^n + g^n + C_v e \tag{6c}$$

$$\dot{\hat{\xi}}_f = -\sigma L_p \hat{J} f^b_m + C_\xi e \tag{6d}$$

$$\hat{f}^n = \hat{R}_\Theta f^b_m + \xi_f, \tag{6e}$$

with estimates $\hat{p}_I$, $\hat{p}^n$, $\hat{v}^n$ and $\hat{f}^n$, $\hat{R}_\Theta$ is from (5), and ξ_f is a correction term on the specific force estimate. (6b)–(6e) are standard kinematic observer equations, and (6a) is an addition from Bryne, Fossen, and Johansen (2015) that comes instead of using the vertical GNSS position measurement height, as mentioned in Section 2. The augmentation is motivated by the fact that a marine vessel in normal operation oscillates in heave about the mean sea surface. It may be assumed that:

(A2) The mean vertical position of the vessel over time is zero (Godhaven, 1998), $p_I = 0$.

p_I is called the *virtual vertical reference*. In (6a) the vertical position estimate $\hat{p}^n_{(3,1)}$ is integrated to give $\hat{p}_I$, which is compared with p_I and used as the driving error for the vertical dynamics. For more details, see Bryne et al. (2015). The driving error is $e := [\tilde{p}_I, \tilde{p}^\top]^\top \in \mathbb{R}^3$ with $\tilde{p} := p^n_m - \hat{p}^n_{(1:2)} \in \mathbb{R}^2$, $\tilde{p}_I := p_I - \hat{p}_I = 0 - \hat{p}_I \in \mathbb{R}$. The correction gain-matrices are

$$C_p = \begin{bmatrix} 0_{2\times1} & K_{pp} \\ k_{ppi} & 0_{1\times2} \end{bmatrix} \quad C_v = \begin{bmatrix} 0_{2\times1} & K_{vp} \\ k_{vpi} & 0_{1\times2} \end{bmatrix} \quad C_\xi = \begin{bmatrix} 0_{2\times1} & K_{\xi p} \\ k_{\xi pi} & 0_{1\times2} \end{bmatrix}.$$

The North and East gain components are $K_{pp}, K_{vp}, K_{\xi p} \in \mathbb{R}^{2\times2}_{>0}$, and the down gains are $k_{pipi}, k_{ppi}, k_{vpi}, k_{\xi pi} \in \mathbb{R}_{>0}$. The signal-based estimation error dynamics are written compactly as

$$\dot{e}_2 = F_2(e_2), \tag{7}$$

with state vector

$$e_2 := x_2 - \hat{x}_2 = [(r - \hat{r})^\top, (b_g - \hat{b}_g)^\top, (p_I - \hat{p}_I), (p^n - \hat{p}^n)^\top, (v^n - \hat{v}^n)^\top, (f^n - \hat{f}^n)^\top]^\top \in \mathbb{R}^{22},$$

[3] For a vector $x \in \mathbb{R}^3$, $S(x)$ denotes a skew-symmetric matrix so that for any $y \in \mathbb{R}^3$, $S(x)y = x \times y$, where $\times$ denotes the cross product. The skew-symmetric part of a matrix X is denoted by $\mathbb{P}_a = \frac{1}{2}(X - X^\top)$. The linear function $\mathrm{vex}(X)$, with X skew symmetric is defined so that $S(\mathrm{vex}(X)) = X$ and $\mathrm{vex}(S(x)) = x$.

with $r := [R_{\Theta(1,:)}, R_{\Theta(2,:)}, R_{\Theta(3,:)}]^\top \in \mathbb{R}^9$ and $\hat{r}$ defined accordingly. ':' denotes all elements of the row/column.

Claim 2. *Under Assumption (A2), with inputs as described in (1), the origin of the signal-based estimation error dynamics (7) is UGES.* □

Proof. See Bryne et al. (2015) and Grip et al. (2015). □

The output from the signal-based observer is written using (2), so that $\hat{\eta}_2 := [\hat{p}^n_{(1,1)}, \hat{p}^n_{(2,1)}, \hat{\Theta}_{(3,1)}]^\top$, $\hat{\nu}_2 := [\hat{v}^b_{(1,1)}, \hat{v}^b_{(2,1)}, \hat{\omega}^b_{(3,1)}]^\top$, where the heading angle estimate $\hat{\Theta}_{(3,1)}$ is extracted from $\hat{R}_\Theta$, and $\hat{v}^b = \hat{R}^\top_\Theta \hat{v}^n$. Because this observer relies on the specific force measurements instead of estimating the bias force, it reacts fast and accurately to transients. Here, no wave filter is included so $\hat{\eta}_2$ and $\hat{\nu}_2$ capture the combined low-frequency and wave-frequency motion. For shorter periods of time this may be acceptable, which is the case during transients.

3.3. Controller

The control objective is to control the vessel to the desired time-varying trajectory $\eta_d(t)$ with the desired velocity trajectory $\nu_d(t)$. The proposed control law is

$$\begin{aligned}\dot{\zeta}_s &= \hat{\eta}_s - \eta_d \\ \tau &= -K_p R^\top(\psi^n_m)(\hat{\eta}_s - \eta_d) - K_d(\hat{\nu}_s - \nu_d) \\ &\quad - K_i R^\top(\psi^n_m)\zeta_s + M\dot{\nu}_d + D_L \nu_d. \end{aligned} \tag{8}$$

$\tau \in \mathbb{R}^3$ is the commanded thrust vector, $K_p, K_d, K_i \in \mathbb{R}^{3\times 3}_{\geq 0}$ are gain-matrices, and $\hat{\eta}_s$ and $\hat{\nu}_s$ are the estimates from the model-based observer when $s = 1$, and from the signal-based observer when $s = 2$. ζ_s compensates for the unknown bias force vector b with dynamics $\dot{b} = -T_b^{-1} b$. The last two terms in (8) are feedforward terms of the desired acceleration and desired velocity. For the stability analysis of the controller, it is assumed that:

(A3) The yaw rate $\omega^b_{(3,1)}$ (also denoted $\nu_{(3,1)}$) is bounded, $|\omega^b_{(3,1)}| < r_{max}$, and K_i and T_b commute with $R(\psi)$[4] (Lindegaard & Fossen, 2003).

The following result is proven in Lindegaard and Fossen (2003).

Claim 3. *If Assumption (A3) holds, and the controller gains are chosen so that the system matrix A_c (see below) is Hurwitz, the origin of the tracking error dynamics, consisting of the control plant model using control input with state feedback, (8) inserted the real states η, ν, is UGES.* □

We note, for later use, that the tracking error dynamics have the form $\dot{e}_0 = T^\top(\psi) A_c T(\psi) e_0$ with

$$e_0 = [\xi^\top, b^\top, (\eta - \eta_d)^\top, (\nu - \nu_d)^\top, \zeta^\top]$$

$$A_c = \begin{bmatrix} A_\omega & 0 & 0 & 0 & 0 \\ 0 & -T_b^{-1} & 0 & 0 & 0 \\ 0 & 0 & 0 & I & 0 \\ 0 & I & -M^{-1}K_p & -M^{-1}(D_L + K_d) & -M^{-}K_i \\ 0 & 0 & I & 0 & 0 \end{bmatrix},$$

$$T(\psi) = \text{blkdiag}([I, R^\top(\psi), R^\top(\psi), I, R^\top(\psi)]),$$

where $T(\psi)$ is a block diagonal matrix. A Lyapunov function of the form $V_0(e_0, \psi) := e_0^\top T^\top(\psi) P T(\psi) e_0$ with $P = P^\top > 0$, where P satisfies the linear matrix inequality (LMI) $PA_c + A_c^\top P < 0$, that verifies the UGES property asserted in Claim 3.

[4] $K_i = \text{diag}([k_1, k_1, k_2])$, $T_b = \text{diag}([t_1, t_1, t_2])$ are used. The North and East gains/time constants are equal, which for a marine vessel is justified, since the environmental changes have roughly the same dominating frequencies in surge and sway.

4. Hybrid system

In this paper we propose a new hybrid strategy for DP systems in order to cope with both stationary and transient dynamics. In general, a hybrid system $\mathcal{H} = (C, F, D, G)$ is written formally as

$$x \in C \;\; \dot{x} \in F(x) \tag{9a}$$

$$x \in D \;\; x^+ \in G(x), \tag{9b}$$

where x is the hybrid state, C is the flow set, F is the flow map, D is the jump set, and G is the jump map. When x is in C, then the states are allowed to flow, and when x is in D the states are allowed to jump (Goebel et al., 2012). In this section the hybrid DP control system is assembled, starting with the performance monitoring and switching logic that choose the appropriate estimates to use in output feedback with (8). The performance monitoring and switching logic dynamics can be written as:

$$\dot{m}_i = 0, \qquad i = \{1, \ldots, n\} \tag{10a}$$

$$\dot{t}_m = -1 \tag{10b}$$

$$\dot{s} = 0 \tag{10c}$$

$$m_i^+ = \begin{cases} \|\hat{\eta}_{1(1:2)} - \hat{\eta}_{2(1:2)}\|, & \text{for } i = 1 \\ m_{i-1}, & \text{for } i = \{2, \ldots, n\} \end{cases} \tag{10d}$$

$$t_m^+ = T \tag{10e}$$

$$s^+ = \begin{cases} 1, & \text{if } \bar{m} \leq \epsilon_{ss} \\ 2, & \text{if } \bar{m} \geq \epsilon_{tr} \\ 2, & \text{if } \nu_{d(3,1)} \geq \delta \\ s, & \text{otherwise,} \end{cases} \tag{10f}$$

where m_i are monitoring states, t_m is a timer, and s is the switching signal. In order to evaluate the performance of the observers, we choose to compute the difference in estimation error in North and East $(p^n_m - \hat{\eta}_{2(1:2)}) - (p^n_m - \hat{\eta}_{1(1:2)}) = (\hat{\eta}_{1(1:2)} - \hat{\eta}_{2(1:2)})$, and take the Euclidean norm of this difference, see (10d). This signal may oscillate a lot, so we take the average of n of the past values that are saved in the shift register of size n with state $m \in \mathbb{R}^n$, i.e., $\bar{m} = \frac{1}{n}\sum_{i=1}^n m_i$. We call $\bar{m}$ the performance monitoring signal, and switch based upon this quantity in (10f). m does not change during flows, (10a). During flows, t_m decreases with unitary rate (10b), and is reset to T during jumps. A new jump is triggered when a new position measurement is available, when $t_m = 0$, so the position measurement has sample time T. The jump map for the switching signal s, including performance and heading change monitoring is (10f), where $\epsilon_{ss} \geq 0$ is the estimation difference we expect to see in steady state, and $\epsilon_{tr} \geq 0$ is the estimation difference we expect to see during a transient. Choose $\epsilon_{tr} > \epsilon_{ss}$ with some margin to provide hysteresis that suppresses unnecessary switching back and forth. The signal-based observer is chosen in closed loop if the desired yaw rate $\nu_{d(3,1)}$ is larger than a threshold $\delta \geq 0$, as we know that the forces on the vessel hull will change rapidly in this situation. s does not change during flows (10c).

For later use, we look closer at the steady state behavior of the performance monitoring states. Inserting for the steady-state observer estimates we have that $\hat{\eta}_{1(1:2)} = \eta_{(1:2)}$ (Claim 1), and $\hat{\eta}_{2(1:2)} = p^n_{(1:2)}$ (Claim 2). During steady state, the performance monitoring states m_i, $i = \{1, \ldots, n\}$, are

$$m_i = \left(\|\eta_{(1:2)} - p^n_{(1:2)}\|\right)_{i-1} = \left(\|\eta_{w(1:2)}\|\right)_{i-1}, \tag{11}$$

corresponding to the norm of the wave-frequency motion $\eta_w = W\xi$ in North and East, for each sample i in the shift register. The wave states ξ go to zero during steady state, since A_ω in (3a) is Hurwitz. In this case $\bar{m}$ is also zero, and we would like to use the model-based observer estimates in output feedback with (8) during steady state. This is because these estimates are wave filtered, and hence reduce the wear and tear on the propulsion

system. During a transient, the observers do not agree, and then $\tilde{m}$ is larger. Since the signal-based observer presumably performs better in transients, these estimates are used in closed loop during these times.

The control plant model and the kinematic model represent, with some overlap, the same underlying dynamics being the motion of the vessel. We assume that:

(A4) The solutions to the control plant model and kinematic model dynamics are forward complete.[5]

Then the solutions exist for all positive time. The tracking error analysis in Lindegaard and Fossen (2003) (Claim 3) makes sure that x_1 behaves as it is meant to, i.e., η converges to η_d and ν converges to ν_d. From the relation between the control plant model and kinematic model (2), we have that $[p^{n\top}_{(1:2)}, \Theta_{(3,1)}]^\top$ goes to η_d, and $[v^{b\top}_{(1:2)}, \omega^b_{(3,1)}]^\top$, goes to ν_d. The heave, roll, and pitch states in the kinematic model are not controlled, and hence do not converge to a reference. Therefore the kinematic model with state x_2 is not included in the hybrid analysis. We define the state vector of the hybrid system as

$$x := (x_1, \zeta_s, \hat{x}_1, \hat{x}_2, m, t_m, s) \in \mathbb{R}^{15} \times \mathbb{R}^3 \times \mathbb{R}^{15} \times \mathbb{R}^{22} \times \mathbb{R}^n \times [0, T] \times \{1, 2\}, \tag{12}$$

consisting of the control plant model state x_1, the integral state in the control law ζ_s, the model-based observer estimates $\hat{x}_1$, the signal-based observer estimates $\hat{x}_2$, the performance monitoring states m, the timer t_m, and the switching signal s. The flow dynamics of the hybrid system constitutes the vessel described by the control plant model, controller, observer, and timer dynamics. The states x_1, ζ_s, $\hat{x}_1$, and $\hat{x}_2$ do not change during jumps, i.e., $x_1^+ = x_1$, $\zeta_s^+ = \zeta_s$, and so on. The dynamics for m, t_m, and s are given by (10). Flows are allowed when $x \in C$, and jumps are allowed when $x \in D$, defined by

$$C := \mathbb{R}^{55+n} \times [0, T] \times \{1, 2\} \tag{13}$$

$$D := \mathbb{R}^{55+n} \times \{0\} \times \{1, 2\}. \tag{14}$$

5. Stability

We are analyzing stability of the set

$$\mathcal{A} := C \cap (\{x_{1d}\} \times \{0\} \times \{x_{1d}\} \times \{x_2\} \times \{0\} \times [0, T] \times \{1, 2\}). \tag{15}$$

This corresponds to the vessel tracking the desired trajectory, with $x_{1d} = [0, 0, \eta_d^\top, \nu_d^\top]^\top$, and the controller integral state ζ_s converging to zero. The model-based estimates being equal to the control plant model state x_1, which goes to x_{1d}, and the signal-based estimates being equal to the kinematic model state x_2. The performance monitoring states m go to zero, as discussed around (11), and the timer t_m and the switching signal s stay within $\mathcal{A}$ by design.

Theorem 1. *Under Assumptions (A1–A4) the set $\mathcal{A}$ given by (15) is GAS for the hybrid system given by the control plant model, the observers (3), (5)–(6), the controller (8), the performance monitoring and switching logic (10), and the flow and jump sets (13)–(14).* □

Proof. The proof follows from Goebel et al. (2009), Corollary 19. By splitting the control law (8) into a state feedback part and a part that is due to estimation error, the tracking error dynamics and observer error dynamics can be written in a cascaded structure,

$$\dot{e}_0 = F_0(e_0) + g(e_0, e_s) \tag{16a}$$

$$\dot{e}_1 = F_1(e_1) \tag{16b}$$

$$\dot{e}_2 = F_2(e_2) \tag{16c}$$

$$e_0^+ = e_0,\ e_1^+ = e_1,\ e_2^+ = e_2. \tag{16d}$$

(16a) is the tracking error dynamics with tracking error $e_0 = [\xi^\top, b^\top, (\eta - \eta_d)^\top, (\nu - \nu_d)^\top, \zeta^\top]^\top$ and estimation errors e_s, with $s = 1$ model-based estimation error, and $s = 2$ signal-based estimation error. $g(e_0, e_s)$ is the additional control input due to estimation error, where $g(e_0, e_s) = K_p R^\top(\psi_m^n)(\eta - \hat{\eta}_s) + K_d(\nu - \hat{\nu}_s) + K_i R^\top(\psi_m^n)(\zeta - \zeta_s)$. The switching signal s decides which observer perturbs the tracking error dynamics. (16b), (16c) are the model-based and signal-based estimation error dynamics. The rest of the observer error dynamics are given by (10). The flow and jump sets for (10) and (16) are:

$$C' := \mathbb{R}^{55+n} \times [0, T] \times \{1, 2\} \tag{17}$$

$$D' := \mathbb{R}^{55+n} \times \{0\} \times \{1, 2\}. \tag{18}$$

To prove Theorem 1, it is sufficient to prove global asymptotic stability (GAS) of the set

$$\mathcal{A}' := \{0_{55+n}\} \times [0, T] \times \{1, 2\}, \tag{19}$$

for the hybrid system $\mathcal{H} := (C', F, D', G)$ given by (10) and (16)–(18). This is done in two steps.

Step 1. We prove GAS of $\mathcal{A}'$ for $\mathcal{H}_\beta := (C_\beta, F, D_\beta, G)$, which is $\mathcal{H}$ with the flow and jump sets intersected with $\beta\mathbb{B} \times \mathbb{R}^{37+n}$ for $\beta > 0$ and unit ball $\mathbb{B} \in \mathbb{R}^{18}$; $C_\beta := C' \cap (\beta\mathbb{B} \times \mathbb{R}^{37+n})$ and $D_\beta := D' \cap (\beta\mathbb{B} \times \mathbb{R}^{37+n})$. Firstly, the compact set

$$\mathcal{A}_1 := \{\beta\mathbb{B}\} \times \{0_{37+n}\} \times [0, T] \times \{1, 2\}, \tag{20}$$

is GAS for $\mathcal{H}_\beta$. This follows from the analysis in Bryne et al. (2015), Fossen and Strand (1999) and Grip et al. (2015) resulting in UGES origin of the observer error dynamics (Claims 1 and 2). Then, we prove GAS of $\mathcal{A}'$ for $\mathcal{H}|_{\mathcal{A}_1} := (C' \cap \mathcal{A}_1, F, D' \cap \mathcal{A}_1, G)$. When the solution is in $\mathcal{A}_1$, we have state feedback so that (16a) is $\dot{e}_0 = F_0(e_0)$, since $e_s = 0$, and $g(e_0, 0) = 0$. The analysis in Lindegaard and Fossen (2003) gives UGES origin of the tracking error dynamics with state feedback (Claim 3). Applying Corollary 19 in Goebel et al. (2009), we have that the compact set $\mathcal{A}_1$ is GAS for $\mathcal{H}_\beta$, and that the compact set $\mathcal{A}' \subset \mathcal{A}_1$ is GAS for $\mathcal{H}|_{\mathcal{A}_1}$. Then $\mathcal{A}'$ is GAS for $\mathcal{H}_\beta$.

Step 2. We use this preliminary result to prove GAS of $\mathcal{A}'$ for $\mathcal{H}$ without restrictions on e_0 in the flow and jump sets. The solutions of $\mathcal{H}$ are the solutions of $\mathcal{H}_\beta$ when $e_0 \in \beta\mathbb{B}$. The only thing left to prove is that the basin of attraction is the entire space, so that for each solution, β can be chosen large enough so that the $\beta\mathbb{B}$ intersection has no effect. The observer solutions e_s can be bounded by $\|e_s(t)\| \leq \lambda_1 \|e_s(t_0)\| e^{-\lambda_2(t - t_0)}$ for $\lambda_1, \lambda_2 > 0$ that are dependent on initial condition $e_s(t_0)$. Integrating $e_s(t)$ over time, we get

$$\int_{t_0}^{\infty} \|e_s(t, t_0, e_s(0))\| dt \leq \phi(\|e_s(t_0)\|), \quad \forall t_0 \geq 0,$$

with $\phi(\|e_s(t_0)\|) = \frac{\lambda_1}{\lambda_2}\|e_s(t_0)\|$. $g(e_0, e_s)$ can be bounded in terms of e_s by $\|g(e_0, e_s)\| \leq \gamma \|e_s\|$, $\gamma \geq \|[K_p,\ K_d,\ K_i]^\top\|$. Then, the only state that can grow unbounded is e_0, but this is ruled out by the following. The Lyapunov function $V_0(e_0, \psi)$, defined below Claim 3, for ((16a)) with $g(e_0, e_s) = 0$ and $F_0(e_0) = T^\top(\psi) A_c T(\psi) e_0$ satisfies

$$\left\| \frac{\partial V_0(e_0, \psi)}{\partial e_0} \right\| \|e_0\| \leq c_1 \|e_0\|^2, \quad \forall \|e_0\| \geq \mu \tag{21a}$$

$$\left\| \frac{\partial V_0(e_0, \psi)}{\partial e_0} \right\| \leq c_2, \quad \forall \|e_0\| \leq \mu \tag{21b}$$

[5] A solution with an unbounded time domain is called complete (Goebel et al., 2009, p. 41).

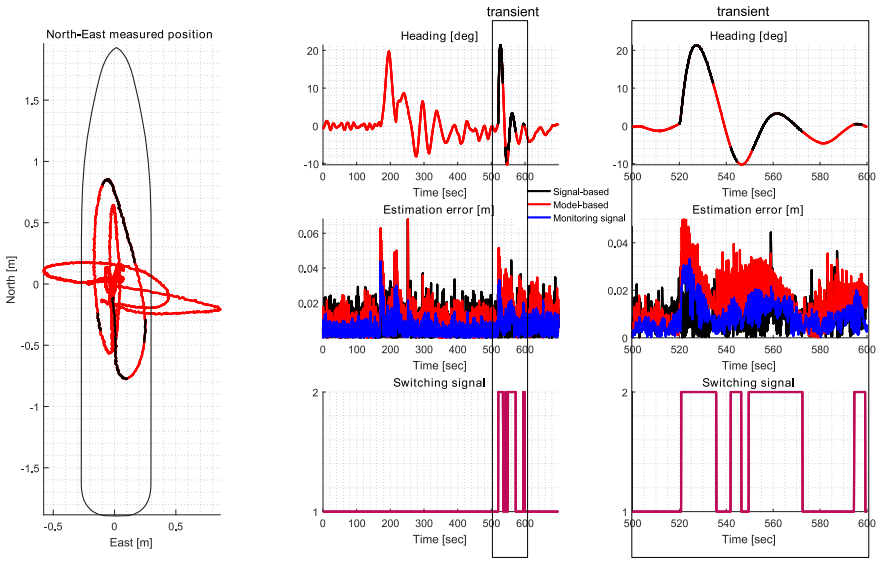

Fig. 2. Closed-loop control: C/S Inocean Cat I Drillship is pushed off position using a boat-hook at time 170 and 520 s. North-East position track (left), heading, estimation error, monitoring signal and switching signal (middle), details of the second transient (right). Position and heading trajectories are red when model-based estimates are used in closed loop, and black for signal-based estimates. Environmental conditions corresponding to rough full-scale sea state with significant wave height $H_s = 3.6$ m, peak period $T_p = 10.4$ s, head sea, no wind nor current, $\epsilon_{tr} = 0.02$, $\epsilon_{ss} = 0.005$, $\delta = 0.05$. (For interpretation of the references to color in this figure legend, the reader is referred to the web version of this article.)

with $c_1 = 2\lambda_{max}(P)$ and $c_2 = 2\lambda_{max}(P)\mu$, with $\lambda_{max}(P)$ being the largest eigenvalue of P. (21b) holds for all headings ψ. (21) ensures that e_0 stays bounded (Loria, Fossen, & Panteley, 2000), so that each solution of $\mathcal{H}$ has to converge to $\mathcal{A}'$ because it is a solution to the system $\mathcal{H}_\beta$ for large enough β and the solutions of $\mathcal{H}_\beta$ converge. Hence, $\mathcal{A}'$ in (19) is GAS for the hybrid system $\mathcal{H}$ given by (10) and (16)–(18), which concludes the proof. □

When applying Assumption (A1) we assume that the control plant model is an exact deterministic model of the real vessel dynamics. Then there may only be switching due to reference changes and due to transients during initialization. However, as shown through experiments in Section 6, switching based on performance is triggered because Assumption (A1) of slowly-varying bias loads does not hold during transients. Performing an analysis of the hybrid system with randomness is a topic for further work, see Teel, Subbaraman, and Sferlazza (2014).

6. Experimental setup, results and discussion

The model-scale experiments were conducted with C/S Inocean Cat I Drillship, a 1:90 scale model with dimensions (length, beam) = (2.578 m, 0.44 m) in the Marine Cybernetics Laboratory (MCLab) at NTNU. The full-scale DP data was collected during the AMOS DP Research Cruise 2016 (ADPRC'16) onboard R/V Gunnerus, see Skjetne et al. (2017) for details. The model-based observer was in both cases tuned using tuning rules in Fossen (2011), Ch. 11, for good steady state, and adequate transient performance. The same IMUs were used to provide input to the signal-based observer both in model-scale and full-scale, showing that the proposed hybrid observer setup is robust to large variations in signal-to-noise ratio. In full-scale, the signal-based observer tuning from (Bryne et al., 2015) was tweaked to work better for R/V Gunnerus, but in the MCLab the tuning was found from scratch. Tuning of the controller in the MCLab was found using standard PID tuning rules (Fossen, 2011, Ch. 12), which were tweaked to work well with both observer estimates in feedback. The algorithms were coded in Matlab/Simulink and run in NI Veristand[6] software.

6.1. Model-scale experiments

Wind loads constitute a lot of the mean forces on the vessel hull, and since wind is not available in the MCLab, the directional dependence of the bias force that is seen in full-scale applications was less prominent in the lab. Hence, switching based on observer performance was triggered by pushing the model off setpoint using a boat-hook, inducing an unknown, rapid transient, see Fig. 2. The model is pushed off setpoint twice; at time 170 and 520 s. In the first transient, the observer is fixed with the model-based observer in closed loop. The vessel spends a long time coming back to the setpoint, since the estimates from the model-based observer (especially the velocity estimate) are off during the transient. In the second transient the observer is allowed to switch based on performance, and chooses the signal-based observer in closed loop for most of the transient, although there is some switching back and forth. The heading reaches steady state somewhat faster when the signal-based observer is in closed loop, *although comparison of the two pushes can be seen only as indications of performance since the conditions were not identical.* Brodtkorb et al. (2016) and the section below compares the model-based observer, signal-based observer and hybrid approach in closed loop and estimation performance on full-scale data, respectively. Switching during heading changes, based on desired yaw rate, worked well in the MCLab. How large δ is chosen should be dependent on the vessel size and the maximum desired yaw rate. The thrust usage when the model-based or the signal-based observer estimates were used in closed loop was not significantly different, though the signal-based estimates made the thrust more oscillatory, as expected.

[6] The Bogacki–Shampine solver (Matlab ode23) was used with fixed step 0.01 s, www.ni.com/veristand/.

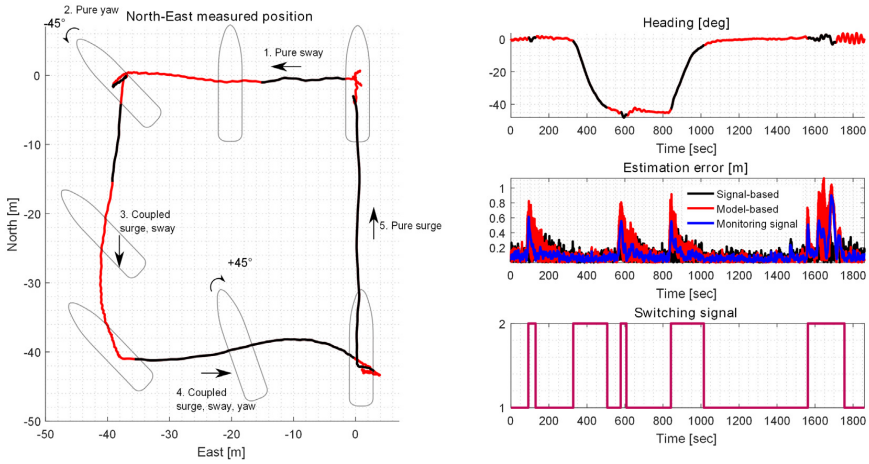

Fig. 3. Estimation: R/V Gunnerus is doing a DP 4 corner maneuver, starting at (0,0) and moving as indicated by the arrows. North-East position track (left), heading, observer estimation error and monitoring signal, and switching signal (right). The position and heading trajectories are red when the model-based estimates should be used in closed loop, and black when the signal-based estimates should be used in closed loop. Environmental conditions: current 0.3 m/s, 290°, wind 7 m/s, 260°, and waves with significant wave height $H_s = 0.2$ m, peak period $T_p = 13.6$ s, and direction 260°. $\epsilon_{tr} = 0.5$, $\epsilon_{ss} = 0.03$, $\delta = 0.2$. (For interpretation of the references to color in this figure legend, the reader is referred to the web version of this article.)

Table 1
Cumulative estimation errors for the model-based, signal-based and hybrid observers at the end of R/V Gunnerus' DP 4 corner maneuver.

Observer	Surge [m]	Sway [m]	Yaw [deg]
Model-based	1368.3	998.0	1372.7
Signal-based	964.3	949.9	902.9
Hybrid	945.1	901.3	1247.3

6.2. Estimation based on full-scale measurements

Fig. 3 shows estimation results on full-scale R/V Gunnerus data from a DP 4 corner maneuver, and that the hybrid observer switches due to transients. If the third and fourth parts of the maneuver were to be done close to other offshore infrastructure, R/V Gunnerus may have been required to either reduce the speed, or choose another control strategy in order to stay on the desired straight-line segments of the square. In the fifth maneuver, a pure surge motion should not induce much transients, however in this dataset the heading oscillates $\pm 3°$, and therefore the signal-based observer is chosen for most of the leg. Depending on the vessel size, propulsion system, and instrumentation, a smarter choice of controller could make the vessel stay on the desired path with a higher speed, reducing the vessel operation time.

Fig. 4 and Table 1 show the cumulative estimation errors over time when the model-based, signal-based and hybrid observers (switching between the model-based and signal-based) are used for estimation on full-scale data. The hybrid observer has the lowest estimation error at the end of the time series in surge and sway, a bit lower than the signal-based observer, and much lower than the model-based observer, which accumulates estimation error fast during transients. The signal-based observer has the smallest estimation error in yaw; 34% lower than the model-based observer, and 28% lower than the hybrid observer. A reason may be that the signal-based observer uses more information about the yaw angle through the yaw rate to construct the estimate. Keep in mind that the maneuver R/V Gunnerus performs in this case includes a lot of transients, and therefore favors the signal-based observer over the model-based observer. In the case where there are more periods of steady state, the model-based observer and hybrid approach are more beneficial.

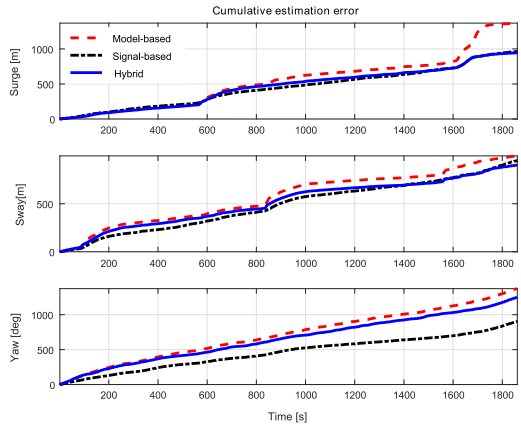

Fig. 4. Cumulative estimation error when the model-based, signal-based and hybrid observers are used for estimation on full scale field data from R/V Gunnerus doing a DP 4-corner maneuver.

7. Conclusion

A general hybrid control strategy for marine control systems providing a redundant design methodology for robustness to system errors was proposed in this paper. An example of a such control system improving the transient vessel response in dynamic positioning was given. Performance was shown through model-scale experiments, and estimation on full-scale field data.

Acknowledgments

Thanks to Vincenzo Calabrò and the rest of the Kongsberg Maritime team, Øivind Kjerstad, Mikkel E. N. Sørensen and Martin Heyn for collaboration during ADPRC'16, and to Torgeir Wahl for assistance in the MCLab.

References

Blanke, M., Kinnaert, M., Lunze, J., & Staroswiecki, M. (2003). *Diagnosis and fault-tolerant control*. Springer.

Brodtkorb, A. H., Værnø, S. A., Teel, A. R., Sørensen, A. J., & Skjetne, R. (2016). Hybrid observer for improved transient performance of a marine vessel in dynamic positioning. *NOLCOS, USA*.

Bryne, T. H., Fossen, T. I., & Johansen, T. A. (2015). A virtual vertical reference concept for GNSS/INS applications at the sea surface. *MCMC, Denmark*.

DNV-GL (2014). *DNV rules for classification of ships, part 6, Ch. 6.*. DNV-GL service documents.

Fossen, T. I. (2011). *Handbook of marine craft hydrodyamics and motion control*. Wiley.

Fossen, T. I., & Strand, J. P. (1999). Passive nonlinear observer design for ships using lyapunov methods: Full-scale experiments with a supply vessel. *Automatica*, *35*(1), 3–16.

Girard, A. R., Howell, A. S., & Hedrick, J. K. (2005). Hybrid supervisory control for real-time embedded bus rapid transit applications. *IEEE Transactions on Vehicular Technology*, *54*(5), 1684–1696. http://dx.doi.org/10.1109/TVT.2005.853466.

Godhaven, J. M. (1998). Adaptive tuning of heave filter in motion sensor. In *OCEANS '98 conference proceedings, volume 1* (pp. 174–178), http://dx.doi.org/10.1109/OCEANS.1998.725731.

Goebel, R., Sanfelice, R., & Teel, A. R. (2009). Hybrid dynamical systems robust stability and control for systems that combine continuous-time and discrete-time dynamics. *IEEE Control Systems Magazine*, 28–93.

Goebel, R., Sanfelice, R. G., & Teel, A. R. (2012). *Hybrid dynamical systems, modelling, stability and robustness*. Princeton University Press.

Grip, H. F., Fossen, T. I., Johansen, T. A., & Saberi, A. (2015). Globally exponentially stable attitude and gyro bias estimation with application to GNSS/INS integration. *Automatica*, 158–166.

Hassani, V., Sørensen, A. J., Pascoal, A. M., & Athans, M. (2017). Robust dynamic positioning of offshore vessels using mixed- synthesis modeling, design, and practice. *Ocean Engineering*, *129*, 389–400.

Hassani, V., Sørensen, A. J., Pascoal, A. M., & Dong, N. T. (2012). Multiple model adaptive dynamic positioning. In *{IFAC} conference on manoeuvring and control of marine craft, Vol. 45*, 27 (pp. 55–60).

Hespanha, J. P., Liberzon, D., & Morse, A. S. (2003). Hysteresis-based switching algorithms for supervisory control of uncertain systems. *Automatica*, *39*(2), 263–272.

Hespanha, J. P., & Morse, A. S. (2002). Switching between stabilizing controllers. *Automatica*, *38*(11), 1905–1917.

Hu, J., Prandini, M., & Sastry, S. (2005). Aircraft conflict prediction in the presence of a spatially correlated wind field. *IEEE Transactions on Intelligent Transportation Systems*, *6*(3), 326–340. http://dx.doi.org/10.1109/TITS.2005.853699.

Kapinski, J., Deshmukh, J. V., Jin, X., Ito, H., & Butts, K. (2016). Simulation-based approaches for verification of embedded control systems: An overview of traditional and advanced modeling, testing, and verification techniques. *IEEE Control Systems*, *36*(6), 45–64. http://dx.doi.org/10.1109/MCS.2016.2602089.

Lindegaard, K. P., & Fossen, T. I. (2003). Fuel-efficient rudder and propeller control allocation for marine craft: experiments with a model ship. *IEEE Transactions on Control Systems Technology*, *11*(6), 850–862.

Loria, A., Fossen, T. I., & Panteley, E. (2000). A separation principle for dynamic positioning of ships: Theoretical and experimental results. *IEEE TCST*, *8*(2), 332–343.

Malladi, B. P., Sanfelice, R. G., Butcher, E., & Wang, J. (2016). Robust hybrid supervisory control for rendezvous and docking of a spacecraft. In *2016 IEEE 55th conference on decision and control* (pp. 3325–3330), http://dx.doi.org/10.1109/CDC.2016.7798769.

Miyazaki, M. R., Sørensen, A. J., & Vartdal, B. J. (2016). Reduction of fuel consumption on hybrid marine power plants by strategic loading with energy storage devices. *IEEE Power and Energy Technology Systems Journal*, *3*(4), 207–217.

Nguyen, T. D., Sørensen, A. J., & Quek, S. T. (2007). Design of hybrid controller for dynamic positioning from calm to extreme sea conditions. *Automatica*, *43*(5), 768–785.

Perez, T., Sørensen, A., & Blanke, M. (2006). Marine vessel models in changing operational conditionsa tutorial. In *14th IFAC symposium on identification and system parameter estimation, IFAC proceedings volumes, Vol. 39*, 1, (pp. 309–314) doi: http://dx.doi.org/10.3182/20060329-3-AU-2901.00044.

Sastry, S., Meyer, G., Tomlin, C., Lygeros, J., Godbole, D., & Pappas, G. (1995). Hybrid control in air traffic management systems. In *Proceedings of 1995 34th IEEE conference on decision and control, Vol. 2* (pp. 1478–1483).

Skjetne, R., Kjerstad, Ø. K., Værnø, S. A. T., Brodtkorb, A. H., Sørensen, A. J., & Sørensen, M. E. N. et al., (2017). AMOS DP Research Campain. *OMAE, Norway*.

Smogeli, Ø., Vik, B., Haugen, O., & Pivano, L. (2014). Risk management for control system software for the maritime and offshore oil and gas industries. In *Proceedings of the IMCA annual seminar, London*.

Sørensen, A. J. (2011). A survey of dynamic positioning control systems. *Annual Reviews in Control*, *35*(1), 123–136.

Teel, A. R., Subbaraman, A., & Sferlazza, A. (2014). Stability analysis for stochastic hybrid systems: A survey. *Automatica*, *50*(10), 2435–2456.

Astrid H. Brodtkorb received her M.Sc. degree in Marine Technology at the Norwegian University of Science and Technology (NTNU) in Trondheim in 2014. She received her Ph.D. degree in Marine Control Systems at the Norwegian Centre of Excellence Autonomous Marine Operations and Systems (NTNU AMOS) in 2017. Her main research interests are hybrid control theory, observers, and sea state estimation applied to dynamic positioning (DP) systems for marine vessels.

Svenn Are Værnø was born in Norway in 1990. He received his M.Sc. degree in marine technology from the Norwegian University of Science and Technology, Trondheim, Norway, in 2014, where he is currently pursuing his Ph.D. degree with the Norwegian Centre of Excellence Autonomous Marine Operations and Systems (NTNU AMOS). His research include marine motion control systems and dynamic positioning.

Andrew R. Teel received his A.B. degree in Engineering Sciences from Dartmouth College in Hanover, New Hampshire, in 1987, and his M.S. and Ph.D. degrees in Electrical Engineering from the University of California, Berkeley, in 1989 and 1992, respectively. After receiving his Ph.D., he was a postdoctoral fellow at the Ecole des Mines de Paris in Fontainebleau, France. In 1992 he joined the faculty of the Electrical Engineering Department at the University of Minnesota, where he was an assistant professor until 1997. Subsequently, he joined the faculty of the Electrical and Computer Engineering Department at the University of California, Santa Barbara, where he is currently a Distinguished Professor and Director of the Center for Control, Dynamical systems, and Computation. His research interests are in nonlinear and hybrid dynamical systems, with a focus on stability analysis and control design. He has received NSF Research Initiation and CAREER Awards, the 1998 IEEE Leon K. Kirchmayer Prize Paper Award, the 1998 George S. Axelby Outstanding Paper Award, and was the recipient of the first SIAM Control and Systems Theory Prize in 1998. He was the recipient of the 1999 Donald P. Eckman Award and the 2001 O. Hugo Schuck Best Paper Award, both given by the American Automatic Control Council, and also received the 2010 IEEE Control Systems Magazine Outstanding Paper Award. In 2016, he received the Certificate of Excellent Achievements from the IFAC Technical Committee on Nonlinear Control Systems. He is Editor-in-Chief for Automatica, and a Fellow of the IEEE and of IFAC.

Asgeir J. Sørensen obtained M.Sc. degree in Marine Technology in 1988 at NTNU, and Ph.D. degree in Engineering Cybernetics at NTNU in 1993. Sørensen has more than 15 years of industrial experience from ABB and Marine Cybernetics (DNV GL). Since 1999 Sørensen has held the position of Professor of Marine Control Systems at the Department of Marine Technology, NTNU. He is currently acting as key scientist and the Director of the Centre for Autonomous Marine Operations and Systems (NTNU AMOS).

Roger Skjetne received his M.Sc. degree in 2000 from the University of California at Santa Barbara (UCSB) and his Ph.D. degree in 2005 from the Norwegian University of Science and Technology (NTNU) on control engineering. He holds an Exxon Mobil prize for his Ph.D. thesis at NTNU. Prior to his studies, he worked as a certified electrician for Aker Elektro AS on numerous oil installations for the North Sea, and in 2004–2009 he was employed in Marine Cybernetics AS, working on Hardware-In-the-Loop simulation for testing marine control systems. From August 2009 he has held the Kongsberg Maritime chair of Professor in Marine Control Engineering at the Department of Marine Technology at NTNU. His research interests are within dynamic positioning of marine vessels, Arctic stationkeeping and Ice Management systems, control of shipboard hybrid electric power systems, nonlinear motion control of marine vehicles, and autonomous marine robots. Presently, Roger Skjetne is leader of the ice management work

package in the CRI Sustainable Arctic Marine and Coastal Technology (SAMCoT), associated researcher in the CoE Centre for Ships and Ocean Structures (CeSOS) and CoE Autonomous Marine Operations and Systems (NTNU AMOS), principal researcher in the CRI on Marine Operations (MOVE), and he was project manager of the KMB Arctic DP research project. In 2017–2018, he is a visiting research scholar at the Center for Control, Dynamical-systems and Computation (CCDC) at UCSB. He is also co-founder of the two companies BluEye Robotics AS and Arctic Integrated Solutions AS.

J.4

Compensation of bias loads in dynamic positioning of marine surface vessels

---

Værnø, S. A., Brodtkorb, A. H., Skjetne, R.

Ocean Engineering 178 (2019) 484–492

Contents lists available at ScienceDirect

Ocean Engineering

journal homepage: www.elsevier.com/locate/oceaneng

Compensation of bias loads in dynamic positioning of marine surface vessels

Svenn A. Værnø*, Astrid H. Brodtkorb, Roger Skjetne

Department of Marine Technology, Norwegian University of Science and Technology, 7052, Trondheim, Norway

ARTICLE INFO

Keywords:
Dynamic positioning
Control design
Observers
Integral control

ABSTRACT

This paper investigates different methods for compensating the mean and slowly varying environmental loads, and unmodeled dynamics (bias loads) in dynamic positioning of marine vessels. Four different methods are compared; using the bias estimate from an observer tuned to estimate position and velocity well, using a wave-filtered version of this bias load, using the estimate from a separate observer tuned to work well for estimating the bias loads, and finally traditional integral action on the tracking errors. The results show that the bias from the bias observer is the best solution, both in transients and steady state. Standard integral action matches the steady state performance, but is slower in transients. The estimate from the observer used for position and velocity is fast in transients, but too oscillatory in the bias state. The wave-filtered version of this has less oscillations, but falls short compared to the other methods due to added phase lag from the extra wave filter. Using a bias estimate from an observer has benefits over typical integral action, such as the possibility of offline or open-loop tuning and avoiding integral windup issues. For the comparison study, a 6 DOF simulation model of a supply vessel is used.

1. Introduction

In control systems for dynamic positioning (DP) of marine vessels it is common to include integral action to compensate for the mean and slowly varying environmental disturbances and unmodeled dynamics. When using a model-based observer, the sum of the environmental disturbances and unmodeled dynamics is estimated in what is typically called a bias load (Fossen and Strand, 1999). Use of this bias load estimate in feedback instead of integral action has been proposed by Loria et al. (2000). However, for output feedback designs it is common in the literature (Sørensen, 2011) to include integral action in the controller even though this load is estimated in the observer. One reason for this could be the assumption that the bias estimate from the observer is too oscillatory to give good performance when used in feedback. Integral action is therefore introduced and tuned such that it is slow, calm (small oscillations), and works well in steady state.

Recently, however, there have been much focus on DP during transient conditions, e.g. due to sudden large wave trains, ice loads, frequent setpoint changes, etc., and the question has been asked if a slow integral action is suitable. As seen for instance in Refsnes and Sørensen (2007), Værnø et al. (2016), Værnø et al. (2017), Kjerstad and Skjetne (2016), Lindegaard (2003), and as discussed in Brodtkorb et al. (2016) and in Brodtkorb et al. (2018), the bias load can vary rapidly, even for common situations such as heading changes. In these instances, effective compensation of the bias load is beneficial. In the following we compare four different approaches for compensating the bias loads, with special focus on transient events. This problem received some attention by Værnø et al. (2016), but here the discussion is more rigorous.

A typical DP system is evaluated through numerical studies and model-scale experiments in Tannuri and Morishita (2006), and a model-based Kalman filter is presented for DP by Fossen and Perez (2009), initially proposed by Balchen et al. (1976). A robust controller presented by Du et al. (2015) uses a high-gain observer, in addition to neural networks to compensate for the unknown environmental disturbances. Typically, fault tolerance and robustness are system design properties that are considered (Blanke et al., 2003). For an overview of the DP system and a historical overview, see Sørensen (2011) and the references therein.

In this paper we refer to the bias compensation by a term $\hat{b}$ in the control law, where $\hat{b}$ is the estimated bias in an observer. Integral action, on the other hand, refers to an integral term ζ in the control law with $\dot{\zeta} = \hat{\eta} - \eta_d(t)$, that is, it integrates the tracking error based on the estimated vessel state $\hat{\eta}$.

Using the bias estimate from a model-based observer instead of typical integral action on the output tracking errors has some benefits. First, if we use the bias estimate from an observer instead of integral action, windup issues in the integrator are of no concern. However, it

* Corresponding author.
E-mail addresses: svenn.are.varno@ntnu.no (S.A. Værnø), astrid.h.brodtkorb@ntnu.no (A.H. Brodtkorb), roger.skjetne@ntnu.no (R. Skjetne).

https://doi.org/10.1016/j.oceaneng.2019.03.010
Received 14 June 2018; Received in revised form 19 January 2019; Accepted 4 March 2019

should be noted that if a separate observer is added to estimate the bias load, this adds similar complexity as an anti-windup filter in the controller (Perez, 2009). Another benefit of using a bias estimate from an observer is tuning. It is easier to tune an observer since you only need offline data series. In addition you can use optimization methods to find satisfactory gains. An advantage of using the integral action is that it can be tuned independently of the bias response time. This means, for instance, that the integral action can be tuned slow to account for steady-state offsets, whereas the bias estimate in the observer can be made faster and letting it live its own life. This tuning separation also applies if there is a separate observer to estimate the bias load.

The main contribution of this paper is an in-depth study into several best practices of compensating the unknown environmental loads and unmodeled dynamics for DP of marine vessels. The analysis of performance is made fair by the use of optimization in tuning of all observers, and also a thorough tuning of controller and integral action. The results are demonstrated through a high-fidelity simulation study. To the authors' knowledge, such a comparison does not exist in the literature. This study is important, as it allows for research-based design choices to be made when developing DP control systems.

Notation and terminology: A column vector is stated as $\text{col}(x, y, z) := [x^\top, y^\top, z^\top]^\top$, $\mathbb{R}_{>0}$ denotes positive real numbers, and $\mathbb{S}$ represents the angle defined on the interval $[-\pi, \pi)$.

2. Problem formulation

There are two reference frames typically used for DP; the North-East-Down (NED)-frame and body-frame. For operations in confined areas (such as DP) the NED-frame can be assumed to be a non-rotating global and inertial frame. This is a tangent plane to the Earth, with the x-axis pointing North, y-axis pointing East, and z-axis pointing down to the center of the Earth. The body-frame is a local frame with origin typically midships, in the centerline, and waterline of the vessel, with the x-axis pointing to the bow, y-axis to starboard, and z-axis down.

We separate between a *simulation verification model (SVM)* and a *control design model (CDM)*. The SVM is intended for observer and controller verification, and is a high-fidelity model. The CDM includes the dynamics that is most important for the operation. For low-speed application such as DP, this typically implies that the Coriolis, centripetal, and nonlinear damping loads are omitted from the model. As shown by Værnø et al. (2019), including nonlinear damping gives a slight improvement. However, because the improvement is not significant, and because it is not important for this study, it is not included in the CDM of this paper.

2.1. Control design model

We consider the 3 degrees of freedom (DOF) CDM (Fossen, 2011),

$$\dot{\xi} = A_w \xi + E_w w_w \tag{1a}$$

$$\dot{\eta} = R(\psi)\nu \tag{1b}$$

$$\dot{b} = w_b \tag{1c}$$

$$M\dot{\nu} = -D\nu + R(\psi)^\top b + \tau + \tau_{wind} \tag{1d}$$

$$y = \eta + C_w \xi + v_y, \tag{1e}$$

where $\xi \in \mathbb{R}^6$ in (1a) is the first order wave-induced dynamics of the vessel, and (1b)-(1d) is the low-frequency vessel dynamics. The first-order wave-induced dynamics makes the vessel oscillate about the setpoint at the wave frequency. Compensating this oscillatory motion causes extra wear and tear on the thrusters, and it is often not possible due to thruster limitations. For both of these reasons, we separate between the low-frequency and wave-frequency dynamics. The wave-frequency dynamics ξ in (1a) are modeled by a mass-spring-damper dynamics, where A_w is a Hurwitz matrix that contains the damping ratio and the peak frequency of the incident waves, and $w_w \in \mathbb{R}^6$ is white noise (Sørensen, 2013). The vector $\eta := \text{col}(\eta_N, \eta_E, \psi) \in \mathbb{R}^2 \times \mathbb{S}$ in (1b) contains the low-frequency North/East position, and heading, respectively, and $\nu := \text{col}(u, v, r) \in \mathbb{R}^3$ is the surge/sway velocity in the body-frame, and the yaw rate, respectively. The rotation matrix $R(\psi)$ rotates a 3 DOF vector from the body to the NED-frame according to

$$R(\psi) = \begin{bmatrix} \cos(\psi) & -\sin(\psi) & 0 \\ \sin(\psi) & \cos(\psi) & 0 \\ 0 & 0 & 1 \end{bmatrix}. \tag{2}$$

$\tau := \text{col}(\tau_{surge}, \tau_{sway}, \tau_{yaw}) \in \mathbb{R}^3$ is the generalized control vector in the body-frame, $\tau_{wind} \in \mathbb{R}^3$ is the wind load, which is measured, and $b := \text{col}(b_N, b_E, b_\psi) \in \mathbb{R}^3$ is the bias load vector, and $w_b \in \mathbb{R}^3$ is white noise. The vector b constitutes the sum of the low-frequency loads, such as the slowly-varying second-order wave loads, current loads, and unmodeled dynamics from errors in the mass, added mass, hydrodynamic damping, wind loads, and thrust mappings. The bias load vector is assumed constant (or slowly-varying) in the NED-frame. Finally, the measurement vector y is the sum of low-frequency North/East position and heading η, the wave-frequency North/East position and heading $C_w\xi$, where $C_\omega = [0_{3\times3} \;\; I_{3\times3}]$, and the measurement noise $v_y \in \mathbb{R}^3$.

2.2. Model-based observer

To estimate the low-frequency position η, velocity ν, and the bias b, a nonlinear observer (NLO) similar to the observer proposed by Fossen and Strand (1999) is chosen. The observer is given by

$$\dot{\hat{\xi}} = A_w \hat{\xi} + K_1 \tilde{y} \tag{3a}$$

$$\dot{\hat{\eta}} = R(\psi)\hat{\nu} + K_2 \tilde{y} \tag{3b}$$

$$\dot{\hat{b}} = K_3 \tilde{y} \tag{3c}$$

$$M\dot{\hat{\nu}} = -D\hat{\nu} + R(\psi)^\top \hat{b} + \tau + \tau_{wind} + K_4 R(\psi)^\top \tilde{y} \tag{3d}$$

$$\hat{y} = \hat{\eta} + C_w \hat{\xi}, \tag{3e}$$

where $\hat{\xi} \in \mathbb{R}^6$, $\hat{\eta} \in \mathbb{R}^2 \times \mathbb{S}$, $\hat{b} \in \mathbb{R}^3$, and $\hat{\nu} \in \mathbb{R}^3$ are the state estimates. The injection gains $K_1 = [K_{11}^\top \;\; K_{12}^\top]^\top \in \mathbb{R}^{6\times3}$, K_2, K_3, $K_4 \in \mathbb{R}^{3\times3}$ are non-negative matrices, and $\tilde{y} = y - \hat{y}$ is the measurement error. The matrices K_3 and K_4 are constant, whereas K_1 and K_2 depend on the peak frequency of the wave spectrum to obtain good wave-filtering. As in (Fossen and Strand, 1999) and many later references, we assume that:

(A1) $R(\psi^m) \approx R(\psi + \psi_w) \approx R(\psi)$. First, because of the low noise on the compass, we assume that the measured heading angle ψ^m is close to the real heading angle, that is, the sum of the low-frequency heading ψ and the wave-frequency heading ψ_w. Second, the heading angle due to wave-induced motion, ψ_w is small (negligible effect on the rotation matrix).

The assumption is justified because the wave-induced heading angle is typically less than 1° for normal sea states, and less than 5° for extreme sea states. Thus, the measured heading angle is used instead of the low-frequency heading angle in the rotation matrix.

2.3. Controller

The controller τ is given by a feedback part τ_{FB} and a reference feedforward part τ_{FF},

$$\tau = \tau_{FB} + \tau_{FF} \tag{4a}$$

$$\tau_{FF} = D\nu_d(t) + M\dot{\nu}_d(t) - \tau_{wind} \tag{4b}$$

$$\tau_{FB} = \tau_{nPD} + \tau_{BR}, \tag{4c}$$

where τ_{nPD} is a nonlinear proportional-derivative (nPD) controller given by

$$\tau_{nPD} = -K_p R(\psi)^\top(\hat{\eta} - \eta_d(t)) - K_d(\hat{\nu} - \nu_d(t)), \tag{4d}$$

and $\eta_d \in \mathbb{R}^2 \times \mathbb{S}$, $\nu_d \in \mathbb{R}^3$, and $\dot{\nu}_d(t) \in \mathbb{R}^3$ are bounded references generated by a guidance system, $K_p \in \mathbb{R}^{3\times3}$ and $K_d \in \mathbb{R}^{3\times3}$ are positive definite gain matrices, and τ_{BR} is a bias rejection term to compensate for $R(\psi)^\top b$ in (1d). Designs for τ_{BR} is the main focus of this paper and will be elaborated in Section 2.4.

2.4. Methods for bias compensation

In the following, four methods for compensating the bias load, τ_{BR} in (4c), are presented:

- Method 1: Direct compensation
- Method 2: Wave-filtered bias estimate
- Method 3: Separate bias observer
- Method 4: Integral action.

All the methods use estimates of η and ν from the same observer in the nPD-controller, called the *position and velocity observer*, based on (3). In order to obtain meaningful results in the comparison of different versions of τ_{BR}, it is important that the observer that provides the estimates of η and ν, as well as the nPD-controller are well tuned. Details about the tuning for position and velocity observer, the nPD-controller, and the bias compensation methods are presented in Section 4.4.

2.4.1. Method 1: Direct compensation

The first method we consider, common in the literature (Loría and Panteley, 1999), is to directly use the bias estimate from the position and velocity observer based on (3), tuned for good η and ν estimates, that is,

$$\tau_{BR} = R(\psi)^\top \hat{b}. \tag{5}$$

2.4.2. Method 2: Wave-filtered bias estimate

When we optimize the observer to work well for position and velocity in transients, we observe that the bias estimate is fast, but very oscillatory in steady state. This is elaborated in Section 4.2. By assumption, the bias load b from (3) is low-frequency, but for sufficiently high tuning of the observer (3) the bias estimate will oscillate due to wave-induced behavior. Therefore, we suggest to add an extra wave filter on the bias estimate before this is sent to the controller.

For this method we make the assumption that the bias load contains a wave-component in addition to the low-frequency part that we want to compensate. Accordingly, we redefine the bias load in (1c) to

$$b := b_{lf} + C_w b_w, \tag{6}$$

where $C_w b_w \in \mathbb{R}^3$ and $b_{lf} \in \mathbb{R}^3$ are the wave-frequency and low-frequency components of the bias load from (1c), respectively.

In the bias wave-filter we treat the bias estimate $\hat{b}$ from the observer (3) as the input to the filter and assume that:

(A2) The bias estimate $\hat{b}$ from (3c) is given as $\hat{b} := b_{lf} + C_w b_w$.

The model used for the bias dynamics has the same wave dynamics as in (3a), where

$$\dot{b}_w = A_w b_w + E_w w_{bw} \tag{7a}$$

$$\dot{b}_{lf} = 0 \tag{7b}$$

and the observer is given as

$$\dot{\hat{b}}_w = A_w \hat{b}_w + K_{b,1}(\omega_0)\tilde{b} \tag{8a}$$

$$\dot{\hat{b}}_{lf} = K_{b,2}\tilde{b} \tag{8b}$$

$$\hat{b}_2 = \hat{b}_{lf} + C_w \hat{b}_w \tag{8c}$$

where $\tilde{b} := \hat{b} - \hat{b}_2$. The low-frequency estimate of the bias is used in feedback, such that τ_{BR} is given as

$$\tau_{BR} = R(\psi)^\top \hat{b}_{lf}. \tag{9}$$

2.4.3. Method 3: Separate bias observer

The third bias compensation method is to use the bias estimate from a separate observer with the same structure as in (3), but with a tuning optimized to find a bias estimate that closely resembles the true low-frequency bias load.

Let us denote the estimate from this bias observer as $\hat{b}_{BO}$, and then τ_{BR} is given as

$$\tau_{BR} = R(\psi)^\top \hat{b}_{BO}. \tag{10}$$

2.4.4. Method 4: Integral action

The last method we consider is perhaps the most common choice for τ_{BR}, and that is integral action in the control law (Sørensen, 2011). A new integral state ζ is defined with dynamics

$$\dot{\zeta} = \hat{\eta} - \eta_d(t), \tag{11}$$

such that

$$\tau_{BR} = -K_i R(\psi)^\top \zeta. \tag{12}$$

2.5. Problem statement

We consider both the case where the bias b is slowly-varying for long periods of time, and also the case when b changes rapidly due to transient events. The objective is to compare the four different model-based approaches for τ_{BR} to compensate the bias loads, in order to gain insight on the efficiency of the methods and make conclusions on when the best overall closed-loop performance is obtained. The comparisons will be based on closed-loop key performance indicators (KPIs) that measure the low-frequency positioning performance and thrust utilization.

3. Setup and implementation

To test the different bias compensation methods, an SVM is used along with two different test maneuvers that include a combination of transients and longer periods of steady state.

3.1. Simulation verification model

The simulation model is a 6 DOF high-fidelity model of a platform supply vessel, with main parameters given in Table 1. The model is based on building blocks from the MSS Toolbox (Fossen and Perez, 2004), and includes Coriolis, centripetal forces, and linear and nonlinear damping; see Appendix A. To give a realistic load variation with heading angle of the vessel, lookup tables are used to calculate the loads acting on the vessel. The model is subject to waves from a sea state taken from the JONSWAP[1] spectrum, with a significant wave height of 6 m, and a peak frequency of 0.53 rad/s. The mean incident wave direction is 190° (head waves) in the North/East frame (Price and Bishop, 1974). The simulation also includes a current with a speed of 0.5 m/s and direction of 30°. The sensor models include realistic noise and sensor effects. The GPS is updated at 1 Hz, and the compass is updated at 10 Hz. The vessel is controlled by (4), which operates at 1 Hz. In addition, a first order lowpass thrust dynamics with a 5 s time constant is included.

[1] Joint North Sea Wave Project.

Table 1
Simulation, platform supply vessel, main parameters.

Parameters	Value
Length between perp.	80 m
Breadth	17.4 m
Draft	5.6 m
Displacement	6150 tons

3.2. Maneuvers

For the simulations presented in Section 5, two maneuvers are performed, both with the environmental conditions described in Section 3.1 above. One training maneuver, which is used to tune the observers and controller, and one test maneuver that uses the same tuning. This is to verify that the tuning is not an overfit to the training maneuver.

Both maneuvers are 1500 s in duration. For the training maneuver there is a combined North/East setpoint change and heading change of 90° at 300 s, and at 600 s there is a change of 45° in the direction of the current. The current direction changes as a first order filtered step response with time constant of 30 s. This is an exaggerated case, not necessarily very realistic, designed to challenge the algorithms. This gives three transient events for a short time frame, and about the last half of the maneuver, the conditions are steady, in order to compare the steady state performance as well. The test maneuver has a combined North/East setpoint and heading change at 300 s, where the heading changes 70°, and at 500 s there is also a combined setpoint and heading change with a heading change of 50°. Finally, at 800 s there is a pure heading change of 90°.

3.3. Closed-loop performance evaluation

To evaluate the closed-loop positioning performance of the algorithms, combinations of the following metrics are used,

$$J^c_{\tilde{\eta}} = \int_{t_0}^{t_f} \left\{ |\eta_N - \eta_{d,N}| + |\eta_E - \eta_{d,E}| + \frac{180}{\pi}|\psi - \psi_d| \right\} dt \tag{13a}$$

$$J^c_{\tau,uv} = \int_{t_0}^{t_f} \left\{ |\tau_{surge}| + |\tau_{sway}| dt \right. \tag{13b}$$

$$J^c_{\tau,r} = \int_{t_0}^{t_f} |\tau_{yaw}| dt, \tag{13c}$$

where the states and the elements of τ are defined in (1), and t_0 and t_f are the initial and final time of the interval. $J^c_{\tilde{\eta}}$ is a positioning performance metric, whereas $J^c_{\tau,uv}$ and $J^c_{\tau,r}$ are control effort metrics.

4. Tuning

In this section the tuning for the observers, nPD-controller and the bias compensation methods are presented. The maneuver used in the tuning is the training maneuver described in Section 3.2.

4.1. Derivative free optimization for tuning

In order to allow for a fair comparison of the bias compensation methods, optimization is used to find observer tuning. Classic optimization methods are not applicable due to a lack of information about the gradient, Hessian, or higher order derivatives. Thus, derivative free optimization (DFO) is used, specifically the MATLAB® function *fminsearch*.

To illustrate how DFO works, consider the example where we have one state variable $x \in \mathbb{R}$ where the objective is to minimize the error $\tilde{x} = x - \hat{x}$, and $\hat{x}$ is our state estimate. The observer has an injection gain $K \in \mathbb{R}$, and we select a cost function that depends on the injection gain and the time of the interval $J(K, t_{int})$, where $t_{int} = t_f - t_0$, and t_f and t_0 are the final and initial time of the interval. We initialize the DFO by selecting an initial guess for K, and the DFO evaluates the cost of J. Thereafter, the DFO algorithm selects values close to the initial K value to see if they provide a lower cost for J. It then selects the K that gave the lowest value and repeats the process. Note that the DFO can get stuck in a local minimum, so several runs with varying initial conditions have to be performed.

The different observer performance evaluations metrics used in this paper are

$$J_{\tilde{\eta}} = \int_{t_0}^{t_f} \left\{ |\eta_N - \hat{\eta}_N| + |\eta_E - \hat{\eta}_E| + \frac{180}{\pi}|\psi - \hat{\psi}| \right\} dt \tag{14a}$$

$$J_{\tilde{\nu}} = \int_{t_0}^{t_f} \left\{ |u - \hat{u}| + |v - \hat{v}| + \frac{180}{\pi}|r - \hat{r}| \right\} dt \tag{14b}$$

$$J_{\tilde{b}_N} = \int_{t_0}^{t_f} |b_N - \hat{b}_N| dt \tag{14c}$$

$$J_{\tilde{b}_E} = \int_{t_0}^{t_f} |b_E - \hat{b}_E| dt \tag{14d}$$

$$J_{\tilde{b}_\psi} = \int_{t_0}^{t_f} |b_\psi - \hat{b}_\psi| dt, \tag{14e}$$

where the states are defined in (1) and the estimates in (3).

4.2. Tuning of position and velocity observer

The injection gains K_1 and K_2 in (3) for the wave and η-dynamics are found by the tuning rules proposed by Fossen and Strand (1999), which give good wave-filtering. The tuning for K_3 and K_4 is optimized for finding good η and ν estimates, and is found by derivative free optimization. The corresponding cost function J used in the DFO is then

$$J = J_{\tilde{\eta}} + c_\nu J_{\tilde{\nu}}, \tag{15}$$

where $J_{\tilde{\eta}}$ and $J_{\tilde{\nu}}$ are given by (14a) and (14b), and $c_\nu \in \mathbb{R}_{>0}$ is a scaling parameter set such that the contributions from the velocity estimation error $c_\nu J_{\tilde{\nu}}$ and the position estimation errors are balanced. The value we used was $c_\nu = 7$. The vessel is controlled by (4) using state estimates together with the integral action (11)–(12). The tuning of the observer is found in several iterations, and for each iteration the observer tuning is updated with the resulting DFO tuning from the previous run. Thereafter, a new closed-loop run was performed, serving as the dataset of the next round of DFO runs, until the observer tuning converged.

The resulting bias estimate from the observer tuned with (15), along with the actual bias load found by solving for b in (1d), are shown in Fig. 1. Note that the bias estimate tracks the actual mean bias load well, but since the bias estimation is not part of the evaluation function (15) it is quite oscillatory in steady state.

4.3. nPD-controller tuning

The tuning for the nonlinear PD-controller is given by the tuning rules outlined in Fossen (2011) by specifying desired eigenfrequencies and damping ratios of the response, as if the system is linear, that is, by setting the rotation matrix to identity. Thereafter, the tuning is adjusted through trial and error using the well-tuned η and ν estimates from the position and velocity observer.

4.4. Tuning of the bias compensation methods

4.4.1. Tuning method 1: direct compensation

The tuning of Method 1 is given by the tuning of the position and velocity observer as outlined in Section 4.2. No further tuning is needed.

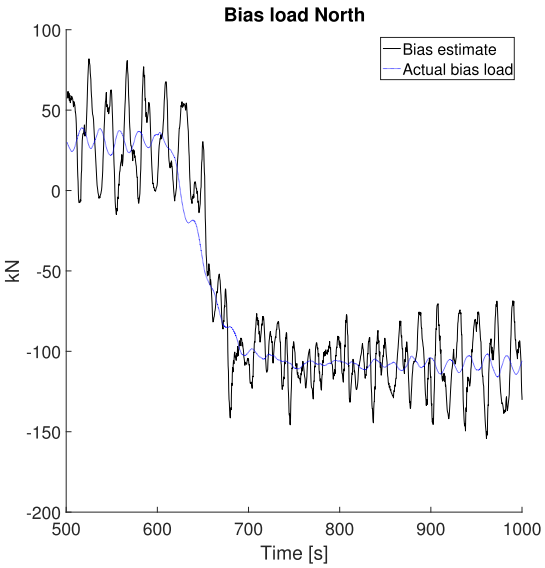

Fig. 1. Bias estimate from the position and velocity observer and the true bias load in the North direction.

4.4.2. Tuning method 2: wave-filtered bias estimate

Method 2 uses the bias estimate $\hat{b}$ from the position and velocity observer in Section 4.2 as input, that is, the bias estimate used in Method 1. The tuning of the matrices K_{b1} and K_{b2} in the wave filter of (8) are found by the tuning rules proposed by Fossen and Strand (1999). That is, K_{b1} and K_{b2} are similar to K_1 and K_2 in (3), respectively.

4.4.3. Tuning method 3: bias observer

For Method 3 the cost function J_{BO} used in the DFO is

$$J_{BO} = c_{b_N} J_{\hat{b}_E} + c_{b_E} J_{\hat{b}_N} + c_{b_\psi} J_{\hat{b}_\psi} \tag{16}$$

where $J_{\hat{b}_N}$, $J_{\hat{b}_E}$, and $J_{\hat{b}_\psi}$ are given by (14c)-(14e), and c_{b_N}, c_{b_E}, $c_{b_\psi} \in \mathbb{R}_{>0}$ are scaling parameters to balance the contributions from the three bias terms. The values used were $c_{b_N} = 0.587$, $c_{b_E} = 1$, and $c_{b_\psi} = 0.055$. This is to make the observer equally responsive to all the three bias forces. For instance, in the training dataset, the North bias force is larger than the East bias force over the maneuver. An equal weighting with $c_{b_N} = c_{b_E}$ would have made the observer more aggressive in observing the North bias. With the chosen weights this is avoided. The DFO tuning process is similar to that of Section 4.2.

4.4.4. Tuning method 4: integral action

For Method 4 the tuning for K_i in (12) was found through extensive trial and error, starting at the tuning given in Fossen (2011). In the following we provide a reasonable documentation for a good K_i-tuning, where it is shown that K_i-values above and below the chosen tuning are less optimal. To document the choice of a good K_i−tuning the cost function J_η^c from (13a) is shown for several values of K_i in Table 2, applied on the maneuver described in Section 3.2 as the main maneuver. The different values for K_i in Table 2 are given as $K_{i,j} = \rho_j K_{i1}$, $j = 1, \ldots, 5$, where ρ_j, $j = 1, \ldots, 5$ are positive scalars that satisfy $\rho_{j+1} > \rho_j$, $j = 1, \ldots, 4$. The results of the table clearly show that K_{i3} gives the minimum value, and the lower and higher values of K_i give less optimal performance.

Table 2
Results for the integral action tuning on the training maneuver. The table shows the KPI in (13a). The KPIs are normalized such that the worst performing has a value of maximum of 100 for the whole maneuver.

Step	K_i [10^5]	J_η^c
1	diag{0.0132, 0.0115, 6.314}	99.88
2	diag{0.0142, 0.0123, 6.765}	99.59
3	diag{0.0151, 0.0131, 7.188}	99.58
4	diag{0.0160, 0.0139, 7.6673}	99.74
5	diag{0.0170, 0.0148, 8.1183}	100.00

Table 3
Summary of the bias compensation methods.

Method	Description
1	Direct comp. from pos/vel observer
2	Wave-filtered bias compensation
3	Comp. from separate bias observer
4	Integral action

5. Results and discussion

5.1. Simulation results

Results for the four different bias rejection methods are presented in the following. See Table 3 for a summary of the methods. The vessel performs the two different maneuvers presented in Section 3.2. The results on the training maneuver are shown in Fig. 2, Fig. 5, and Table 4. Fig. 2 has three plots. The upper left plot shows the low-frequency position and heading for the run with Method 1. The lower left plot shows the different bias rejection terms in surge only, and the right plot shows the cumulative error J_η^c of the positioning performance from (13a). Table 4 shows all the performance indices from (13) both for the whole maneuver and also for the steady-state time interval from 1000 to 1500 s. Fig. 5 shows the thrust KPIs $J_{\tau,uv}^c$ in (13b) and $J_{\tau,r}^c$ in (13c) for the training maneuver and the test maneuver.

The results for the training maneuver show that Method 3 (the bias observer) has the best overall performance. It is both fast over transients and calm in steady state. As seen from Table 4 and from Fig. 5, the thrust effort of Methods 3 and 4 are about equal, and lower than Methods 1 and 2, which also are approximately equal. During the steady period, the thrust effort of all four methods are similar, but Methods 3 and 4 have a lower positioning error than Methods 1 and 2.

Fig. 3 shows the bias rejection terms in surge for the four different methods in the upper plot. This is the same as the lower left plot of Fig. 2 zooming in on the transient at 600 s. The lower plot of Fig. 3 shows the difference between τ_{BR} and true bias force for the different methods for the respective simulations. As observed from Fig. 3, all four methods are quite fast in the transient, with Method 4 as the slowest. In steady state Method 4 is very calm, while Methods 2 and 3 are much calmer than Method 1.

As observed, Methods 1 and 2 have similar closed-loop performance. Even though Method 2 has smaller oscillations than Method 1, it also has a slight lag due to the extra filter, as observed from Fig. 3. The lag seems to make Method 2 underperform Method 1 during transients, and the two effects (lower oscillations and added lag) cancel in steady state, making the two methods similar in their steady-state performance. Method 3 has a good balance between steady-state and transient performance, and therefore has a better overall performance compared to Methods 1 and 2.

The results for the test maneuver is shown in Fig. 4, Fig. 5, and Table 5. The tuning used for the observers and controllers are the same as those used for the training maneuver. Similar type of results are seen. In the test maneuver there are more transient events and less steady

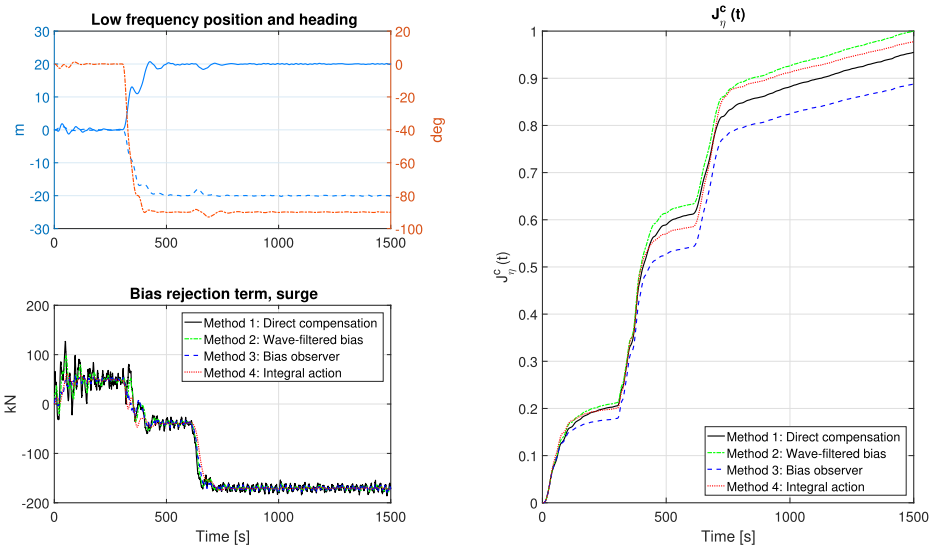

Fig. 2. Results for the four different bias rejection methods for the training maneuver. The right plot shows the KPI in (13a). The KPI is normalized such that the worst performing has a maximum of 1 for the whole maneuver.

Table 4
Results for the training maneuver. The table shows the KPIs from (13). The KPIs are normalized such that the worst performing has a value of maximum 100 (for the whole maneuver). The time interval 1000–1500 s is in steady state.

Time:	0–1500 s			1000–1500 s		
Controller	J^c_η	$J^c_{\tau,uv}$	$J_{\tau,r}$	J^c_η	$J^c_{\tau,uv}$	$J_{\tau,r}$
Method 1	95.5	100.0	99.5	7.3	42.4	29.6
Method 2	100.0	99.1	100.0	7.3	42.4	29.6
Method 3	88.8	97.5	98.7	6.3	42.4	29.6
Method 4	97.8	97.7	98.9	6.5	42.4	29.6

state than in the training maneuver. That is why Method 4 performs worse overall (in positioning performance) than in the training maneuver. However, note that Method 4 has the lowest thrust consumption. Method 3 still performs best, and Method 4 has the best steady-state behavior, and Method 3 has close to the same steady-state performance. This shows that the same tuning and observations also apply well for the test maneuver.

5.2. General discussion

The findings presented in Section 5.1 justify that using a bias estimate from a separate bias observer, with tuning optimized to estimate the bias, is the best way of compensating the bias loads in DP. This is better than the traditional integral action based on the tracking errors, since it mainly outperforms the integral action in transients. In addition, the results show that using the bias estimate (in feedback) from a single observer optimized for position and velocity estimates underperforms compared to using the separate bias observer both in transients and in steady state. The wave-filtered version of this bias estimate (from the position and velocity observer) underperforms the non-wave-filtered version, seemingly due to the added phase lag from the extra wave-filter. Using a separate bias observer is the best option among those presented in the paper. Direct integral action and bias compensation from the single position/velocity/bias observer have similar performance. If there are longer periods of steady state conditions,

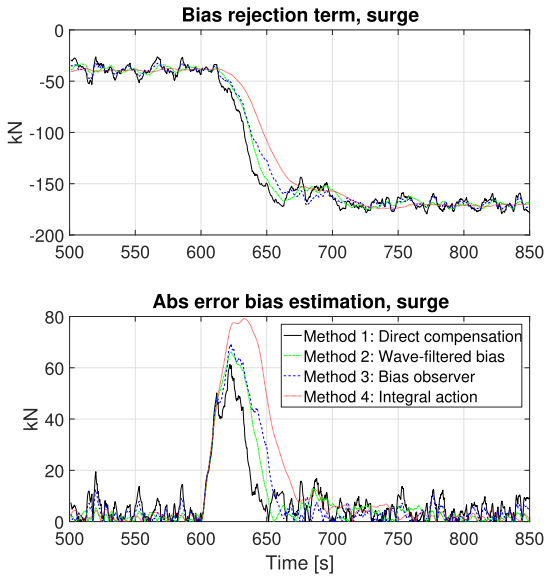

Fig. 3. The top plot shows the bias rejection term in surge for the four different methods on the training maneuver. The bottom plot shows the error between τ_{BR} and the true bias in surge (absolute value).

integral action is better than the single observer bias compensation, and vice versa for transient conditions.

6. Conclusion

In this paper, four methods for compensating the mean and slowly varying environmental loads (and unmodeled dynamics) for DP of marine vessels have been investigated. A high-fidelity simulation model

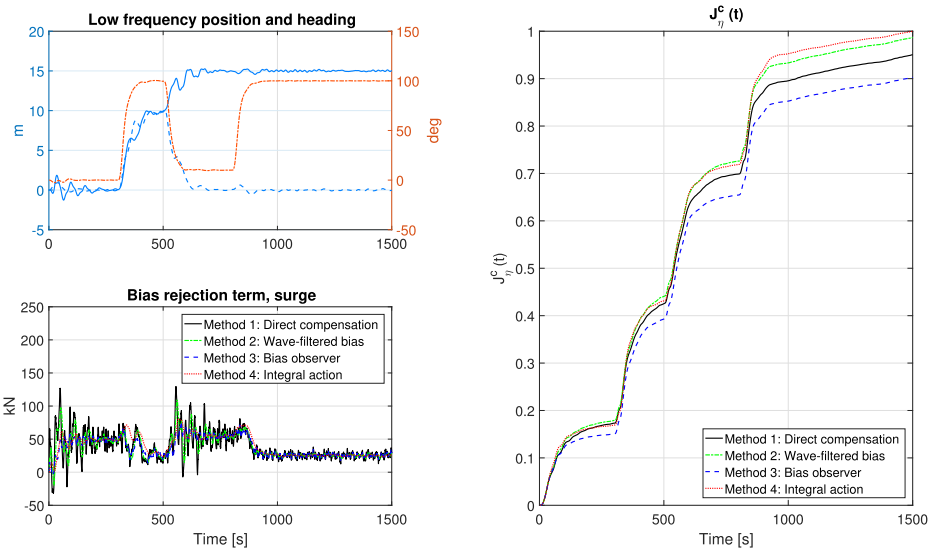

Fig. 4. Results for the four different bias rejection methods, on the test maneuver. The right plot shows the KPI in (13a). The KPI is normalized such that the worst performing has a maximum of 1 for the whole maneuver.

was used to compare the methods, using two different maneuvers; one training maneuver for tuning and one test maneuver for verification. All methods were tuned to work well for the training maneuver. Then this tuning was applied for the test maneuver to verify the gains, and similar performances were shown. The standard integral action was compared to three variations of using the bias estimate from a model-based observer. The results indicated that the best method to compensate the bias loads was using the bias estimate from a separate bias observer, for which the tuning was optimized to estimate the bias loads. This method displayed both the best transient and steady state behavior given the maneuvers in this paper.

Table 5
Results for the test maneuver. The table shows the KPIs from (13). The KPIs are normalized such that the worst performing has a value of maximum 100 (for the whole maneuver). The time interval 1000–1500 s is in steady state.

Time:	0–1500 s			1000–1500 s		
Controller	J^c_η	$J^c_{\tau,uv}$	$J_{\tau,r}$	J^c_η	$J^c_{\tau,uv}$	$J_{\tau,r}$
Method 1	95.1	100.0	99.4	5.5	24.3	24.4
Method 2	98.7	94.2	99.4	5.4	22.1	24.4
Method 3	90.3	92.0	99.5	5.0	22.0	24.4
Method 4	100.0	90.5	100.0	4.7	21.3	24.3

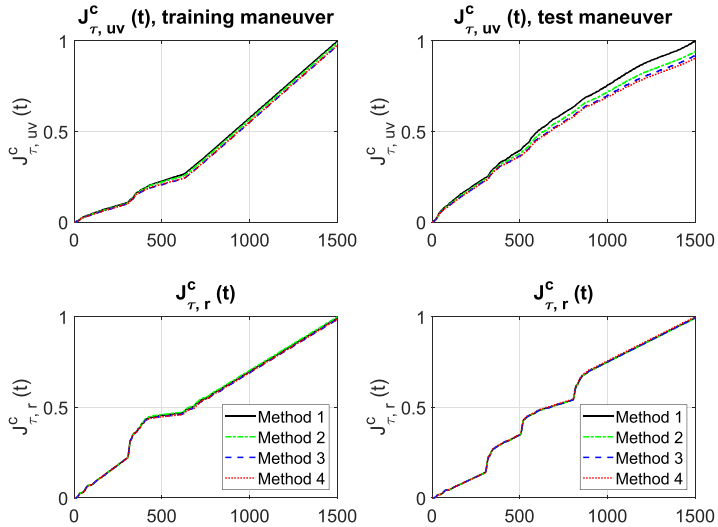

Fig. 5. Cumulative thrust results for the four different bias rejection methods, on the training maneuver (left) and the test maneuver (right). The top plots show the KPI in (13b) and the bottom plots show the KPI in (13c). The KPIs are normalized such that the worst performing has a maximum of 1 for the whole maneuver.

Acknowledgements

This work was supported by the Research Council of Norway, partly through the Centre of Excellence NTNU AMOS, project no. 223254, and partly through Centre for Research-based Innovation MOVE, project no. 237929. The authors would like to thank Vincenzo Calabrò from Norwegian Subsea for helpful discussion and input.

Appendix. Simulation verification model

The kinetics used in the SVM of the supply vessel, see Section 3.1, is (Sørensen, 2013)

$$M\dot{\nu} + C_{RB}(\nu)\nu + C_A(\nu_r)\nu_r + D_L\nu + d_{NL}(\nu_r) + G\eta = \tau + \tau_{env}, \tag{17}$$

where $M \in \mathbb{R}^{6\times6}$ is the inertia matrix, $C_{RB}(\nu) \in \mathbb{R}^{6\times6}$ and $C_A(\nu_r) \in \mathbb{R}^{6\times6}$ are the rigid body and added mass Coriolis matrices, respectively, $\nu \in \mathbb{R}^6$ and $\nu_r \in \mathbb{R}^6$ are the velocity and relative velocity, respectively, $D_L \in \mathbb{R}^{6\times6}$ is the linear damping matrix, $d_{NL}(\nu_r) \in \mathbb{R}^6$ is the non-linear damping vector, $G \in \mathbb{R}^{6\times6}$ is the restoring matrix, $\tau \in \mathbb{R}^6$ is the thrust vector, and $\tau_{env} \in \mathbb{R}^6$ is the environmental load vector. The inertia matrix for the SVM is a sum of the rigid body mass and the added mass, $M := M_{RB} + M_A$,

$$M_{RB} = \begin{bmatrix} mI_{3\times3} & -mS(r_g^b) \\ mS(r_g^b) & I_b \end{bmatrix} = 10^8 \cdot \begin{bmatrix} 0.0615 & 0 & 0 & 0 & -0.3198 & 0 \\ 0 & 0.0615 & 0 & 0.3198 & 0 & -0.1414 \\ 0 & 0 & 0.0615 & 0 & 0.1414 & 0 \\ 0 & 0.3198 & 0 & 31.4290 & 0 & -0.7355 \\ -0.3198 & 0 & 0.1414 & 0 & 4.2767 & 0 \\ 0 & -0.1414 & 0 & -0.7355 & 0 & 16.6653 \end{bmatrix} \tag{18}$$

$$M_A = 10^8 \cdot \begin{bmatrix} 0.0053 & 0 & -0.0036 & 0 & -0.7101 & 0 \\ 0 & 0.0518 & 0 & 0.1135 & 0 & 0.0095 \\ -0.0036 & 0 & 0.1993 & 0 & 1.9683 & 0 \\ 0 & 0.1128 & 0 & 2.6167 & 0 & -1.9025 \\ -0.7070 & 0 & 1.9664 & 0 & 177.7000 & 0 \\ 0 & 0.0095 & 0 & -1.9082 & 0 & 15.2660 \end{bmatrix} \tag{19}$$

where m is the mass of the ship, here $m = 6150$ tons, and $I_b := I_g - mS^2(r_g^b)$, where I_g is the inertia matrix about the body's center of gravity, $r_g^b = \mathrm{col}(-2.3m,\ 0,\ -5.2m)$. The matrix $S(\lambda)$, where $\lambda = \mathrm{col}(\lambda_1, \lambda_2, \lambda_3) \in \mathbb{R}^3$, denotes a skew-symmetric matrix,

$$S(\lambda) = \begin{bmatrix} 0 & -\lambda_3 & \lambda_2 \\ \lambda_3 & 0 & -\lambda_1 \\ -\lambda_2 & \lambda_1 & 0 \end{bmatrix}. \tag{20}$$

The rigid body and added mass Coriolis matrices are calculated online during simulations from the inertia matrices M_{RB} and M_A given above, and the velocity ν and relative velocity ν_r. The rigid body Coriolis can be written as Fossen (2011):

$$C_{RB}(\nu) = \begin{bmatrix} 0_{3\times3} & -mS(\nu_1) - mS(\nu_2)S(r_g^b) \\ -mS(\nu_1) + mS(r_g^b)S(\nu_2) & -S(I_b\nu_2) \end{bmatrix}, \tag{21}$$

where the linear and angular velocities are written as $\nu_1 = \mathrm{col}(u, v, w)$, $\nu_2 = \mathrm{col}(p, q, r)$. The added mass Coriolis is calculated in a similar way, see Sørensen (2013) for a complete representation. The nonlinear damping is calculated from a look-up table. The linear damping matrix D_L, and restoring force matrix G are

$$D_L = 10^8 \cdot \begin{bmatrix} 0.0017 & 0 & 0 & 0 & -0.0115 & 0 \\ 0 & 0.0014 & 0 & 0.0147 & 0 & -0.0065 \\ 0 & 0 & 0.0387 & 0 & 0.0891 & 0 \\ 0 & 0.0147 & 0 & 1.6800 & 0 & -0.0338 \\ -0.0115 & 0 & 0.0891 & 0 & 16.5299 & 0 \\ 0 & -0.0065 & 0 & -0.0338 & 0 & 0.6386 \end{bmatrix}$$

$$G = 10^9 \cdot \begin{bmatrix} 0 & 0 & 0 & 0 & 0 & 0 \\ 0 & 0 & 0 & 0 & 0 & 0 \\ 0 & 0 & 0.0141 & 0 & 0.0324 & 0 \\ 0 & 0 & 0 & 0.1931 & 0 & 0 \\ 0 & 0 & 0.0324 & 0 & 4.2977 & 0 \\ 0 & 0 & 0 & 0 & 0 & 0 \end{bmatrix}.$$

References

Balchen, J.G., Jenssen, N.A., Sælid, S., 1976. Dynamic positioning using kalman filtering and optimal control theory. IFAC/IFIP symposium on automation in offshore oil field operation 183, 186.

Blanke, M., Kinnaert, M., Lunze, J., Staroswiecki, M., 2003. Diagnosis and Fault-Tolerant Control. Springer.

Brodtkorb, A.H., Værnø, S.A., Teel, A.R., Sørensen, A.J., Skjetne, R., 2016. Hybrid observer for improved transient performance of a marine vessel in dynamic positioning. In: Proceedings of the IFAC Symposium on Nonlinear Control Systems 2016, vol. 49. pp. 345–350 (18).

Brodtkorb, A.H., Værnø, S.A., Teel, A.R., Sørensen, A.J., Skjetne, R., 2018. Hybrid controller concept for dynamic positioning of marine vessels with experimental results. Automatica 93, 489–497.

Du, J., Hu, X., Liu, H., Chen, C.P., 2015. Adaptive robust output feedback control for a marine dynamic positioning system based on a high-gain observer. IEEE Trans. Neural Netw. Learning Syst. 26 (11), 2775–2786.

Fossen, T.I., 2011. Handbook of Marine Craft Hydrodynamics and Motion Control. John Wiley & Sons.
Fossen, T.I., Perez, T., 2004. Marine Systems Simulator (Mss). https://github.com/cybergalactic/MSS, Accessed date: 24 February 2017.
Fossen, T.I., Perez, T., 2009. Kalman filtering for positioning and heading control of ships and offshore rigs. IEEE Control Syst. Mag. 29 (6), 32–46.
Fossen, T.I., Strand, J.P., 1999. Passive nonlinear observer design for ships using lyapunov methods: full-scale experiments with a supply vessel. Automatica 35 (1), 3–16.
Kjerstad, Ø.K., Skjetne, R., 2016. Disturbance rejection by acceleration feedforward for marine surface vessels. IEEE Access 4, 2656–2669.
Lindegaard, K.-P., 2003. Acceleration Feedback in Dynamic Positioning. PhD thesis. Norwegian University of Science and Technology, Trondheim, Norway.
Loria, A., Fossen, T.I., Panteley, E., 2000. A separation principle for dynamic positioning of ships: theoretical and experimental results. IEEE Trans. Control Syst. Technol. 8 (2), 332–343.
Loría, A., Panteley, E., 1999. A Separation Principle for a Class of Euler-Lagrange Systems, New Directions In Nonlinear Observer Design. Springer, pp. 229–247.
Perez, T., 2009. Anti-wind-up designs for dynamic positioning of marine vehicles with control allocation. IFAC Proceedings Volumes 42 (18), 243–248.
Price, W.G., Bishop, R.E.D., 1974. Probabilistic Theory of Ship Dynamics. Halsted Press.
Refsnes, J.E., Sørensen, A.J., 2007. Comparison of two observers for marine vessels in ocean current. IFAC Proceedings Volumes 40 (17), 32–37.
Sørensen, A.J., 2011. A survey of dynamic positioning control systems. Annu. Rev. Contr. 35 (1), 123–136.
Sørensen, A.J., 2013. Marine Control Systems - Lecture Notes. Department of Marine Technology, Norwegian Univ. of Sci. and Tech.
Tannuri, E.A., Morishita, H.M., 2006. Experimental and numerical evaluation of a typical dynamic positioning system. Appl. Ocean Res. 28 (2), 133–146.
Værnø, S.A., Brodtkorb, A.H., Skjetne, R., Calabrò, V., 2017. Time-varying Model-Based Observer for Marine Surface Vessels in Dynamic Positioning. IEEE Access.
Værnø, S.A., Brodtkorb, A.H., Skjetne, R., Sørensen, A.J., 2016. An output feedback controller with improved transient response of marine vessels in dynamic positioning. In: Proceedings of the IFAC Conference on Control Applications in Marine Systems 2016, vol. 49. pp. 133–138 (23).
Værnø, S.A., Skjetne, R., Kjerstad, Ø.K., Calabrò, V., 2019. Comparison of control design models and observers for dynamic positioning of surface vessels. Contr. Eng. Pract. 85, 235–245.

Chapter 7

International Refereed Conference Papers

C.1

An Output Feedback Controller with Improved Transient Response of Marine Vessels in Dynamic Positioning

---

Værnø, S. A., Brodtkorb, A. H., Skjetne, R., Sørensen, A. J.

Available online at www.sciencedirect.com

ScienceDirect

IFAC-PapersOnLine 49-23 (2016) 133–138

IFAC Papers Online
CONFERENCE PAPER ARCHIVE

An Output Feedback Controller with Improved Transient Response of Marine Vessels in Dynamic Positioning ⋆

Svenn Are T. Værnø * **Astrid H. Brodtkorb** * **Roger Skjetne** * **Asgeir J. Sørensen** *

* *Centre for Autonomous Marine Operations (NTNU AMOS), Department of Marine Technology, Norwegian University of Science and Technology (NTNU), Otto Nielsens vei 10, 7491 Trondheim, Norway (e-mail: svenn.are.varno@ntnu.no,astrid.h.brodtkorb@ntnu.no, roger.skjetne@ntnu.no,asgeir.sorensen@ntnu.no)*

Abstract: An output feedback controller for dynamic positioning (DP) of marine surface vessels is developed. The proposed algorithm has good performance during transients as well as good steady state performance. The method achieves this by a flexible injection gain in the bias estimation dynamics in the observer. In addition, the traditional integral action is replaced by a filtered bias estimate from the observer. Both these elements combined provide good DP performance in transients, as well as calm behavior in steady state. A simulation study is performed showing the benefit of the proposed output feedback controller, and a stability analysis is performed to show uniform asymptotic stability.

Keywords: Dynamic positioning; Observers; Output feedback; Integral action

1. INTRODUCTION

A surface vessel performing dynamic positioning (DP) has to keep position and orientation (stationkeeping) or do low speed tracking while compensating for the slowly-varying loads that affect the vessel. These loads are typically due to current, mean wind loads, and second order wave loads. The sum of these loads together with unmodeled dynamics, is lumped into the bias load vector. For model-based observer designs it is important to estimate this bias in order to achieve good estimation of the velocity, and thereby the position of the vessel. In addition, this bias load needs to be compensated in the controller to keep the desired position. This is typically achieved through integral action in the control law.

In standard model-based observer designs (Fossen, 2011), the tuning of the bias observer is set low to ensure good performance of the observer in steady state. Since the bias is typically slowly-varying, low tuning will lead to less oscillations in the bias estimate, and therefore also less oscillations in the velocity and position estimates. However, when there is a significant transient in the bias force, for instance by a heading change, a wave train, or a mooring line that breaks (for position mooring), the bias estimate will take some time to converge to the new value. This is problematic for transient performance of the DP system, since the velocities will not be estimated correctly over the course of the transient.

The objective of this paper is to construct a model-based observer and controller with good performance in both transients as well as in steady state. This will be achieved by two changes from the standard model-based design. The first is to allow for a flexible bias estimation in the observer. The injection gain in the bias dynamics will be allowed to take values ranging from a nominal gain matrix to higher gains and a more aggressive tuning. The second contribution is to add a lowpass-filtered bias estimate which has a less oscillatory and smoother characteristics than the direct bias estimate. This filtered estimate will be used to compensate for the bias in the controller. There are two reasons for this implementation. From the literature, the two existing options for compensating the bias is to either use the bias estimate from the observer (Loría and Panteley, 1999), or to add integral action in the controller (Sørensen, 2011). The integral action in the controller finds the bias estimate based on the tracking errors. Since the control performance depends on the convergence of the observer, it is reasonable to believe that the bias estimate in the observer will always be faster than the integral action based on tracking errors (with reasonable tuning).

However, if we use a filtered version of the bias estimate, we allow for fast bias convergence in the observer, without having to send this noisy estimate directly to the controller. At the same time the bias compensation term in the controller is oscillating less than the direct bias estimate itself, and this is most likely faster than integral action based on tracking errors. This is a similar idea as used in L1 adaptive control (Hovakimyan and Cao, 2010).

In addition, there is a tuning benefit of using the bias estimate from the observer, both because tuning an ob-

⋆ Research partly funded by the Research Council of Norway (RCN) project no. 223254: CoE NTNU AMOS, and partly by RCN project no. 237929: CRI MOVE.

10.1016/j.ifacol.2016.10.333

server does not require the system to be in closed loop, and because tuning of integral action (on tracking errors) heavily depends on how fast the observer estimates converge. This is especially beneficial in the current design, since the proposed observer have time-varying gains.

Similar use of time-varying gains is present in the literature. See for instance Tutturen and Skjetne (2015) where hybrid integral action for DP of marine vessels is proposed, and Lekkas and Fossen (2014) where the authors propose to use a time-varying lookahead distance as a function of the cross track error in a line-of-sight algorithm. In Belleter et al. (2013, 2015) a wave encounter frequency estimator is proposed, where the frequency adaption law has a time-varying gain. In Bryne et al. (2014) time-varying gains are proposed for an inertial observer (aided by GNSS) for DP, in order to improve convergence and suppress sensor noise.

2. PROBLEM FORMULATION

In the following we will separate between a simulation model and a control design model. The simulation model has higher fidelity and is used for simulation and verification of observer and control designs. Because of the low-speed nature of the dynamic positioning operations, the control design models typically neglect centripetal and Coriolis terms, as well as nonlinear damping; see (Sørensen, 2005, 2011), and (Fossen, 2011). The control design model considered here is a horizontal motion 3 degree of freedom (DOF) model, with the dynamics

$$\dot{\xi} = A_w \xi + E_w w_w \tag{1a}$$
$$\dot{\eta} = R(\psi)\nu \tag{1b}$$
$$\dot{b} = w_b \tag{1c}$$
$$M\dot{\nu} = -D\nu + R(\psi)^\top b + u \tag{1d}$$
$$y = \eta + C_w \xi + v_y, \tag{1e}$$

where $\xi \in \mathbb{R}^6$ is the state of a synthetic white noise-driven model of the vessel motion due to the 1st order wave loads. In normal operating conditions it is beneficial to counteract the low frequency part of the wave motion only, and the model therefore consists of a wave model (1a) and a low frequency part (1b) - (1d), which consists of the low frequency position in north and east, as well as the heading angle, $\eta := [N, E, \psi]^\top \in \mathbb{R}^3$, the velocities in surge, sway, and the yaw rate, $\nu := [u, v, r]^\top \in \mathbb{R}^3$, the slowly varying NED-fixed bias force $b \in \mathbb{R}^3$ that constitutes the sum of all slowly-varying perturbation loads, such as current, mean wind, 2nd order waves, and unmodeled dynamics. In (1b) the kinematic relation is described by the 3 DOF rotation matrix from the body to the NED frame $R(\psi) \in \mathbb{R}^{3\times 3}$,

$$R(\psi) = \begin{bmatrix} \cos(\psi) & -\sin(\psi) & 0 \\ \sin(\psi) & \cos(\psi) & 0 \\ 0 & 0 & 1 \end{bmatrix}, \tag{2}$$

and the time derivative of $R(\psi)$ is given by $\dot{R} = rS$, where

$$S = \begin{bmatrix} 0 & -1 & 0 \\ 1 & 0 & 0 \\ 0 & 0 & 0 \end{bmatrix}, \tag{3}$$

and $r = \dot{\psi} \in \mathbb{R}$ is the yaw rate. In (1d), $M \in \mathbb{R}^{3\times 3}$ is the inertia matrix including added mass, $D \in \mathbb{D}^{3\times 3}$ is the linear damping matrix, and $u \in \mathbb{R}^3$ is the control input vector. The measurements $y \in \mathbb{R}^3$ in (1e) measure the actual position of the vessel, that is, the sum of the low frequency and wave frequency position, where $C_w = [0\ I] \in \mathbb{R}^{3\times 6}$, and $v_y \in \mathbb{R}^3$ is the measurement noise.

The control objective of the paper is to construct an output feedback tracking controller for DP, that has good performance in both steady state as well as in transients. This output feedback controller will track a reference trajectory given by an open-loop reference system (Sørensen, 2011).

Below are some assumptions relevant for the observer and control design.

Assumption 1. Starboard/port symmetry, $M = M^\top > 0$, and $\dot{M} = 0$. The damping matrix satisfies $D + D^\top > 0$.

Assumption 2. Because of physical limitations of the thrusters, the yaw rate is bounded, by $|r| \leq r_{max} < \infty$.

3. OUTPUT FEEDBACK DESIGN

3.1 Model-based observer

The model-based observer considered is similar to the traditional "nonlinear passive observer" presented in Fossen and Strand (1999) with an additional state $\hat{b}_f$, which is a lowpass-filtered version of $\hat{b}$. By copying the dynamics of (1), neglecting the noise terms, and adding injection terms we get the observer dynamics as

$$\dot{\hat{\xi}} = A_w \hat{\xi} + K_{1,\omega} \bar{y} \tag{4a}$$
$$\dot{\hat{\eta}} = R(\psi)\hat{\nu} + K_2 \bar{y} \tag{4b}$$
$$\dot{\hat{b}} = K_3 \bar{y} \tag{4c}$$
$$\dot{\hat{b}}_f = -T_f^{-1}[\hat{b}_f - \hat{b}] \tag{4d}$$
$$M\dot{\hat{\nu}} = -D\hat{\nu} + R(\psi)^\top \hat{b} + u + K_4 R(\psi)^\top \bar{y} \tag{4e}$$
$$\hat{y} = \hat{\eta} + C_w \hat{\xi}, \tag{4f}$$

where $\hat{\xi} \in \mathbb{R}^6, \hat{\eta}, \hat{b}, \hat{b}_f, \hat{\nu} \in \mathbb{R}^3$ are the state estimates, $K_{1,\omega} \in \mathbb{R}^{6\times 3}, K_2, K_3, K_4 \in \mathbb{R}^{3\times 3}$ are non-negative gain matrices, and $\bar{y} = y - \hat{y}$ is the measurement error. The underlying assumptions for the observer are:

Assumption 3. (a) $R(\psi + \psi_w) \approx R(\psi)$. That is, the heading angle due to wave-induced motion is small.
(b) The frequency used in the wave filter does not change. It corresponds to the peak frequency of the wave spectra of the incoming sea state.

By defining the estimation error states $\bar{\eta} := \eta - \hat{\eta}$, $\bar{\nu} := \nu - \hat{\nu}$, $\bar{b} := b - \hat{b}$, $\bar{b}_f := b - \hat{b}_f$, and subtracting the observer equations (4) from the control design model (1), we get the observer error system,

$$\dot{\bar{\xi}} = A_w \bar{\xi} - K_{1,\omega} \bar{y} \tag{5a}$$
$$\dot{\bar{\eta}} = R(\psi)\bar{\nu} - K_2 \bar{y} \tag{5b}$$
$$\dot{\bar{b}} = -K_3 \bar{y} \tag{5c}$$
$$\dot{\bar{b}}_f = -T_f^{-1}[\bar{b}_f - \bar{b}] \tag{5d}$$
$$M\dot{\bar{\nu}} = -D\bar{\nu} + R(\psi)^\top \bar{b} - K_4 R(\psi)^\top \bar{y}. \tag{5e}$$

3.2 Varying bias gain

To improve the transient response, we want the injection gain K_3 in (4c) to vary. In steady-state it is desired that K_3 stays close to a nominal gain such that the bias estimate is calm. Whenever the vessel experiences transients, K_3 should increase to make the bias estimate more reactive, and when the vessel again reaches steady state, the gain should return to the nominal gain. To solve this, K_3 is allowed to take a range of values within $K_3(t) \in [K_{3,min}, K_{3,max}]$, $\forall t \geq 0$. We let $K_3(t) := \kappa(t) K_{3,min}$, where $\kappa(t) \in [\kappa_{min}, \kappa_{max}]$, $\forall t \geq 0$. The update law for κ is given by

$$\kappa = \max\{1, \beta\}, \tag{6a}$$

$$\beta = \min\{\varepsilon_{r_d}|r_d(t)| + \varepsilon_\eta|\bar{\eta}_f| + \kappa_{max}e^{-\varepsilon_t t}, \kappa_{max}\}, \tag{6b}$$

$$\dot{\bar{\eta}}_f = -T_{\eta_f}^{-1}\{\bar{\eta}_f - \bar{y}\}. \tag{6c}$$

The first term in (6b) contains a constant $\varepsilon_{r_d} \geq 0$ and the desired yaw rate $r_d(t) \in \mathbb{R}$, related to a heading change. The second term is a performance term that triggers a higher gain when the observer error is large, and the third term only makes κ large during the initial transient. In (6c) T_{η_f} is a positive definite diagonal matrix with filter time constants, and these time constants and the size of $\varepsilon_\eta \geq 0$ are tuned such that κ approach κ_{min} at steady state.

In order to have a convenient expression for K_3 in the further analysis we introduce $\lambda \in [0, 1]$ and write $K_3 := K_{3,\lambda}$ as

$$K_{3\lambda} := \lambda K_{3,min} + (1 - \lambda) K_{3,max}. \tag{7}$$

3.3 Output feedback tracking control

The control law consists of a reference feedforward term and a feedback term. The feedback part consists of a nonlinear PD-term, and a bias rejection term, which is the filtered bias estimate from (4d),

$$u = u_{FB} + u_{FF} \tag{8}$$

$$u_{FF} = M\dot{\nu}_d(t) + D\nu_d(t) \tag{9}$$

$$\begin{aligned} u_{FB} &= -K_p R(\psi)^\top(\hat{\eta} - \eta_d(t)) - K_d(\hat{\nu} - \nu_d(t)) - R(\psi)^\top \hat{b}_f \\ &= -K_p R(\psi)^\top(\bar{\eta} - \bar{\eta}) - K_d(\bar{\nu} - \bar{\nu}) - R(\psi)^\top(b - \bar{b}_f). \end{aligned} \tag{10}$$

where $\eta_d(t)$, $\nu_d(t)$, $\dot{\nu}_d(t)$ are the desired references generated by a reference generator. By defining the tracking error states $\tilde{\eta} := \eta - \eta_d(t)$, $\tilde{\nu} := \nu - \nu_d(t)$, the kinematics in (1b) along with the kinetics in (1d) inserted for (8) gives the tracking error system,

$$\dot{\tilde{\eta}} = R(\psi)\tilde{\nu} \tag{11a}$$

$$M\dot{\tilde{\nu}} = -(D + K_d)\tilde{\nu} - K_p R(\psi)^\top \tilde{\eta} \tag{11b}$$

$$+ K_d\bar{\nu} + K_p R(\psi)^\top \bar{\eta} + R(\psi)^\top \bar{b}_f \tag{11c}$$

4. STABILITY ANALYSIS

We collect all error states in $x := col(x_c, x_o)$, where $x_c := col(\tilde{\eta}, \tilde{\nu})$, $x_o := col(\bar{\xi}, \bar{\eta}, \bar{b}, \bar{b}_f, \bar{\nu})$ and combining (5), (7), and (11) the total error dynamic becomes

$$\dot{x} = A_\lambda(\psi)x \tag{12}$$

where

$$A_\lambda(\psi) = \begin{bmatrix} A_c(\psi) & B_{co}(\psi) \\ 0_{18\times 6} & A_{o,\lambda}(\psi) \end{bmatrix}, \tag{13}$$

and

$$A_c := \begin{bmatrix} 0 & R(\psi) \\ -M^{-1}K_p R(\psi)^\top & -M^{-1}(D + K_d) \end{bmatrix}, \tag{14a}$$

$$B_{co} := \begin{bmatrix} 0_{3\times 18} \\ 0_{3\times 6} \;\; M^{-1}K_p R(\psi)^\top \;\; 0_{3\times 3} \;\; M^{-1}R(\psi)^\top \;\; M^{-1}K_d \end{bmatrix}, \tag{14b}$$

$$A_{o,\lambda} := \begin{bmatrix} A_w - K_{1,\omega}C_w & -K_{1,\omega} & 0 & 0 & 0 \\ -K_2 C_w & -K_2 & 0 & 0 & R(\psi) \\ -K_{3,\lambda}C_w & -K_{3,\lambda} & 0 & 0 & 0) \\ 0 & 0 & T_f^{-1} & -T_f^{-1} & 0 \\ -M^{-1}K_4 R(\psi)^\top C_w & -M^{-1}K_4 R(\psi)^\top & M^{-1} & 0 & -M^{-1}D \end{bmatrix}. \tag{14c}$$

The dynamics (12) can be written (Lindegaard, 2003),

$$\dot{x} = T(\psi)^\top A_\lambda(0) T(\psi) x, \tag{15}$$

if the matrices $K_{1,\omega}$, K_2, $K_{3,\lambda}$, and T_f^{-1} commute with the rotation matrix $R(\psi)$. The transformation matrix $T(\psi)$ is given as

$$T(\psi) = \text{diag}\{T_c(\psi), T_o(\psi)\} \tag{16a}$$

$$T_c(\psi) = \text{diag}\{R(\psi)^\top, I\} \tag{16b}$$

$$T_o(\psi) = \text{diag}\{R(\psi)^\top, \ldots, R(\psi)^\top, I\}. \tag{16c}$$

By inserting (7) we can write

$$A_\lambda(0) = \lambda A_{min} + (1 - \lambda)A_{max}, \tag{17}$$

where A_{min} contains $K_{3,min}$ and A_{max} contains $K_{3,max}$.

Proposition 1. The equilibrium $x = 0$ of (12,) where $K_{3,\lambda}$ can arbitrarily take any value in $[K_{3,min}, K_{3,max}]$, is uniformly asymptotically stable under the following conditions:

- The matrices $K_{1,\omega}$, K_2, $K_{3,\lambda}$, and T_f^{-1} commute with the rotation matrix $R(\psi)$.
- The following LMI's are satisfied,

$$A_{min}^\top P + PA_{min} + r_{max}(S_T P - PS_T) < -Q \tag{18a}$$

$$A_{min}^\top P + PA_{min} - r_{max}(S_T P - PS_T) < -Q \tag{18b}$$

$$A_{max}^\top P + PA_{max} + r_{max}(S_T P - PS_T) < -Q \tag{18c}$$

$$A_{max}^\top P + PA_{max} - r_{max}(S_T P - PS_T) < -Q, \tag{18d}$$

  where $S_T = \text{diag}\{S, 0, S, \ldots, S, 0\}$, and P and Q are symmetric positive definite matrices.

Proof. Consider the transformation $z = T(\psi)x$ given by (16), and notice that $T(\psi)^{-1} = T(\psi)^\top$. From (15) we get

$$\begin{aligned} \dot{z} &= T(\psi)T(\psi)^\top A_\lambda(0)z + \dot{T}(\psi)T(\psi)^\top z \\ &= A_\lambda(0)z - rS_T z \end{aligned} \tag{19}$$

where r is the yaw rate. We introduce a quadratic Lyapunov function $V(z) = z^\top P z$, and from (19) we define $f(z) := A_\lambda(0)z$ and $g_r(z) := -rS_T z$ such that (19) becomes

$$\dot{z} = f(z) + g_r(z), \tag{20}$$

where $f(z) := \lambda f_{min}(z) + (1-\lambda)f_{max}(z)$. From (18a)-(18d) and $r \in [-r_{max}, r_{max}]$ we have

$$\langle \nabla V(z), f_{min}(z) + g_r(z) \rangle \leq -\alpha(|z|) \tag{21a}$$

$$\langle \nabla V(z), f_{max}(z) + g_r(z) \rangle \leq -\alpha(|z|), \tag{21b}$$

where $\alpha(|z|)$ is a positive definite function. Finally, we get

$$\begin{aligned} &\langle \nabla V(z), \lambda f_{min}(z) + (1-\lambda)f_{max}(z) + g_r(z) \rangle \leq \\ &\lambda\langle \nabla V(z), f_{min}(z) + g_r(z) \rangle + (1-\lambda)\langle \nabla V(z), f_{max}(z) + g_r(z) \rangle \\ &\leq -\lambda\alpha(z) - (1-\lambda)\alpha(z) \leq -\alpha(z), \end{aligned} \tag{22}$$

and this concludes the proof.

Table 1. Supply vessel, main parameters

Parameters	Value
Length between perp.	80 m
Breadth	17.4 m
Draft	5.6 m
Displacment	6150 tons

If the observer and controller gains are set such that A_{min} and A_{max} are Hurwitz, and if the ratio of $\kappa_{max}/\kappa_{min}$ is not very large (in practice, up to 5), it is easy to satisfy (18) for a maximum yaw rate far above "normal" yaw rates.

5. SIMULATION RESULTS AND DISCUSSION

The simulations are performed in MATLAB/Simulink on a high fidelity model based on building blocks from the MSS Toolbox (MSS, 2010). The case simulated is a platform supply vessel in an environment consisting of waves, wind, and current. See Table 1 for the main parameters of the vessel. The sea state is very rough with significant wave height of 6 meters, and a peak frequency of 0.53 rad/s taken from the JONSWAP [1] spectrum. The mean incident wave heading is 190° in the north-east frame (Price and Bishop, 1974). The current has a speed of 0.5 m/s and direction of 180°, and the wind has a mean velocity of 5 m/s with a direction of 160°. A first order model for the thrust dynamics is included, and the time constants for thrust force is set to 5 seconds. The GPS measurements have realistic noise properties, and are sampled at 1 Hz, and the measurements are processed by a zero-order hold element before they are sent to the observer.

Three different output feedback controllers are compared to illustrate the benefit of changing the gain K_3 in (4c). The only difference between the three setups is a variation of allowed values for κ from (6a). For two of the output feedback controllers the κ-value is fixed, where the "nominal" controller has $\kappa = \kappa_{min}$ for steady conditions, while the "aggressive" controller has $\kappa = \kappa_{max}$ for transient conditions. The last controller is our proposed algorithm in (6) where $\kappa \in [\kappa_{min}, \kappa_{max}]$, called the "flexible" controller. Even though the difference between these three systems is in the observer we often just write "controller" to describe the system. However, when just the observer performance is discussed, "observer" is used.

At the beginning of the simulation, the position and orientation of the vessel is at $\eta = [0, 0, 0]^\top$. At 1000 seconds there is a setpoint change 20 meters north, 20 meters east, and to heading -90°. Due to the ship hull shape this maneuver will change the bias force experienced by the vessel in the body frame, as well as in the NED frame. After 3000 seconds the direction of the current changes to 90°, to see how the vessel responds to a sudden change in bias force that is not known in advance. The current direction changes as a first order filtered step with time constant 30 seconds.

In Figure 1 the cumulative low-frequency position tracking error of the vessel is shown for the three controllers. The left part starts from the instance of the heading change, and the right part is a zoom-in on the steady period 2000-3000 seconds. The top plots show the combined error in north and east, and the bottom plots show the error in yaw. From the left part it can be observed that the aggressive and flexible controller perform much better than the nominal controller in the transient regime, that is, just after 1000 seconds, and just after 3000 seconds. From the right part of Figure 1 it can be observed that after the system reaches steady state, the flexible and nominal controller perform better than the aggressive controller, and this is due to lower oscillations of the bias and velocity estimates from the observer. This implies that since the flexible and aggressive controllers have similar performance in transients, the flexible controller will eventually perform better.

From the left part of Figure 1 it is observed that already around 2000 seconds the flexible controller has a lower cumulative position deviation. This is because the heading change is a transient known in advance, and the flexible controller can react fast, and go to a higher value for κ quickly. This is observed from Figure 4, where κ for the flexible controller is shown ($\kappa_{max} = 2.5$). In addition, we can observe from Figure 4 that at 3000 seconds it takes a bit more time for κ to go to κ_{max} than at 1000 seconds. This is natural since this increase is based on the estimation error in the observer, and not a command in the reference system as with the heading change. Even though κ will be slower for the "unknown" transients, we see from Figure 1 that the flexible controller has a similar performance to the aggressive controller, and will eventually outperform the aggressive controller if the steady state conditions persist.

In Figure 2 the cumulative bias estimation error (in the body frame) from the observer is plotted for the entire simulated case study. The combined error of surge and sway is shown in the top plot, and the yaw error is shown in the bottom plot. Here we see the same trend as in Figure 1, but the trend is even clearer. The flexible observer is superior to both the aggressive and nominal observer. Even the nominal observer performs better than the aggressive observer after 5000 seconds for the error in surge and sway.

In Figure 3 the bias in surge is plotted, along with the observer estimate, and the filtered bias estimate for the flexible controller. It is observed that the bias estimate (and the filtered estimate) converge to their new bias values quite fast, and within 200 seconds after a transient steady state conditions are reached.

6. CONCLUSION

The proposed output feedback controller was shown to have good closed-loop properties in both transients and steady state. Both the flexible bias estimation, and the filtering of the bias estimate used in the control law, contributed to a good overall performance for the system.

For the flexible bias estimation, the lowest tuning should be quite responsive to ensure good overall responsiveness. There are a couple of reasons for this. If we failed to detect a transient, or the detection was slow, a moderate nominal tuning vastly improved the performance in the transient compared to a very low nominal tuning. That is, if excellent positioning capabilities is the goal, the tuning should have a fairly high minimum. In the presented

[1] Joint North Sea Wave Project

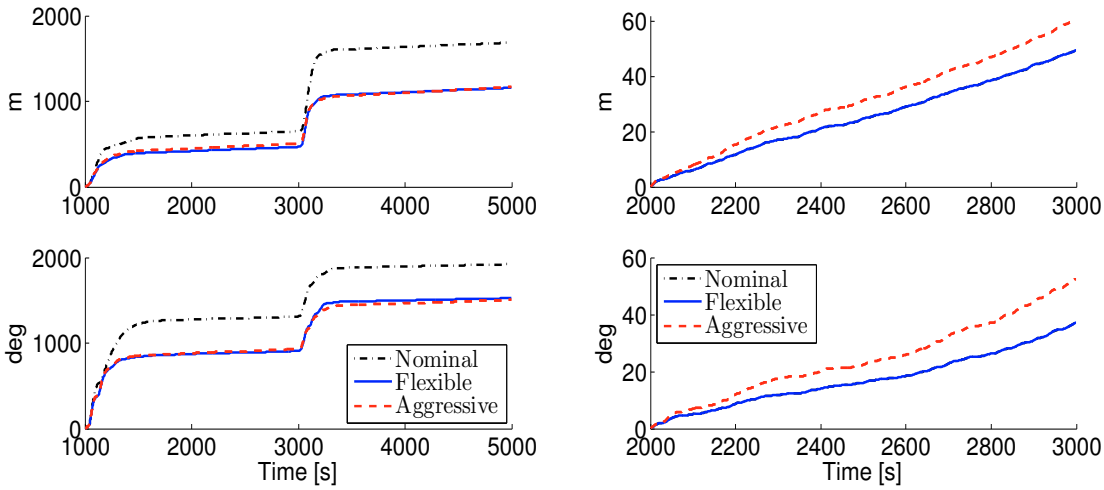

Fig. 1. Cumulative low frequency position tracking error in north and east combined (top plots), and yaw (bottom plots). The right plot is a zoom-in on the steady period 2000-3000s (the flexible and nominal controllers overlap because of steady state conditions).

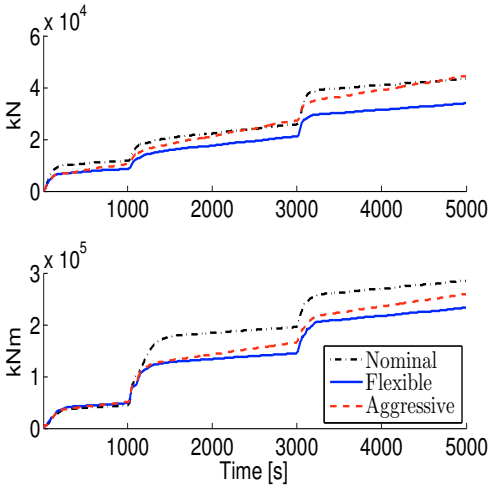

Fig. 2. Cumulative bias estimation error in surge and sway combined (top), and yaw (bottom).

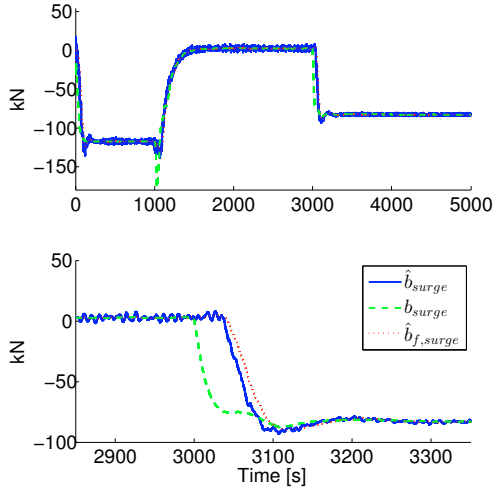

Fig. 3. Bias estimate (blue, solid), actual bias (green, dashed), and filtered bias estimate (red, dotted), all in surge. For the entire simulation (top) and zoom-in (bottom).

simulation case study all the bias estimate tunings were quite fast, and they all converged within 300 seconds.

REFERENCES

(2010). Mss. marine systems simulator. `http://www.marinecontrol.org`. Accessed: 2015-02-24.

Belleter, D.J., Breu, D.A., Fossen, T.I., and Nijmeijer, H. (2013). A globally k-exponentially stable nonlinear observer for the wave encounter frequency. *IFAC Proceedings Volumes*, 46(33), 209–214.

Belleter, D.J., Galeazzi, R., and Fossen, T.I. (2015). Experimental verification of a global exponential stable nonlinear wave encounter frequency estimator. *Ocean Engineering*, 97, 48–56.

Bryne, T.H., Fossen, T.I., and Johansen, T.A. (2014). Nonlinear observer with time-varying gains for inertial navigation aided by satellite reference systems in dynamic positioning. In *Control and Automation (MED), 2014 22nd Mediterranean Conference of*, 1353–1360. IEEE.

Fossen, T.I. (2011). *Handbook of marine craft hydrodynamics and motion control*. John Wiley & Sons.

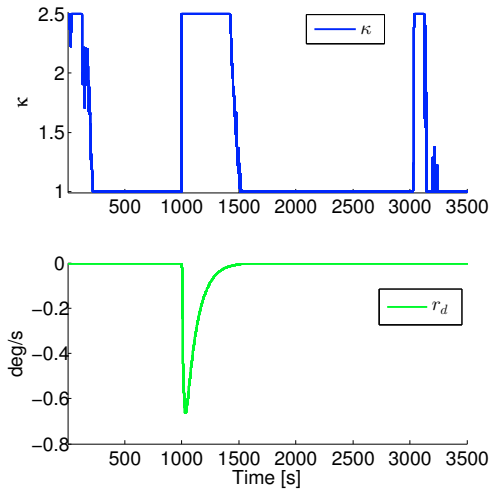

Fig. 4. Plot of κ (top) and desired yaw rate (bottom).

Fossen, T.I. and Strand, J.P. (1999). Passive nonlinear observer design for ships using lyapunov methods: full-scale experiments with a supply vessel. *Automatica*, 35(1), 3–16.

Hovakimyan, N. and Cao, C. (2010). *L1 adaptive control theory: guaranteed robustness with fast adaptation*, volume 21. Siam.

Lekkas, A.M. and Fossen, T.I. (2014). Integral los path following for curved paths based on a monotone cubic hermite spline parametrization. *IEEE Transactions on Control Systems Technology*, 22(6), 2287–2301.

Lindegaard, K.P. (2003). Acceleration feedback in dynamic positioning.

Loría, A. and Panteley, E. (1999). A separation principle for a class of euler-lagrange systems. In *New Directions in nonlinear observer design*, 229–247. Springer.

Price, W.G. and Bishop, R.E.D. (1974). *Probabilistic theory of ship dynamics*. Halsted Press.

Sørensen, A.J. (2005). Structural issues in the design and operation of marine control systems. *Annual Reviews in Control*, 29(1), 125–149.

Sørensen, A.J. (2011). A survey of dynamic positioning control systems. *Annual reviews in control*, 35(1), 123–136.

Tutturen, S.A. and Skjetne, R. (2015). Hybrid control to improve transient response of integral action in dynamic positioning of marine vessels. *IFAC-PapersOnLine*, 48(16), 166–171.

C.2

Hybrid observer for improved transient performance of a marine vessel in dynamic positioning

---

Brodtkorb, A. H., **Værnø, S. A.**, Teel, A. R., Sørensen, A. J., Skjetne, R.

Available online at www.sciencedirect.com

ScienceDirect

IFAC-PapersOnLine 49-18 (2016) 345–350

IFAC Papers Online
CONFERENCE PAPER ARCHIVE

Hybrid observer for improved transient performance of a marine vessel in dynamic positioning ⋆

Astrid H. Brodtkorb * **Svenn A. Værnø** * **Andrew R. Teel** **
Asgeir J. Sørensen * **Roger Skjetne** *

* *Centre for Autonomous Marine Operations (NTNU AMOS), Department of Marine Technology, Norwegian University of Science and Technology (NTNU), Otto Nielsens vei 10, 7491 Trondheim, Norway (e-mails: astrid.h.brodtkorb@ntnu.no, svenn.are.varno@ntnu.no, asgeir.sorensen@ntnu.no, roger.skjetne@ntnu.no).*
** *Department of Electrical and Computational Engineering, University of California Santa Barbara, CA USA (e-mail: teel@ece.ucsb.edu)*

Abstract: Dynamic positioning (DP) systems are used on marine vessels for automatic station keeping and tracking operations solely by use of thrusters. Observers are key components of DP systems, and two main types are proposed in this paper. The model-based type is used in steady state conditions since it is especially good at filtering out first order wave induced motions and predicting states in the case of signal loss, and the signal-based type typically has superior performance during transients. In this paper a hybrid observer including a signal-based part and a model-based part with a performance monitoring function is proposed. The observer part that provides the best estimate of the vessel position and heading is used in closed-loop control, thereby allowing for improved transient response while maintaining good steady-state performance. The contributions of this paper include the design of a hybrid signal-based and model-based observer with performance monitoring, stability analysis of the vessel with hybrid estimates in output feedback control, and simulations of a platform supply vessel during a setpoint and heading change.

Keywords: Dynamic positioning, observers, hybrid systems, output feedback control

1. INTRODUCTION

Marine operations are moving further from shore and into harsher environments, and with it requirements for the DP vessel's operational window, safety functions and energy-efficiency become stricter. Vessels that are doing operations with longer duration experience changing sea states with varying wind and wave directions, with suboptimal heading at times. Large forces and moments act on the vessel, making quick and precise control essential, especially when operating close to other offshore infrastructures.

There are many unknown factors at sea that may cause transients in the vessel response depending on the type of operations: wave trains, ice loads, mooring line break, etc. However, many transients are triggered by the operator, which makes them easier to account for with proactive control strategies, e.g. heading and setpoint changes, pipelay operations, well intervention operations, the lowering of a jack-up vessel from jacked-up to floating, etc. In this work the transient response of a DP vessel is improved by combining two observers.

⋆ This work was supported by the Research Council of Norway through the Centres of Excellence funding scheme, project number 23254 - AMOS, and in part by NSF grant number ECCS-1508757 and AFOSR grant number FA9550-15-1-0155.

The model-based observer, like the Extended Kalman filter (Tannuri and Morishita, 2006), (Hassani et al., 2013), or the nonlinear passive observer (Fossen and Strand, 1999), are commonly used in DP systems. The model-based observer uses noisy position and heading angle measurements to estimate the low frequency position, heading, and velocity of the vessel. A key feature of this observer type is the wave filter, which eliminates the wave frequency vessel motion from the output feedback control law. This reduces the wear and tear on the machinery as well as reducing the energy consumption.

The signal-based observer, also referred to as a kinematic, or sensor-based observer, is based on the kinematic equations, see for instance Mahony et al. (2008), Hua (2010), Grip et al. (2012), and Bryne et al. (2015). It is especially well suited during transients, as it uses linear acceleration measurements to predict velocity and position. In this implementation no wave filter was included in this observer, but it is ongoing work by Bryne et al. (2016). As a result this observer estimates the total vessel motion, including low frequency and wave frequency motion. When inserted into the control law it gives an oscillatory thrust command.

Earlier hybrid control theory has been applied to dynamic positioning in a changing sea state, see Nguyen et al.

2405-8963 © 2016, IFAC (International Federation of Automatic Control) Hosting by Elsevier Ltd. All rights reserved.
Peer review under responsibility of International Federation of Automatic Control.
10.1016/j.ifacol.2016.10.189

(2007) and Brodtkorb et al. (2014), and for changing operational modes (Nguyen et al., 2008). These all consist of a bank of controllers and observers with a supervisory mechanism that monitors performance and chooses the best controller/observer pair. Dwell-time and hysteresis switching were applied to avoid chattering. In this paper we apply an output feedback DP controller, using analysis from Loria et al. (2000). Related to this, Prieur and Teel (2011) looks at output feedback control using a hybrid controller with a nonlinear globally stabilizing part, and a linear locally stabilizing part.

The main contributions of this paper includes the design, analysis, and simulation of a hybrid observer with a model-based part and a signal-based part for improving the transient vessel response in an uncertain marine environment. A performance monitoring function keeps track of the mean estimation error over a time period for the observers, and the estimates from the better-performing observer are used in closed-loop output feedback control using a nonlinear proportional, integral, derivative (nPID) controller. Hysteresis is applied in order to limit the number of jumps for the system, and this is important for the stability of the system.

The organization of the paper is as follows: In Section 2 typical instrumentation for DP vessels is discussed, and two mathematical models of marine DP vessels are presented. A model-based and a signal-based observer are introduced in Section 3, and Section 4 presents the output feedback control algorithm. The hybrid signal-based and model-based observer in closed loop control is modeled in Section 5, and stability is discussed in Section 6. Simulation results for a platform supply vessel doing a setpoint change are presented and discussed in Section 7. Section 8 concludes the paper.

2. MARINE VESSEL MODELING AND DYNAMIC POSITIONING

Two reference frames are used in this paper: the North-East-Down (NED) reference frame which is a local Earth-fixed frame, and the body frame, which is body-fixed.

2.1 Instrumentation

DP vessels have statutory class requirements on the on-board instrumentation, and system redundancy. Vessels have positioning systems, e.g. GNSS, acoustics, or laser, a compass measuring heading angle, and an inertial measurement unit (IMU) that combines gyroscopes for measuring angular rates and accelerometers for measuring linear acceleration. The measurements are taken at different sampling rates ranging from 0.1-2 Hz for acoustics, 0.5-4 Hz for GNSS position measurements, to 100-200 Hz for IMU angular velocity and acceleration measurements. The measurements are in this paper assumed to be of the form

$$p^n = [N, E]^\top \tag{1a}$$
$$\psi_c = \psi \tag{1b}$$
$$\omega^b_{imu} = \omega^b + b_g \tag{1c}$$
$$f^b_{imu} = R(\Theta)(\dot{v}^n - g^n), \tag{1d}$$

where the measurements in the NED frame have superscript n, and measurements in the body frame have superscript b. $p^n \in \mathbb{R}^2$ is the measured position in north and east. A heave measurement may also be obtained through GNSS, but it is typically of low quality and is not used here. $\psi_c \in \mathbb{R}$ is measured heading angle (ψ is used in the remainder of the paper), $\omega^b_{imu} \in \mathbb{R}^3$ is measured angular rate ω^b, $f^b_{imu} \in \mathbb{R}^3$ is measured linear acceleration, $\Theta = [\phi,\ \theta,\ \psi]^\top \in \mathbb{R}^3$ is the orientation in roll, pitch and yaw, $R(\Theta) \in \mathbb{R}^{3\times3}$ is the rotation matrix about the z, y, x axes, $g^n \in \mathbb{R}^3$ is acceleration due to gravity, and $b_g \in \mathbb{R}$ is the gyro bias. Measurement noise is disregarded in the stability analysis, but inserted in simulations.

2.2 Marine vessel modeling

Two models of the same system are presented.

Control plant model The control plant model for a vessel is a simplification of the real vessel dynamics. It is different for the various vessel types, operational and environmental conditions, and the design problem under consideration (e.g. observer design or feedback control design); see Fossen (2011) or Sørensen (2013). A surface vessel in DP with starboard/port symmetry, $M = M^\top$, has largest motions in the horizontal plane (surge, sway, and yaw), so the heave, roll, and pitch dynamics are neglected. The control plant model in this case is:

$$\dot{\xi} = A_w \xi + E_w w_w, \tag{2a}$$
$$\dot{\eta} = R(\psi)\nu, \tag{2b}$$
$$\dot{b} = -T_b^{-1} b + E_w w_b \tag{2c}$$
$$M\dot{\nu} = -D\nu + R^\top(\psi) b + u, \tag{2d}$$
$$y = \eta + W\xi + v_y; \tag{2e}$$

where the states of the system include the 3 DOF North, East position and heading $\eta := [N, E, \psi]^\top$ and body-fixed velocity ν in surge, sway and yaw. In normal operational conditions we want to control only the low frequency part of the vessel motion, and the wave filter in (2a) allows us to separate the motion into a wave frequency part, and a low frequency part. The wave filter has a state $\xi \in \mathbb{R}^6$ and system matrix $A_w \in \mathbb{R}^{6\times6}$ that contains the peak wave frequency and damping. It is driven by zero mean white noise w_w. (2b-d) are the low frequency dynamics of the vessel. (2b) is the 3 DOF kinematics that transforms velocity from the body to the NED frame; $R(\psi)$ is the rotation matrix about the z-axis,

$$R(\psi) = \begin{bmatrix} \cos(\psi) & -\sin(\psi) & 0 \\ \sin(\psi) & \cos(\psi) & 0 \\ 0 & 0 & 1 \end{bmatrix}. \tag{3}$$

The wave frequency part of the heading angle, ψ_w, is assumed to be small, $R(\psi+\psi_w) \approx R(\psi)$. (2c) is a bias force model with state $b \in \mathbb{R}^3$, accounting for *slowly-varying* environmental disturbances from mean wind, current, and second-order wave loads and unmodeled vessel dynamics. T_b is the Markov time constant, and w_b zero mean white noise. Note that the bias force model does not capture rapidly varying disturbances. In (2d) $M \in \mathbb{R}^{3\times3}$ is the inertia matrix including added mass for asymptotic values of wave frequency equal to zero, $D \in \mathbb{R}^{3\times3}$ is the linear damping coefficient matrix, and $u \in \mathbb{R}^3$ is the control input. (2e) is the measurement $y = [(p^n)^\top\ \psi]^\top \in \mathbb{R}^3$ of

position and heading including low frequency motion η, wave frequency motion $W\xi$ with $W = [0_{3\times3},\ I_{3\times3}]$, and measurement noise v_y.

Kinematic model The kinematic model is based on fundamental principles of inertia, relating position, velocity and acceleration of the vessel in 6 DOF. It represents the same vessel as in (2), but now the acceleration and angular velocities are inputs as well as the position and heading. The dynamics are split into a translational part and an angular part. The translational part is written as

$$\dot{p}^n = v^n \tag{4a}$$
$$\dot{v}^n = R(\Theta) f^b_{imu} + g^n. \tag{4b}$$

p^n is the north, east and down (heave) position and v^n is the NED velocity. The acceleration measurements from the IMU are rotated directly to the NED frame. The orientation of the vessel is Θ in roll, pitch, and yaw angles, and $R(\Theta)$ is the 6 DOF rotation matrix about the z, y, x-axes. Gravity is also acting on the vessel. The attitude part is written as

$$\dot{\Theta} = T(\Theta)\omega^b \tag{5}$$

with the velocity transformation matrix $T(\Theta)$ and angular rate ω^b.

Relating the two models, we have that

$$\eta = [p^n(1),\ p^n(2),\ \psi]^\top,$$
$$\nu = R(\psi)^\top [v^n(1),\ v^n(2),\ \omega^b(3)]^\top. \tag{6}$$

3. OBSERVERS USED IN DYNAMIC POSITIONING

The two observers are briefly presented in this section. The reader is referred to Fossen and Strand (1999), Fossen (2011) for details on the model-based observer, and to Grip et al. (2012), Grip et al. (2013), Bryne et al. (2014), and Bryne et al. (2015) for details on the signal-based observer.

3.1 Model-based observer

We have chosen to work with the nonlinear passive observer (Fossen and Strand, 1999) since it is an intuitive observer to tune, and it has global stability results. This is based on the control plant model (2) taking in position and heading measurements, and commanded thrust u from the controller (see Section 4). It is a 3 DOF observer, and the algorithm can be written as

$$\dot{\hat{\xi}} = A_\omega \hat{\xi} + K_{1,\omega}\tilde{y} \tag{7a}$$
$$\dot{\hat{\eta}} = R(\psi)\hat{\nu} + K_2\tilde{y} \tag{7b}$$
$$\dot{\hat{b}} = T_b^{-1}\hat{b} + K_3\tilde{y} \tag{7c}$$
$$M\dot{\hat{\nu}} = -D\hat{\nu} + R^\top(\psi)\hat{b} + u + R^\top(\psi)K_4\tilde{y} \tag{7d}$$
$$\hat{y} = \hat{\eta} + C_\omega\hat{\xi}, \tag{7e}$$

where $\hat{\xi}, \hat{\eta}, \hat{v}, \hat{b} \in \mathbb{R}^3$ are the estimates of the states in (2), $\tilde{y} = y - \hat{y}$ is the measurement estimation error and $K_{1,\omega} \in \mathbb{R}^{6\times3}_{>0}, K_2, K_3, K_4 \in \mathbb{R}^{3\times3}_{>0}$ are observer gains chosen to satisfy the Kalman-Yakubovich-Popov (KYP) lemma (Khalil, 2002). The wave filter contains estimates of the peak wave frequency and damping in $A_\omega \in \mathbb{R}^{6\times6}$, and $C_\omega = W$ from (2). The key feature in this observer is the wave filter. This means that the wave frequency motion $W\xi$ is separated from the low frequency motion η, and the output from this observer is the *low frequency motion* estimate of the vessel: $\hat{\eta}_1 := \hat{\eta}$ and $\hat{\nu}_1 := \hat{\nu}$.

Define the estimation errors as $\tilde{(\cdot)}:=(\cdot)$ - $\hat{(\cdot)}$, and collect them in the state $x_1 := [\tilde{\nu}^\top,\ \tilde{\eta}^\top,\ \tilde{\xi}^\top,\ \tilde{b}^\top]^\top$. The error dynamics of (2) and the model-based observer (7) is written compactly as

$$\dot{x}_1 = F_1(x_1, p^n, \psi). \tag{8}$$

3.2 Signal-based observer

The signal-based observer is a 6 DOF observer, and is based on the kinematic relations (4) and (5). The attitude is represented using quaternions, q.

Attitude observer Write the attitude observer dynamics as

$$\dot{\hat{q}} = T(\hat{q})(\omega^b_{imu} - \hat{b}_g + \hat{\sigma}) \tag{9a}$$
$$\dot{\hat{b}}_g = Proj(\hat{b}_g, -k_I\hat{\sigma}), \tag{9b}$$

with the correction term

$$\hat{\sigma} = k_1 c^b \times R(\hat{q})^\top c^n + k_2 f^b_{imu} \times R(\hat{q})^\top \hat{f}^n \tag{10}$$

where $\hat{q}$ is the attitude estimate, $T(\hat{q})$ is the velocity transformation matrix, $\hat{b}_g$ is the gyro bias estimate, and a bias compensated angular rate estimate is provided as well $\hat{\omega}^b$. The projection function used is found in (Grip et al., 2012, Appendix). The symbol $\times$ represents the cross product, $c^b = [\cos(\psi),\ -\sin(\psi),\ 0]^\top$, ψ is measured by the compass, and $c^n = [1,\ 0,\ 0]^\top$ is a reference vector. f^b_{imu} is the measured acceleration and $\hat{f}^n$ is the estimated acceleration in NED. Choose the gains $k_1 \geq k_P,\ k_2 \geq k_P$, with $k_P > 0$ sufficiently large.

Translational Observer The translational observer is based on (4). The equations are taken from Bryne et al. (2015), as we use a virtual vertical reference in heave in stead of the low quality GNSS measurement. The algorithm is

$$\dot{\hat{p}}^n_I = \hat{p}^n_z + k_{pipi}\tilde{p}_I \tag{11a}$$
$$\dot{\hat{p}}^n = \hat{v}^n + \theta^2 \begin{bmatrix} 0_{2\times1} & K_{pp} \\ k_{ppi} & 0_{1\times2} \end{bmatrix} \begin{bmatrix} \tilde{p}_I \\ \tilde{p} \end{bmatrix} \tag{11b}$$
$$\dot{\hat{v}}^n = \hat{f}^n + g^n + \theta^3 \begin{bmatrix} 0_{2\times1} & K_{vp} \\ k_{vpi} & 0_{1\times2} \end{bmatrix} \begin{bmatrix} \tilde{p}_I \\ \tilde{p} \end{bmatrix} \tag{11c}$$
$$\dot{\xi}_f = -R(\hat{q})S(\hat{\sigma})f^b_{imu} + \theta^4 \begin{bmatrix} 0_{2\times1} & K_{\xi p} \\ k_{\xi pi} & 0_{1\times2} \end{bmatrix} \begin{bmatrix} \tilde{p}_I \\ \tilde{p} \end{bmatrix} \tag{11d}$$
$$\hat{f}^n = R(\hat{q})f^b_{imu} + \xi_f. \tag{11e}$$

The driving errors are defined as: $\tilde{p} = p^n - \hat{p}^n \in \mathbb{R}^2, \tilde{p}_I = p_I - \hat{p}_I = 0 - \hat{p}_I \in \mathbb{R}$. $R(\hat{q})$ is the rotation matrix in roll, pitch, and yaw represented with quaternion estimates from (9). ξ_f is a correction term on the acceleration estimate. $K_{pp}, K_{vp}, K_{\xi p} \in \mathbb{R}^{2\times2}_{>0}$, and $k_{pipi}, k_{ppi}, k_{vpi}, k_{\xi pi} \in \mathbb{R}_{>0}$. $\theta \geq 1$ is a high gain. The equation (11a) includes only the virtual heave part of the position estimate, i.e. it is scalar.

The estimation error state can be written compactly as $x_2 := [\tilde{q}^\top, \tilde{b}_g^\top, \tilde{p}_I, \tilde{p}^\top, \tilde{v}^\top, \tilde{f}^\top]^\top$, with estimation errors defined as before, $\tilde{(\cdot)}:=(\cdot)$ - $\hat{(\cdot)}$. The error dynamics can be written compactly as

$$\dot{x}_2 = F_2(x_2, p^n, \psi, \omega^b_{imu}, f^b_{imu}). \tag{12}$$

The signal-based estimation error dynamics (12) has the origin uniformly locally exponentially stable (ULES) with almost global attractivity (Grip et al. (2012) and Bryne et al. (2015)). The attractivity is almost global but not global; hence, the convergence rate from points near the boundary of the basin of attraction, particularly those corresponding to yaw estimation error equal to 180 degrees, is slow.

The output from the signal-based observer is transformed so it has the same form as the output from the model-based observer using (6)

$$\begin{aligned}\hat{\eta}_2 &:= [\hat{p}^n(1),\ \hat{p}^n(2),\ \hat{\psi}_2]^\top \\ \hat{\nu}_2 &:= R(\hat{\psi}_2)^\top [v^n(1),\ v^n(2),\ \hat{\omega}^b(3)]^\top \end{aligned} \tag{13}$$

where $\hat{\psi}_2$ is the heading angle estimate we get when converting from quaternions $\hat{q}$ to Euler angles, and the velocity output is transformed from the NED frame to the body frame. Because this observer relies on acceleration measurements and does not include a bias force estimation model, it reacts fast and accurately to transients. The downside to this is that the estimates are not wave filtered, so $\hat{\eta}_2$ and $\hat{\nu}_2$ will cause an oscillatory control input.

4. CONTROLLER

The control objective is to control the vessel to the desired time-varying setpoint $\eta_d(t)$ with the desired velocity trajectory $\nu_d(t)$:

$$\begin{aligned}\lim_{t\to\infty} \eta(t) - \eta_d(t) &= 0 \\ \lim_{t\to\infty} \nu(t) - \nu_d(t) &= 0.\end{aligned}$$

We write the tracking error dynamics as $x_0 := [\nu - \nu_d,\ \eta - \eta_d,\ \zeta - K_i^{-1} b]$, with the integral state in the controller ζ defined below.

The control objective is achieved by combining feedforward of the desired trajectory and output feedback using a nonlinear proportional, integral, derivative (nPID) algorithm. The algorithm is

$$\dot{\zeta} = (\hat{\eta}_s - \eta_d) \tag{14a}$$

$$u = -K_p R^\top(\psi)(\hat{\eta}_s - \eta_d) - K_d(\hat{\nu}_s - \nu_d) \tag{14b}$$

$$- K_i R^\top(\psi)\zeta + M\dot{\nu}_d + D\nu_d. \tag{14c}$$

$u \in \mathbb{R}^3$ is the commanded thrust, $K_p, K_d, K_i \in \mathbb{R}^{3\times 3}$ are the proportional, derivative and integral gains, and $\hat{\eta}_s$ and $\hat{\nu}_s$ are the estimates from the model-based observer when $s = 1$, and from the signal-based observer when $s = 2$. ζ compensates for the unknown bias force in (2d), which is commonly assumed constant for control design. The integral action error is $\zeta - K_i^{-1} b$. K_i should be picked so it can commute with the rotation matrix, i.e. $K_i R(\psi) = R(\psi) K_i$. The last two terms in (14b) are feedforward terms of the desired acceleration times inertia and desired velocity times damping.

Loria et al. (2000) showed that the feedback control law (14) using model-based estimates renders the closed-loop vessel and output feedback controller UGAS.

Following a similar approach for the other observer renders the closed-loop vessel and output feedback controller using signal-based estimates uniformly locally asymptotically stable (ULAS). We conclude local because the desired behavior of the observer error dynamics (12) is predicated on the derivative of the tracking error, $\dot{x}_0$, being bounded. It is not clear whether the region of attraction for the origin of the signal-based output feedback controller and vessel is almost global. The simulations in Section 7 indicate that the basin of attraction when the signal-based estimates are used in feedback is fairly large, but further research on this problem is required to make rigorous statements about the basin of attraction of the origin for (12), (14), (4) and (5).

5. HYBRID SIGNAL-BASED AND MODEL-BASED OBSERVER IN CLOSED-LOOP CONTROL

The observers flow in parallel in the hybrid observer design, and the position and velocity in surge, sway, and yaw from the observer that performs best is used in output feedback with (14). The estimation errors are monitored, and switching is limited by hysteresis.

5.1 Plant, controller, and observer

The flow dynamics of the hybrid system constitutes the marine vessel, controller, and observer dynamics is

$$\dot{\eta} = R(\psi)\nu, \tag{15a}$$

$$M\dot{\nu} = -D_L\nu + R^\top(\psi)b + u \tag{15b}$$

$$\dot{\zeta} = \hat{\eta}_s - \eta_d \tag{15c}$$

$$\begin{aligned} u = &-R^\top(\psi)K_p(\hat{\eta}_s - \eta_d) - K_d(\hat{\nu}_s - \nu_d) \\ &- R^\top(\psi)K_i\zeta + M\dot{\nu}_d + D\nu_d \end{aligned} \tag{15d}$$

$$\dot{x}_1 = F_1(x_1, p^n, \psi) \tag{15e}$$

$$\dot{x}_2 = F_2(x_2, p^n, \psi, \omega^b_{imu}, f^b_{imu}) \tag{15f}$$

$$\dot{s} = 0, \tag{15g}$$

with $\eta, \nu, \hat{\eta}_s, \hat{\nu}_s \in \mathbb{R}^3$. (15a-b) are the vessel dynamics, (15c-d) is the control algorithm with output feedback and reference feedforward, (15e) is the model-based observer (7), and (15f) is the signal-based observer from (9) and (11). $s \in \{1, 2\}$ is a logic variable that indicates if the model-based or signal-based estimates are used in closed-loop control. $s = 1$ is model-based and $s = 2$ is the signal-based estimates, as decided by the performance monitoring and switching logic.

5.2 Performance monitoring and switching logic

The performance monitoring function computes the estimation errors of the two observers in position and heading over a time period to make sure the system does not switch unnecessarily often. In order to make a fair comparison, the total (low frequency and wave frequency) estimates are compared with the measured position and heading where north and east positions are measured in meters and heading in degrees. The model-based estimate, including wave frequency components, is $\hat{y}_1 := \hat{y}$ from (7), and the signal-based position and heading estimates are $\hat{y}_2 := \hat{\eta}_2$.

We sample y, $\hat{y}_1$, and $\hat{y}_2$ every $T > 0$ seconds and $N \in \mathbb{Z}_{\geq 1}$ consecutive measurements are stored in the state of three different shift registers with states $\chi_k \in \mathbb{R}^{3N}$, $k = \{0, 1, 2\}$. $\chi_{k,i} \in \mathbb{R}^3$, $i \in \{1, \ldots, N\}$ are the stored measurements and estimates. The state component $\chi_{k,1}$ contains the most recent samples, and $\chi_{k,N}$ contains the least recent samples; see (17a-f).

Let $\ell \in \mathbb{R}$ be a counter that triggers a performance check of the observer. This happens every LT seconds where $L \in \mathbb{Z}_{\geq 1}$. Let us define the *shift register mean value* for the measurements: $\bar{\chi}_0 := \frac{1}{N}\sum_{i=1}^{N} \chi_{0,i}$, model-based: $\bar{\chi}_1 := \frac{1}{N}\sum_{i=1}^{N} \chi_{1,i}$, and signal-based: $\bar{\chi}_2 := \frac{1}{N}\sum_{i=1}^{N} \chi_{2,i}$. We switch to the other observer if it performs better than the one currently in feedback with a hysteresis margin of $\varepsilon > 0$; see (17g-i).

The jumps for these variables are allowed when

$$(x_0, x_1, x_2, \chi_k, \tau, \ell, s) \in D \tag{16}$$

$$D := \mathbb{R}^9 \times \mathbb{R}^{15} \times \mathbb{R}^{16} \times \mathbb{R}^{3Nk} \times \{T\} \times \{0, \ldots, L\} \times \{1, 2\}$$

x_0 is the tracking error defined in Section 4. The jumps satisfy

$$\chi_{0,1}^{+} = y \tag{17a}$$
$$\chi_{1,1}^{+} = \hat{y}_1 \tag{17b}$$
$$\chi_{2,1}^{+} = \hat{y}_2 \tag{17c}$$
$$\chi_{k,2}^{+} = \chi_{k,1}, \quad k = \{0, 1, 2\} \tag{17d}$$
$$\vdots \tag{17e}$$
$$\chi_{k,N}^{+} = \chi_{k,N-1}, \ k = \{0, 1, 2\} \tag{17f}$$
$$\tau^{+} = 0 \tag{17g}$$
$$\ell^{+} = \begin{cases} \ell + 1 & \ell \in \{0, \ldots, L-1\} \\ 0 & \ell = L \end{cases} \tag{17h}$$
$$s^{+} \in \begin{cases} s & \ell \in \{0, \ldots, L-1\} \\ 3 - s & \ell = L, \ |\bar{\chi}_0 - \bar{\chi}_{3-s}| \leq |\bar{\chi}_0 - \bar{\chi}_s| - \varepsilon \\ s & \ell = L, \ |\bar{\chi}_0 - \bar{\chi}_{3-s}| \geq |\bar{\chi}_0 - \bar{\chi}_s| - \varepsilon. \end{cases} \tag{17i}$$

All the states introduced in this section remain constant during flows, except for τ that satisfies $\dot{\tau} = 1$. Flows are allowed when

$$(x_0, x_1, x_2, \chi_k, \tau, \ell, s) \in C \tag{18}$$

$$C := \mathbb{R}^9 \times \mathbb{R}^{15} \times \mathbb{R}^{16} \times \mathbb{R}^{3Nk} \times [0, \ T] \times \{0, \ldots, L\} \times \{1, 2\}.$$

6. STABILITY

The stability results used to analyze the set are based on invariance and uniform convergence according to Proposition 7.5 of Goebel et al. (2012). Consider the set

$$\mathcal{A} := \{0\} \times \{0\} \times \{0\} \times \Psi \times [0, \ T] \times \{0, \ldots, L\} \times \{1, 2\}, \tag{19}$$

with $\Psi := \{\chi_{0,ss}\} \times \{\chi_{1,ss}\} \times \{\chi_{2,ss}\}$ and $\chi_{k,ss}$, $k = \{0, 1, 2\}$ are the steady-state values of the shift register with saved measurements and estimates of the total vessel motion. The set $\mathcal{A}$ is compact because its components are closed and bounded sets.

Theorem 1. The set $\mathcal{A}$ defined in (19) is uniformly locally asymptotically stable (ULAS) for the hybrid system defined in (15)-(18).

Proof: The set $\mathcal{A}$ is:

(i) strongly forward invariant. If the solution starts inside the set $\mathcal{A}$, the observer in closed loop, regardless of which, will keep the solution within $\mathcal{A}$ during flows. During jumps the solution still remains in $\mathcal{A}$ since jumping from the set of values $\mathcal{A} \cap D$, will yield a solution that still is in $\mathcal{A}$.

(ii) uniformly attractive from a neighborhood of itself. Since each observer is converging, at least locally, it follows from the switching condition in (17i) that the number of switches will be uniformly bounded, at least from initial conditions sufficiently close to the set $\mathcal{A}$, and that the last switching time can also be uniformly bounded. That is there exists a T such that

$$|\bar{\chi}_0(t) - \bar{\chi}_1(t)| + |\bar{\chi}_0(t) - \bar{\chi}_2(t)| \leq \varepsilon \quad \forall t \geq T,$$

and there will be no more switching. Then, because of uniform attractivity in the absence of switching, we also have uniform attractivity with the switching. □

7. SIMULATION RESULTS AND DISCUSSION

Simulations are done in Matlab/Simulink with a platform supply vessel in a marine environment with waves, wind and current. The high fidelity simulation model is based on the MSS GNC toolbox (Fossen and Perez, 2010) with realistic measurement noise and sample time. The sea state is very rough with significant wave height 4 meters, peak frequency 0.6 rad/s taken from the JONSWAP [1] spectrum, with mean incident wave heading 150° in the North-East frame (Price and Bishop, 1974). The current speed is 0.5 m/s with direction 180°, and the wind speed and direction are taken as expectation values based on the wave parameters.

The case simulated is a setpoint change where the vessel moves 20 meters North and East, and changes heading from $\psi = 0°$ to $\psi = -90°$. The change happens at 2500 seconds so the observer parts have ample time to converge to steady state first. Figure 1 shows the estimation error for the signal-based and model-based observer parts after the initialization phase. The switching variable s indicates which observer estimates are used in closed loop.

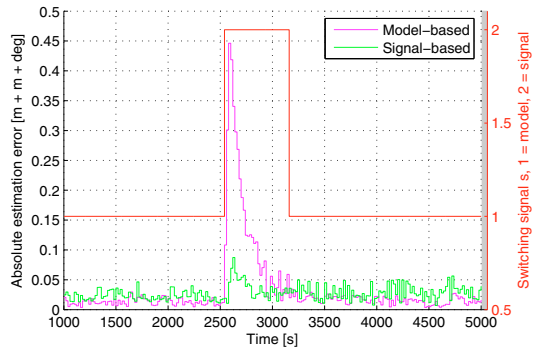

Fig. 1. Estimation error for the signal-based and model-based parts. The estimates used in closed-loop s is indicated, with axis to the right.

At initialization the model-based observer is chosen in feedback, as it takes time for the gyro bias estimate $\hat{b}_g$ in the signal-based observer to converge. The bias force estimate $\hat{b}$ in the model-based observer converges after about 500 seconds. When the vessel changes heading,

[1] Joint North Sea Wave Project.

the forces on the hull due to current, wind and waves changes rapidly. This induces a transient in the model-based part since the bias force estimate takes time to converge to the new value. 40 seconds after the vessel starts the setpoint change, the signal-based observer performs better and is used in feedback. 700 seconds later the model-based bias force estimate $\hat{b}$ has converged to the new value and is used in feedback once more. While performing better during the setpoint change, the signal-based part has higher estimation error during steady state, as seen clearly in the figure. The simulation results indicate that the basin of attraction for the signal-based estimates in output feedback control is fairly large, since it includes points from where we end up switching.

The vessel response is more oscillatory when the signal-based observer is used in closed-loop. This is because the signal-based observer does not include a wave filter and has oscillatory estimates. It therefore induces some wave frequency motion on the system through the control law, approximately ± 1 meter. This motion is insignificant compared with the motion due to the 4 meter waves, however, the vessel uses more energy and in a real system the wear and tear on the machinery would be increased.

8. CONCLUSION

The hybrid observer with a signal-based and a model-based part was shown to have good performance in simulations of a DP vessel in a rough sea state. The observer used in output feedback with a nonlinear PID tracking controller, was shown uniformly locally asymptotically stable.

REFERENCES

Brodtkorb, A.H., Sørensen, A.J., and Teel, A.R. (2014). Increasing the operation window of dynamic positioned vessels using the concept of hybrid control. *ASME 2014 33rd International Conference on Ocean, Offshore and Arctic Engineering Volume 1A: Offshore Technology San Francisco, California, USA, June 813, 2014*.

Bryne, T.H., Fossen, T.I., and Johansen, T.A. (2014). Nonlinear observer with time-varying gains for inertial navigation aided by satellite reference systems in dynamic positioning. *2014 22nd Mediterranean Conference on Control and Automation, MED 2014*, 1353–1360.

Bryne, T.H., Fossen, T.I., and Johansen, T.A. (2015). A virtual vertical reference concept for GNSS/INS applications at the sea surface. *10th Conference on Maneouvring and Control of Marine Craft, MCMC August 24-26 2015 Copenhagen, Denmark*.

Bryne, T.H., Fossen, T.I., and Johansen, T.A. (2016). Design of inertial navigation systems for marine craft with adaptive wave filtering by triple-redundant sensor packages. *To appear in: International Journal of Adaptive Control and Signal Processing*.

Fossen, T.I. (2011). *Handbook of Marine Craft Hydrodyamics and Motion Control*. Wiley.

Fossen, T.I. and Perez, T. (2010). Marine systems simulator, viewed 27.01.2016. URL `http://www.marinecontrol.org`.

Fossen, T.I. and Strand, J.P. (1999). Passive nonlinear observer design for ships using lyapunov methods: full-scale experiments with a supply vessel. *Automatica*, 35(1), 3 – 16.

Goebel, R., Sanfelice, R.G., and Teel, A.R. (2012). *Hybrid Dynamical Systems, Modelling, Stability and Robustness*. Princeton University Press.

Grip, H.F., Fossen, T.I., Johansen, T.A., and Saberi, A. (2013). Nonlinear observer for gnss-aided inertial navigation with quaternion-based attitude estimation. *Proceedings of the American Control Conference*, 272–279.

Grip, H., Fossen, T., Johansen, T., and Saberi, A. (2012). Attitude estimation using biased gyro and vector measurements with time-varying reference vectors. *IEEE Transactions on Automatic Control*, 57(5), 1332–1338. doi:10.1109/TAC.2011.2173415.

Hassani, V., Sørensen, A.J., and Pascoal, A.M. (2013). A novel methodology for robust dynamic positioning of marine vessels: Theory and experiments. *Proceedings of the American Control Conference*, 560–565.

Hua, M.D. (2010). Attitude estimation for accelerated vehicles using GPS/INS measurements. *Control Engineering Practice*, 18(7), 723 – 732. Special Issue on Aerial Robotics.

Khalil, H. (2002). *Nonlinear Systems, Second Edition*. Prentice Hall,.

Loria, A., Fossen, T.I., and Panteley, E. (2000). A separation principle for dynamic positioning of ships: Theoretical and experimental results. *IEEE Transactions on Control Systems Technology*, 8(2), 332–343. doi: 10.1109/87.826804.

Mahony, R., Hamel, T., and Pflimlin, J.M. (2008). Nonlinear complementary filters on the special orthogonal group. *IEEE Transactions on Automatic Control*, 53(5), 1203–1218.

Nguyen, T.D., Sørensen, A.J., and Quek, S.T. (2008). Multi-operational controller structure for station keeping and transit operations of marine vessels. *IEEE Transactions on Control Systems Technology*, 16(3), 491–498.

Nguyen, T.D., Sørensen, A.J., and Tong Quek, S.T. (2007). Design of hybrid controller for dynamic positioning from calm to extreme sea conditions. *Automatica*, 43(5), 768–785.

Price, W.G. and Bishop, R.E.D. (1974). *Probalistic Theory of Ships*. Chapman and Hall, London.

Prieur, C. and Teel, A. (2011). Uniting local and global output feedback controllers. *IEEE Transactions on Automatic Control*, 56(7), 1636–1649. doi: 10.1109/TAC.2010.2091436.

Sørensen, A.J. (2013). *Marine Control Systems, Propulsion and Motion Control of Ships and Ocean structures, Lecture Notes*. Department of Marine Technology, NTNU.

Tannuri, E.A. and Morishita, H.M. (2006). Experimental and numerical evaluation of a typical dynamic positioning system. *Applied Ocean Research*, 28(2), 133–146.

C.3

Hybrid Control to Improve Transient Response of Integral Action in Dynamic Positioning of Marine Vessels

---

Værnø, S. A., Skjetne, R.,

Available online at www.sciencedirect.com

ScienceDirect

IFAC-PapersOnLine 48-16 (2015) 166–171

IFAC Papers Online CONFERENCE PAPER ARCHIVE

Hybrid Control to Improve Transient Response of Integral Action in Dynamic Positioning of Marine Vessels ⋆

Svenn Are Tutturen * **Roger Skjetne** *

* *Centre for Autonomous Marine Operations (AMOS), Department of Marine Technology, Norwegian University of Science and Technology (NTNU), Otto Nielsens vei 10, 7491 Trondheim, Norway (e-mail: svenn.are.tutturen@ntnu.no, roger.skjetne@ntnu.no)*

Abstract: A hybrid control approach for integral action in the PID control law for dynamically positioned marine vessels is considered. The proposed method is essentially a resetting of the integration gain when the control performance deteriorates. The method allows for a flexible tuning, and could be useful when there are long periods of normal operating conditions, but abnormal events may occur. In that case the hybrid controller will have a low tuning in the normal regime and switch to a more aggressive tuning in the abnormal regime. Stability of the hybrid system is investigated, and a simulation case is performed.

Keywords: Dynamic positioning; Integral action; Hybrid dynamical systems

1. INTRODUCTION

Dynamically positioned (DP) vessels normally experience wave loads, wind loads, and currents. The loads the integral action part of the controller compensate for are slowly varying forces, almost constant for long periods of time. Because of this the integral action is normally tuned very low, such that it does not induce unnecessary oscillation in the closed loop system. Also, the tuning could be low to avoid that the integral action compensates for motion due to 1^{st} order wave loads. Even though this motion is filtered out with a wave filter [Fossen 2011], the exact knowledge of the peak frequency of the wave spectrum is uncertain, and perfect filtering is difficult. Therefore, there is some oscillatory motion left that the integral action ideally should not compensate for.

One issue with a low tuning of the integral action is that it will spend some time building up to the correct value. This is especially the case at initialization, or when large changes in force occur. This could for instance be caused by ice forces, a tension line that breaks, or a sudden wave train. In these instances, it is of interest to improve the transient response of the integral action.

Hybrid control of DP vessels has been considered in several papers in the literature. A framework with several continuous controller and observer-pairs based on the work in Hespanha [2001] was proposed for hybrid control of DP vessels in Nguyen et al. [2007]. The operational window of a DP vessel is extended by switching between different observer-controller pairs depending on the sea state. Using the same type of continuous controller and observer-pair methodology as in Nguyen et al. [2007], a hybrid control approach was proposed to combine dynamic positioning, maneuvering, and transit operation in Nguyen et al. [2008], and also to be applied for switching control for position mooring in Nguyen and Sørensen [2009]. See [Sørensen 2013] for an overview. In Brodtkorb et al. [2014] the control problem considered in Nguyen et al. [2007] is analyzed in the framework of Goebel et al. [2012], which is the framework used in this paper as well.

The main contribution of the paper is a novel control structure that allows for increased flexibility in integral action in the PID control law, for dynamically positioned marine vessels. This is achieved by a hybrid global/local controller approach. A hybrid control framework is used, and particularly the methods analyzed in [Goebel et al. 2012, Ch. 3] have motivated the method presented here.

The idea of the proposed hybrid controller is that close to the desired position the nominal local integrator is active. When the vessel is far off target, for instance due to a rapid disturbance, the global and more aggressive integral action is turned on. The benefit is that the aggressive integral action will give a faster response to a disturbance. When close to the desired values, this aggressive part is turned off, and the system is back to the nominally tuned integral action. Stability of the hybrid system is analyzed, and a simulation study is performed to demonstrate the benefit of the approach.

Notation: The time derivative is denoted by dot notation, such that $\dot{x}$ is the time derivative of x. The minimum and maximum eigenvalue of a matrix P are denoted by $\lambda_{min}(P)$ and $\lambda_{max}(P)$, respectively.

2. PROBLEM STATEMENT

Given the 3 degree of freedom (DOF) control design model of a DP system [Fossen 2011],

⋆ This work was supported by the Research Council of Norway through the Centres of Excellence funding scheme, project number 223254 - AMOS.

2405-8963 © 2015, IFAC (International Federation of Automatic Control) Hosting by Elsevier Ltd. All rights reserved.
Peer review under responsibility of International Federation of Automatic Control.
10.1016/j.ifacol.2015.10.275

$$\dot{\eta} = R(\psi)\nu \tag{1a}$$
$$M\dot{\nu} = -D\nu + R(\psi)^\top b + \tau, \tag{1b}$$

where $\eta = [N, E, \psi]^\top \in \mathbb{R}^3$ is a vector containing the North/East positions and heading, and $\nu = [u, v, r]^\top \in \mathbb{R}^3$ contains the surge/sway velocities and yaw rate, $\tau \in \mathbb{R}^3$ is the control input, and $R(\psi) \in \mathbb{R}^{3\times 3}$ is the 3 DOF rotation matrix,

$$R(\psi) = \begin{bmatrix} \cos(\psi) & -\sin(\psi) & 0 \\ \sin(\psi) & \cos(\psi) & 0 \\ 0 & 0 & 1 \end{bmatrix}. \tag{2}$$

The mass matrix is $M = M^\top > 0$, and $D > 0$ is the damping matrix. The disturbance or bias vector $b \in \mathbb{R}^3$ contains all the remaining forces affecting the vessel, such as current, second order wave forces, and unmodeled dynamics [Sørensen 2013]. It is common to assume b is constant. The task of the integral action is to compensate this bias.

Due to saturation limits in the thrusters and bounded environmental loads, we make the following assumption.

Assumption 1 The yaw rate $r := \dot{\psi}$ is bounded, with $|r| \leq r_{max} < \infty$.

In the following, the position and velocity are assumed measured. The velocity is normally found through a state observer, but to simplify the analysis, velocity is assumed known. The proposed integral action integrates the position error.

3. HYBRID CONTROLLER APPROACH

In hybrid control, continuous and discrete dynamics are combined [Goebel et al. 2012]. The continuous dynamics is called "flow", which is allowed on a flow set $\mathcal{C}$. The discrete dynamics is called "jump", which is allowed on a jump set $\mathcal{D}$.

Consider a case with two different controllers for the same system dynamics. One controller works locally, and has good performance around the equilibrium. The other "global" controller is used when the states are far from the equilibrium.

In the following, this controller structure will be used for PID control of a DP plant. Under normal conditions the local integral action will be active. The global integral action will first activate under large disturbance events that deteriorate the control performance. The global integral action will then be more aggressive in response to the disturbance.

The system setup is similar to the local/global control structure of Goebel et al. [2012], but here both controllers are globally stable. Another difference is that Goebel et al. [2012] assumes full state knowledge. Here, knowledge of the position and the velocity is assumed known, but the bias force is not known.

4. FLOW DYNAMICS

The integrator state ξ is given the dynamics

$$\dot{\xi} = L\eta, \tag{3}$$

where the properties that the matrix $L \in \mathbb{R}^{3\times 3}$ needs to satisfy will be elaborated later.

The controller considered is the standard DP PID-control law

$$\tau = -K_p R(\psi)^\top \eta - K_d \nu - K_i R(\psi)^\top \xi, \tag{4}$$

where K_p, K_d, $K_i \in \mathbb{R}^{3\times 3}$ are all positive definite matrices, and K_i commutes with the rotation matrix, that is, $K_i R(\psi) = R(\psi) K_i$. Let the integral action error be $\tilde{\xi} = \xi - K_i^{-1} b$. Then the resulting error dynamics becomes

$$\dot{\tilde{\xi}} = L\eta \tag{5a}$$
$$\dot{\eta} = R(\psi)\nu \tag{5b}$$
$$M\dot{\nu} = -K_p R(\psi)^\top \eta - (D + K_d)\nu - K_i R(\psi)^\top \tilde{\xi}. \tag{5c}$$

Collecting the error states in a state vector $x \in \mathbb{R}^9$,

$$x = \begin{bmatrix} \tilde{\xi} \\ \eta \\ \nu \end{bmatrix}, \tag{6}$$

the error dynamics becomes

$$\dot{x} = F_0(\psi) x, \tag{7}$$

where

$$F_0(\psi) = \begin{bmatrix} 0 & L & 0 \\ 0 & 0 & R(\psi) \\ -M^{-1}K_i R(\psi)^\top & -M^{-1}K_p R(\psi)^\top & -M^{-1}(D + K_d) \end{bmatrix}. \tag{8}$$

Consider the global diffeomorphism, similar to the one proposed by Lindegaard [2003],

$$x = T(\psi) z, \tag{9}$$

where

$$T(\psi) = \text{diag}\{R(\psi), R(\psi), I\}. \tag{10}$$

The z-dynamics becomes

$$\begin{aligned} \dot{z} &= \dot{T}(\psi)^\top x + T(\psi)^\top \dot{x} \\ &= \dot{T}^\top(\psi) T(\psi) z + T(\psi)^\top F_0(\psi) T(\psi) z \end{aligned} \tag{11}$$

First, consider the term $T(\psi)^\top F_0(\psi) T(\psi)$,

$$T(\psi)^\top F_0(\psi) T(\psi) = \begin{bmatrix} 0 & R(\psi)^\top L R(\psi) & 0 \\ 0 & 0 & I \\ -M^{-1}K_i & -M^{-1}K_p & -M^{-1}(D + K_d) \end{bmatrix} \tag{12}$$

Given that L commutes with the rotation matrix $R(\psi)$, that is, $R(\psi)L = LR(\psi)$, then $A_0 := T(\psi)^\top F_0 T(\psi)$ becomes

$$A_0 = \begin{bmatrix} 0 & L & 0 \\ 0 & 0 & I \\ -M^{-1}K_i & -M^{-1}K_p & -M^{-1}(D + K_d) \end{bmatrix}. \tag{13}$$

For a specification of what the K_i and L matrix needs to satisfy to commute with $R(\psi)$, see [Fossen 2011, ch. 11].

Now, consider the second term $\dot{T}(\psi)^\top T(\psi) z$. Since $\dot{R}(\psi) = R(\psi) S r$, where

$$S = \begin{bmatrix} 0 & -1 & 0 \\ 1 & 0 & 0 \\ 0 & 0 & 0 \end{bmatrix}, \tag{14}$$

the term $\dot{T}(\psi)^\top$ can be written as

$$\begin{aligned} \dot{T}(\psi)^\top &= \text{diag}\{\dot{R}(\psi)^\top,\ \dot{R}(\psi)^\top,\ 0\} \\ &= \text{diag}\{-\dot{\psi} S R(\psi)^\top,\ -\dot{\psi} S R(\psi)^\top,\ 0\} \\ &= -r S_T T(\psi)^\top, \end{aligned} \tag{15}$$

where

$$S_T = \text{diag}\{S,\ \ S,\ \ 0\} = -S_T^\top. \tag{16}$$

This gives

$$\dot{T}(\psi)^\top T(\psi)z = -rS_T T(\psi)^\top T(\psi)z = -rS_T z, \tag{17}$$

which finally gives the z-dynamics as

$$\dot{z} = A_0 z - rS_T z. \tag{18}$$

Let A_0 be Hurwitz, and choose a Lyapunov function candidate as

$$V(z) = z^\top P z, \tag{19}$$

where $P = P^\top > 0$ and

$$A_0^\top P + PA_0 = -G_0 < 0. \tag{20}$$

The time derivative of V along the trajectories of z becomes

$$\dot{V} = z^\top [A_0^\top P + PA_0 - r(S_T^\top P + PS_T)]z \tag{21a}$$

$$\leq [-\lambda_{min}(G_0) + 2r_{max}\lambda_{max}(P)]|z|^2. \tag{21b}$$

For (21b) to be negative definite, r_{max} needs to be very small, due to the structure of A_0. A less conservative estimate of r_{max} is found in Lindegaard [2003], and is based on (21a). Given A_0, r_{max}, P and G are found from an LMI optimization problem, such that

$$\dot{V} = z^\top [A_0^\top P + PA_0 - r(S_T^\top P + PS_T)]z$$
$$\leq -G|z|^2 < 0 \quad \forall\ |r| \leq r_{max}. \tag{22}$$

For how to find this r_{max}, see [Lindegaard 2003, Corollary 5.1].

5. HYBRID SYSTEM ANALYSIS

The condition for switching between the two controllers is the norm of the position error, $|\eta|$. Two scalar quantities $\eta_1^* = 0$ and $\eta_2^* > 0$ are defined, and switching is based on an idea that is similar to what was proposed in Brodtkorb et al. [2014], where switching between different DP controllers was decided based on the estimated peak frequency of the wave spectrum. In the following, the switching will be based on the position error. When $|\eta|$ is closer to η_1^* than η_2^*, that is, $\text{abs}(|\eta| - \eta_1^*) < \text{abs}(|\eta| - \eta_2^*)$, the local controller is used, and similarly the global controller is used when $|\eta|$ is closer to η_2^*.

For the hybrid system the closed loop dynamics can be described by

$$\dot{z} = f(z, L_q), \tag{23}$$

where $f(z, L_q)$ is given by (18), and L_q is the L-matrix from (5a). This L-matrix is the only difference between the local and global controller. The variable $q \in \{1, 2\} =: \mathcal{Q}$ is a switching variable between the two controllers, where L_1 is the L-matrix used in the local controller, and L_2 is used by the global controller ($\|L_2\| \geq \|L_1\|$).

The system will include dwell-time switching, and the timer variable τ has continuous dynamics $\dot{\tau} = 1$. When $\tau = T$ jumps are allowed, and the preferred controller is decided based on a check of whether $|\eta|$ is closer to η_1^* than η_2^*, and vice versa. This can be formally written as $q = \text{argmin}_{\alpha\in\mathcal{Q}}[\text{abs}(|\eta| - \eta_\alpha^*)]$ [Brodtkorb et al. 2014].

From (19)-(22), given A_0 Hurwitz, a Lyapunov function on the form

$$W_i(z) = z^\top P_i z,\ \ P_i = P_i^\top > 0,\ \ i = 1, 2,\ \ z \in \mathbb{R}^9, \tag{24}$$

can be found for both the local and global closed-loop system.

$$\alpha_1(|z|) \leq W_i(z) \leq \alpha_2(|z|), \tag{25}$$

where $\alpha_1(|z|) = \min\{\lambda_{min}(P_1), \lambda_{min}(P_2)\}|z|^2 =: p_m|z|^2$, and $\alpha_2(|z|) = \max\{\lambda_{max}(P_1), \lambda_{max}(P_2)\} =: p_M|z|^2$. Define the augmented state space as

$$z_e := \begin{bmatrix} z \\ \tau \\ q \end{bmatrix} \in \mathbb{R}^{11}. \tag{26}$$

Then the hybrid system becomes

$$\left.\begin{aligned} \dot{z} &= f(z, L_q) \\ \dot{q} &= 0 \\ \dot{\tau} &= 1 \end{aligned}\right\} \tau \in [0, T] \tag{27}$$

$$\left.\begin{aligned} z^+ &= z \\ q^+ &= \text{argmin}_{\alpha\in Q}[\text{abs}(|\eta| - \eta_\alpha^*)] \\ \tau^+ &= 0 \end{aligned}\right\} \tau = T, \tag{28}$$

where the flow set is

$$\mathcal{C} := \mathbb{R}^8 \times [-r_{max}, r_{max}] \times \mathcal{Q} \times [0, T], \tag{29}$$

and the jump set is

$$\mathcal{D} := \mathbb{R}^8 \times [-r_{max}, r_{max}] \times \mathcal{Q} \times \{T\}. \tag{30}$$

The goal is to prove that the set

$$\mathcal{A} = \{z_e :\ \ z = 0,\ \ q \in \mathcal{Q},\ \ \tau \in [0, T]\} \tag{31}$$

is uniformly globally (pre-) asymptotically stable. The relevant theorem from Goebel et al. [2012] is given in Appendix A. Note that the distance to the set $|z_e|_\mathcal{A} = |z|$.

For any scalar $\mu > 0$, consider the following Lyapunov function

$$V(z_e) = \text{e}^{\mu\tau} W_q(z) W_{3-q}(z), \tag{32}$$

and notice that

$$p_m^2|z|^4 \leq V(z_e) \leq p_M^2 \text{e}^{\mu T}|z|^4,$$

such that condition(A.1) is satisfied for $\alpha_1(|z|) := p_m^2|z|^4$ and $\alpha_2(|z|) := p_M^2 \text{e}^{\mu T}|z|^4$.

Define $G_m := \min\{\lambda_{min}(G_1), \lambda_{min}(G_2)\}$, such that local controller satisfies

$$\langle \nabla W_1, f(z, \kappa_1\rangle \leq -\lambda_{min}(G_1)|z|^2$$
$$\leq -G_m|z|^2\ \ \forall z \in \mathbb{R}^9, \tag{33}$$

and the global controller satisfies

$$\langle \nabla W_2, f(z, \kappa_2\rangle \leq -\lambda_{min}(G_2)|z|^2$$
$$\leq -G_m|z|^2\ \ \forall z \in \mathbb{R}^9. \tag{34}$$

Consider next the flow dynamics of $V(z_e)$,

$$\langle V(z_e), f\rangle = \text{e}^{\mu\tau}[\mu V(z_e) + \langle \nabla W_1, f(z, \kappa_1\rangle W_2(z)$$
$$+ \langle \nabla W_2, f(z, \kappa_2\rangle W_1(z)]$$
$$\leq \text{e}^{\mu\tau}[\mu p_M^2 \text{e}^{\mu T}|z|^4 - 2G_m p_m|z|^4], \tag{35}$$

and let $T := \frac{\varsigma}{\mu}$, such that for $\mu = \varepsilon\frac{2G_m p_m}{p_M^2 \text{e}^\varsigma}$, $\varepsilon < 1$, the flow dynamics becomes

$$\langle \nabla V(z_e), f_q\rangle \leq -\rho_1|z|^4,\ \ \forall x \in \mathcal{C}, f \in F(x) \tag{36}$$

where $\rho_1 = (1-\varepsilon)2G_m p_m \text{e}^{\mu\tau} > 0$, such that the Lyapunov function decrease in flow, and condition (A.2) is satisfied.

Let $V(g)$ be the value of $V(z_e)$ after a jump, and $V(z_e)$ the value right before a jump. Looking at the jump dynamics, $V(g) - V(z_e)$ becomes

$$V(g) - V(z_e) = W_{q^+} W_{3-q^+} - \mathrm{e}^{\mu T} W_q W_{3-q}$$
$$= -(\mathrm{e}^{\mu T} - 1) W_q W_{3-q}$$
$$\leq -\rho_2 |z|^4, \quad \forall x \in \mathcal{D}, g \in G(D) \qquad (37)$$

where $\rho_2 > 0$ since $\mathrm{e}^{\mu T} > 1$ for $T > 0$, and since both W_1 and W_2 are scalar quantities, $W_1 W_2 = W_2 W_1$.

Note that in the stability proof there was only a demand for the timer variable T to be strictly larger than zero. The reason for this is because the switching is between two vector fields that are globally stable, and the switch between them is performed only to achieve better performance, so the dwell time need not be large.

6. SIMULATION CASE STUDY

As a case study a vessel simulated in MATLAB/Simulink, using the MSS Toolbox [MSS 2010] is considered. The simulated vessel is a model ship called Cybership III (CS3), which is used for experiments in the Marine Cybernetics Lab (MC-lab) at the Norwegian University of Science and Technology.

The vessel model used is given by (1), where the mass and damping matrices are given in Appendix B.

The case study will compare the hybrid local/global controller implementation to a non-switching PID control law. Good tuning rules are stated in [Fossen 2011, Ch. 12]. A damping ratio corresponding to critical damping is chosen, and design time constants for the closed loop system and the controller gains are given in Appendix B.

The comparison is performed between the hybrid controller, a non-switching controller with nominal integral action (named "low gain"), and a non-switching controller with aggressive integral action (named "high gain"). For the local controller, we use $L = I_{3\times 3}$, and for the global controller we use $L = 3I_{3\times 3}$. For the hybrid controller, other relevant parameters are the timer variable T that is set to $T = 2$s, and $\eta_1^* = 0$, and $\eta_2^* = 1.0$.

The vessel is initialized in $(\eta, \nu) = 0$. The bias force b is acting in the NED frame, and in both North and East direction there is a sine wave of amplitude $0.3N$ with a frequency of $0.1Hz$. In North direction there is also a ramp component equal to $0.001t$ to illustrate a slowly varying bias. In both North, East, and yaw there is a step disturbance at $t = 500s$ of magnitude $5N$ in North, $3N$ in East, and $1Nm$ in yaw. In yaw there is also a white noise component with variance 0.001. See Figure 3.

The results are shown in figures 1 to 4. In Figure 1 the error in position is shown, and also the switching signal q. From the plot of q it is observed that the global controller is active right after the step inputs, and some seconds later the controller switches back to the nominal integral action. Note that all controllers show similar ability to maintain position in normal conditions, but after the step disturbance the low tuned controller is slower to get back to position. This is illustrated more clearly in Figure 2 where the cumulative error in position is shown.

In Figure 3 the bias force is shown. Also, the integral action of the three controllers are plotted. Note that in North and East up to $t = 500s$ the high gain controller has a higher integral action amplitude, and therefore spends more control action trying to compensate for the sine waves. This is also illustrated in Figure 4 where the cumulative control action is shown between $t = 200s$ and $t = 300s$. This figure illustrates that the high gain controller spends more control effort than the hybrid and the low gain controllers (those two are equal in this time interval), whereas Figure 2 shows that this does not give a considerable gain in position performance. Note that the hybrid solution gives a trade-off between the two controllers, where the integral action is relaxed in the normal regime, and responsive when there is a step change in b. This ensures that the position offset is maintained close to the level of the high gain integral action controller, without the additional control effort in the normal regime.

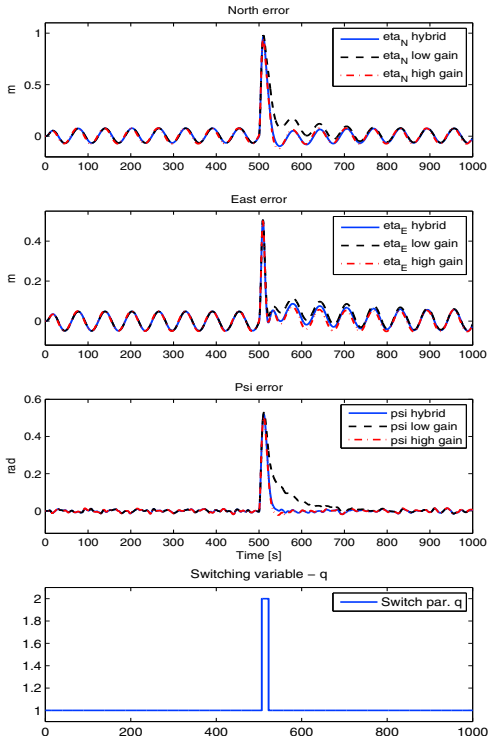

Fig. 1. North position error (top), East position error (second), yaw angle error (third), q (bottom).

7. CONCLUSION

In the following a hybrid control approach for integral action in the PID control law for dynamically positioned marine vessels is considered. The proposed approach allows the integral action to work aggressively when there is a large change is external force affecting the vessel, and to work slowly in normal conditions. The controller is shown to be uniformly globally asymptotically stable, and the benefit of the design is illustrated through simulations.

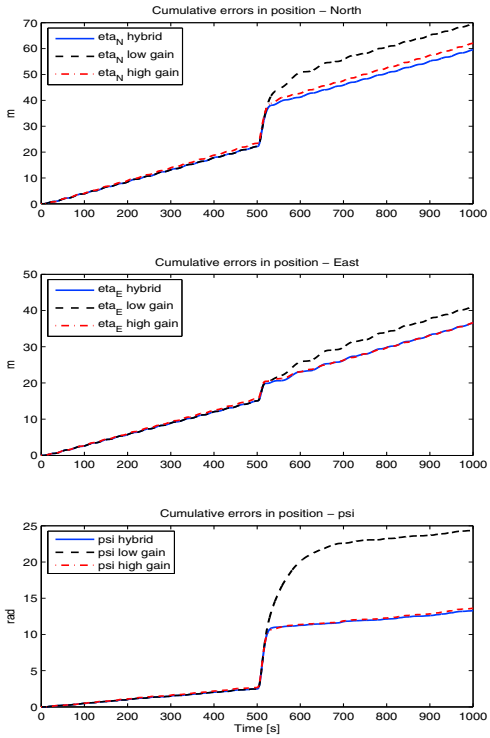

Fig. 2. Comulative position error. North (top), East (middle), yaw (bottom).

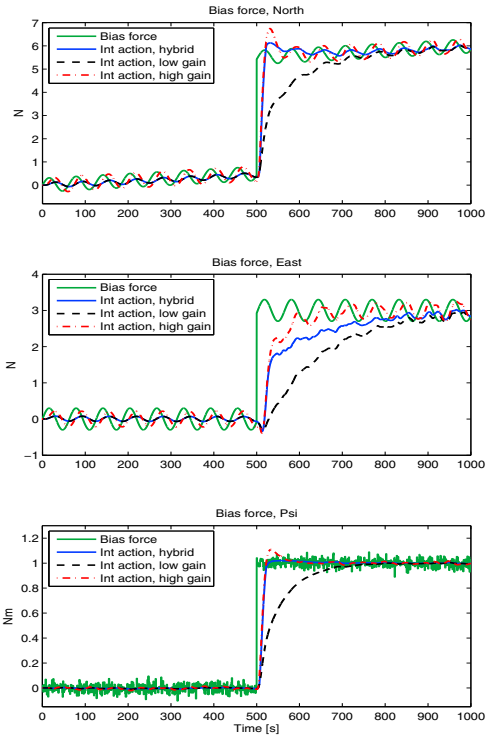

Fig. 3. Bias force and integral action. North (top), East (middle), yaw (bottom).

Appendix A. STABILITY THEOREM

Theorem 1. (Goebel et al. [2012] Theorem 3.18). (Sufficient Lyapunov conditions)
Let $\mathcal{H} = (C, F, \mathcal{D}, G)$ be a hybrid system and let $\mathcal{A} \subset \mathbb{R}^n$ be closed. If V is a Lyapunov function candidate for $\mathcal{H}$ and there exists α_1, $\alpha_2 \in K_\infty$, and a continuous positive definite function ρ such that

$$\alpha_1(|x|_A) \leq V(x) \leq \alpha_2(|x|_A) \quad \forall x \in C \cup \mathcal{D} \cup G(\mathcal{D}) \quad \text{(A.1)}$$
$$\langle \nabla V(x), f \rangle \leq -\rho(|x|_A) \quad \forall x \in C, f \in F(x) \quad \text{(A.2)}$$
$$V(g) - V(x) \leq -\rho(|x|_A) \quad \forall x \in \mathcal{D}, g \in G(\mathcal{D}) \quad \text{(A.3)}$$

then $\mathcal{A}$ is uniformly globally pre-asymptotically stable for $\mathcal{H}$.

Note on pre-asymptotically [Goebel et al. 2012, p. 45]: Pre-asymptotically indicates the possibility of a maximal solution that is not complete, even though it may be bounded. By including "pre-" this phenomena is included. Lyapunov functions do not guarantee existence or completeness of solutions, so this inclusion is reasonable.

Appendix B. CASE STUDY - DIMENSIONS AND TUNING

Parameters Cybership III

Mass matrix M,

$$M = \begin{bmatrix} 76.88 & 0 & 0 \\ 0 & 149.58 & -1.07 \\ 0 & -1.07 & 34.10 \end{bmatrix},$$

and damping matrix D,

$$D = \begin{bmatrix} 12.20 & 0 & 0 \\ 0 & 11.87 & 0.59 \\ 0 & 0.59 & 4.37 \end{bmatrix}.$$

Controller tuning

Critical damping is chosen for all degrees of freedom (DOF), such that the damping ratio ζ becomes

$$\zeta = \text{diag}\{1.0,\ 1.0,\ 1.0\}.$$

The design time constants

$$T_n = \left[T_{n_{surge}}, T_{n_{sway}}, T_{n_{yaw}}\right] = [15,\ 15,\ 20]\,[s],$$

and corresponding design natural frequencies

$$\omega_n = \text{diag}\{\left[\frac{2\pi}{T_{n_{surge}}}, \frac{2\pi}{T_{n_{sway}}}, \frac{2\pi}{T_{n_{yaw}}}\right]\},$$

and from Table 12.2 in [Fossen 2011, p. 374], the P and D-tuning become

$$K_p = \text{diag}\{M\omega_n^2\} = \text{diag}\{13.49,\ 26.24,\ 3.36\}$$
$$K_d = \text{diag}\{2M\zeta\omega_n - D\} = \text{diag}\{52.20,\ 113.44,\ 17.06\},$$

and K_i is assigned as follows

$$K_i = \text{diag}\{0.16,\ 0.16,\ 0.05\}.$$

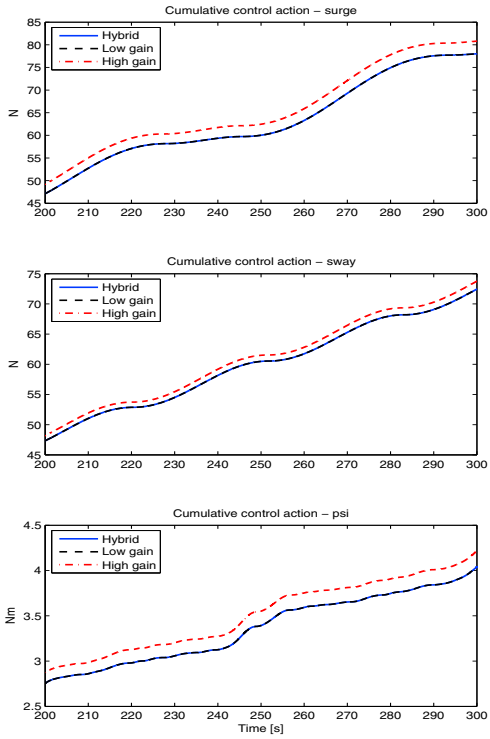

Fig. 4. Cumulative control action. Surge (top), sway (middle), yaw (bottom).

REFERENCES

(2010). Mss. marine systems simulator. `http://www.marinecontrol.org`. Accessed: 2015-02-24.

Brodtkorb, A.H., Sørensen, A.J., and Teel, A.R. (2014). Increasing the operation window for dynamic positioned vessels using the concept of hybrid control. In *ASME 2014 33rd International Conference on Ocean, Offshore and Arctic Engineering*, V01AT01A046–V01AT01A046. American Society of Mechanical Engineers.

Fossen, T.I. (2011). *Handbook of marine craft hydrodynamics and motion control*. John Wiley & Sons.

Goebel, R., Sanfelice, R.G., and Teel, A.R. (2012). *Hybrid Dynamical Systems: modeling, stability, and robustness*. Princeton University Press.

Hespanha, J.P. (2001). Tutorial on supervisory control. In *Lecture Notes for the workshop Control using Logic and Switching for the 40th Conf. on Decision and Contr., Orlando, Florida*.

Lindegaard, K.P. (2003). *Acceleration feedback in dynamic positioning*. Ph.D. thesis, PhD thesis, Norwegian University of Science and Technology, Trondheim.

Nguyen, D.T. and Sørensen, A.J. (2009). Switching control for thruster-assisted position mooring. *Control Engineering Practice*, 17(9), 985–994.

Nguyen, T.D., Sorensen, A.J., and Quek, S.T. (2008). Multi-operational controller structure for station keeping and transit operations of marine vessels. *Control Systems Technology, IEEE Transactions on*, 16(3), 491–498.

Nguyen, T.D., Sørensen, A.J., and Tong Quek, S. (2007). Design of hybrid controller for dynamic positioning from calm to extreme sea conditions. *Automatica*, 43(5), 768–785.

Sørensen, A.J. (2013). *Marine Control Systems - Lecture notes*. Department of Marine Technology, Norwegian Univ. of Sci. and Tech.

C.4

A Robust Dynamic Positioning Tracking Control Law Mitigating Integral Windup

---

Kjerstad, Ø. K., **Værnø, S. A.** , Skjetne, R.

Available online at www.sciencedirect.com

ScienceDirect

IFAC-PapersOnLine 49-23 (2016) 239–244

IFAC Papers Online
CONFERENCE PAPER ARCHIVE

A Robust Dynamic Positioning Tracking Control Law Mitigating Integral Windup ⋆

Øivind K. Kjerstad [*,**] **Svenn Are T. Værnø** [***]
Roger Skjetne [***]

[*] *Arctic Technology Department, University Center in Svalbard, Norway (e-mail: oivind.kjerstad@unis.no)*
[**] *Department of Civil and Transport Engineering, Norwegian University of Science and Technology, Norway*
[***] *Department of Marine Technology, Norwegian University of Science and Technology, Norway*

Abstract: This paper deals with the design of a tracking control law for dynamic positioning of marine vessels subject to disturbances. It shows that the integral windup problem can be mitigated by removing the position setpoint in the proportional error term and injecting the velocity setpoint in the integral state. This creates an internal reference point in the control law for the vessel to follow. Control of the transient convergence trajectories is achieved without compromising stability by constraining the internal convergence velocity. The proposed control law provides the same functionality as a conventional tracking control law in combination with a reference filter, but with lower complexity and fewer tuning parameters. A closed-loop simulation case study verifies the theoretical findings and show feasible and robust performance.

Keywords: Nonlinear control design; Integral windup; Setpoint tracking; Dynamic positioning

1. INTRODUCTION

Dynamic positioning (DP) of a marine vessel is defined as keeping location (either a fixed position and heading or low-speed tracking) exclusively by means of onboard thrusters (IMO, 1994). State-of-the-art marine control systems employ the structure of Figure 1 and are designed using continuous model-based control methods relying on measurements of position, heading, and sometimes angular velocity (Fossen, 2011; Sørensen, 2012). Since the 1960's the control law principle has relied on proportional position and damping terms together with integral action in PID-like structures to calculate forces and moments needed for positioning (Breivik et al., 2015). Proportional feedback is still state-of-the-art, but modern designs include nonlinear terms to handle reference frame transformations and guarantee stability. Although such control laws have good track record in most sea states, the nonlinear PID structure has issues with respect to integral windup and integral settling time during setpoint changes.

To avoid overshoot, oscillations, and instabilities, integral windup is typically dealt with by slow integral action update together with a reference filter providing a smooth time-varying reference trajectory. Additional remedies such as bounding the integral action output and integrator resetting may also be applied (Sørensen, 2012). Although these methods mitigate integral windup, the trade-off is typically reduction in performance and/or increased system complexity with more tuning parameters.

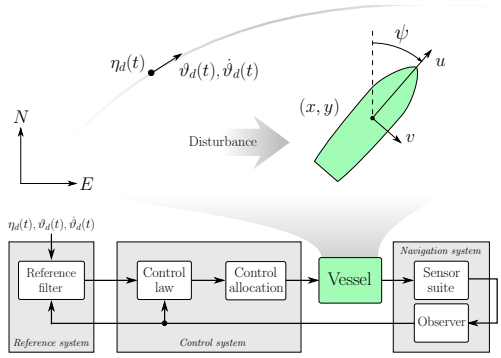

Fig. 1. Reference frames, desired trajectory, and signal flow in guidance, navigation, and control of marine vessels.

To deal with integral windup in LTI systems, Phelan (1977) proposed the pseudo-derivative feedback (PDF) control law. It is structurally similar to PID (Ohm, 1994) and a special case of the weighted reference PID by Åström and Hägglund (1995). The only difference from conventional PID is the lack of setpoint error in the proportional term. This vastly improves integral windup (and thereby reduces the need for the mentioned remedies). Although PDF is as simple as PID, and has demonstrated feasible experimental performance (Nikolic and Milivojevic, 1998; Setiawan et al., 2000), it has received little attention in marine applications. In the authors best knowledge, only Vahedipour and Bobis (1993) considers the method for autopilot design. Thus, the objective and contribution of this paper is to extend the PDF control law for LTI point

⋆ Research partly funded by the Research Council of Norway project no. 203471: CRI SAMCoT, and project no. 223254: CoE AMOS.

10.1016/j.ifacol.2016.10.349

stabilization to nonlinear tracking control for DP of marine vessels in presence of disturbances. Since PDF for LTI is not well know, an example is presented next.

Terminology and notation: In UGS, UGES, etc., stands G for Global, S for Stable, U for Uniform, and E for Exponential. LTI means linear time-invariant, and ISS means input-to-state-stable. The smallest and largest eigenvalues of a matrix $A \in \mathbb{R}^{n\times n}$ is denoted $\lambda_{\min}(A)$ and $\lambda_{\max}(A)$, respectively. $\mathbb{R}_{>0}$ denote positive real numbers and positive definite matrices.

1.1 Example

Consider the scalar second order system for which a point stabilization control law is to be designed,

$$m\ddot{q} + a\dot{q} = u + b \tag{1a}$$
$$\dot{b} = 0 \tag{1b}$$

where q, $\dot{q}$, $\ddot{q} \in \mathbb{R}$ is the position, velocity, and acceleration, respectively, $m, a \in \mathbb{R}_{>0}$ are known system parameters, and $b \in \mathbb{R}$ is a constant unknown bias. Full state feedback is assumed (i.e., $y := \begin{bmatrix} q & \dot{q} \end{bmatrix}^\top$), which enables PID and PDF control laws as,

$$u_{PID} = -k_p(q - q_d) - k_d(\dot{q} - \dot{q}_d) - k_i \int_0^t (q - q_d)\, dt \tag{2}$$

$$u_{PDF} = -l_p q - l_d \dot{q} - l_i \int_0^t (q - q_d)\, dt, \tag{3}$$

where $q_d \in \mathbb{R}$ is the setpoint, $\dot{q}_d \in \mathbb{R}$ is the desired velocity, $k_{p,d,i} \in \mathbb{R}$ are the PID gains, and $l_{p,d,i} \in \mathbb{R}$ are the PDF gains. The closed-loop transfer functions are thus,

$$q_{PID}(s) = \frac{(k_d s^2 + k_p s + k_i) q_d + bs}{ms^3 + (a + k_d)s^2 + k_p s + k_i} \tag{4}$$

$$q_{PDF}(s) = \frac{l_i q_d + bs}{ms^3 + (a + l_d)s^2 + l_p s + l_i}. \tag{5}$$

Notice that (4) and (5) have equal characteristic polynomial and disturbance rejection properties (provided equal tuning), but differ in the number of zeros.

Figure 2 shows a setpoint unit step of (1) comparing (2) to (3) with system parameters $m = 10$, $a = 2$, and $b = 2$. The PID is used with and without the following filter,

$$q_d'(s) = \frac{\omega_0^2 q_d}{s^2 + 2\zeta\omega_0 s + \omega_0^2}, \tag{6}$$

for smooth reference generation (replacing q_d, $\dot{q}_d$ with q_d', $\dot{q}_d'$ in (2)). (4) and (5) were designed with equal poles (s = -0.75, -0.25, and -0.25), and the PID reference filter was set to provide quick transient, but avoid overshoot ($\omega_0 = 0.21$ and $\zeta = 1$). The results show that the PDF obtains feasible performance which is comparable to the PID with a reference filter, but with the benefit of fewer tuning variables.

2. PROBLEM FORMULATION

The aim of this paper is to design a nonlinear tracking control law for DP using the PDF concept. As illustrated in Figure 1 the control objective is to track a desired time-varying North-East-Down (NED) trajectory parameterized by $\eta_d(t)$, $\vartheta_d(t)$, $\dot{\vartheta}_d(t) \in \mathbb{R}^3$. To achieve this the following control design model is applied,

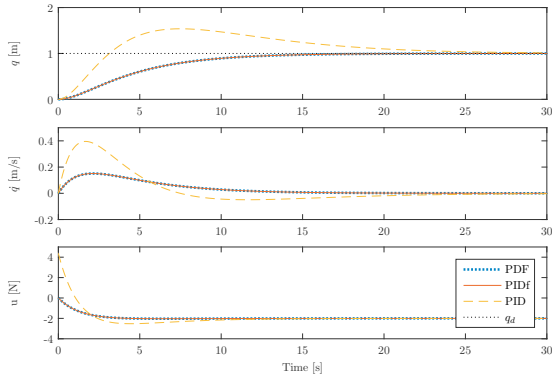

Fig. 2. Reference step simulation example results. PIDf denotes the use of a second order reference filter.

$$\dot{\eta} = R(\psi)\nu \tag{7a}$$
$$\dot{b} = 0 \tag{7b}$$
$$M\dot{\nu} + D\nu = \tau + MR^\top(\psi)b, \tag{7c}$$

where $\eta \in \mathbb{R}^3$ is the position and heading given in the NED frame, $R(\psi) \in \mathbb{R}^{3\times3}$ is the rotation matrix between the NED and vessel's body-fixed frame, $b \in \mathbb{R}^3$ is a bias state describing unmodeled dynamics and external loads, $M \in \mathbb{R}^{3\times3}_{>0}$ is the vessel inertia and added mass matrix, $\nu \in \mathbb{R}^3$ is the vessel's body-fixed linear and angular velocity, $D \in \mathbb{R}^{3\times3}_{>0}$ is a linear damping matrix, and $\tau \in \mathbb{R}^3$ is the control input. The design model is derived from the state-of-the-art models found in (Fossen, 2011; Sørensen, 2012) with one minor difference. The bias term is multiplied with the mass matrix M in (7c). This modification is reasonable as any external load may be described as mass times an acceleration. For the control design, ideal state feedback measurements of η and ν are assumed together with the following rotation matrix properties,

$$R(\psi)R(\psi)^\top = I \tag{8a}$$
$$\dot{R} = R(\psi)S(r), \tag{8b}$$

where $I \in \mathbb{R}^{3\times3}$ is the identity matrix, $S(r) \in \mathbb{R}^{3\times3}$ is a skew-symmetric matrix, and $r \in \mathbb{R}$ is the yaw-rate (for further details, see (Fossen, 2011)). For simplicity and readability, the arguments of $R(\psi)$ and $S(r)$ are dropped in the remainder of the paper.

For τ, the following nonlinear PDF tracking control law structure is proposed,

$$\tau = M(\tau_{FF} + \tau_{FB}) \tag{9a}$$
$$\tau_{FB} = R^\top(\xi - K_p\eta) - K_{D1}\nu + K_{D2}\nu_d \tag{9b}$$
$$\dot{\xi} = K_i(\eta_d - \eta) + \beta\vartheta_d, \tag{9c}$$

where $\tau_{FF} \in \mathbb{R}^3$ is a design feedforward term, $\beta \in \mathbb{R}^{3\times3}$ and $K_{p,D1,D2,i} \in \mathbb{R}^{3\times3}$ will be state-dependent design matrices, and $\xi \in \mathbb{R}^3$ is an integral action state. Similar to the example, the difference from conventional nonlinear PID control designs for marine vessels (as seen in e.g. (Sørensen, 2011)) is the lack of η_d in (9b), and inclusion of $\beta\vartheta_d$ in (9c). Hence, the problem treated in this paper is to design τ_{FF}, $K_{p,D1,D2,i}$, and β such that the vessel converges to, and tracks, the desired time-varying setpoint with feasible convergence trajectories.

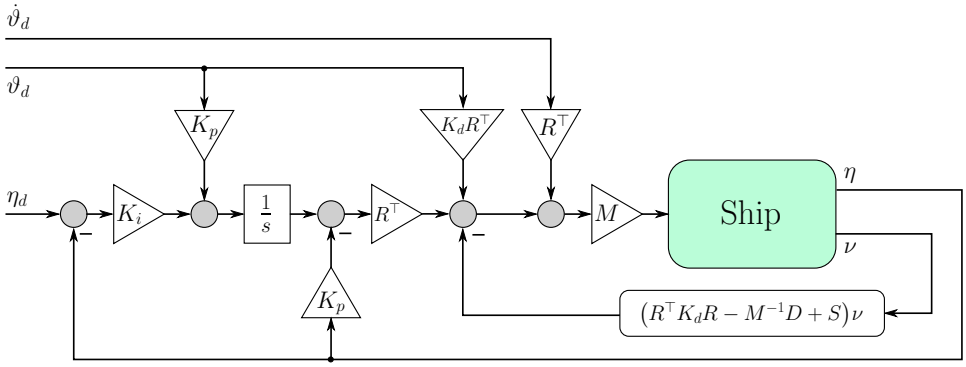

Fig. 3. Block diagram showing the nominal nonlinear tracking control law for DP.

3. CONTROL DESIGN

First, τ_{FF}, $K_{p,D1,D2,i}$, and β are derived to provide a nominal control law. Then, the results are extended to impose internal velocity constraints in (9c) such that feasible convergence trajectories are obtained. Finally, a set of tuning laws are proposed.

3.1 Nominal tracking design

To formalize the control law (9) the design model (7) is transformed to NED by $\vartheta := R\nu$ and $\vartheta_d := R\nu_d$, where $\nu_d \in \mathbb{R}^3$ is the body-fixed desired trajectory. This can be written as,

$$\dot{\eta} = \vartheta \tag{10a}$$
$$\dot{b} = 0 \tag{10b}$$
$$\dot{\vartheta} = RSR^\top\vartheta + RM^{-1}\left(\tau - DR^\top\vartheta + MR^\top b\right). \tag{10c}$$

Inserting (9) in (10c) gives the closed-loop dynamics,

$$\dot{\vartheta} = R\tau_{FF} + \xi - K_p\eta + b + RK_{D2}R^\top\vartheta_d - R(K_{D1} + M^{-1}D - S)R^\top\vartheta. \tag{11}$$

From this it can be seen that choosing,

$$K_{D1} = R^\top K_d R - M^{-1}D + S \tag{12}$$
$$K_{D2} = R^\top K_d R, \tag{13}$$

where $K_d \in \mathbb{R}^{3\times3}$ is a gain matrix, the NED velocity dynamics become,

$$\dot{\vartheta} = R\tau_{FF} + \xi - K_p\eta + b - K_d(\vartheta - \vartheta_d). \tag{14}$$

To investigate the closed-loop stability properties and determine τ_{FF} and β, the following error variables are proposed,

$$e_1 = \eta_d - \eta \tag{15a}$$
$$e_2 = \vartheta_d - \vartheta \tag{15b}$$
$$e_3 = \xi - K_p\eta + b. \tag{15c}$$

Differentiating these give the closed-loop error dynamics,

$$\dot{e}_1 = e_2 \tag{16a}$$
$$\dot{e}_2 = \dot{\vartheta}_d - R\tau_{FF} - K_d\, e_2 - e_3 \tag{16b}$$
$$\dot{e}_3 = K_i e_1 + \beta\vartheta_d - K_p\vartheta. \tag{16c}$$

By choosing $\tau_{FF} = R^\top\dot{\vartheta}_d$ and $\beta = K_p$ the error dynamics become linear.

Theorem 1. The tracking control law (9) with

$$\tau_{FF} = R^\top\dot{\vartheta}_d \tag{17a}$$
$$K_{D1} = R^\top K_d R - M^{-1}D + S \tag{17b}$$
$$K_{D2} = R^\top K_d R \tag{17c}$$
$$\beta = K_p, \tag{17d}$$

render the equilibrium (e_1, e_2, $e_3 = 0$) of (16) UGES if the gains K_p, K_d, and K_i are designed to make the matrix

$$A = \begin{bmatrix} 0 & I & 0 \\ 0 & -K_d & -I \\ K_i & K_p & 0 \end{bmatrix}, \tag{18}$$

Hurwitz.

Proof. Letting $e = col(e_1, e_2, e_3)$ gives $\dot{e} = Ae$, which is UGES.

The integral windup problem is dealt with by the fact that the integral state ξ acts as an internal reference model (and integral action). This is possible as ξ is the only entry point of η_d (see Figure 3). Thus, there is no need for an external reference filter in order to avoid integral windup. A major benefit is that it reduces the overall control system complexity and mitigates the need for complex integral state handling logic. Since the control law (9), with (17), renders the closed-loop UGES, it is also ISS, and will be ideal for use in both a separation principle with an observer, and in more complex changing disturbance environments.

3.2 Constraining the convergence velocity

In DP it is beneficial to limit the velocity of the vessel as it converges to $\eta_d(t)$, $\vartheta_d(t)$, and $\dot{\vartheta}_d(t)$, so that it remains in the low velocity range. In conventional PID-like control designs this is typically achieved by limiting the velocity in the reference filter. In the proposed design, which has no reference filter, the convergence velocity may be impacted through tuning of K_i, K_p, and K_d, or by constraining $\dot{\xi}$. The second option is pursued as the tuning method is a trade-off that reduces the freedom of the response design. Since ϑ_d is given by the desired trajectory it should not be constrained in (9c) as that may lead to improper tracking. However, the proportional term $K_i(\eta_d - \eta)$ which

governs the convergence velocity may. Thus, the following modification to (9c) is proposed,

$$\dot{\xi} = \text{sat}(K_i e_1) + K_p \vartheta_d \tag{19}$$

where the saturation operator is defined by a maximum vector, denoted $\vartheta_{\max} \in \mathbb{R}^3_{>0}$. This is evaluated for the different elements in $K_i e_1$ so that $\text{sat}(K_i e_1) \in [-\vartheta_{\max}\ \vartheta_{\max}]$.

Before proceeding to analyze the impact of this modification, we note that (9) with (17) and (19) can be written as,

$$\dot{e} = Ae + Bu \tag{20a}$$
$$y = Ce \tag{20b}$$
$$u = -\phi(y), \tag{20c}$$

where $B \in \mathbb{R}^{9\times 3} := [0\ 0\ I]^\top$, $u \in \mathbb{R}^3$, $C \in \mathbb{R}^{3\times 9} := [I\ 0\ 0]$, (A,B) is controllable, (A,C) is observable, and $\phi : \mathbb{R}^3 \to \mathbb{R}^3$ is a memoryless nonlinearity, locally Lipschitz in y.

Theorem 2. The tracking control law (9) with (17) and (19) render the system absolutely stable if (18) is Hurwitz, and

$$\gamma_1 \gamma_2 < 1, \tag{21}$$

where $\gamma_2 := \lambda_{max}(K_i)$ and $\gamma_1 := \sup_{\omega\in\mathbb{R}} \|G(s)\|_2$, where $G(s) \in \mathbb{R}^{3\times 3}$ is the transfer function matrix of (20).

Proof. First note that $G(s)$ is Hurwitz since A is Hurwitz. The second condition of the circle criterion (Theorem 7.1 in (Khalil, 2001)), states that (20) is absolutely stable if $\phi \in [K_1,\ K_2]$, with $K = K_2 - K_1 = K^\top > 0$, and $Z(s) = [I + K_2 G(s)][I + K_1 G(s)]^{-1}$ strictly positive real (SPR).

The sector $[K_1,\ K_2]$ is established by noting that ϕ satisfies

$$\|\phi(y)\|_2 \le \gamma_2 \|y\|_2, \quad \forall y \in \mathbb{R}^3, \tag{22}$$

by choosing $\gamma_2 = \lambda_{max}(K_i)$. From this it follows that $K_1 = -\gamma_2 I$ and $K_2 = \gamma_2 I$, and $K^\top > 0$.

Lemma 6.1 in (Khalil, 2001) states that $Z(s)$ is SPR if $Z(s)$ is Hurwitz, $Z(j\omega) + Z^\top(j\omega) > 0\ \forall \omega \in \mathbb{R}$, and $Z(\infty) + Z^\top(\infty) > 0$. To show that these hold we define

$$\gamma_1 = \sup_{\omega\in\mathbb{R}} \|G(s)\|_2, \tag{23}$$

and note that γ_1 is finite as $G(s)$ is Hurwitz. The analysis showing $Z(s)$ SPR with (22) and (23) is identical to Example 7.1 in (Khalil, 2001), and therefore left out here. Then, the second condition of the multivariable circle criterion is satisfied, and we conclude that (20) is absolutely stable if $\gamma_1\gamma_2 < 1$.

3.3 Control synthesis

Since the nominal error dynamics (16) are linear, tuning laws based on the closed-loop transfer function can be proposed. By assuming that $K_{p,d,i}$ are diagonal, $\vartheta_d = 0$, $\dot{\vartheta}_d = 0$, and $b = 0$, it may be shown that each degree of freedom has the following transfer function,

$$h(s) = \frac{k_i}{s^3 + k_d s^2 + k_p s + k_i}, \tag{24}$$

where $k_i,\ k_p,\ k_d \in \mathbb{R}$ are diagonal terms of K_i, K_p, and K_d, respectively. To determine these, the following characteristic polynomial is proposed,

$$c(s) = (s+\alpha)(s^2 + 2\zeta\omega_0 + \omega_0^2) \tag{25a}$$
$$= s^3 + (2\zeta\omega_0 + \alpha)s^2 + (\omega_0^2 + 2\zeta\omega_0\alpha)s + \alpha\omega_0^2, \tag{25b}$$

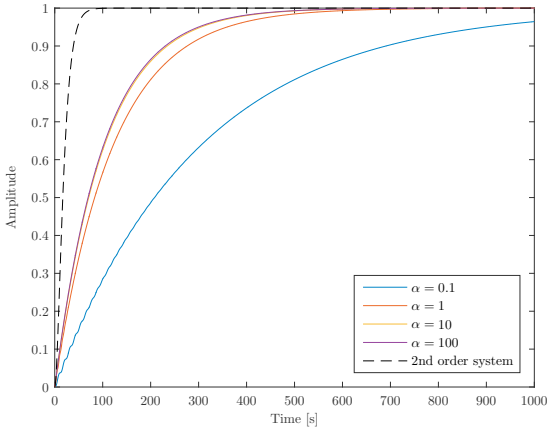

Fig. 4. Comparison of different α values for use in control parameter tuning.

where $\zeta \in \mathbb{R}$ is the damping factor, $\omega_0 \in \mathbb{R}$ is the natural frequency, and $\alpha \in \mathbb{R}$ is a filtering coefficient. From (24) and (25) it is found that,

$$k_d = 2\zeta\omega_0 + \alpha \tag{26a}$$
$$k_p = \omega_0^2 + 2\zeta\omega_0\alpha \tag{26b}$$
$$k_i = \alpha\omega_0^2. \tag{26c}$$

As the impact of α on the closed-loop dynamics is not well-known, Figure 4 shows a unit step comparison of (24) using a range of α values. For each value the control gains were calculated as in (26) using $\zeta = 1$ and $\omega_0 = 0.1$. It can be seen that α acts as an inverse first order lowpass filter time constant for the 2nd order system defined by ζ and ω_0. General tuning laws for the control law (9) with (17) are therefore proposed as,

$$K_p = diag\left(\begin{bmatrix} 2\zeta_x\omega_{0x} + \alpha_x \\ 2\zeta_y\omega_{0y} + \alpha_y \\ 2\zeta_\psi\omega_{0\psi} + \alpha_\psi \end{bmatrix}\right) \tag{27a}$$
$$K_d = diag\left(\begin{bmatrix} \omega_{0x}^2 + 2\zeta_x\omega_{0x}\alpha_x \\ \omega_{0y}^2 + 2\zeta_y\omega_{0y}\alpha_y \\ \omega_{0\psi}^2 + 2\zeta_\psi\omega_{0\psi}\alpha_\psi \end{bmatrix}\right) \tag{27b}$$
$$K_i = diag\left(\begin{bmatrix} \alpha_x\omega_{0x}^2 \\ \alpha_y\omega_{0y}^2 \\ \alpha_\psi\omega_{0\psi}^2 \end{bmatrix}\right), \tag{27c}$$

where the subscripts x, y, and ψ denote the parameter of the degree of freedom. It must be mentioned that other tuning methods may provide equal or better results as the above rely on assumptions of diagonal K_p, K_d, and K_i matrices and the specific characteristic equation given in (25). Yet, (27) provide an intuitive approach and give feasible results.

4. SIMULATION CASE STUDY

A simulation case study implementing (7) is conducted to verify the proposed PDF control design and evaluate its feasibility. The vessel in scope is the construction and intervention vessel for Arctic operations (CIVArctic), seen in Figure 5. It is a multi-purpose vessel capable of operating in open water on the Norwegian Continental Shelf and in first year in the High North (Berg, 2012). Table 1 gives its main particulars.

Fig. 5. The construction and intervention vessel for Arctic operations. Courtesy of (Berg, 2012).

Table 1. CIVArctic main parameters.

Parameter	Value
Length between perp.	109.3 m
Breadth at water line	24 m
Draught	6.5 m
Mass (normal load)	$11.85 \cdot 10^6$ kg

The simulation scenario is point stabilization followed by setpoint tracking subject to constant disturbance ($b = [25\ 0\ 0]^\top$). For the point stabilization we consider static setpoints given by $\eta_d(t) = \eta_d$ (implying $\vartheta_d(t), \dot{\vartheta}_d(t) = 0$), where η_d is changed twice with an interval of 250 seconds (at $t = 250s,\ 500s$). At $t = 750$ seconds the vessel's control objective changes from point stabilization to setpoint tracking where the objective is to follow a linear trajectory parametrized by $\eta_d(t)$, $\vartheta_d(t)$, and $\dot{\vartheta}_d(t)$.

The nonlinear PDF design (9) using (17), with and without the convergence velocity constraints given in (19), is compared to the following nonlinear PID control law,

$$\tau_{PID} = M(\tau_{FF} + \tau_{FB}) \tag{28a}$$

$$\tau_{FB} = R^\top (\xi - K_p(\eta - \eta_d)) - K_{D1}\nu + K_{D2}\nu_d \tag{28b}$$

$$\dot{\xi} = K_i(\eta_d - \eta) \tag{28c}$$

where τ_{FF}, K_{D1}, and K_{D2} are given in (17). The error dynamics of (28) can be shown to be UGES by following the approach of Section 3.1. As both the PID and the PDF control laws have (24) as the characteristic equation, they are tuned equally with the method proposed in (27), using $\zeta = 1$, $\omega_0 = 0.06$, and $\alpha = 10$ (for all degrees of freedom).

To produce feasible transient PID performance, we propose the following general reference filter for setpoint tracking,

$$\ddot{\eta}_r = \dot{\vartheta}_d + \omega_{0r}^2\sigma + 2\zeta_r\omega_{0r}(\vartheta_d - \dot{\eta}_r) \tag{29a}$$

$$\ddot{\sigma} = \omega_{0\sigma}^2(\eta_d - \eta_r - \sigma) - 2\zeta_\sigma\omega_{0\sigma}\dot{\sigma}, \tag{29b}$$

where $\eta_r \in \mathbb{R}^3$ is the reference position and heading, $\omega_{0r}, \zeta_r, \omega_{0\sigma}, \zeta_\sigma \in \mathbb{R}_{>0}$ are positive scalars, and $\sigma \in \mathbb{R}^3$ is a reference acceleration state. For the simulation case this is applied with $\zeta_{r,\sigma} = 1$, $\omega_{0r} = 0.04$, and $\omega_{0r} = 0.5$. The initial condition of the PID reference position and the internal PDF reference state are both set to $\eta_r(0) = \xi(0) = \eta(0)$. For the PDF control law with velocity constraints, these are set to $\vartheta_{max} = [0.35\ \ 0.35\ \ 0.0175]^\top$.

Figures 6 and 7 show that all four closed-loop systems accomplish the control objective during both point stabilization and setpoint tracking, and that all are significantly

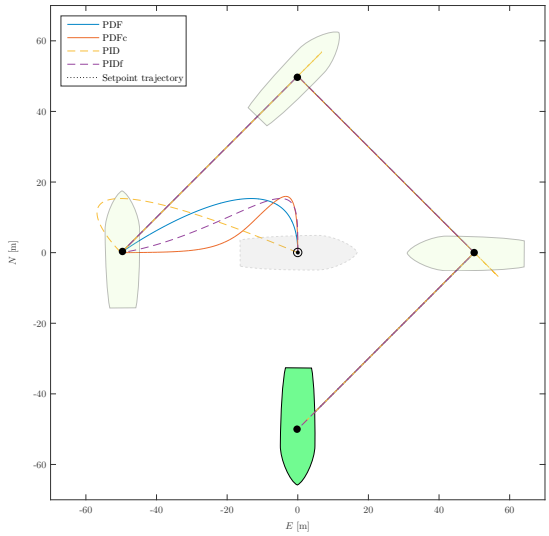

Fig. 6. The position trajectories of the control laws compared to the setpoints ans setpoint trajectory. PDFc denotes velocity constraint and PIDf denotes use of reference filter.

affected at initialization due to the unknown environmental bias. As expected, the PID without a reference filter has less feasible transient performance during point stabilization setpoint changes compared to the others due to integral windup. For setpoint tracking (initialized at the vessel position) there is no difference in performance.

Note that the PDF velocity constraints only affect the transient convergence velocity, and not the total motion. This can be seen in Figure 7 where the limitations are respected during point stabilization as the resulting velocity is solely due to convergence. During setpoint tracking the total motion is mostly a result of the setpoint motion which is unaffected by the convergence limitations. Overall, the results indicate that the extension of the PDF concept to the nonlinear DP tracking problem is valid and that performance comparable to nonlinear PID control laws using a reference filter can be achieved.

5. DISCUSSION AND CONCLUSIONS

The main implications of the presented design are:

- Reduced number of tuning variables and implementation complexity.
- Ease of constraining the convergence velocity.

The reduced control system implementation complexity comes from the fact that the PDF control do not require a reference filter to achieve feasible convergence transients (as it mitigates integral windup). This simplifies synthesis and tuning and allows for designing highly reactive system responses without special attention to the integral action dynamics. Especially in harsh environment applications which includes effects such as wave trains, ship-ice interaction effects, ship-to-ship interaction effects, current surges,

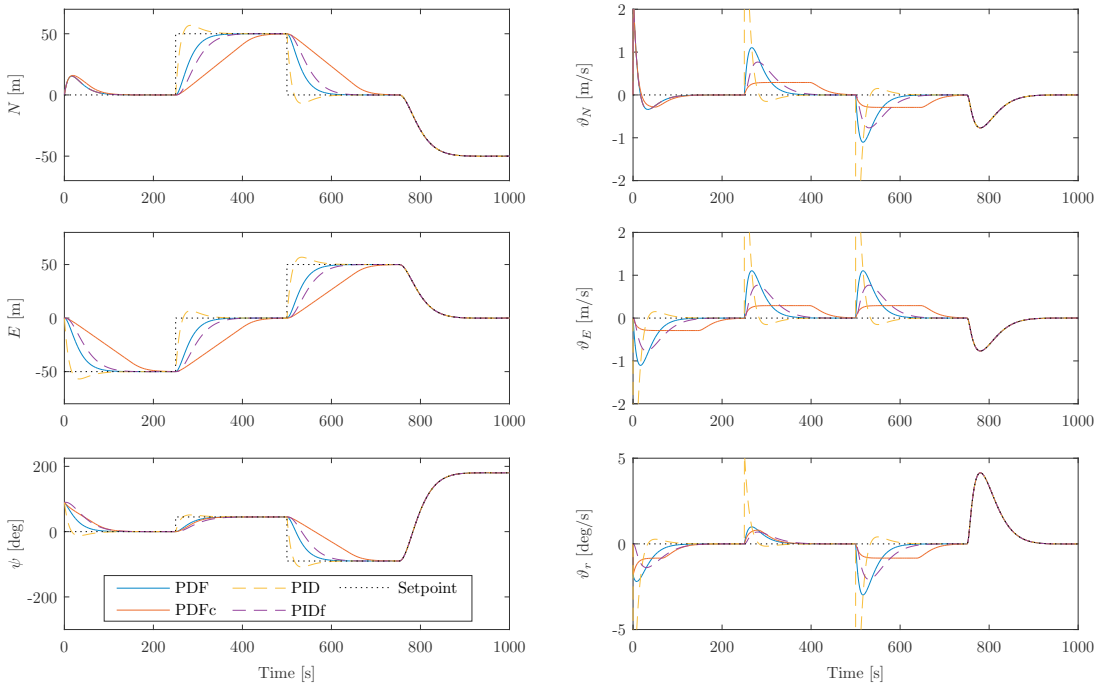

Fig. 7. Simulation case study results. The left column shows position and heading. The right column shows the linear velocity and angular rate. All signals are presented in the NED frame.

and effects from operations with heavy equipment in the sea or at the sea floor this can be of particular importance.

This paper has presented a robust tracking control law for DP of marine vessels that mitigates the integral windup problem often encountered in conventional PID-like designs. It is achieved by a subtle change in the control law feedback structure that allows the integral state to act as a reference point (and integral action). The proposed control law was analyzed and found to have uniform global exponential stability with respect to its error variables when subject to constant disturbance. Further, a method to constrain the convergence velocity was proposed and shown to render the error system absolutely stable. Together these mitigate the need for an explicit reference filter. A simulation case study verified the findings.

ACKNOWLEDGEMENTS

The authors would like to thank the CIVArctic project for the vessel model applied in the simulations.

REFERENCES

Åström, K. and Hägglund, T. (1995). *PID Controllers: Theory, Design, and Tuning*. ISA: The Instrumentation, Systems, and Automation Society.

Berg, T.E. (2012). Summary report - RCN project no. 188913/I40, Construction and intervention vessel for Arctic conditions. Technical report, MARINTEK.

Breivik, M., Kvaal, S., and Østby, P. (2015). From Eureka to K-Pos: Dynamic Positioning as a Highly Successful and Important Marine Control Technology. In *Proceedings of IFAC MCMC*.

Fossen, T.I. (2011). *Handbook of Marine Craft Hydrodynamics and Motion Control*. Wiley.

International Maritime Organization (1994). Guidelines for vessels with dynamic positioning systems. Technical report. MSC/circ.645.

Khalil, H.K. (2001). *Nonlinear Systems*. Pearson.

Nikolic, I. and Milivojevic, I. (1998). Application of pseudo-derivative feedback in industrial robot controllers. *Facta Universitatis, Automatic Control and Robotics*.

Ohm, D.Y. (1994). Analysis of pid and pdf compensators for motion control systems. In *Conference Record of the IEEE Industry Applications Society Annual Meeting*.

Phelan, R.M. (1977). *Automatic Control Systems*. Cornell University Press.

Setiawan, A., Albright, L.D., and Phelan, R.M. (2000). Application of pseudo-derivative-feedback algorithm in greenhouse air temperature control. *Computers and Electronics in Agriculture*, 26(3), 283 – 302.

Sørensen, A.J. (2011). A survey of dynamic positioning control systems. *Annual Reviews in Control*, 35(1).

Sørensen, A.J. (2012). *Marine Control Systems: Propulsion and Motion Control of Ships and Ocean Structures*. Department of Marine Technology, NTNU, Norway.

Vahedipour, A. and Bobis, J. (1993). Cascade pseudo derivative feedback control algorithm and its application to design of autopilots. In *Proceedings of the IECON*.

C.5

AMOS DP Research Cruise 2016: Academic Full-scale Testing of Experimental Dynamic Positioning Control Algorithms Onboard R/V Gunnerus

---

Skjetne, R., Sørensen, M. E. N., Breivik, M., **Værnø, S. A.**, Brodtkorb, A. H., Sørensen, A. J., Kjerstad, Ø. K., Calabrò, V., Vinje, B. O.

Part III

Concluding Remarks

Chapter 8

Conclusions and Further Work

The research questions of the thesis were stated in Chapter 1.1 as:

1. In model-based observer and controller design for DP, how does different control design models compare, and how does different estimation algorithms compare?
2. How can we improve observer and controller design to better handle transient events in DP?
3. What is the best way of compensating the transient bias loads in the DP controller?

Research question 1 was addressed by (J.1), where the comparisons were made fair by derivative free optimization on a high-fidelity simulation model and experimental data. For the control design model results, the current models including nonlinear damping performed the best for the simulation results, and the bias load models performed the best for the experimental results. Including nonlinear damping had a positive effect for the current models, especially for transient performance, whereas the effect was negligible for the bias load models. The reason the current models performed better in simulation data can be explained by less uncertain and unmodeled dynamics compared to the results on the full-scale experimental data. The results showed surprisingly small differences between the observer algorithms, showing that DP is dominantly a linear process. When using the nonlinear damping model, the EKF and UKF had very similar performance, and when using only linear damping the LTV-KF, the EKF, and the UKF had similar performance. There was no notable performance deterioration when using the measured yaw angle in the rotation matrix for the LTV-KF compared to as a state for the EKF/UKF.

For the research question 2, the observer performance has received the most attention of this thesis. In (J.2), a version of a model-based nonlinear observer with time-varying gains has been proposed and analyzed with regards to stability. This observer has a good steady-state and transient performance. Performance of the observer is shown through a closed-loop high-fidelity simulation study, on experimental data, and through a full-scale closed-loop verification on R/V Gunnerus during the ADPRC' 16. The time-varying

observer performs slightly better than a well tuned fixed-gain observer, especially if in between the transients, there are long periods of steady state. As a second contribution to improve observer design presented by (J.3), a hybrid observer that combines a kinematic and a model-based observer is proposed, and stability is proven. The hybrid observer switches to the kinematic observer in transients, while the model-based observer is used in steady state. This observer performance is shown through a high-fidelity simulation study, closed-loop experimental data in the MC-lab, and through full-scale experimental data from R/V Gunnerus on ADPRC' 16. Both these observer contributions improve the overall performance of the DP system, as expected.

The control aspect of research question 2 has a similar challenge as the observer challenge, as discussed in Section 2.4, and this is addressed by (C.3) that propose hybrid integral action as a solution to improve controller performance during transients. The integral action switches between aggressive tuning in transients, to achieve better bias load compensation, and relaxed tuning in steady state, to lower the control oscillations and improve wave-filtering. Performance is shown through a simulation study, and the results are as expected. The control action is calm in steady state, and responsive in transient, leading to an overall good performance. In addition, pseudo-derivative control is proposed for DP by (C.4). This simplifies the control design since it does not need a reference filter, and it mitigates windup issues with the integral action.

Finally, research question 3 was addressed by (J.4) where different bias compensation methods were compared. Traditional integral action was compared to using different versions of a bias load estimate from a model-based observer. The results clearly show that using a model-based observer optimized for bias estimation is the best solution in compensation of the bias loads in the controller. However, the results in this paper is a simulation study, and experimental verification would be interesting as further work.

To improve transient behavior in DP, there are a lot of further work that can be done. These may include:

- Investigate further how the kinematic observer with wave-filter by Bryne et al. (2017) behaves in transients. As mentioned in Chapter 2.4, this is a promising design. However, it needs more study, and it should be compared in a rigorous way to a model-based observer, considering normal steady state and transient conditions, as well as dead reckoning.
- Perform another and thorough analysis of damping identification, especially for experimental results, to further investigate the performance of the different control design models.
- Investigate how well the *acceleration feedforward* proposed by Kjerstad and Skjetne (2016) in transient conditions when the vessel operates in waves, with special attention on compensating the low-frequency loads.

Bibliography

Audet, C. and Hare, W. (2017). *Derivative-Free and Blackbox Optimization*, Springer Int. Publ.

Balchen, J. G., Jenssen, N. A., Mathisen, E. and Sælid, S. (1980). A dynamic positioning system based on kalman filtering and optimal control, *Modeling, Identification and Control* 1(3): 135.

Balchen, J. G., Jenssen, N. A. and Sælid, S. (1976). Dynamic positioning using kalman filtering and optimal control theory, *IFAC/IFIP symposium on automation in offshore oil field operation*, Vol. 183, p. 186.

Bjørnø, J., Heyn, H.-M., Skjetne, R., Dahl, A. R. and Frederich, P. (2017). Modeling, parameter identification and thruster-assisted position mooring of c/s inocean cat i drillship, *ASME 2017 36th International Conference on Ocean, Offshore and Arctic Engineering*, American Society of Mechanical Engineers Digital Collection.

Breivik, M. (2010). *Topics in guided motion control of marine vehicles*, PhD thesis, Norwegian University of Science and Technology, Trondheim, Norway.

Brodtkorb, A. H., Sørensen, A. J. and Teel, A. R. (2014). Increasing the operation window for dynamic positioned vessels using the concept of hybrid control, *ASME 2014 33rd International Conference on Ocean, Offshore and Arctic Engineering*, American Society of Mechanical Engineers, pp. V01AT01A046–V01AT01A046.

Bryne, T. H., Fossen, T. I. and Johansen, T. A. (2014). Nonlinear observer with time-varying gains for inertial navigation aided by satellite reference systems in dynamic positioning, *Control and Automation (MED), 2014 22nd Mediterranean Conference of*, IEEE, pp. 1353–1360.

Bryne, T. H., Fossen, T. I. and Johansen, T. A. (2017). Design of inertial navigation systems for marine craft with adaptive wave filtering aided by triple-redundant sensor packages, *International Journal of Adaptive Control and Signal Processing* 31(4): 522–544.

DNV GL (2019). Rules for classification: Ships - part 6 additional class notations - chapter 3 navigation, manoeuvring and position keeping, *Technical Report Pt.6, Ch.3*, DNV GL. Amended Oct. 2019.

Faltinsen, O. M. (1990). *Sea loads on ships and ocean structures*, Cambridge University Press.

Fay, H. (1989). Dynamic positioning systems, principles, design and applications (france: Editions), *Technip, Paris* .

Fossen, T. I. (1994). *Guidance and control of ocean vehicles*, John Wiley & Sons Inc.

Fossen, T. I. (2011). *Handbook of marine craft hydrodynamics and motion control*, John Wiley & Sons.

Fossen, T. I. and Perez, T. (2009). Kalman filtering for positioning and heading control of ships and offshore rigs, *IEEE Control Systems* 29(6): 32–46.

Fossen, T. I., Sagatun, S. I. and Sørensen, A. J. (1996). Identification of dynamically positioned ships, *Control Engineering Practice* 4(3): 369–376.

Fossen, T. I. and Strand, J. P. (1999). Passive nonlinear observer design for ships using lyapunov methods: full-scale experiments with a supply vessel, *Automatica* 35(1): 3–16.

Fung, P. and Grimble, M. (1983). Dynamic ship positioning using a self-tuning kalman filter, *IEEE Transactions on Automatic Control* 28(3): 339–350.

Goebel, R., Sanfelice, R. G. and Teel, A. R. (2009). Hybrid dynamical systems, *IEEE Control Systems* 29(2): 28–93.

Grimble, M. J., Patton, R. and Wise, D. (1980). Use of kalman filtering techniques in dynamic ship-positioning systems, *IEE Proceedings D (Control Theory and Applications)*, Vol. 127, IET, pp. 93–102.

Grip, H. F., Fossen, T. I., Johansen, T. A. and Saberi, A. (2015). Globally exponentially stable attitude and gyro bias estimation with application to gnss/ins integration, *Automatica* 51: 158–166.

Grip, H. F., Fossero, T. I., Johansent, T. A. and Saberi, A. (2012). A nonlinear observer for integration of gnss and imu measurements with gyro bias estimation, *American Control Conference (ACC), 2012*, IEEE, pp. 4607–4612.

Hamel, T. and Mahony, R. (2006). Attitude estimation on so [3] based on direct inertial measurements, *Robotics and Automation, 2006. ICRA 2006. Proceedings 2006 IEEE International Conference on*, IEEE, pp. 2170–2175.

Hassani, V., Pascoal, A. M., Aguiar, A. P. et al. (2012). Multiple model adaptive wave filtering for dynamic positioning of marine vessels, *American Control Conference (ACC), 2012*, IEEE, pp. 6222–6228.

Hespanha, J. P. (2001). Tutorial on supervisory control, *Lecture Notes for the workshop Control using Logic and Switching for the 40th Conf. on Decision and Contr., Orlando, Florida*.

International Maritime Organization (1994). Guidelines for vessels with dynamic positioning systems., *Technical Report MSC/circ. 645*.

Jenssen, N. A. (1981). *Estimation and control in dynamic positioning of vessels*, PhD thesis, NTH (NTNU), Trondheim, Norway.

Katebi, M., Grimble, M. and Zhang, Y. (1997). H∞ robust control design for dynamic ship positioning, *IEE Proceedings-Control Theory and Applications* 144(2): 110–120.

Katebi, M., Yamamoto, I., Matsuura, M., Grimble, M., Hirayama, H. and Okamoto, N. (2001). Robust dynamic ship positioning control system design and applications, *International Journal of Robust and Nonlinear Control* 11(13): 1257–1284.

Katebi, M., Zhang, Y. and Grimble, M. (1997). Nonlinear dynamic ship positioning, *In Proceedings of the IFAC 13th IFAC World Congress* 13: 303–380.

Kjerstad, Ø. K. (2016). *Dynamic Positioning of Marine Vessels in Ice*, PhD thesis, NTNU, Trondheim, Norway.
URL: *http://hdl.handle.net/11250/2391724*

Kjerstad, Ø. K., Metrikin, I., Løset, S. and Skjetne, R. (2015). Experimental and phenomenological investigation of dynamic positioning in managed ice, *CRST* 111: 67–79.

Kjerstad, Ø. K. and Skjetne, R. (2016). Disturbance rejection by acceleration feedforward for marine surface vessels, *IEEE Access* 4: 2656–2669.

Lagarias, J. C., Reeds, J. A., Wright, M. H. and Wright, P. E. (1998). Convergence properties of the nelder–mead simplex method in low dimensions, *SIAM Journal on optimization* 9(1): 112–147.

Lindegaard, K.-P. (2003). *Acceleration feedback in dynamic positioning*, PhD thesis, Norwegian University of Science and Technology, Trondheim, Norway.

Loría, A. and Panteley, E. (1999). A separation principle for a class of euler-lagrange systems, *New Directions in nonlinear observer design*, Springer, pp. 229–247.

Løvås, H. S. (2019). *DP Autotuning by use of Derivative-free Optimization*, Master's thesis, Norwegian University of Science and Technology, Trondheim, Norway.

Mahony, R., Hamel, T. and Pflimlin, J.-M. (2008). Nonlinear complementary filters on the special orthogonal group, *IEEE Transactions on automatic control* 53(5): 1203–1218.

Mandžuka, S. and Vukić, Z. (1995). Use of optimal constrained covariance control (oc 3) in dynamic positioning of floating vessels, *IFAC Proceedings Volumes* 28(2): 9–15.

MATLAB (2016). *version 9.1.0 (R2016b)*, The MathWorks Inc., Natick, Massachusetts.

MTEC/ICMASS (2019). International Maritime and Port Technology and Development Conference, and the International Conference on Maritime Autonomous Surface Ships (MTEC/ICMASS 2019), *Journal of Physics* 1357.
URL: *https://iopscience.iop.org/issue/1742-6596/1357/1*

Nguyen, T. D., Sørensen, A. J. and Quek, S. T. (2007). Design of hybrid controller for dynamic positioning from calm to extreme sea conditions, *Automatica* 43(5): 768–785.

Nguyen, T. D., Sorensen, A. J. and Quek, S. T. (2008). Multi-operational controller structure for station keeping and transit operations of marine vessels, *IEEE Transactions on Control Systems Technology* 16(3): 491–498.

Reddy, N. P., Zadeh, M. K., Thieme, C. A., Skjetne, R., Aanondsen, S. A., Breivik, M. and Eide, E. (2019). Zero-emission autonomous ferries for urban water transport: Cheaper, cleaner alternative to bridges and manned vessels, *IEEE Electrification Magazine* 7(4): 32–45.

Refsnes, J. E. G. (2007). *Nonlinear model-based control of slender body AUVs*, PhD thesis, Norwegian University of Science and Technology, Trondheim, Norway.

Refsnes, J. E. and Sørensen, A. J. (2007). Comparison of two observers for marine vessels in ocean current, *In Proceedings of the IFAC Conference on Control Applications in Marine Systems 2007* 40(17): 32–37.

Saelid, S., Jenssen, N. and Balchen, J. (1983). Design and analysis of a dynamic positioning system based on kalman filtering and optimal control, *IEEE Transactions on Automatic Control* 28(3): 331–339.

Salcudean, S. (1991). A globally convergent angular velocity observer for rigid body motion, *IEEE transactions on Automatic Control* 36(12): 1493–1497.

Simon, D. (2006). *Optimal state estimation: Kalman, H infinity, and nonlinear approaches*, John Wiley & Sons.

Skjetne, R. (2005). *The maneuvering problem*, PhD thesis, Norwegian University of Science and Technology, Trondheim, Norway.

Skjetne, R. and Egeland, O. (2006). Hardware-in-the-loop testing of marine control system, *Modeling, Identification and Control* 27(4): 239.

Skjetne, R., Sørensen, M. E. N., Breivik, M., Værnø, S. A., Brodtkorb, A. H., Sørensen, A. J., Kjerstad, Ø. K., Calabrò, V. and Vinje, B. O. (2017). AMOS DP research cruise 2016: Academic full-scale testing of experimental dynamic positioning control algorithms onboard r/v gunnerus, *ASME 2017 36th International Conference on Ocean, Offshore and Arctic Engineering*, American Society of Mechanical Engineers.

Smogeli, Ø. N. (2006). *Control of Marine Propellers: From normal to extreme conditions*, PhD thesis, NTNU, Trondheim, Norway.

Sørensen, A. J. (2011). A survey of dynamic positioning control systems, *Annual reviews in control* 35(1): 123–136.

Sørensen, A. J. (2013). *Marine Control Systems - Lecture notes*, Department of Marine Technology, Norwegian Univ. of Sci. and Tech.

Sørensen, A. J., Sagatun, S. I. and Fossen, T. I. (1996). Design of a dynamic positioning system using model-based control, *Control Engineering Practice* 4(3): 359–368.

Sørensen, A. J., Skjetne, R., Bø, T., Miyazaki, M. R., Johansen, T. A., Utne, I. B. and Pedersen, E. (2017). Toward safer, smarter, and greener ships: Using hybrid marine power plants, *IEEE Electrification Magazine* 5(3): 68–73.

Strand, J. and Fossen, T. (1999). Nonlinear passive observer design for ships with adaptive wave filtering, *New Directions in nonlinear observer design* pp. 113–134.

Tannuri, E. A. and Donha, D. C. (2000). H∞ controller design for dynamic positioning of a turret moored FPSO, *IFAC Proceedings Volumes* 33(21): 263–268.

Tannuri, E. and Morishita, H. (2006). Experimental and numerical evaluation of a typical dynamic positioning system, *Applied Ocean Research* 28(2): 133–146.

Thienel, J. and Sanner, R. M. (2003). A coupled nonlinear spacecraft attitude controller and observer with an unknown constant gyro bias and gyro noise, *IEEE Transactions on Automatic Control* 48(11): 2011–2015.

Værnø, S. A., Skjetne, R., Kjerstad, Ø. K. and Calabrò, V. (2019). Comparison of control design models and observers for dynamic positioning of surface vessels, *Control Engineering Practice* 85: 235–245.

Vasconcelos, J. F., Silvestre, C. and Oliveira, P. (2008). A nonlinear observer for rigid body attitude estimation using vector observations, *IFAC Proceedings Volumes* 41(2): 8599–8604.

Vik, B. and Fossen, T. I. (2001). A nonlinear observer for gps and ins integration, *Decision and Control, 2001. Proceedings of the 40th IEEE Conference on*, Vol. 3, IEEE, pp. 2956–2961.

Previous PhD theses published at the Department of Marine Technology

Previous PhD theses published at the Department of Marine Technology (earlier: Faculty of Marine Technology)
NORWEGIAN UNIVERSITY OF SCIENCE AND TECHNOLOGY

Report No.	Author	Title
	Kavlie, Dag	Optimization of Plane Elastic Grillages, 1967
	Hansen, Hans R.	Man-Machine Communication and Data-Storage Methods in Ship Structural Design, 1971
	Gisvold, Kaare M.	A Method for non-linear mixed -integer programming and its Application to Design Problems, 1971
	Lund, Sverre	Tanker Frame Optimalization by means of SUMT-Transformation and Behaviour Models, 1971
	Vinje, Tor	On Vibration of Spherical Shells Interacting with Fluid, 1972
	Lorentz, Jan D.	Tank Arrangement for Crude Oil Carriers in Accordance with the new Anti-Pollution Regulations, 1975
	Carlsen, Carl A.	Computer-Aided Design of Tanker Structures, 1975
	Larsen, Carl M.	Static and Dynamic Analysis of Offshore Pipelines during Installation, 1976
UR-79-01	Brigt Hatlestad, MK	The finite element method used in a fatigue evaluation of fixed offshore platforms. (Dr.Ing. Thesis)
UR-79-02	Erik Pettersen, MK	Analysis and design of cellular structures. (Dr.Ing. Thesis)
UR-79-03	Sverre Valsgård, MK	Finite difference and finite element methods applied to nonlinear analysis of plated structures. (Dr.Ing. Thesis)
UR-79-04	Nils T. Nordsve, MK	Finite element collapse analysis of structural members considering imperfections and stresses due to fabrication. (Dr.Ing. Thesis)
UR-79-05	Ivar J. Fylling, MK	Analysis of towline forces in ocean towing systems. (Dr.Ing. Thesis)
UR-80-06	Nils Sandsmark, MM	Analysis of Stationary and Transient Heat Conduction by the Use of the Finite Element Method. (Dr.Ing. Thesis)
UR-80-09	Sverre Haver, MK	Analysis of uncertainties related to the stochastic modeling of ocean waves. (Dr.Ing. Thesis)
UR-81-15	Odland, Jonas	On the Strength of welded Ring stiffened cylindrical Shells primarily subjected to axial Compression
UR-82-17	Engesvik, Knut	Analysis of Uncertainties in the fatigue Capacity of

		Welded Joints
UR-82-18	Rye, Henrik	Ocean wave groups
UR-83-30	Eide, Oddvar Inge	On Cumulative Fatigue Damage in Steel Welded Joints
UR-83-33	Mo, Olav	Stochastic Time Domain Analysis of Slender Offshore Structures
UR-83-34	Amdahl, Jørgen	Energy absorption in Ship-platform impacts
UR-84-37	Mørch, Morten	Motions and mooring forces of semi submersibles as determined by full-scale measurements and theoretical analysis
UR-84-38	Soares, C. Guedes	Probabilistic models for load effects in ship structures
UR-84-39	Aarsnes, Jan V.	Current forces on ships
UR-84-40	Czujko, Jerzy	Collapse Analysis of Plates subjected to Biaxial Compression and Lateral Load
UR-85-46	Alf G. Engseth, MK	Finite element collapse analysis of tubular steel offshore structures. (Dr.Ing. Thesis)
UR-86-47	Dengody Sheshappa, MP	A Computer Design Model for Optimizing Fishing Vessel Designs Based on Techno-Economic Analysis. (Dr.Ing. Thesis)
UR-86-48	Vidar Aanesland, MH	A Theoretical and Numerical Study of Ship Wave Resistance. (Dr.Ing. Thesis)
UR-86-49	Heinz-Joachim Wessel, MK	Fracture Mechanics Analysis of Crack Growth in Plate Girders. (Dr.Ing. Thesis)
UR-86-50	Jon Taby, MK	Ultimate and Post-ultimate Strength of Dented Tubular Members. (Dr.Ing. Thesis)
UR-86-51	Walter Lian, MH	A Numerical Study of Two-Dimensional Separated Flow Past Bluff Bodies at Moderate KC-Numbers. (Dr.Ing. Thesis)
UR-86-52	Bjørn Sortland, MH	Force Measurements in Oscillating Flow on Ship Sections and Circular Cylinders in a U-Tube Water Tank. (Dr.Ing. Thesis)
UR-86-53	Kurt Strand, MM	A System Dynamic Approach to One-dimensional Fluid Flow. (Dr.Ing. Thesis)
UR-86-54	Arne Edvin Løken, MH	Three Dimensional Second Order Hydrodynamic Effects on Ocean Structures in Waves. (Dr.Ing. Thesis)
UR-86-55	Sigurd Falch, MH	A Numerical Study of Slamming of Two-Dimensional Bodies. (Dr.Ing. Thesis)
UR-87-56	Arne Braathen, MH	Application of a Vortex Tracking Method to the Prediction of Roll Damping of a Two-Dimension Floating Body. (Dr.Ing. Thesis)

UR-87-57	Bernt Leira, MK	Gaussian Vector Processes for Reliability Analysis involving Wave-Induced Load Effects. (Dr.Ing. Thesis)
UR-87-58	Magnus Småvik, MM	Thermal Load and Process Characteristics in a Two-Stroke Diesel Engine with Thermal Barriers (in Norwegian). (Dr.Ing. Thesis)
MTA-88-59	Bernt Arild Bremdal, MP	An Investigation of Marine Installation Processes – A Knowledge - Based Planning Approach. (Dr.Ing. Thesis)
MTA-88-60	Xu Jun, MK	Non-linear Dynamic Analysis of Space-framed Offshore Structures. (Dr.Ing. Thesis)
MTA-89-61	Gang Miao, MH	Hydrodynamic Forces and Dynamic Responses of Circular Cylinders in Wave Zones. (Dr.Ing. Thesis)
MTA-89-62	Martin Greenhow, MH	Linear and Non-Linear Studies of Waves and Floating Bodies. Part I and Part II. (Dr.Techn. Thesis)
MTA-89-63	Chang Li, MH	Force Coefficients of Spheres and Cubes in Oscillatory Flow with and without Current. (Dr.Ing. Thesis
MTA-89-64	Hu Ying, MP	A Study of Marketing and Design in Development of Marine Transport Systems. (Dr.Ing. Thesis)
MTA-89-65	Arild Jæger, MH	Seakeeping, Dynamic Stability and Performance of a Wedge Shaped Planing Hull. (Dr.Ing. Thesis)
MTA-89-66	Chan Siu Hung, MM	The dynamic characteristics of tilting-pad bearings
MTA-89-67	Kim Wikstrøm, MP	Analysis av projekteringen for ett offshore projekt. (Licenciat-avhandling)
MTA-89-68	Jiao Guoyang, MK	Reliability Analysis of Crack Growth under Random Loading, considering Model Updating. (Dr.Ing. Thesis)
MTA-89-69	Arnt Olufsen, MK	Uncertainty and Reliability Analysis of Fixed Offshore Structures. (Dr.Ing. Thesis)
MTA-89-70	Wu Yu-Lin, MR	System Reliability Analyses of Offshore Structures using improved Truss and Beam Models. (Dr.Ing. Thesis)
MTA-90-71	Jan Roger Hoff, MH	Three-dimensional Green function of a vessel with forward speed in waves. (Dr.Ing. Thesis)
MTA-90-72	Rong Zhao, MH	Slow-Drift Motions of a Moored Two-Dimensional Body in Irregular Waves. (Dr.Ing. Thesis)
MTA-90-73	Atle Minsaas, MP	Economical Risk Analysis. (Dr.Ing. Thesis)
MTA-90-74	Knut-Aril Farnes, MK	Long-term Statistics of Response in Non-linear Marine Structures. (Dr.Ing. Thesis)
MTA-90-75	Torbjørn Sotberg, MK	Application of Reliability Methods for Safety Assessment of Submarine Pipelines. (Dr.Ing.

		Thesis)
MTA-90-76	Zeuthen, Steffen, MP	SEAMAID. A computational model of the design process in a constraint-based logic programming environment. An example from the offshore domain. (Dr.Ing. Thesis)
MTA-91-77	Haagensen, Sven, MM	Fuel Dependant Cyclic Variability in a Spark Ignition Engine - An Optical Approach. (Dr.Ing. Thesis)
MTA-91-78	Løland, Geir, MH	Current forces on and flow through fish farms. (Dr.Ing. Thesis)
MTA-91-79	Hoen, Christopher, MK	System Identification of Structures Excited by Stochastic Load Processes. (Dr.Ing. Thesis)
MTA-91-80	Haugen, Stein, MK	Probabilistic Evaluation of Frequency of Collision between Ships and Offshore Platforms. (Dr.Ing. Thesis)
MTA-91-81	Sødahl, Nils, MK	Methods for Design and Analysis of Flexible Risers. (Dr.Ing. Thesis)
MTA-91-82	Ormberg, Harald, MK	Non-linear Response Analysis of Floating Fish Farm Systems. (Dr.Ing. Thesis)
MTA-91-83	Marley, Mark J., MK	Time Variant Reliability under Fatigue Degradation. (Dr.Ing. Thesis)
MTA-91-84	Krokstad, Jørgen R., MH	Second-order Loads in Multidirectional Seas. (Dr.Ing. Thesis)
MTA-91-85	Molteberg, Gunnar A., MM	The Application of System Identification Techniques to Performance Monitoring of Four Stroke Turbocharged Diesel Engines. (Dr.Ing. Thesis)
MTA-92-86	Mørch, Hans Jørgen Bjelke, MH	Aspects of Hydrofoil Design: with Emphasis on Hydrofoil Interaction in Calm Water. (Dr.Ing. Thesis)
MTA-92-87	Chan Siu Hung, MM	Nonlinear Analysis of Rotordynamic Instabilities in Highspeed Turbomachinery. (Dr.Ing. Thesis)
MTA-92-88	Bessason, Bjarni, MK	Assessment of Earthquake Loading and Response of Seismically Isolated Bridges. (Dr.Ing. Thesis)
MTA-92-89	Langli, Geir, MP	Improving Operational Safety through exploitation of Design Knowledge - an investigation of offshore platform safety. (Dr.Ing. Thesis)
MTA-92-90	Sævik, Svein, MK	On Stresses and Fatigue in Flexible Pipes. (Dr.Ing. Thesis)
MTA-92-91	Ask, Tor Ø., MM	Ignition and Flame Growth in Lean Gas-Air Mixtures. An Experimental Study with a Schlieren System. (Dr.Ing. Thesis)
MTA-86-92	Hessen, Gunnar, MK	Fracture Mechanics Analysis of Stiffened Tubular Members. (Dr.Ing. Thesis)

MTA-93-93	Steinebach, Christian, MM	Knowledge Based Systems for Diagnosis of Rotating Machinery. (Dr.Ing. Thesis)
MTA-93-94	Dalane, Jan Inge, MK	System Reliability in Design and Maintenance of Fixed Offshore Structures. (Dr.Ing. Thesis)
MTA-93-95	Steen, Sverre, MH	Cobblestone Effect on SES. (Dr.Ing. Thesis)
MTA-93-96	Karunakaran, Daniel, MK	Nonlinear Dynamic Response and Reliability Analysis of Drag-dominated Offshore Platforms. (Dr.Ing. Thesis)
MTA-93-97	Hagen, Arnulf, MP	The Framework of a Design Process Language. (Dr.Ing. Thesis)
MTA-93-98	Nordrik, Rune, MM	Investigation of Spark Ignition and Autoignition in Methane and Air Using Computational Fluid Dynamics and Chemical Reaction Kinetics. A Numerical Study of Ignition Processes in Internal Combustion Engines. (Dr.Ing. Thesis)
MTA-94-99	Passano, Elizabeth, MK	Efficient Analysis of Nonlinear Slender Marine Structures. (Dr.Ing. Thesis)
MTA-94-100	Kvålsvold, Jan, MH	Hydroelastic Modelling of Wetdeck Slamming on Multihull Vessels. (Dr.Ing. Thesis)
MTA-94-102	Bech, Sidsel M., MK	Experimental and Numerical Determination of Stiffness and Strength of GRP/PVC Sandwich Structures. (Dr.Ing. Thesis)
MTA-95-103	Paulsen, Hallvard, MM	A Study of Transient Jet and Spray using a Schlieren Method and Digital Image Processing. (Dr.Ing. Thesis)
MTA-95-104	Hovde, Geir Olav, MK	Fatigue and Overload Reliability of Offshore Structural Systems, Considering the Effect of Inspection and Repair. (Dr.Ing. Thesis)
MTA-95-105	Wang, Xiaozhi, MK	Reliability Analysis of Production Ships with Emphasis on Load Combination and Ultimate Strength. (Dr.Ing. Thesis)
MTA-95-106	Ulstein, Tore, MH	Nonlinear Effects of a Flexible Stern Seal Bag on Cobblestone Oscillations of an SES. (Dr.Ing. Thesis)
MTA-95-107	Solaas, Frøydis, MH	Analytical and Numerical Studies of Sloshing in Tanks. (Dr.Ing. Thesis)
MTA-95-108	Hellan, Øyvind, MK	Nonlinear Pushover and Cyclic Analyses in Ultimate Limit State Design and Reassessment of Tubular Steel Offshore Structures. (Dr.Ing. Thesis)
MTA-95-109	Hermundstad, Ole A., MK	Theoretical and Experimental Hydroelastic Analysis of High Speed Vessels. (Dr.Ing. Thesis)
MTA-96-110	Bratland, Anne K., MH	Wave-Current Interaction Effects on Large-Volume Bodies in Water of Finite Depth. (Dr.Ing. Thesis)
MTA-96-111	Herfjord, Kjell, MH	A Study of Two-dimensional Separated Flow by a Combination of the Finite Element Method and

		Navier-Stokes Equations. (Dr.Ing. Thesis)
MTA-96-112	Æsøy, Vilmar, MM	Hot Surface Assisted Compression Ignition in a Direct Injection Natural Gas Engine. (Dr.Ing. Thesis)
MTA-96-113	Eknes, Monika L., MK	Escalation Scenarios Initiated by Gas Explosions on Offshore Installations. (Dr.Ing. Thesis)
MTA-96-114	Erikstad, Stein O., MP	A Decision Support Model for Preliminary Ship Design. (Dr.Ing. Thesis)
MTA-96-115	Pedersen, Egil, MH	A Nautical Study of Towed Marine Seismic Streamer Cable Configurations. (Dr.Ing. Thesis)
MTA-97-116	Moksnes, Paul O., MM	Modelling Two-Phase Thermo-Fluid Systems Using Bond Graphs. (Dr.Ing. Thesis)
MTA-97-117	Halse, Karl H., MK	On Vortex Shedding and Prediction of Vortex-Induced Vibrations of Circular Cylinders. (Dr.Ing. Thesis)
MTA-97-118	Igland, Ragnar T., MK	Reliability Analysis of Pipelines during Laying, considering Ultimate Strength under Combined Loads. (Dr.Ing. Thesis)
MTA-97-119	Pedersen, Hans-P., MP	Levendefiskteknologi for fiskefartøy. (Dr.Ing. Thesis)
MTA-98-120	Vikestad, Kyrre, MK	Multi-Frequency Response of a Cylinder Subjected to Vortex Shedding and Support Motions. (Dr.Ing. Thesis)
MTA-98-121	Azadi, Mohammad R. E., MK	Analysis of Static and Dynamic Pile-Soil-Jacket Behaviour. (Dr.Ing. Thesis)
MTA-98-122	Ulltang, Terje, MP	A Communication Model for Product Information. (Dr.Ing. Thesis)
MTA-98-123	Torbergsen, Erik, MM	Impeller/Diffuser Interaction Forces in Centrifugal Pumps. (Dr.Ing. Thesis)
MTA-98-124	Hansen, Edmond, MH	A Discrete Element Model to Study Marginal Ice Zone Dynamics and the Behaviour of Vessels Moored in Broken Ice. (Dr.Ing. Thesis)
MTA-98-125	Videiro, Paulo M., MK	Reliability Based Design of Marine Structures. (Dr.Ing. Thesis)
MTA-99-126	Mainçon, Philippe, MK	Fatigue Reliability of Long Welds Application to Titanium Risers. (Dr.Ing. Thesis)
MTA-99-127	Haugen, Elin M., MH	Hydroelastic Analysis of Slamming on Stiffened Plates with Application to Catamaran Wetdecks. (Dr.Ing. Thesis)
MTA-99-128	Langhelle, Nina K., MK	Experimental Validation and Calibration of Nonlinear Finite Element Models for Use in Design of Aluminium Structures Exposed to Fire. (Dr.Ing. Thesis)
MTA-99-	Berstad, Are J., MK	Calculation of Fatigue Damage in Ship Structures.

129		(Dr.Ing. Thesis)
MTA-99-130	Andersen, Trond M., MM	Short Term Maintenance Planning. (Dr.Ing. Thesis)
MTA-99-131	Tveiten, Bård Wathne, MK	Fatigue Assessment of Welded Aluminium Ship Details. (Dr.Ing. Thesis)
MTA-99-132	Søreide, Fredrik, MP	Applications of underwater technology in deep water archaeology. Principles and practice. (Dr.Ing. Thesis)
MTA-99-133	Tønnessen, Rune, MH	A Finite Element Method Applied to Unsteady Viscous Flow Around 2D Blunt Bodies With Sharp Corners. (Dr.Ing. Thesis)
MTA-99-134	Elvekrok, Dag R., MP	Engineering Integration in Field Development Projects in the Norwegian Oil and Gas Industry. The Supplier Management of Norne. (Dr.Ing. Thesis)
MTA-99-135	Fagerholt, Kjetil, MP	Optimeringsbaserte Metoder for Ruteplanlegging innen skipsfart. (Dr.Ing. Thesis)
MTA-99-136	Bysveen, Marie, MM	Visualization in Two Directions on a Dynamic Combustion Rig for Studies of Fuel Quality. (Dr.Ing. Thesis)
MTA-2000-137	Storteig, Eskild, MM	Dynamic characteristics and leakage performance of liquid annular seals in centrifugal pumps. (Dr.Ing. Thesis)
MTA-2000-138	Sagli, Gro, MK	Model uncertainty and simplified estimates of long term extremes of hull girder loads in ships. (Dr.Ing. Thesis)
MTA-2000-139	Tronstad, Harald, MK	Nonlinear analysis and design of cable net structures like fishing gear based on the finite element method. (Dr.Ing. Thesis)
MTA-2000-140	Kroneberg, André, MP	Innovation in shipping by using scenarios. (Dr.Ing. Thesis)
MTA-2000-141	Haslum, Herbjørn Alf, MH	Simplified methods applied to nonlinear motion of spar platforms. (Dr.Ing. Thesis)
MTA-2001-142	Samdal, Ole Johan, MM	Modelling of Degradation Mechanisms and Stressor Interaction on Static Mechanical Equipment Residual Lifetime. (Dr.Ing. Thesis)
MTA-2001-143	Baarholm, Rolf Jarle, MH	Theoretical and experimental studies of wave impact underneath decks of offshore platforms. (Dr.Ing. Thesis)
MTA-2001-144	Wang, Lihua, MK	Probabilistic Analysis of Nonlinear Wave-induced Loads on Ships. (Dr.Ing. Thesis)
MTA-2001-145	Kristensen, Odd H. Holt, MK	Ultimate Capacity of Aluminium Plates under Multiple Loads, Considering HAZ Properties. (Dr.Ing. Thesis)
MTA-2001-146	Greco, Marilena, MH	A Two-Dimensional Study of Green-Water

		Loading. (Dr.Ing. Thesis)
MTA-2001-147	Heggelund, Svein E., MK	Calculation of Global Design Loads and Load Effects in Large High Speed Catamarans. (Dr.Ing. Thesis)
MTA-2001-148	Babalola, Olusegun T., MK	Fatigue Strength of Titanium Risers – Defect Sensitivity. (Dr.Ing. Thesis)
MTA-2001-149	Mohammed, Abuu K., MK	Nonlinear Shell Finite Elements for Ultimate Strength and Collapse Analysis of Ship Structures. (Dr.Ing. Thesis)
MTA-2002-150	Holmedal, Lars E., MH	Wave-current interactions in the vicinity of the sea bed. (Dr.Ing. Thesis)
MTA-2002-151	Rognebakke, Olav F., MH	Sloshing in rectangular tanks and interaction with ship motions. (Dr.Ing. Thesis)
MTA-2002-152	Lader, Pål Furset, MH	Geometry and Kinematics of Breaking Waves. (Dr.Ing. Thesis)
MTA-2002-153	Yang, Qinzheng, MH	Wash and wave resistance of ships in finite water depth. (Dr.Ing. Thesis)
MTA-2002-154	Melhus, Øyvin, MM	Utilization of VOC in Diesel Engines. Ignition and combustion of VOC released by crude oil tankers. (Dr.Ing. Thesis)
MTA-2002-155	Ronæss, Marit, MH	Wave Induced Motions of Two Ships Advancing on Parallel Course. (Dr.Ing. Thesis)
MTA-2002-156	Økland, Ole D., MK	Numerical and experimental investigation of whipping in twin hull vessels exposed to severe wet deck slamming. (Dr.Ing. Thesis)
MTA-2002-157	Ge, Chunhua, MK	Global Hydroelastic Response of Catamarans due to Wet Deck Slamming. (Dr.Ing. Thesis)
MTA-2002-158	Byklum, Eirik, MK	Nonlinear Shell Finite Elements for Ultimate Strength and Collapse Analysis of Ship Structures. (Dr.Ing. Thesis)
IMT-2003-1	Chen, Haibo, MK	Probabilistic Evaluation of FPSO-Tanker Collision in Tandem Offloading Operation. (Dr.Ing. Thesis)
IMT-2003-2	Skaugset, Kjetil Bjørn, MK	On the Suppression of Vortex Induced Vibrations of Circular Cylinders by Radial Water Jets. (Dr.Ing. Thesis)
IMT-2003-3	Chezhian, Muthu	Three-Dimensional Analysis of Slamming. (Dr.Ing. Thesis)
IMT-2003-4	Buhaug, Øyvind	Deposit Formation on Cylinder Liner Surfaces in Medium Speed Engines. (Dr.Ing. Thesis)
IMT-2003-5	Tregde, Vidar	Aspects of Ship Design: Optimization of Aft Hull with Inverse Geometry Design. (Dr.Ing. Thesis)
IMT-	Wist, Hanne Therese	Statistical Properties of Successive Ocean Wave

2003-6		Parameters. (Dr.Ing. Thesis)
IMT-2004-7	Ransau, Samuel	Numerical Methods for Flows with Evolving Interfaces. (Dr.Ing. Thesis)
IMT-2004-8	Soma, Torkel	Blue-Chip or Sub-Standard. A data interrogation approach of identity safety characteristics of shipping organization. (Dr.Ing. Thesis)
IMT-2004-9	Ersdal, Svein	An experimental study of hydrodynamic forces on cylinders and cables in near axial flow. (Dr.Ing. Thesis)
IMT-2005-10	Brodtkorb, Per Andreas	The Probability of Occurrence of Dangerous Wave Situations at Sea. (Dr.Ing. Thesis)
IMT-2005-11	Yttervik, Rune	Ocean current variability in relation to offshore engineering. (Dr.Ing. Thesis)
IMT-2005-12	Fredheim, Arne	Current Forces on Net-Structures. (Dr.Ing. Thesis)
IMT-2005-13	Heggernes, Kjetil	Flow around marine structures. (Dr.Ing. Thesis
IMT-2005-14	Fouques, Sebastien	Lagrangian Modelling of Ocean Surface Waves and Synthetic Aperture Radar Wave Measurements. (Dr.Ing. Thesis)
IMT-2006-15	Holm, Håvard	Numerical calculation of viscous free surface flow around marine structures. (Dr.Ing. Thesis)
IMT-2006-16	Bjørheim, Lars G.	Failure Assessment of Long Through Thickness Fatigue Cracks in Ship Hulls. (Dr.Ing. Thesis)
IMT-2006-17	Hansson, Lisbeth	Safety Management for Prevention of Occupational Accidents. (Dr.Ing. Thesis)
IMT-2006-18	Zhu, Xinying	Application of the CIP Method to Strongly Nonlinear Wave-Body Interaction Problems. (Dr.Ing. Thesis)
IMT-2006-19	Reite, Karl Johan	Modelling and Control of Trawl Systems. (Dr.Ing. Thesis)
IMT-2006-20	Smogeli, Øyvind Notland	Control of Marine Propellers. From Normal to Extreme Conditions. (Dr.Ing. Thesis)
IMT-2007-21	Storhaug, Gaute	Experimental Investigation of Wave Induced Vibrations and Their Effect on the Fatigue Loading of Ships. (Dr.Ing. Thesis)
IMT-2007-22	Sun, Hui	A Boundary Element Method Applied to Strongly Nonlinear Wave-Body Interaction Problems. (PhD Thesis, CeSOS)
IMT-2007-23	Rustad, Anne Marthine	Modelling and Control of Top Tensioned Risers. (PhD Thesis, CeSOS)
IMT-2007-24	Johansen, Vegar	Modelling flexible slender system for real-time simulations and control applications
IMT-2007-25	Wroldsen, Anders Sunde	Modelling and control of tensegrity structures.

		(PhD Thesis, CeSOS)
IMT-2007-26	Aronsen, Kristoffer Høye	An experimental investigation of in-line and combined inline and cross flow vortex induced vibrations. (Dr. avhandling, IMT)
IMT-2007-27	Gao, Zhen	Stochastic Response Analysis of Mooring Systems with Emphasis on Frequency-domain Analysis of Fatigue due to Wide-band Response Processes (PhD Thesis, CeSOS)
IMT-2007-28	Thorstensen, Tom Anders	Lifetime Profit Modelling of Ageing Systems Utilizing Information about Technical Condition. (Dr.ing. thesis, IMT)
IMT-2008-29	Refsnes, Jon Erling Gorset	Nonlinear Model-Based Control of Slender Body AUVs (PhD Thesis, IMT)
IMT-2008-30	Berntsen, Per Ivar B.	Structural Reliability Based Position Mooring. (PhD-Thesis, IMT)
IMT-2008-31	Ye, Naiquan	Fatigue Assessment of Aluminium Welded Box-stiffener Joints in Ships (Dr.ing. thesis, IMT)
IMT-2008-32	Radan, Damir	Integrated Control of Marine Electrical Power Systems. (PhD-Thesis, IMT)
IMT-2008-33	Thomassen, Paul	Methods for Dynamic Response Analysis and Fatigue Life Estimation of Floating Fish Cages. (Dr.ing. thesis, IMT)
IMT-2008-34	Pákozdi, Csaba	A Smoothed Particle Hydrodynamics Study of Two-dimensional Nonlinear Sloshing in Rectangular Tanks. (Dr.ing.thesis, IMT/ CeSOS)
IMT-2007-35	Grytøyr, Guttorm	A Higher-Order Boundary Element Method and Applications to Marine Hydrodynamics. (Dr.ing.thesis, IMT)
IMT-2008-36	Drummen, Ingo	Experimental and Numerical Investigation of Nonlinear Wave-Induced Load Effects in Containerships considering Hydroelasticity. (PhD thesis, CeSOS)
IMT-2008-37	Skejic, Renato	Maneuvering and Seakeeping of a Singel Ship and of Two Ships in Interaction. (PhD-Thesis, CeSOS)
IMT-2008-38	Harlem, Alf	An Age-Based Replacement Model for Repairable Systems with Attention to High-Speed Marine Diesel Engines. (PhD-Thesis, IMT)
IMT-2008-39	Alsos, Hagbart S.	Ship Grounding. Analysis of Ductile Fracture, Bottom Damage and Hull Girder Response. (PhD-thesis, IMT)
IMT-2008-40	Graczyk, Mateusz	Experimental Investigation of Sloshing Loading and Load Effects in Membrane LNG Tanks Subjected to Random Excitation. (PhD-thesis, CeSOS)
IMT-2008-41	Taghipour, Reza	Efficient Prediction of Dynamic Response for Flexible amd Multi-body Marine Structures. (PhD-

		thesis, CeSOS)
IMT-2008-42	Ruth, Eivind	Propulsion control and thrust allocation on marine vessels. (PhD thesis, CeSOS)
IMT-2008-43	Nystad, Bent Helge	Technical Condition Indexes and Remaining Useful Life of Aggregated Systems. PhD thesis, IMT
IMT-2008-44	Soni, Prashant Kumar	Hydrodynamic Coefficients for Vortex Induced Vibrations of Flexible Beams, PhD thesis, CeSOS
IMT-2009-45	Amlashi, Hadi K.K.	Ultimate Strength and Reliability-based Design of Ship Hulls with Emphasis on Combined Global and Local Loads. PhD Thesis, IMT
IMT-2009-46	Pedersen, Tom Arne	Bond Graph Modelling of Marine Power Systems. PhD Thesis, IMT
IMT-2009-47	Kristiansen, Trygve	Two-Dimensional Numerical and Experimental Studies of Piston-Mode Resonance. PhD-Thesis, CeSOS
IMT-2009-48	Ong, Muk Chen	Applications of a Standard High Reynolds Number Model and a Stochastic Scour Prediction Model for Marine Structures. PhD-thesis, IMT
IMT-2009-49	Hong, Lin	Simplified Analysis and Design of Ships subjected to Collision and Grounding. PhD-thesis, IMT
IMT-2009-50	Koushan, Kamran	Vortex Induced Vibrations of Free Span Pipelines, PhD thesis, IMT
IMT-2009-51	Korsvik, Jarl Eirik	Heuristic Methods for Ship Routing and Scheduling. PhD-thesis, IMT
IMT-2009-52	Lee, Jihoon	Experimental Investigation and Numerical in Analyzing the Ocean Current Displacement of Longlines. Ph.d.-Thesis, IMT.
IMT-2009-53	Vestbøstad, Tone Gran	A Numerical Study of Wave-in-Deck Impact usin a Two-Dimensional Constrained Interpolation Profile Method, Ph.d.thesis, CeSOS.
IMT-2009-54	Bruun, Kristine	Bond Graph Modelling of Fuel Cells for Marine Power Plants. Ph.d.-thesis, IMT
IMT 2009-55	Holstad, Anders	Numerical Investigation of Turbulence in a Sekwed Three-Dimensional Channel Flow, Ph.d.-thesis, IMT.
IMT 2009-56	Ayala-Uraga, Efren	Reliability-Based Assessment of Deteriorating Ship-shaped Offshore Structures, Ph.d.-thesis, IMT
IMT 2009-57	Kong, Xiangjun	A Numerical Study of a Damaged Ship in Beam Sea Waves. Ph.d.-thesis, IMT/CeSOS.
IMT 2010-58	Kristiansen, David	Wave Induced Effects on Floaters of Aquaculture Plants, Ph.d.-thesis, CeSOS.

IMT 2010-59	Ludvigsen, Martin	An ROV-Toolbox for Optical and Acoustic Scientific Seabed Investigation. Ph.d.-thesis IMT.
IMT 2010-60	Hals, Jørgen	Modelling and Phase Control of Wave-Energy Converters. Ph.d.thesis, CeSOS.
IMT 2010- 61	Shu, Zhi	Uncertainty Assessment of Wave Loads and Ultimate Strength of Tankers and Bulk Carriers in a Reliability Framework. Ph.d. Thesis, IMT/ CeSOS
IMT 2010-62	Shao, Yanlin	Numerical Potential-Flow Studies on Weakly-Nonlinear Wave-Body Interactions with/without Small Forward Speed, Ph.d.thesis,CeSOS.
IMT 2010-63	Califano, Andrea	Dynamic Loads on Marine Propellers due to Intermittent Ventilation. Ph.d.thesis, IMT.
IMT 2010-64	El Khoury, George	Numerical Simulations of Massively Separated Turbulent Flows, Ph.d.-thesis, IMT
IMT 2010-65	Seim, Knut Sponheim	Mixing Process in Dense Overflows with Emphasis on the Faroe Bank Channel Overflow. Ph.d.thesis, IMT
IMT 2010-66	Jia, Huirong	Structural Analysis of Intect and Damaged Ships in a Collission Risk Analysis Perspective. Ph.d.thesis CeSoS.
IMT 2010-67	Jiao, Linlin	Wave-Induced Effects on a Pontoon-type Very Large Floating Structures (VLFS). Ph.D.-thesis, CeSOS.
IMT 2010-68	Abrahamsen, Bjørn Christian	Sloshing Induced Tank Roof with Entrapped Air Pocket. Ph.d.thesis, CeSOS.
IMT 2011-69	Karimirad, Madjid	Stochastic Dynamic Response Analysis of Spar-Type Wind Turbines with Catenary or Taut Mooring Systems. Ph.d.-thesis, CeSOS.
IMT - 2011-70	Erlend Meland	Condition Monitoring of Safety Critical Valves. Ph.d.-thesis, IMT.
IMT – 2011-71	Yang, Limin	Stochastic Dynamic System Analysis of Wave Energy Converter with Hydraulic Power Take-Off, with Particular Reference to Wear Damage Analysis, Ph.d. Thesis, CeSOS.
IMT – 2011-72	Visscher, Jan	Application of Particla Image Velocimetry on Turbulent Marine Flows, Ph.d.Thesis, IMT.
IMT – 2011-73	Su, Biao	Numerical Predictions of Global and Local Ice Loads on Ships. Ph.d.Thesis, CeSOS.
IMT – 2011-74	Liu, Zhenhui	Analytical and Numerical Analysis of Iceberg Collision with Ship Structures. Ph.d.Thesis, IMT.
IMT – 2011-75	Aarsæther, Karl Gunnar	Modeling and Analysis of Ship Traffic by Observation and Numerical Simulation. Ph.d.Thesis, IMT.

Imt – 2011-76	Wu, Jie	Hydrodynamic Force Identification from Stochastic Vortex Induced Vibration Experiments with Slender Beams. Ph.d.Thesis, IMT.
Imt – 2011-77	Amini, Hamid	Azimuth Propulsors in Off-design Conditions. Ph.d.Thesis, IMT.
IMT – 2011-78	Nguyen, Tan-Hoi	Toward a System of Real-Time Prediction and Monitoring of Bottom Damage Conditions During Ship Grounding. Ph.d.thesis, IMT.
IMT- 2011-79	Tavakoli, Mohammad T.	Assessment of Oil Spill in Ship Collision and Grounding, Ph.d.thesis, IMT.
IMT- 2011-80	Guo, Bingjie	Numerical and Experimental Investigation of Added Resistance in Waves. Ph.d.Thesis, IMT.
IMT- 2011-81	Chen, Qiaofeng	Ultimate Strength of Aluminium Panels, considering HAZ Effects, IMT
IMT- 2012-82	Kota, Ravikiran S.	Wave Loads on Decks of Offshore Structures in Random Seas, CeSOS.
IMT- 2012-83	Sten, Ronny	Dynamic Simulation of Deep Water Drilling Risers with Heave Compensating System, IMT.
IMT- 2012-84	Berle, Øyvind	Risk and resilience in global maritime supply chains, IMT.
IMT- 2012-85	Fang, Shaoji	Fault Tolerant Position Mooring Control Based on Structural Reliability, CeSOS.
IMT- 2012-86	You, Jikun	Numerical studies on wave forces and moored ship motions in intermediate and shallow water, CeSOS.
IMT- 2012-87	Xiang ,Xu	Maneuvering of two interacting ships in waves, CeSOS
IMT- 2012-88	Dong, Wenbin	Time-domain fatigue response and reliability analysis of offshore wind turbines with emphasis on welded tubular joints and gear components, CeSOS
IMT- 2012-89	Zhu, Suji	Investigation of Wave-Induced Nonlinear Load Effects in Open Ships considering Hull Girder Vibrations in Bending and Torsion, CeSOS
IMT- 2012-90	Zhou, Li	Numerical and Experimental Investigation of Station-keeping in Level Ice, CeSOS
IMT- 2012-91	Ushakov, Sergey	Particulate matter emission characteristics from diesel enignes operating on conventional and alternative marine fuels, IMT
IMT- 2013-1	Yin, Decao	Experimental and Numerical Analysis of Combined In-line and Cross-flow Vortex Induced Vibrations, CeSOS

IMT-2013-2	Kurniawan, Adi	Modelling and geometry optimisation of wave energy converters, CeSOS
IMT-2013-3	Al Ryati, Nabil	Technical condition indexes doe auxiliary marine diesel engines, IMT
IMT-2013-4	Firoozkoohi, Reza	Experimental, numerical and analytical investigation of the effect of screens on sloshing, CeSOS
IMT-2013-5	Ommani, Babak	Potential-Flow Predictions of a Semi-Displacement Vessel Including Applications to Calm Water Broaching, CeSOS
IMT-2013-6	Xing, Yihan	Modelling and analysis of the gearbox in a floating spar-type wind turbine, CeSOS
IMT-7-2013	Balland, Océane	Optimization models for reducing air emissions from ships, IMT
IMT-8-2013	Yang, Dan	Transitional wake flow behind an inclined flat plate-----Computation and analysis, IMT
IMT-9-2013	Abdillah, Suyuthi	Prediction of Extreme Loads and Fatigue Damage for a Ship Hull due to Ice Action, IMT
IMT-10-2013	Ramìrez, Pedro Agustìn Pèrez	Ageing management and life extension of technical systems- Concepts and methods applied to oil and gas facilities, IMT
IMT-11-2013	Chuang, Zhenju	Experimental and Numerical Investigation of Speed Loss due to Seakeeping and Maneuvering. IMT
IMT-12-2013	Etemaddar, Mahmoud	Load and Response Analysis of Wind Turbines under Atmospheric Icing and Controller System Faults with Emphasis on Spar Type Floating Wind Turbines, IMT
IMT-13-2013	Lindstad, Haakon	Strategies and measures for reducing maritime CO2 emissons, IMT
IMT-14-2013	Haris, Sabril	Damage interaction analysis of ship collisions, IMT
IMT-15-2013	Shainee, Mohamed	Conceptual Design, Numerical and Experimental Investigation of a SPM Cage Concept for Offshore Mariculture, IMT
IMT-16-2013	Gansel, Lars	Flow past porous cylinders and effects of biofouling and fish behavior on the flow in and around Atlantic salmon net cages, IMT
IMT-17-2013	Gaspar, Henrique	Handling Aspects of Complexity in Conceptual Ship Design, IMT
IMT-18-2013	Thys, Maxime	Theoretical and Experimental Investigation of a Free Running Fishing Vessel at Small Frequency of Encounter, CeSOS
IMT-19-2013	Aglen, Ida	VIV in Free Spanning Pipelines, CeSOS

IMT-1-2014	Song, An	Theoretical and experimental studies of wave diffraction and radiation loads on a horizontally submerged perforated plate, CeSOS
IMT-2-2014	Rogne, Øyvind Ygre	Numerical and Experimental Investigation of a Hinged 5-body Wave Energy Converter, CeSOS
IMT-3-2014	Dai, Lijuan	Safe and efficient operation and maintenance of offshore wind farms ,IMT
IMT-4-2014	Bachynski, Erin Elizabeth	Design and Dynamic Analysis of Tension Leg Platform Wind Turbines, CeSOS
IMT-5-2014	Wang, Jingbo	Water Entry of Freefall Wedged – Wedge motions and Cavity Dynamics, CeSOS
IMT-6-2014	Kim, Ekaterina	Experimental and numerical studies related to the coupled behavior of ice mass and steel structures during accidental collisions, IMT
IMT-7-2014	Tan, Xiang	Numerical investigation of ship's continuous- mode icebreaking in leverl ice, CeSOS
IMT-8-2014	Muliawan, Made Jaya	Design and Analysis of Combined Floating Wave and Wind Power Facilities, with Emphasis on Extreme Load Effects of the Mooring System, CeSOS
IMT-9-2014	Jiang, Zhiyu	Long-term response analysis of wind turbines with an emphasis on fault and shutdown conditions, IMT
IMT-10-2014	Dukan, Fredrik	ROV Motion Control Systems, IMT
IMT-11-2014	Grimsmo, Nils I.	Dynamic simulations of hydraulic cylinder for heave compensation of deep water drilling risers, IMT
IMT-12-2014	Kvittem, Marit I.	Modelling and response analysis for fatigue design of a semisubmersible wind turbine, CeSOS
IMT-13-2014	Akhtar, Juned	The Effects of Human Fatigue on Risk at Sea, IMT
IMT-14-2014	Syahroni, Nur	Fatigue Assessment of Welded Joints Taking into Account Effects of Residual Stress, IMT
IMT-1-2015	Bøckmann, Eirik	Wave Propulsion of ships, IMT
IMT-2-2015	Wang, Kai	Modelling and dynamic analysis of a semi-submersible floating vertical axis wind turbine, CeSOS
IMT-3-2015	Fredriksen, Arnt Gunvald	A numerical and experimental study of a two-dimensional body with moonpool in waves and current, CeSOS
IMT-4-2015	Jose Patricio Gallardo Canabes	Numerical studies of viscous flow around bluff bodies, IMT

IMT-5-2015	Vegard Longva	Formulation and application of finite element techniques for slender marine structures subjected to contact interactions, IMT
IMT-6-2015	Jacobus De Vaal	Aerodynamic modelling of floating wind turbines, CeSOS
IMT-7-2015	Fachri Nasution	Fatigue Performance of Copper Power Conductors, IMT
IMT-8-2015	Oleh I Karpa	Development of bivariate extreme value distributions for applications in marine technology,CeSOS
IMT-9-2015	Daniel de Almeida Fernandes	An output feedback motion control system for ROVs, AMOS
IMT-10-2015	Bo Zhao	Particle Filter for Fault Diagnosis: Application to Dynamic Positioning Vessel and Underwater Robotics, CeSOS
IMT-11-2015	Wenting Zhu	Impact of emission allocation in maritime transportation, IMT
IMT-12-2015	Amir Rasekhi Nejad	Dynamic Analysis and Design of Gearboxes in Offshore Wind Turbines in a Structural Reliability Perspective, CeSOS
IMT-13-2015	Arturo Jesùs Ortega Malca	Dynamic Response of Flexibles Risers due to Unsteady Slug Flow, CeSOS
IMT-14-2015	Dagfinn Husjord	Guidance and decision-support system for safe navigation of ships operating in close proximity, IMT
IMT-15-2015	Anirban Bhattacharyya	Ducted Propellers: Behaviour in Waves and Scale Effects, IMT
IMT-16-2015	Qin Zhang	Image Processing for Ice Parameter Identification in Ice Management, IMT
IMT-1-2016	Vincentius Rumawas	Human Factors in Ship Design and Operation: An Experiential Learning, IMT
IMT-2-2016	Martin Storheim	Structural response in ship-platform and ship-ice collisions, IMT
IMT-3-2016	Mia Abrahamsen Prsic	Numerical Simulations of the Flow around single and Tandem Circular Cylinders Close to a Plane Wall, IMT
IMT-4-2016	Tufan Arslan	Large-eddy simulations of cross-flow around ship sections, IMT

IMT-5-2016	Pierre Yves-Henry	Parametrisation of aquatic vegetation in hydraulic and coastal research,IMT
IMT-6-2016	Lin Li	Dynamic Analysis of the Instalation of Monopiles for Offshore Wind Turbines, CeSOS
IMT-7-2016	Øivind Kåre Kjerstad	Dynamic Positioning of Marine Vessels in Ice, IMT
IMT-8-2016	Xiaopeng Wu	Numerical Analysis of Anchor Handling and Fish Trawling Operations in a Safety Perspective, CeSOS
IMT-9-2016	Zhengshun Cheng	Integrated Dynamic Analysis of Floating Vertical Axis Wind Turbines, CeSOS
IMT-10-2016	Ling Wan	Experimental and Numerical Study of a Combined Offshore Wind and Wave Energy Converter Concept
IMT-11-2016	Wei Chai	Stochastic dynamic analysis and reliability evaluation of the roll motion for ships in random seas, CeSOS
IMT-12-2016	Øyvind Selnes Patricksson	Decision support for conceptual ship design with focus on a changing life cycle and future uncertainty, IMT
IMT-13-2016	Mats Jørgen Thorsen	Time domain analysis of vortex-induced vibrations, IMT
IMT-14-2016	Edgar McGuinness	Safety in the Norwegian Fishing Fleet – Analysis and measures for improvement, IMT
IMT-15-2016	Sepideh Jafarzadeh	Energy effiency and emission abatement in the fishing fleet, IMT
IMT-16-2016	Wilson Ivan Guachamin Acero	Assessment of marine operations for offshore wind turbine installation with emphasis on response-based operational limits, IMT
IMT-17-2016	Mauro Candeloro	Tools and Methods for Autonomous Operations on Seabed and Water Coumn using Underwater Vehicles, IMT
IMT-18-2016	Valentin Chabaud	Real-Time Hybrid Model Testing of Floating Wind Tubines, IMT
IMT-1-2017	Mohammad Saud Afzal	Three-dimensional streaming in a sea bed boundary layer
IMT-2-2017	Peng Li	A Theoretical and Experimental Study of Wave-induced Hydroelastic Response of a Circular Floating Collar
IMT-3-2017	Martin Bergström	A simulation-based design method for arctic maritime transport systems

IMT-4-2017	Bhushan Taskar	The effect of waves on marine propellers and propulsion
IMT-5-2017	Mohsen Bardestani	A two-dimensional numerical and experimental study of a floater with net and sinker tube in waves and current
IMT-6-2017	Fatemeh Hoseini Dadmarzi	Direct Numerical Simualtion of turbulent wakes behind different plate configurations
IMT-7-2017	Michel R. Miyazaki	Modeling and control of hybrid marine power plants
IMT-8-2017	Giri Rajasekhar Gunnu	Safety and effiency enhancement of anchor handling operations with particular emphasis on the stability of anchor handling vessels
IMT-9-2017	Kevin Koosup Yum	Transient Performance and Emissions of a Turbocharged Diesel Engine for Marine Power Plants
IMT-10-2017	Zhaolong Yu	Hydrodynamic and structural aspects of ship collisions
IMT-11-2017	Martin Hassel	Risk Analysis and Modelling of Allisions between Passing Vessels and Offshore Installations
IMT-12-2017	Astrid H. Brodtkorb	Hybrid Control of Marine Vessels – Dynamic Positioning in Varying Conditions
IMT-13-2017	Kjersti Bruserud	Simultaneous stochastic model of waves and current for prediction of structural design loads
IMT-14-2017	Finn-Idar Grøtta Giske	Long-Term Extreme Response Analysis of Marine Structures Using Inverse Reliability Methods
IMT-15-2017	Stian Skjong	Modeling and Simulation of Maritime Systems and Operations for Virtual Prototyping using co-Simulations
IMT-1-2018	Yingguang Chu	Virtual Prototyping for Marine Crane Design and Operations
IMT-2-2018	Sergey Gavrilin	Validation of ship manoeuvring simulation models
IMT-3-2018	Jeevith Hegde	Tools and methods to manage risk in autonomous subsea inspection,maintenance and repair operations
IMT-4-2018	Ida M. Strand	Sea Loads on Closed Flexible Fish Cages
IMT-5-2018	Erlend Kvinge Jørgensen	Navigation and Control of Underwater Robotic Vehicles

IMT-6-2018	Bård Stovner	Aided Intertial Navigation of Underwater Vehicles
IMT-7-2018	Erlend Liavåg Grotle	Thermodynamic Response Enhanced by Sloshing in Marine LNG Fuel Tanks
IMT-8-2018	Børge Rokseth	Safety and Verification of Advanced Maritime Vessels
IMT-9-2018	Jan Vidar Ulveseter	Advances in Semi-Empirical Time Domain Modelling of Vortex-Induced Vibrations
IMT-10-2018	Chenyu Luan	Design and analysis for a steel braceless semi-submersible hull for supporting a 5-MW horizontal axis wind turbine
IMT-11-2018	Carl Fredrik Rehn	Ship Design under Uncertainty
IMT-12-2018	Øyvind Ødegård	Towards Autonomous Operations and Systems in Marine Archaeology
IMT-13-2018	Stein Melvær Nornes	Guidance and Control of Marine Robotics for Ocean Mapping and Monitoring
IMT-14-2018	Petter Norgren	Autonomous Underwater Vehicles in Arctic Marine Operations: Arctic marine research and ice monitoring
IMT-15-2018	Minjoo Choi	Modular Adaptable Ship Design for Handling Uncertainty in the Future Operating Context
MT-16-2018	Ole Alexander Eidsvik	Dynamics of Remotely Operated Underwater Vehicle Systems
IMT-17-2018	Mahdi Ghane	Fault Diagnosis of Floating Wind Turbine Drivetrain- Methodologies and Applications
IMT-18-2018	Christoph Alexander Thieme	Risk Analysis and Modelling of Autonomous Marine Systems
IMT-19-2018	Yugao Shen	Operational limits for floating-collar fish farms in waves and current, without and with well-boat presence
IMT-20-2018	Tianjiao Dai	Investigations of Shear Interaction and Stresses in Flexible Pipes and Umbilicals
IMT-21-2018	Sigurd Solheim Pettersen	Resilience by Latent Capabilities in Marine Systems
IMT-22-2018	Thomas Sauder	Fidelity of Cyber-physical Empirical Methods. Application to the Active Truncation of Slender Marine Structures
IMT-23-2018	Jan-Tore Horn	Statistical and Modelling Uncertainties in the Design of Offshore Wind Turbines

IMT-24-2018	Anna Swider	Data Mining Methods for the Analysis of Power Systems of Vessels
IMT-1-2019	Zhao He	Hydrodynamic study of a moored fish farming cage with fish influence
IMT-2-2019	Isar Ghamari	Numerical and Experimental Study on the Ship Parametric Roll Resonance and the Effect of Anti-Roll Tank
IMT-3-2019	Håkon Strandenes	Turbulent Flow Simulations at Higher Reynolds Numbers
IMT-4-2019	Siri Mariane Holen	Safety in Norwegian Fish Farming – Concepts and Methods for Improvement
IMT-5-2019	Ping Fu	Reliability Analysis of Wake-Induced Riser Collision
IMT-6-2019	Vladimir Krivopolianskii	Experimental Investigation of Injection and Combustion Processes in Marine Gas Engines using Constant Volume Rig
IMT-7-2019	Anna Maria Kozlowska	Hydrodynamic Loads on Marine Propellers Subject to Ventilation and out of Water Condition.
IMT-8-2019	Hans-Martin Heyn	Motion Sensing on Vessels Operating in Sea Ice: A Local Ice Monitoring System for Transit and Stationkeeping Operations under the Influence of Sea Ice
IMT-9-2019|	Stefan Vilsen	Method for Real-Time Hybrid Model Testing of Ocean Structures – Case on Slender Marine Systems
IMT-10-2019	Finn-Christian W. Hanssen	Non-Linear Wave-Body Interaction in Severe Waves
IMT-11-2019	Trygve Olav Fossum	Adaptive Sampling for Marine Robotics
IMT-12-2019	Jørgen Bremnes Nielsen	Modeling and Simulation for Design Evaluation
IMT-13-2019	Yuna Zhao	Numerical modelling and dyncamic analysis of offshore wind turbine blade installation
IMT-14-2019	Daniela Myland	Experimental and Theoretical Investigations on the Ship Resistance in Level Ice
IMT-15-2019	Zhengru Ren	Advanced control algorithms to support automated offshore wind turbine installation
IMT-16-2019	Drazen Polic	Ice-propeller impact analysis using an inverse propulsion machinery simulation approach
IMT-17-2019	Endre Sandvik	Sea passage scenario simulation for ship system performance evaluation

IMT-18-2019	Loup Suja-Thauvin	Response of Monopile Wind Turbines to Higher Order Wave Loads
IMT-19-2019	Emil Smilden	Structural control of offshore wind turbines – Increasing the role of control design in offshore wind farm development
IMT-20-2019	Aleksandar-Sasa Milakovic	On equivalent ice thickness and machine learning in ship ice transit simulations
IMT-1-2020	Amrit Shankar Verma	Modelling, Analysis and Response-based Operability Assessment of Offshore Wind Turbine Blade Installation with Emphasis on Impact Damages
IMT-2-2020	Bent Oddvar Arnesen Haugaløkken	Autonomous Technology for Inspection, Maintenance and Repair Operations in the Norwegian Aquaculture
IMT-3-2020	Seongpil Cho	Model-based fault detection and diagnosis of a blade pitch system in floating wind turbines
IMT-4-2020	Jose Jorge Garcia Agis	Effectiveness in Decision-Making in Ship Design under Uncertainty
IMT-5-2020	Thomas H. Viuff	Uncertainty Assessment of Wave-and Current-induced Global Response of Floating Bridges
IMT-6-2020	Fredrik Mentzoni	Hydrodynamic Loads on Complex Structures in the Wave Zone
IMT-7-2020	Senthuran Ravinthrakumar	Numerical and Experimental Studies of Resonant Flow in Moonpools in Operational Conditions
IMT-8-2020	Stian Skaalvik Sandøy	Acoustic-based Probabilistic Localization and Mapping using Unmanned Underwater Vehicles for Aquaculture Operations
IMT-9-2020	Kun Xu	Design and Analysis of Mooring System for Semi-submersible Floating Wind Turbine in Shallow Water
IMT-10-2020	Jianxun Zhu	Cavity Flows and Wake Behind an Elliptic Cylinder Translating Above the Wall
IMT-11-2020	Sandra Hogenboom	Decision-making within Dynamic Positioning Operations in the Offshore Industry – A Human Factors based Approach
IMT-12-2020	Woongshik Nam	Structural Resistance of Ship and Offshore Structures Exposed to the Risk of Brittle Failure
IMT-13-2020	Svenn Are Tutturen Værnø	Transient Performance in Dynamic Positioning of Ships: Investigation of Residual Load Models and Control Methods for Effective Compensation